THE BIOMECHANICS OF THORACIC SKELETAL RESPONSE

ANDREW ROBB KEMPER

Dissertation submitted to the faculty of the
Virginia Polytechnic Institute and State University
in partial fulfillment of the requirements for the degree of

Doctor of Philosophy
In
Biomedical Engineering

Warren N. Hardy
H. Clay Gabler
Joel D. Stitzel
Michael L. Madigan
P. Gunnar Brolinson

March 30, 2010

Blacksburg, Virginia

Keywords: Thorax, Injury, Bone, Rib, Clavicle, Stress, Strain, Tension, Bending, Failure

Copyright 2010, Andrew R. Kemper

THE BIOMECHANICS OF THORACIC SKELETAL RESPONSE

Andrew Robb Kemper

ABSTRACT

The National Highway Traffic Safety Administration (NHTSA) reported that in 2008 there were a total of 37,261 automotive related fatalities, 26,689 of which were vehicle occupants. It has been reported that in automotive collisions chest injuries rank second only to head injuries in overall number of fatalities and serious injuries. In frontal collisions, chest injuries constitute 37.6% of all AIS 3+ injuries, 46.3% of all AIS 4+ injuries, and 43.3% of all AIS 5+ injuries. In side impact collisions, it has been reported that thoracic injuries are the most common type of serious injury (AIS≥3) to vehicle occupants in both near side and far side crashes which do not involve a rollover. In addition, rib fractures are the most frequent type of thoracic injury observed in both frontal and side impact automotive collisions.

Anthropomorphic test devices (ATDs), i.e. crash test dummies, and finite element models (FEMs) have proved to be integral tools in the assessment and mitigation of thoracic injury risk. However, the validation of both of these tools is contingent on the availability of relevant biomechanical data. In order to develop and validate FEMs and ATDs with improved thoracic injury risk assessment capabilities, it is necessary to generate biomechanical data currently not presented in the literature. Therefore, the purpose of this dissertation is to present novel material, structural, and global thoracic skeletal response data as well as quantify thoracic injury timing in both frontal belt loading and side impact tests using cadaveric specimens.

ACKNOWLEDGEMENTS

I would like to thank all of the people who played an important role in the completion of my degree. Without the help, advice, and encouragement of these individuals this achievement would not have been possible.

First of all, I would like to express gratitude to my doctoral committee chairman, Dr. Warren Hardy for his support and guidance. He has provided me with a wealth of knowledge and advice. I know that I am a better engineer and researcher thanks to the time I have spent learning from Dr. Hardy.

I would also like to thank Dr. Joel Stitzel, Dr. Clay Gabler, Dr. Mike Madigan, and Dr. Gunnar Brolinson for serving on my doctoral committee. They have all played significant roles in my academic achievements and understanding of injury biomechanics.

I do not think I could ever adequately thank Dr. Stefan Duma for all of the opportunities, knowledge, support, and guidance he has provided me throughout my years at Virginia Tech. Dr. Duma has been integral to my successes and achievements in the field of injury biomechanics. I am extremely grateful for everything he has done for me as a mentor, role model, and friend.

A lot of this research would not have been possible with out the help and participation of my fellow lab mates. I have worked with too many people during my time at Virginia Tech to list them all. Nevertheless, I greatly appreciate all of the work that everyone contributed to this research.

Finally, my heartfelt gratitude goes to my family for their unconditional love, patience, and support throughout my education. My parents have always emphasized the importance of moral principles, work ethics, and responsibility. The encouragement from both my brother and sister has always helped me in times of need.

TABLE OF CONTENTS

LIST OF FIGURES

LIST OF TABLES

CHAPTER 1

Introduction and Research Objectives

Introduction

The National Highway Traffic Safety Administration (NHTSA) reported that in 2008 there were a total of 37,261 automotive related fatalities, 26,689 of which were vehicle occupants (Traffic Safety Facts, 2008). It has been reported that in automotive collisions chest injuries rank second only to head injuries in overall number of fatalities and serious injuries (Cavanaugh, 1993). Elhagediab and Rouhana (1998) examined the incidence of injuries due to frontal impacts in the National Automotive Sampling System - Crashworthiness Data System (NASS-CDS) from 1988 to 1994 with respect to the Abbreviated Injury Scale (AIS), where AIS is a system used by researchers and trauma centers to rank and compare the severity of injuries on a scale of 0 (no injury) to 6 (certain death) based on threat to life. They found that chest injuries constituted 37.6% of all AIS 3+ injuries, 46.3% of all AIS 4+ injuries, and 43.3% of all AIS 5+ injuries. For side impact collisions, it has been reported that thoracic injuries are the most common type of serious injury (AIS≥3) to vehicle occupants in both near side and far side crashes which do not involve a rollover (Gabler et al., 2005; Samaha et al., 2003).

A number of studies have reported that skeletal injuries are the most frequent type of thoracic injury observed in both frontal and side impact automotive collisions. Data from the Crash Injury Research and Engineering Network (CIREN) showed that rib fractures were the most serious injury sustained by 40% of the patients over 60 who died of chest injuries from automobile collisions (Kent et al., 2005b). Furthermore, previous cadaveric laboratory studies

have shown that rib fractures are the most common skeletal injury in frontal belted sled tests and the most frequent thoracic maximum AIS in side impacts (Cromack and Ziper, 1975; Patrick, 1976; Ramet and Cesari, 1979; Morgan et al., 1986; Crandall et al., 1997; Pintar et al., 1997; Kallieris et al., 1998; Viano, 1989; Kuppa et al., 2003). In addition to rib fractures, clavicle fractures are frequently observed in automotive collisions. An analysis of the NASS-CDS found that over 9,700 three-point belt restrained occupants incur a clavicle fracture every year. Although clavicle fractures due not pose as high of a threat to life (AIS=2) as numerous rib fractures, they can result in either temporary or long term loss of functional capacity. Mid-clavicle fractures are of special concern since they may lead to significant morbidity due to a high rate of nonunion, 22% to 33%, when treated non-operatively (Nordqvist, 2000).

Finite Element Models (FEMs) of the human thorax are becoming an integral tool in the reduction of automotive related thoracic injuries because they provide a relatively inexpensive, both temporally and monetarily, means to assess the effectiveness of both existing and advanced safety restraint systems. A major advantage to FEMs is that they allow for the prediction of injury based on the calculation of physical variables, such as stress and strain, that are mechanically related to injury. However, the response of thoracic skeletal tissue, i.e. the clavicle and rib cage, must be locally and globally validated based on component level tests as well as whole cadaver tests in order to accurately predict injury. The level of validation is contingent on the availability of biomechanical data presented in the literature. There have been some studies that have investigated the biomechanical response of the clavicle in three-point bending (Bolte et al., 2000; Proubasta et al., 2002). However, these studies have been limited to a single loading direction and low impact speeds. In regard to the rib cage, it has been shown that the structural

response and the distribution of rib fractures vary with respect to the region and distribution of an externally applied load (Kent et al., 2001; Shaw et al., 2005). Regional variation in the structural response of bone within an individual can be a result of changes in the bone geometry, bone material properties, or both. Accounting for differences in these parameters increases the complexity of thoracic models, but can have a considerable affect on both the global response and predicted injuries (Stitzel et al., 2003; Kent et al., 2005b). Although the literature suggests that regional differences in the structural response of human ribs are most likely due to regional changes in geometry, there has been no research evaluating the influence of material, structural, and geometric properties on the response of human ribs in a controlled data set. In order to more accurately model the human rib cage, changes in the structural response with respect to material and geometric properties need to be investigated in a controlled study.

Regardless of how advanced FEMs of the human body become, they will never replace the need to perform regulatory full-scale vehicle crash tests designed to ensure occupant safety. In these tests, injury risk is assessed with the use of Anthropomorphic Test Devices (ATDs), i.e. crash test dummies. The response of ATDs must meet the thoracic impact response requirements set forth by the Anthropomorphic Test Devices Working Group of the International Standards Organization (ISO/TC22/SC12/WG5) to ensure that it is representative to that of a human, i.e. biofidelic. These response requirements are based on the results of numerous cadaveric studies which use a variety of dynamic impact conditions. The current ATDs approved by NHTSA to assess injury risk in frontal impacts are the Hybrid III- 50^{th} Percentile dummy, which represents a 50^{th} percentile male, and the Hybrid III- 5^{th} Percentile dummy, which represents a 5^{th} percentile female. Traditionally, the only dummy certified by NHSTA to assess injury risk in side impacts

was the Department of Transportation Side Impact Dummy (DOT SID), which represents a 50th percentile male. Recently, however, NHSTA approved the use of two additional side impact ATDs. These include the Euro Side Impact Dummy-2 with rib extensions (ES-2re), which represents a 50th percentile male, and the SID-IIs, which represents a 5th percentile female. It is important to note that the arm of the DOT SID is positioned parallel to the torso, while the arms of the ES-2re and SID-IIs are positioned such that the angle between the arm and torso is 40 degrees.

Although there have been numerous studies which have investigated the tolerance of the thorax in side impact loading, research regarding the effect of the arm on the response and tolerance of the thorax is quite limited. In fact, there are only two studies to the authors' knowledge which have investigated the influence of the arm on thoracic response in a controlled study (Stalnaker et al., 1979; and Cesari et al., 1981). These studies both concluded that the arm provides some protection against thoracic injury compared to impacts directly to the rib cage. However, it is difficult to determine how the position of the arm relative to the thorax, 20 degrees versus parallel with the thorax, affects the thoracic response due to the differences in test conditions between the two studies. In addition, no studies have quantified the response of human cadavers during side impact loading with the arm placed at 40-45 degrees, which is the arm position specified for both the ES-2re and SID-IIs. In order to determine the true effect of arm position on thoracic response, each of these arm positions needs to be evaluated in single controlled study.

In order for automotive manufactures to sell a vehicle in the United States, the vehicle must first pass standard safety compliance tests regulated by NHTSA. The risk of thoracic injury is assessed with the use of either a frontal or side impact ATD, depending on the specific test and impact direction. These tests are purely pass/fail based on whether or not the dummy response exceeds the injury criteria specified by NHTSA. The Federal Motor Vehicle Safety Standard for frontal impacts (FMVSS 208- Fixed Barrier) specifies that the chest compression cannot exceed 63 mm for the belted male dummy and 52 mm for the belted female dummy during a 48 kph impact into a rigid wall with frontal engagement. The traditional FMVSS for side impact (FMVSS 214- Moving Deformable Barrier) specifies that the Thoracic Trauma Index (TTI), which is based on the rib and spine acceleration, for the DOT SID cannot exceed 85 g's when a stationary vehicle is struck on the driver side with a deformable barrier traveling at 52.9 kph. The new FMVSS for side impact (FMVSS 214- Pole) specifies that the lateral rib deflection of the ES-2re cannot exceed 44 mm when the driver side of a vehicle, traveling up to 32 kph, strikes a 25.4 cm diameter pole, which is centered on the front passenger. Currently, the injury criterion for the SID-IIs is still under development.

Although the current thoracic injury criteria for both frontal and side impact dummies provides a biomechanically-based metric for injury risk, they are limited by the fact that they were developed based on the results of cadaveric studies which rely primarily on censored rib fracture data (Eppinger, 1976; Morgan et al., 1986; Viano, 1989; Morgan et al., 1994; Pintar et al., 1997; Kuppa and Eppinger, 1998; Kuppa et al., 2003). In other words, it is not possible to determine the exact loads, accelerations, or displacements at the time of fracture. Rather, it is only known that an injury occurred at some point during the impact test. Consequently, these studies rely on

statistical regression models to develop injury risk functions with respect to global criteria, such as peak chest deflection or peak acceleration. Kent (2002) noted that one of the problems with global methods used to develop thoracic injury criteria is that the criteria correlate with injury without necessarily being functionally related to injury, in contrast to stress and strain. Although previous studies have shown the ability to detect when selected rib fractures occur, no method has been successful at mapping the exact fracture timing of the entire thorax during dynamic thoracic belt loading or lateral impacts to the thorax (Cormier et al, 2005; Charpail et al., 2005; Trosseille et al., 2008). In addition, there has been no attempt to evaluate the effects of thoracic strain gages, which requires the removal the periosteum and adhesive, on the structural response of whole ribs. Logically, the ability to map the exact timing of rib fractures over the entire thorax could improve and clarify the foundation of thoracic injury criteria in both frontal and side impact loading, which could potentially lead to the mitigation of thoracic injuries and fatalities.

In summary, although anthropomorphic test devices and finite element models are integral tools in the assessment and mitigation of thoracic injury risk, the level of validation of both of these tools is contingent on the availability of biomechanical data presented in the literature. In order to develop and validate FEMs and ATDs with improved thoracic injury risk assessment capabilities, it is necessary to generate biomechanical data currently not provided within the literature. Therefore, the purpose of this dissertation is to present novel material, structural, and global thoracic skeletal response data as well as to quantify thoracic injury timing in both frontal belt loading and side impact tests using cadaveric specimens.

Research Objectives

The studies in this dissertation are expected to yield several new and significant contributions to the field of injury biomechanics. The research objectives from these studies are designed to generate material, structural, and global thoracic skeletal response data not currently addressed in the literature. These studies will provide data that can be used to develop and validate FEMs and ATDs with improved thoracic injury risk assessment capabilities, which could potentially lead to the mitigation of thoracic injuries and fatalities resulting from automotive collisions. In order to achieve this ultimate goal, there are multiple research objectives that are addressed:

1. Determine if the removal of the periosteum, application of a strain gage, or hydration level have any significant effects on the structural response of human ribs in dynamic three-point bending.
2. Determine the effect of loading direction on the biomechanical response of the human clavicle when subjected to dynamic three-point bending.
3. Determine which variables, material properties or geometry, contribute to regional variation in the strength of human ribs.
4. Determine the effect of costovertebral articulation during dynamic frontal belt loading performed on human cadaver thoraces.
5. Determine non-censored rib fracture data during dynamic frontal belt loading performed on human cadaver thoraces and correlate injury timing to sternum deflection.
6. Determine the influence of arm position on thoracic response during both non-destructive and destructive dynamic side impact loading.
7. Determine non-censored rib fracture data during destructive dynamic side impact loading and correlate injury timing to rib deflection.

CHAPTER 2

Effect of the Periosteum, Strain Gages, and Hydration on the Structural Response of Human Ribs

Introduction

In automotive accidents, chest injuries rank second only to head injury in overall number of fatalities and serious injuries (Cavanaugh 1993). Mulligan (1996) reported that thoracic injury is the principle causative factor in 30% of automotive deaths. In addition, previous studies using restrained cadavers in impact sled tests have frequently found rib fractures to be the most common skeletal injury (Cromack and Ziper, 1975; Patrick, 1976; Kallieris et al., 1998,). Finite element models of the human thorax are becoming an integral tool in the reduction of these injuries. However, these models must be validated based on biomechanical data in order to accurately predict injury. Previous researchers have performed three-point bending tests on whole rib sections to evaluate the properties of the ribs (Granik and Stein, 1973; Cormier et al., 2005; Yoganandan and Pintar, 2005). A number of studies have quantified the strain and fracture timing of *in situ* ribs and whole rib sections by removing the periosteum and gluing strain gages directly to the external portion of the cortical shell (Cormier et al, 2005; Charpail et al., 2005; Trosseille et al., 2008). However, this may have a significant effect on the structural response of the ribs due to the fact that the rib cortical shell is relatively thin, approximately 1 mm on average (Mohr et al., 2007). To explain, a whole rib or rib section with a strain gage attached could be thought of as a composite material because the ratio of cortical shell thickness to the combined thickness of the adhesive and strain gage is relatively small. However, there has been no attempt to evaluate the effects of removing the periosteum and application of an

adhesive and strain gage on the structural response of whole rib sections. Therefore, the primary purpose of this study was to determine if either the removal of the periosteum or the application of a strain gage has any significant effect on the structural response of human ribs. In addition, the effect of hydration level was evaluated in order to determine the most appropriate method for storing bone samples prior to testing.

Methods

A total of 48 dynamic three-point bending tests were performed on 24 matched fresh frozen human cadaver rib specimens obtained from five male unembalmed frozen and thawed post mortem human thoraces (Table 1). Freezing was used as a means to preserve the specimens because numerous previous studies have indicated that freezing does not significantly affect the material properties of cortical bone when frozen to a temperature of -20° C (Frankel, 1960; Sedlin, 1965; Weaver, 1966; Linde and Sorensen, 1993; Griffon et al., 1995; Hamer et al., 1996).

For comparison with the standard population, the bone mineral density (BMD) of each cadaver was determined by the Osteogram technique (Hardy et al. 2001a; Stitzel et al., 2003; Kemper et al., 2005). For this technique, the left hand of each cadaver was x-rayed next to an aluminum calibration wedge. The x-ray was then processed by CompuMed Incorporated (CompuMed, Inc., Los Angeles, CA) to obtain the BMD, T-Score, and Z-score for each subject. This type of BMD measurement, however, only provides an indication of overall bone quality and does not account for local changes in bone density or composition. Therefore, the BMD obtained through this method is referred to as the "global BMD." The T-score is the number of standard deviations from the average value of healthy living individuals between 25 and 50 years of age. The Z-score is the number of standard deviations from the average value of healthy living individuals of

similar age. The World Health Organization classifies normal bone as T-scores of -1.0 or greater, osteopenia as T-scores between -1.0 and -2.5, and osteoporosis as T-scores below -2.5 (Wolf and Pfleger, 2003).

Table 1: Subject information for periosteum, strain gage, and hydration rib testing.

Subject ID	Gender	Age (years)	Mass (kg)	Global BMD	T-score	Z-score
sm52	M	42	85.91	92.1	-1.7	-1.3
sm48	M	45	53.18	120.1	0.9	0.9
sm37	M	56	81.36	105.3	-0.5	0.3
sm40	M	66	66.36	79.4	-2.9	-1.4
sm50	M	72	75.91	105.1	-0.5	1.2

Matched left and right rib specimens were dissected from anterior and lateral regions of ribs 8-10 of the five human thoraces (Figure 1). The specimens were approximately 11.43 cm long. It should be noted that anterior specimens were taken at least 10 mm from the costochondral joint. Specimens of each matched set were then potted side by side in a polyvinyl chloride (PVC) square pot filled with polymethyl methacrylate (PMMA) fast cast compound while using a custom jig to ensure the matching orientation. A fiberglass pin was placed through each PVC square pot to act as a pivot on the three-point bending test setup. In order to provide a rigid fixation in the potting compound, the soft tissue and periosteum were removed from the anterior end of each specimen and a one inch plastic pin was inserted through the prepped region. The specimens were kept hydrated during preparation by spraying saline directly on the specimens.

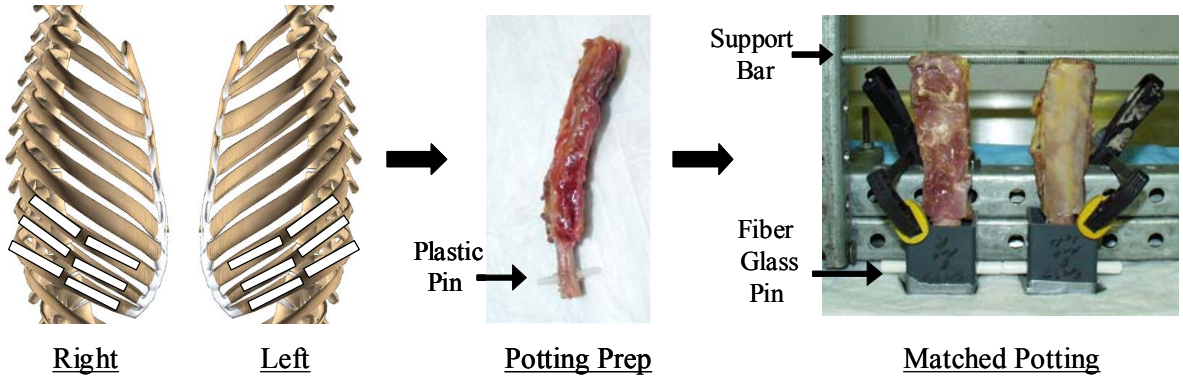

Figure 1: Three-point bending matched pair specimen procurement, preparation, and potting.

The matched rib pairs were randomly divided into three test groups. In the first test group, matched specimens were tested to determine the effects of leaving the periosteum and soft tissue intact, which is representative of the *in vivo* condition, versus removing the periosteum and all soft tissue, which is normally done to attach a strain gage (Table 2). In the second test group, matched specimens were tested to determine the effects of placing a strain gage on the tension side of the specimen (Table 3). For the second test group, the soft tissue and periosteum were removed only in the active region at the location of the strain gage. In the third test group, matched specimens were tested to determine the effects of immersing the specimens in saline versus wrapping the specimens in saline-soaked gauze (Table 4). All specimens in the hydration test group were sealed in a plastic bag and refrigerated for five days. The soft tissue and periosteum were not removed in the third test group. For the first and second test group, specimens were kept hydrated by wrapping the specimens in saline-soaked gauze.

Table 2: Matched pair three-point bending specimens - periosteum test group.

Subject Number	Side of Thorax	Rib Number	Location	Periosteum
sm37	Right	9	Lateral	**Yes**
sm37	Left	10	Anterior	**Yes**
sm48	Left	8	Lateral	**Yes**
sm48	Left	9	Anterior	**Yes**
sm52	Right	8	Anterior	**Yes**
sm52	Left	9	Lateral	**Yes**
sm52	Left	10	Anterior	**Yes**
sm37	Left	9	Lateral	No
sm37	Right	10	Anterior	No
sm48	Right	8	Lateral	No
sm48	Right	9	Anterior	No
sm52	Left	8	Anterior	No
sm52	Right	9	Lateral	No
sm52	Right	10	Anterior	No

Table 3: Matched pair three-point bending specimens - strain gage test group.

Subject Number	Side of Thorax	Rib Number	Location	Strain Gage
sm40	Right	8	Anterior	**Yes**
sm40	Left	8	Lateral	**Yes**
sm40	Right	9	Anterior	**Yes**
sm40	Left	9	Lateral	**Yes**
sm40	Right	10	Anterior	**Yes**
sm50	Left	8	Lateral	**Yes**
sm50	Right	8	Anterior	**Yes**
sm50	Left	9	Lateral	**Yes**
sm50	Right	9	Anterior	**Yes**
sm40	Left	8	Anterior	No
sm40	Right	8	Lateral	No
sm40	Left	9	Anterior	No
sm40	Right	9	Lateral	No
sm40	Left	10	Anterior	No
sm50	Right	8	Lateral	No
sm50	Left	8	Anterior	No
sm50	Right	9	Lateral	No
sm50	Left	9	Anterior	No

Table 4: Matched pair three-point bending specimens - hydration test group.

Subject Number	Side of Thorax	Rib Number	Location	Soaked
sm37	Right	8	Lateral	**Yes**
sm37	Left	10	Lateral	**Yes**
sm48	Left	8	Anterior	**Yes**
sm48	Left	9	Lateral	**Yes**
sm48	Right	10	Anterior	**Yes**
sm52	Right	8	Lateral	**Yes**
sm52	Left	9	Anterior	**Yes**
sm52	Left	10	Lateral	**Yes**
sm37	Left	8	Lateral	No
sm37	Right	10	Lateral	No
sm48	Right	8	Anterior	No
sm48	Right	9	Lateral	No
sm48	Left	10	Anterior	No
sm52	Left	8	Lateral	No
sm52	Right	9	Anterior	No
sm52	Right	10	Lateral	No

Once the specimens were potted, a microCT (Scanco Medical, VivaCT- 40, Switzerland) was used to obtain a detailed cross-sectional image, 38 micron isentropic resolution, of each specimen at the point of the impactor blade contact. This was done by first obtaining a scout image of the potted specimen. A cross-sectional image at the exact location of the impactor contact could then be obtained by performing the CT scan 50.8 mm from the center of a fiberglass pin placed through the PVC square pot (Figure 2). Potting the specimens using non-metallic materials prior to scanning ensured that the CT slice was taken at the exact location and specimen orientation as that seen in the initial testing conditions.

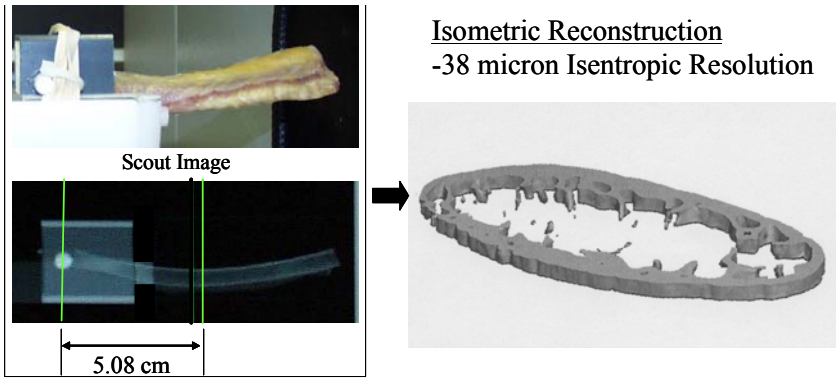

Figure 2: MicroCT image obtained at point of loading.

The cross-sectional microCT image was then thresholded (Hounsfield unit of 300) to obtain the shape of the cortical shell (Figure 3). Finally, the image was converted to black and white, and Matlab © (Matworks, Inc., Matlab-R12, Natick, MA) was used to calculate the area moment of inertia (I) and the distance from the tension side to the neutral axis (c). The neutral axis of the image was found by first calculating the area of bone in each row. This was done by taking the sum of ones, where each "one" was a 0.038 mm x 0.038 mm pixel which represented bone, multiplied by 0.00144 to obtain the area. The area of bone in each row was multiplied by the distance that row was from an assumed neutral axis, and then summed above and below an assumed neutral axis. The neutral axis was determined to be the row where the sum above the assumed neutral axis is equal to the sum below the assumed neutral axis. The distance to the neutral axis (c) was calculated by summing the number of rows between the neutral axis and the bottom of the image, and then multiplying that sum by 0.038 to obtain the distance in millimeters. The moment of inertia (I_{xx}) about the neutral axis was found by calculating the area of bone in a row times the distance that row was from the neutral axis squared, and then summing that value for the entire image. It should be noted that the cortical bone was assumed to be homogeneous and the neutral axis was assumed to be perpendicular to the direction of loading.

Binary Image Thresholded Image

Figure 3: Rib cross-section before and after thresholding.

The primary component of the three-point bending test setup was a servo-hydraulic Material Testing System (MTS Systems Corporation, MTS-810, Eden Prairie, MN). The three-point bending setup was designed so that the potted specimen end was pinned and the un-potted end was simply supported (Figure 4). The testing span was fixed at 10.16 cm. Specimens were oriented so that the specimen was bent in the internal to external direction by the impactor blade. This placed the external surface of the rib in tension, which would be expected when the thorax is compressed in the anterior-posterior direction. The impactor displacement rate of 17.78 cm/s yielded a strain rate of approximately 0.5 s^{-1}. The impactor and reaction support assembly were instrumented with single-axis load cells (Interface, Inc., 1210- 2,224 N, Scottsdale, Arizona). An accelerometer (Endevco Corporation, 7264B-2000 G, San Juan Capistrano, CA) was attached to the impactor head to allow for inertial compensation. Impactor displacement (d) was measured using the MTS internal linear variable displacement transducer (LVDT). Data from the load cells and accelerometers were recorded at a sampling rate of 30 kHz (Iotech, Wavebook-16, Cleveland, OH), and filtered to SAE channel filter class (CFC) 180 (SAE J211, 1995). The peak values were defined as the point at which continued impactor displacement no longer resulted in an incremental increase in measured force. Bending moment was calculated as the product of one half the measured reaction force (P_R) and one half the testing span (L) (Equation 1). Bending

stress was estimated as the product of the moment and distance from the tension side to the neutral axis (c) divided by the area moment of inertia (I_{xx}) (Equation 2). Bending strain was estimated based on the product of impactor displacement and distance from the tension side to the neutral axis divided by the testing span squared (Equation 3).

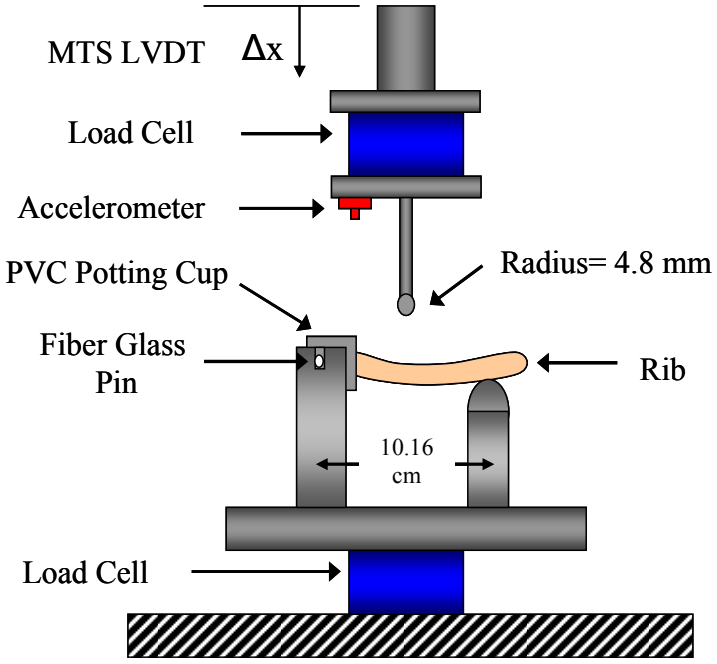

Figure 4: Rib three-point bending test setup.

$$M = \left(\frac{P_R}{2}\right) \cdot \left(\frac{L}{2}\right) \qquad \text{(Eqn. 1)}$$

$$\sigma = \left(\frac{Mc}{I_{xx}}\right) \qquad \text{(Eqn. 2)}$$

$$\varepsilon = \left(\frac{12dc}{L^2}\right) \qquad \text{(Eqn. 3)}$$

Results

The average peak values and corresponding standard deviations for each test group were tabulated (Table 5 to Table 7). In addition, moment versus deflection and estimated stress versus estimated strain were plotted for each test group (Figure 5 to Figure 10).

Table 5: Averages and standard deviations for periosteum test group.

		I_{xx}	c	Peak Moment	Peak Displacement	Estimated Peak Stress	Estimated Peak Strain	Peak Strain (Gage)
		(mm^4)	(mm)	(Nm)	(mm)	(MPa)	(μstrain)	(μstrain)
Periosteum	AVG	100.29	3.41	5.77	5.73	222.20	22087	N/A
	STDEV	90.32	1.13	1.34	3.77	42.25	6271	N/A
No Periosteum	AVG	103.97	3.25	5.07	6.06	213.94	18329	N/A
	STDEV	96.29	0.81	1.49	3.98	35.22	4242	N/A

Table 6: Averages and standard deviations for strain gage test group.

		I_{xx}	c	Peak Moment	Peak Displacement	Estimated Peak Stress	Estimated Peak Strain	Peak Strain (Gage)
		(mm^4)	(mm)	(Nm)	(mm)	(MPa)	(μstrain)	(μstrain)
Strain Gage	AVG	96.27	3.34	4.38	3.89	147.78	15200	12386
	STDEV	38.38	0.43	2.35	1.08	53.98	5036	8239
No Strain Gage	AVG	100.49	3.12	4.50	3.85	142.38	13853	N/A
	STDEV	63.31	0.61	3.02	1.38	47.19	5489	N/A

Table 7: Averages and standard deviations for hydration test group.

		I_{xx}	c	Peak Moment	Peak Displacement	Estimated Peak Stress	Estimated Peak Strain	Peak Strain (Gage)
		(mm^4)	(mm)	(Nm)	(mm)	(MPa)	(μstrain)	(μstrain)
Immersed	AVG	114.29	3.57	6.01	6.43	223.45	26642	N/A
	STDEV	87.66	0.96	3.11	2.32	50.35	8090	N/A
Soaked Gauze	AVG	127.89	3.69	6.57	6.59	223.74	27658	N/A
	STDEV	110.28	0.90	3.84	2.40	38.41	10025	N/A

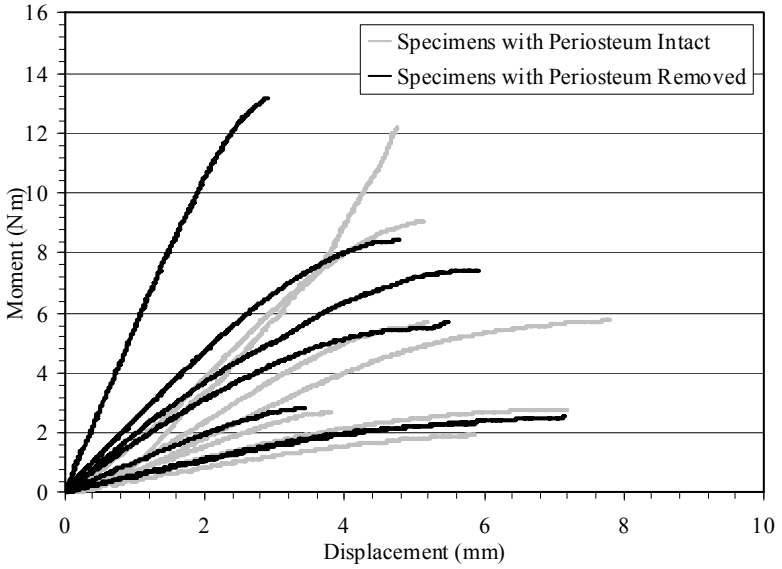

Figure 5: Moment versus displacement for periosteum vs. no periosteum matched rib tests.

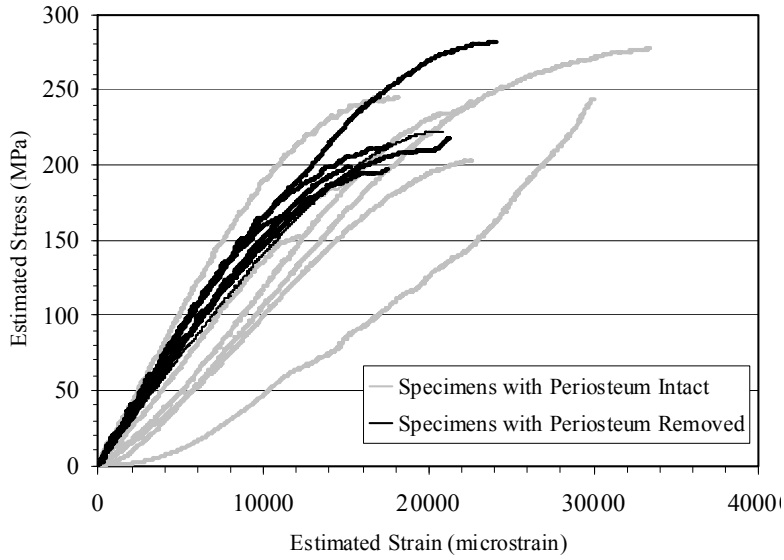

Figure 6: Estimated stress versus strain for periosteum vs. no periosteum matched rib tests.

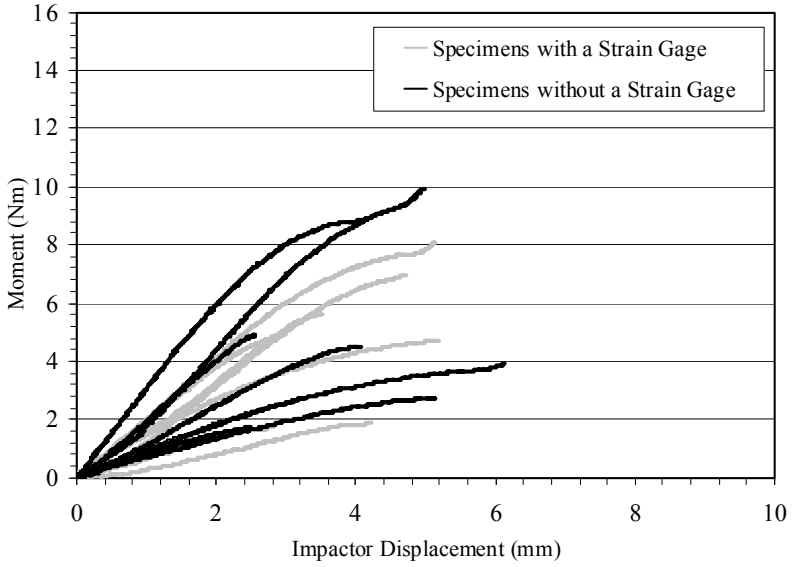

Figure 7: Moment versus displacement for strain gage vs. no strain gage matched rib tests.

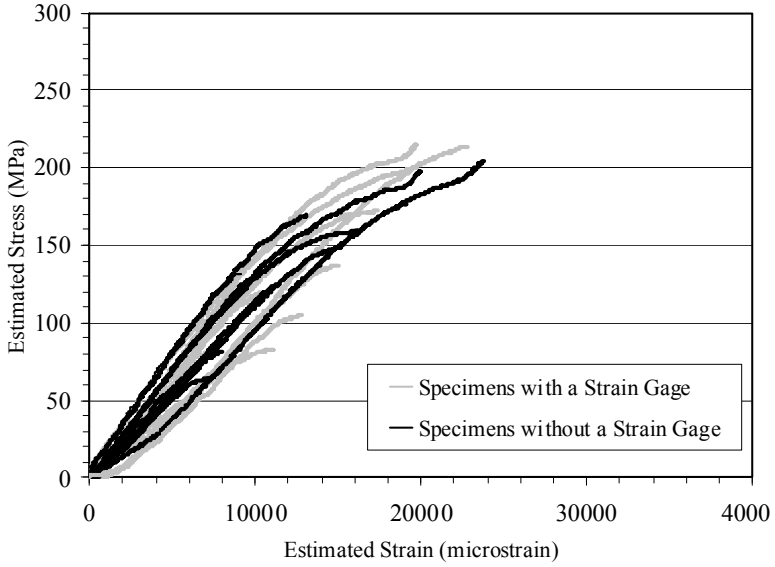

Figure 8: Estimated Stress versus strain for strain gage vs. no strain gage matched rib tests.

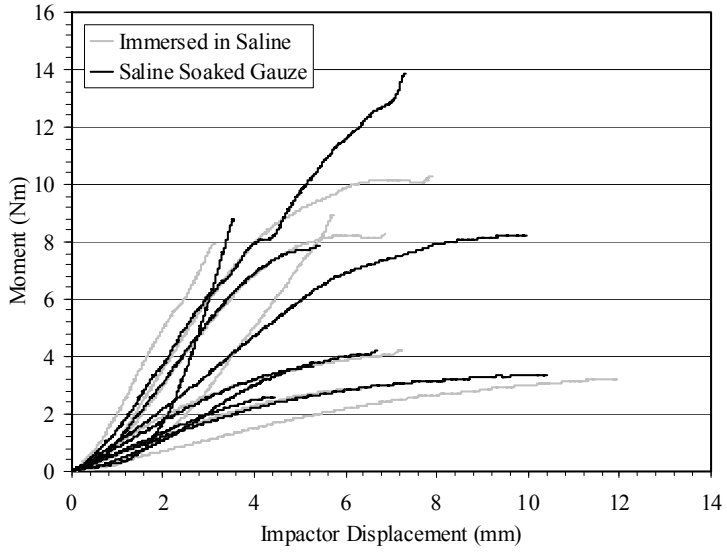

Figure 9: Moment versus displacement for soaked vs. not soaked matched rib tests.

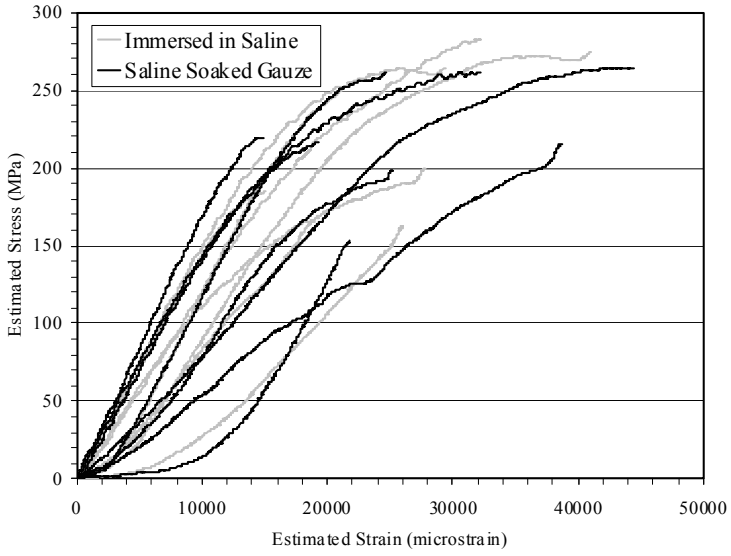

Figure 10: Estimated Stress versus strain for soaked vs. not soaked matched rib tests.

A paired Student's t-test for the means showed that there were no significant differences in the area moment of inertia, distance to the neutral axis, peak moment, peak displacement, estimated peak stress, or estimated peak strain between matched specimens in any of the three test groups (Table 8). Significance was defined as a two-tailed p-value of ≤ 0.05.

Table 8: Statistical comparison for each rib test group.

Comparison Group		I_{xx}	c	Peak Moment	Peak Displacement	Estimated Peak Stress	Estimated Peak Strain
		(mm^4)	(mm)	(Nm)	(mm)	(MPa)	(μstrain)
Periosteum vs. No Periosteum	p-value	0.60	0.29	0.14	0.13	0.42	0.15
Strain Gage vs. No Strain Gage	p-value	0.76	0.20	0.81	0.91	0.59	0.29
Immersed vs. Saline Gauze	p-value	0.35	0.42	0.45	0.75	0.98	0.62

Discussion

Although three-point bending provides the overall structural response of human rib sections, there are inherent limitations that introduce uncertainty in the calculated material properties, i.e. stress and strain. First, the linear-elastic beam equations used to calculate stress and strain do not take plasticity into account, which results in an overestimation of ultimate stress. Burstein et al. (1972) estimated that linear-elastic beam equations over predict the ultimate tensile stress by a factor of 1.56 for square cross-sections, and by a factor of 2.1 for circular cross-sections (Burstein et al., 1972). Funk et al. (2004) reported that calculating material properties based on deflection data from whole bone three-point bending under predicted the elastic modulus and

ultimate strain by approximately 40%, when compared to strain gage data, due to the presence of shear or a varying bending rigidity (EI) along the length of the bone. Second, the linear-elastic beam equations were derived for straight beam specimens. However, numerous authors have shown that the assumption of a straight beam results in negligible error in the calculated stress and strain of whole rib specimens compared to curved beam equations due to the fact that the ratio of radius of curvature to specimen height is fairly large for rib specimens (Granik and Stein, 1973; Cormier et al., 2005). Due to the limitations associated with the calculation of stress and strain from three-point bending performed on whole rib specimens, the stress and strain values reported in the current study are denoted as "estimated."

Three-point bending tests will always be limited by the need to indirectly determine stress and strain rather than measuring them directly. Some authors have attempted to determine true stress and strain values of bone samples tested in three-point bending using correction factors and post-yield shape factors (Stitzel et al., 2003; Funk et al., 2004). However, these methods must be validated with respect to the true material properties determined through tension or compression testing performed on isolated cortical bone coupons. Ultimately, the limitations of the three-point bending tests used in the current study can be ignored in regards to the comparison between test conditions because the calculated stress and strain are used primarily as a means to compare between matched specimens while controlling for cross-section geometry. However, the peak stress and strain values reported in the current study are not the true values and should be regarded with caution.

Conclusions

A total of 48 three-point bending tests were performed on 24 matched whole rib sections obtained from male human thoraces in order to determine the effects of the periosteum as well as the attachment of a strain gage. The detailed preparation and testing methods presented in this study proved to be an accurate means of preparing and testing matched rib specimens in order to directly compare the effects of the periosteum and attachment of a strain gage. The results of the study showed that there were no statistical differences in the area moment of inertia, distance to the neutral axis, peak moment, peak displacement, estimated peak stress, or estimated peak strain between matched specimens in any of the three test groups. Therefore, neither the removal of the periosteum nor the application of a strain gage has any significant effect on the structural response of human ribs in dynamic three-point bending. In addition, wrapping whole rib specimens in saline soaked gauze while placed in a plastic bag and refrigerated is a suitable method for maintaining specimen hydration during specimen storage. Finally, the peak stress and strain values reported in the current study are not the true values, given the limitations associated with the calculation of stress and strain from three-point bending, and should be regarded with caution.

CHAPTER 3

Material and Structural Properties of Human Ribs from Dynamic Tension and Bending Tests

Introduction

In automotive accidents, chest injuries rank second only to head injuries in overall number of fatalities and serious injuries (Cavanaugh, 1993). Elhagediab and Rouhana (1998) examined incidence of injuries due to frontal impacts in the National Automotive Sampling System (NASS) from 1988 to 1994, and found that chest injuries constituted 37.6% of all AIS 3+ injuries, 46.3% of all AIS 4+ injuries, and 43.3% of all AIS 5+ injuries. Kent et al. (2005a) showed that 47% of drivers over 64 years of age, 33% of drivers age 34 through 64, and 24% of drivers age 16 through 33 who died in a frontal crash sustained a fatal chest injury. Furthermore, data from the Crash Injury Research and Engineering Network (CIREN) showed that rib fractures were the most serious injury sustained by 40% of the patients over 60 who died of chest injuries from automobile collisions (Kent et al., 2005b). Similarly, previous studies using restrained cadavers in impact sled tests have frequently found rib fractures to be the most common skeletal injury (Cromack and Ziper, 1975; Patrick, 1976; Ramet and Cesari, 1979; Crandall et al., 1997; Kallieris et al., 1998).

In an effort to determine the properties of human ribs, numerous authors have performed three-point bending tests on either whole rib sections or cortical bone coupons. The majority of the literature has focused on the structural response of whole rib sections in three-point bending (Granik and Stein, 1973; Stein and Granik, 1976; Sacreste et al., 1982; Yoganandan and Pintar,

1998; Cormier et al., 2005). Sacreste et al. (1982) performed three-point bending tests on whole rib sections and used the data for the development of the bone condition factor (BCF). Stein and Granik (1976) reported that there were no significant differences in the bending strength or cross-sectional geometry between the 6th and 7th ribs. Yoganandan and Pintar (1998) reported that the mechanical behavior of the ribs was not significantly different between the 7th and 8th ribs. Cormier et al. (2005) conducted three-point bending tests on whole rib sections taken from anterior, lateral, and posterior regions, and reported significant differences in the structural response with respect to both by rib level and rib region. In addition, Yoganandan and Pintar (1998) and Cormier et al. (2005) both reported significant differences in cross-sectional geometry with respect to rib level. In order to determine the material properties of human rib cortical bone, Stitzel et al. (2003) performed dynamic three-point bending tests on small rectangular cortical bone coupons from the anterior, lateral, and posterior locations of the rib cages of four cadavers. Stitzel et al. (2003) reported that material response varied significantly with respect to both region and rib level.

Although three-point bending provides the overall structural response of human rib sections, there are inherent limitations that introduce uncertainty in the calculated material properties. First, three-point bending of whole rib sections is confounded by the irregular cross-sectional geometry and curvature of human ribs. Second, linear-elastic beam equations used by previous authors ignore the plastic behavior of bone, which results in an overestimation of ultimate stress. Burstein et al. (1972) estimated that linear-elastic beam equations over predict the ultimate tensile stress by a factor of 1.56 for square cross-sections, and by a factor of 2.1 for circular cross-sections. Funk et al. (2004) reported that calculating material properties based on

deflection data from whole bone three-point bending under predicted the elastic modulus and ultimate strain by approximately 40%, when compared to strain gage data, due to the presence of shear or a varying bending rigidity (EI) along the length of the bone.

Three-point bending tests will always be limited by the need to indirectly stress and strain, which requires assumptions and correction factors, rather than measuring them directly. Therefore, the ideal method for determining the material properties of cortical bone is tension or compression testing performed on isolated cortical bone coupons. Kemper et al. (2005) investigated the tensile material properties of 117 rib cortical bone coupons obtained from ribs 1 through 12. In contrast to the findings of Stitzel et al. (2003), Kemper et al. (2005) reported that the material properties of human rib cortical bone, specifically the modulus and ultimate stress, do not vary significantly by thoracic region or rib level.

Finite element models (FEM) of the human thorax, which allow for the calculation of physical variables mechanically related to injury, are becoming an integral tool in the reduction of thoracic injuries and improving crashworthiness (Rouhana et al., 2003; Kemper et al., 2005). Most models can provide an assessment of injury by comparing the predicted stress, typically Von Mises stress, to the injuries observed in matched post mortem human subject (PMHS) tests. As finite element models of humans become more and more refined, accounting for changes in the material properties of bone with respect to static versus dynamic loading, different bones, age, plasticity, and the effects of geometry become more critical factors. Accounting for these different parameters makes determining standard values for the material properties of human cortical bone extremely difficult, but it can have a large effect on the response of FEMs. Stitzel

et al. (2003) modified the rib cage of the THUMS FEM and found that changes in the material properties with respect to region resulted in changes in the fracture patterns. In order to investigate the effects of aging on the response of the human thorax, Kent et al. (2005) modified the angle of the ribs, the material properties of the cortical and trabecular bone, and cortical bone thickness of a commercially available finite element model of the 50th percentile male thorax (Thorax, H-Model, ESI Software S.A., Cedex, France). Kent et al. (2005b) found that that the structural and material changes played approximately equal roles in the decrease of the force deflection response of the thorax. Therefore, variations in the structural response of whole bone sections can be a result of changes in the bone geometry, bone material properties, or both.

In order to more fully understand the injury tolerance of human ribs, changes in both the structural response and the material response must be investigated. Although the literature suggests that regional differences in the structural response of ribs are most likely due to regional changes in geometry, there has been no research that directly compares the tension coupon testing to whole rib three-point bending in a controlled data set. Therefore, the purpose of this study was to conduct matched tension coupon testing and whole rib three-point bending on a controlled data set in order to determine which variables contribute to regional variation in the strength of human ribs.

Methods

This study presents 94 matched tests on human rib specimens; 46 tension coupon tests, 48 three-point bending tests. Contralateral matched specimens were dissected from anterior and lateral regions of ribs 4 through 7 of six male unembalmed frozen and thawed post mortem human

subjects ranging from 42 to 81 years of age (Table 9). Freezing was used as a means to preserve the specimens because numerous previous studies have indicated that freezing does not significantly affect the material properties of cortical bone when frozen to a temperature of -20° C (Frankel, 1960; Sedlin, 1965; Weaver, 1966; Linde and Sorensen, 1993; Griffon et al., 1995; Hamer et al., 1996).

For comparison with the standard population, the bone mineral density (BMD) of each cadaver was determined by the Osteogram technique (Hardy et al. 2001a; Stitzel et al., 2003; Kemper et al., 2005). For this technique, the left hand of each cadaver was x-rayed next to an aluminum calibration wedge. The x-ray was then processed by CompuMed Incorporated (CompuMed, Inc., Los Angeles, CA) to obtain the BMD, T-Score, and Z-score for each subject. This type of BMD measurement, however, only provides an indication of overall bone quality and does not account for local changes in bone density or composition. Therefore, the BMD obtained through this method is referred to as the "global BMD." The T-score is the number of standard deviations from the average value of healthy living individuals between 25 and 50 years of age. The Z-score is the number of standard deviations from the average value of healthy living individuals of similar age. The World Health Organization classifies normal bone as T-scores of -1.0 or greater, osteopenia as T-scores between -1.0 and -2.5, and osteoporosis as T-scores below -2.5 (Wolf and Pfleger, 2003). Global BMD for subject 6 was not obtained due to the fact that the upper limb was not available for x-ray. However, the lack of a global BMD measurement for subject 6 was not critical because a local mineral density was determined for all three-point specimens.

The three-point bending specimens, whole rib sections approximately 10 cm long, were dissected from one side of the rib cage (Figure 11). Tension coupons, isolated cortical bone milled into a dog bone shape, were taken from the opposite side of the thorax as the three-point bending specimens at corresponding anatomical locations. The methodology is presented in three parts: specimen preparation, preparation of cortical bone tension coupons and whole rib three-point bending specimens; testing configuration, detailing the MTS setup and measurement devices; and statistical analysis, the analysis of variance (ANOVA) of the material property data.

Table 9: Subject and Osteogram data for cadavers used in rib testing.

Subject ID	Gender	Age (years)	Mass (kg)	Height (cm)	Global BMD	T-score	Z-score	Cause of Death
Sm1	M	56	81.4	170.2	105.3	-0.5	0.3	lung cancer
Sm2	M	66	66.4	177.8	79.4	-2.9	-1.4	suicide
Sm3	M	45	53.2	165.1	120.1	0.9	0.9	suicide
Sm4	M	72	75.9	167.6	105.1	-0.5	1.2	septicemia
Sm5	M	42	85.9	170.2	92.1	-1.7	-1.3	cirrhosis of the liver
Sm6	M	81	86.4	182.9	N/A	N/A	N/A	fibrosis

Note: N/A = Not available

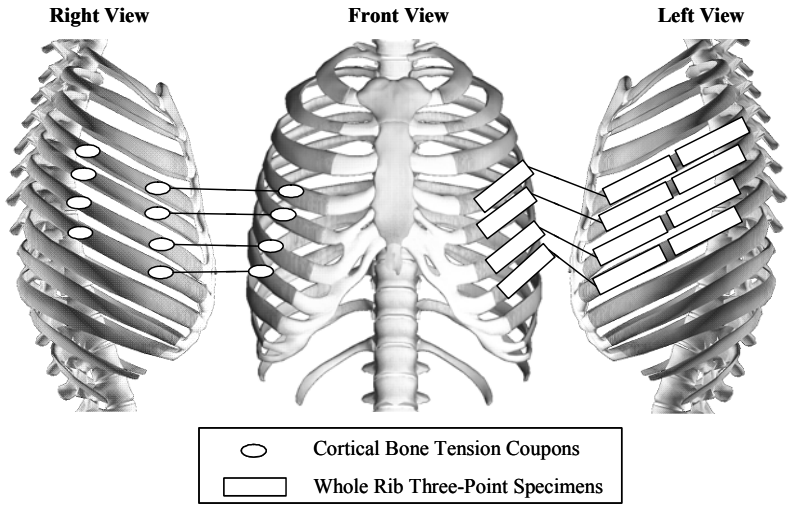

Figure 11: Locations of the matched tension and three-point bending rib specimens.
Note: anterior shown twice

Specimen Preparation

Tension Coupons

In order to create the bone coupon for tension testing, numerous steps of detailed preparation were required (Kemper et al., 2005) (Figure 12). First, an oscillating bone saw (Mopec, Inc., Standard Autopsy Saw- BD040, Detroit, MI) was used to remove the rib cage from the body as a whole. Then, sections from the anterior and lateral regions of the rib cage, approximately 10.16 cm long, were cut from ribs 4 through 7. It should be noted that anterior specimens were taken at least 10 mm from the costochondral joint. Next, a rectangular coupon was obtained from the center of the anterior and lateral rib sections. However, not all of the locations designated in Figure 11 could be obtained from each body due to curvature, insufficient size, and/or thickness. The rectangular bone coupon was prepared by first removing the tissue and periosteum from the bone surface. Then the rib section was placed in a bone chuck and mounted to a pivoting arm on the low speed diamond saw (South Bay Technology, Diamond Saw- 650, San Clemente, CA). The rib section was cut to the final length with the use of a micrometer, which controlled the position of the pivoting arm. Once the specimen was cut to the correct final length, two parallel cuts were made along the axis of the rib specimen on the external surface. The diamond saw blade was kept in a normal saline bath and was operated at a low cutting speed to minimize the heat created from friction and to provide specimen hydration. Numerous authors have reported significant differences in the material properties of dry bone compared to wet bone (Yamada, 1970; Evans, 1951; Dempster, 1952). Therefore, normal saline was sprayed directly on the bone samples to maintain proper specimen hydration at all times during preparation and testing (Reilly et al., 1974).

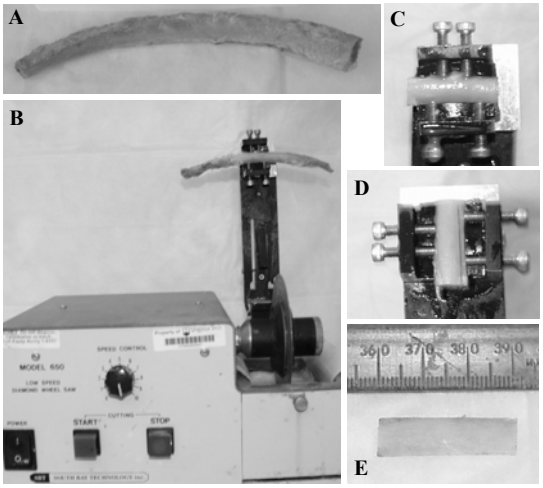

Figure 12: Method for obtaining rectangular samples of isolated rib cortical bone.

The resulting rectangular coupon of rib cortical bone was then milled using a small Computer Numerical Control (CNC) machine (MAXNC Inc., MAXNC-10, Chandler, AZ). Since the rib coupon was cut to the final specimen length and width with the low speed diamond saw, it was necessary to mill a rectangular alignment pocket in the plastic mill base in order to precisely position the rib coupon before clamping. Once the rib coupon was placed in the alignment pocket, a specially designed grip was used to clamp down the specimen for milling. The mill base was contained inside a watertight steel container mounted to the mill base. This container was filled with normal saline before the specimen was milled in order to keep the specimen cool and wet during the milling process. The mill ran a single code to cut the dog bone contour and drill the alignment pin holes in the grips with micrometer precision (Figure 13). The specimen design and dimensions were based on those used by previous researchers (Wood, 1971; Crowninshield and Pope, 1974; Yuehuei and Draughn, 2000; Kemper, 2005). Finally, each side of the dog bone specimens were manually wet sanded with 240, 320, 400, and 600 grit sandpaper and measured with calipers until a constant thickness, less than 0.0254 mm difference, was obtained throughout the entire specimen.

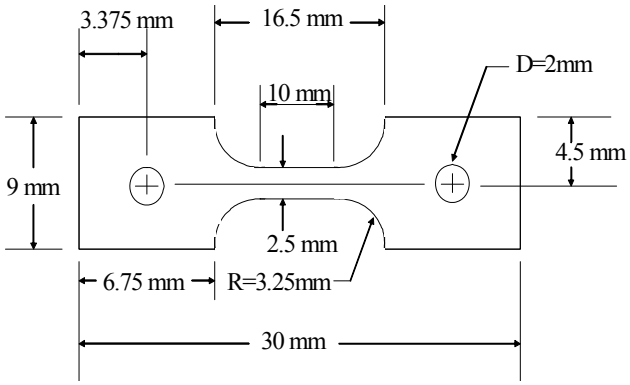

Figure 13: Rib cortical bone 'dog bone' tension specimen dimensions.

Three-Point Bending Specimens

A number of detailed steps were required to prepare the rib specimens for testing (Figure 14). First, matched anterior and lateral rib specimens from ribs 4 through 7 were dissected from one side of the thorax. The specimens were approximately 10.16 cm long. It should be noted that anterior specimens were taken at least 10 mm from the costochondral joint. The soft tissue and periosteum were removed from the anterior end of each specimen and a one inch long plastic pin was inserted through the prepped region. This was done in order to provide a rigid fixation in the potting compound. Specimens were then potted in a polyvinyl chloride (PVC) square pot filled with a two-part potting compound (US Composites, Easy-Flo 60, West Palm Beach, FL) while using a custom jig to control the specimen orientation. Potting the specimens using non-metallic materials prior to scanning ensured the Computed Tomography (CT) could be performed with no adverse affects on the imaging process. Finally, a small area was prepared for the strain gage application by removing the periosteum and soft tissue from the tension side, 41.275 mm from the center of a fiberglass pin placed through the PVC square pot to act as a pivot on the test setup. Normal saline was sprayed directly on the samples to maintain proper specimen hydration at all times during preparation and testing (Reilly et al., 1974).

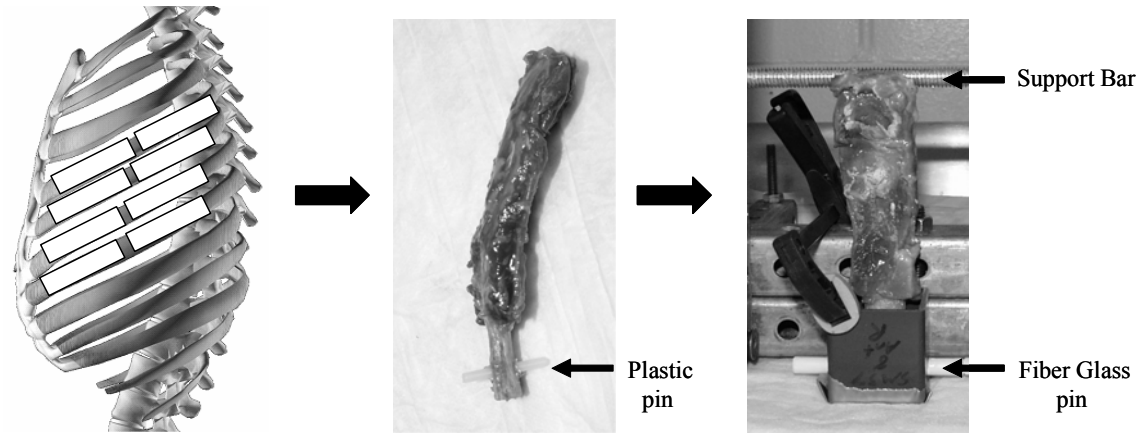

Figure 14: Three-point bending specimen procurement, preparation, and potting.

Once the specimens were potted, a microCT (Scanco Medical, VivaCT- 40, Switzerland) was used to obtain a detailed cross-sectional image, 38 micron isentropic resolution, of each specimen at the point of the impactor blade contact (Figure 15). This was done by first obtaining a scout image of the potted specimen. A cross-sectional image at the exact location of the impactor blade contact could then be obtained by performing the microCT scan 41.275 mm from the center of the fiberglass pin. Potting the specimens using non-metallic materials prior to scanning ensured that the CT slice was taken at the exact location and specimen orientation as that seen in the initial testing conditions, while having no adverse affects on the imaging process. The local mineral density was determined using the calibrated microCT software, in units of milligrams of hydroxyapatite per cubic centimeter (mg HA/ ccm), for each specimen by taking an average of all the pixels in the image (Ito, 2005; DaPont et al., 2006). The cross-sectional microCT image was then thresholded (Hounsfield unit of 300) to obtain the shape of the cortical shell. The image was converted to binary black (0) and white (1), where pixels designated as 1 represented bone. Custom Matlab © (Matworks, Inc., Matlab- R12, Natick, MA) code was then used to calculate the area moment of inertia (I_{xx})**,** the distance from the tension side to the neutral axis (c), radius of gyration (k), the cortical bone cross-sectional area, the superior cortical bone

thickness, the inferior cortical bone thickness, the external cortical bone thickness, and internal cortical bone thickness. The trabecular bone area was determined by subtracting the area of the thresholded cortical shell from the area of the non-thresholded image.

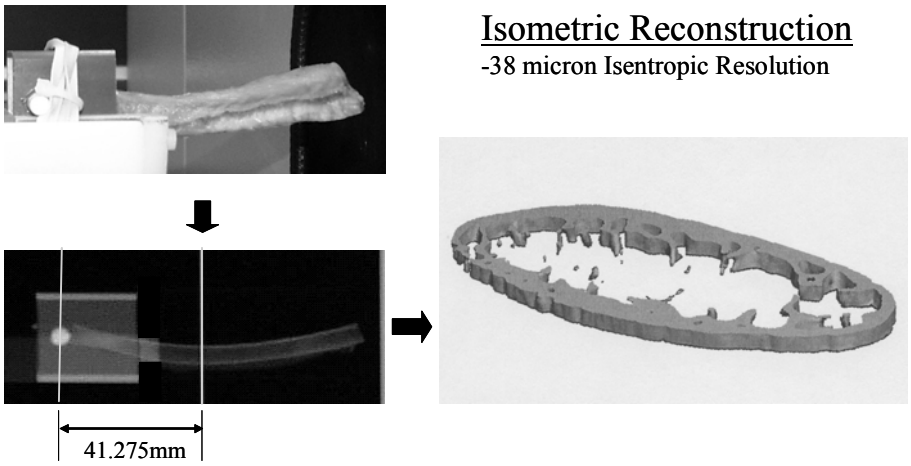

Figure 15: Cross-sectional image at the exact location of the impactor blade contact point using microCT.

The neutral axis of the image was found by first calculating the area of bone in each row. This was done by taking the sum of ones, where each "one" was a 0.038 mm x 0.038 mm pixel which represented bone, multiplied by 0.00144 to obtain the area. The area of bone in each row was multiplied by the distance that row was from an assumed neutral axis, and then summed above and below an assumed neutral axis. The neutral axis was determined to be the row where the sum above the assumed neutral axis is equal to the sum below the assumed neutral axis. The distance to the neutral axis (c) was calculated by summing the number of rows between the neutral axis and the bottom of the image, and then multiplying that sum by 0.038 to obtain the distance in millimeters. The moment of inertia (I_{xx}) about the neutral axis was found by calculating the area of bone in a row times the distance that row was from the neutral axis squared, and then adding that value up for the entire image. The radius of gyration (k) was

calculated as the square root of the ratio of the area moment of inertia to the cortical bone area. The superior and inferior cortical bone thicknesses were calculated by taking the average of the number of rows which contained a one from the edge of the image to the y neutral axis ± 15 columns (± 0.57 mm) about the x neutral axis, and then multiplying that average by 0.038 to obtain the thickness in millimeters. The external and internal cortical bone thicknesses were calculated by taking the average of the number of columns which contained a one from the edge of the image to the x neutral axis ± 15 rows (± 0.57 mm) about the y neutral axis, and then multiplying that average by 0.038 to obtain the thickness in millimeters.

Testing Configurations

Tension Coupon Testing

A high-rate servo-hydraulic Material Testing System (MTS Systems Corporation, MTS- 810, Eden Prairie, MN) machine was used with a custom designed slack adaptor and coupon grips (Figure 16). The three main sources of misalignment in a material testing setup were addressed in order to minimize variable bending stresses, which result in a reduction in both strength and ductility (Kemper et al., 2005). Since the MTS requires approximately 1 cm to accelerate to the desired velocity, a slack adaptor was designed and fabricated to allow time for the machine to reach the desired velocity before pulling the specimen into tension. In addition, this ensured that a constant strain rate was applied to the specimen rather than a range of rates as the MTS reached the target velocity. Using the MTS and the custom designed slack adapter and grips, the coupons were pulled in tension beyond the point of failure at a target rate of 0.5 strains/s. This rate corresponds to the average strain rate resulting from dynamic seat belt loading of the rib cage (Duma et al., 2005). The reaction support was instrumented with single-axis load cell (Interface,

Inc., 1210- 2,224 N, Scottsdale, Arizona). Displacement was measured with an extensometer (MTS Systems Corporation, 632.13F-20-1.5mm, Eden Prairie, MN) placed directly on the gage length of each coupon. The data was collected at 30 kHz and filtered at SAE channel filter class (CFC) 180 (SAE J211, 1995). Stress was calculated by dividing the force measurement by the cross-sectional area at the specimen gage length. Strain was determined using the Lagrangian formulation of dividing the change in length between the extensometer arms by the initial length between the extensometer gage arms. The modulus of elasticity, E, was defined as the slope between 30% and 70% of the yield point.

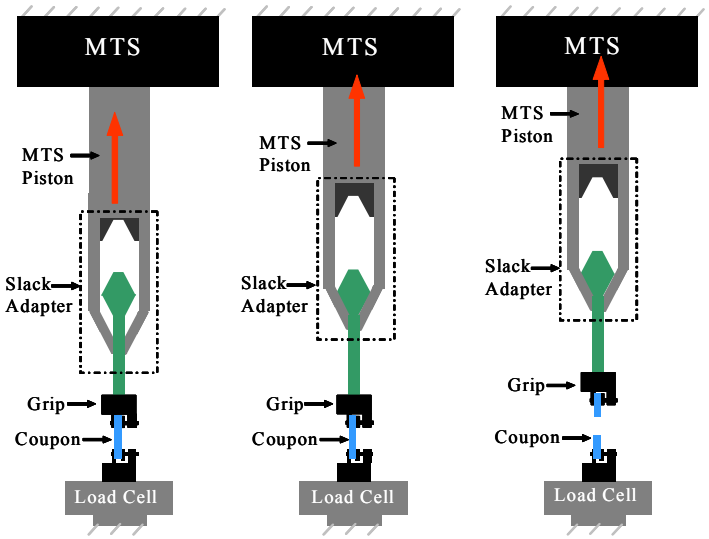

Figure 16: Illustration of the slack adaptor operation used for rib tension coupon testing.

Whole Rib Three-Point Bending

The primary component of the three-point bending test setup was a servo-hydraulic Material Testing System (MTS Systems Corporation, MTS- 810, Eden Prairie, MN) (Figure 17). The three-point bending setup was designed so that the potted specimen end was pinned and the unpotted end was simply supported. The testing span was fixed at 8.255 cm. Specimens were oriented so that the specimen was bent in the internal to external direction by the impactor blade.

This placed the external surface of the rib in tension, which would be expected when the thorax is compressed in the anterior-posterior direction. The impactor displacement rate of 17.78 cm/s yields a strain rate of approximately 0.7 s^{-1}, which is similar to that seen in a belted 35 mph automotive crash (Duma et al., 2005). The impactor and reaction support assembly were instrumented with single-axis load cells (Interface, Inc., 1210- 2,224 N, Scottsdale, Arizona). An accelerometer (Endevco Corporation- 7264B-2000G, San Juan Capistrano, CA) was attached to the impactor head to allow for inertial compensation. Strain was measured using a single-axis strain gage (Vishay Micro-Measurement, CEA-06-062UW-350, Shelton, CT), oriented with the axis of the rib, directly under the point of loading on the tensile side of the specimen.

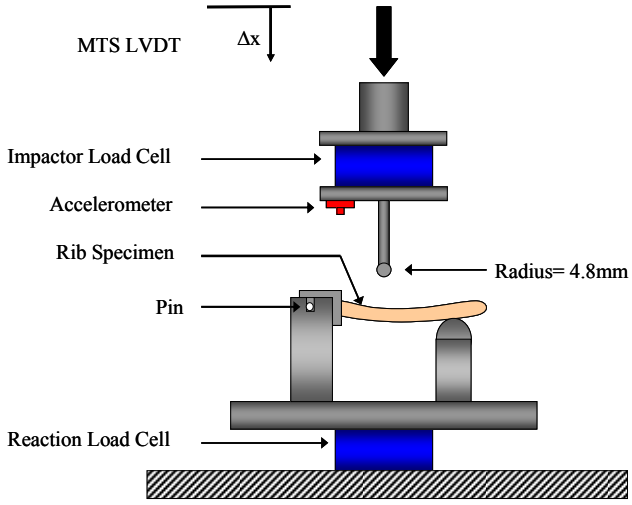

Figure 17: Rib three-point bending test setup.

All data were recorded at a sampling rate of 30 kHz (Iotech Inc., Wavebook-16, Cleveland, OH). Load cell and accelerometer data were filtered at SAE channel filter class (CFC) 180, while strain gage and impactor displacement data were not filtered (SAE J211, 1995). The moment was calculated as one half the reaction load cell, P_R, multiplied by one half of the testing span, L, (Equation 1). Bending stress, σ, was calculated assuming a linear-elastic beam equation (Equation 2), where M is the moment, c is the distance from the neutral axis, and I_{xx} is the cross

sectional area moment of inertia. The stiffness, K, was defined as the slope between two points in the elastic region of the force versus displacement curve, 30% and 70% of the yield point. The modulus of elasticity, E, was defined as the slope between two points in the elastic region of the stress versus strain curve, 30% and 70% of the yield point.

Statistical Analysis

Statistical analyses were performed on the dependent variables ultimate stress, ultimate strain, and elastic modulus by using an analysis of variance (ANOVA) and a correlation analysis. The factors age, mass, and global BMD were treated as between-subject factors and rib level and anatomical region as within-subject factors. The goal of the statistical analysis was to determine if there were any statistical differences in material and structural properties with respect to anatomical region, rib level, age, global BMD, or local mineral density. Evaluation of the data using a full model was not feasible due to the small number of cadavers. Therefore, only models with single between-subject factors and single within-subject factors were considered. Two types of statistical models were used. First, a mixed effect ANOVA was used to determine any interaction effects between the between-subject variables and the within-subject variables (Littell et al., 1996). For the tension coupons, a Satterwaithe approximation to the degrees of freedom was used to assess significance of a factor in order to account for unbalanced data (Milliken and Johnson, 1984). Age, global BMD, and gender were treated as between-subject variables, while rib level and region were treated as within-subject variables. Global BMD and age were treated as continuous rather than as factors. Second, a randomized block ANOVA, where each cadaver was treated as a block, was used to determine the significance of rib level, anatomical region, and their interaction. Finally, a Pearson Correlation Analysis for the data averaged by cadaver,

to account for repeated measured data, was used to evaluate the strength of the relationship between continuous factors (age, mass, global BMD, and local mineral density) and the dependent variables. Significance was determined by a p-value ≤ 0.05 and abs(r) ≥ 0.5.

Results

Tension Coupon Testing

The stress versus strain plots of both anterior and lateral tension coupons from each cadaver are presented in this section (Figure 18 to Figure 29). The average strain rate for all specimens was 0.6 s^{-1}. The material property values for each anterior and lateral specimen are reported (Table 10 and Table 11). There was only one location in which a specimen could not be obtained, Cadaver 1, rib 6-anterior. It should be noted that due to imperfections in the cortical bone, 5 specimens did not break within the 10 mm gage length, which is the area in which the extensometer measured the local strain. This resulted in uncertainty in the ultimate stress, ultimate strain, and strain energy density past the point of yielding for the specimens that had fractures outside of the gage length. The uncertainty in the ultimate strain was due to the fact that the local strain was not directly measured outside of the gage length. However, the modulus of elasticity is still valid for these tests under the assumption that the coupon strains evenly up to the yield point. The test specimens that had fractures outside of the grip area are designated by an asterisk (*) in the tables and plots presented in this paper. For the final analysis and averages, all data was used for the modulus of elasticity, and only the tests that failed inside the active area were used for the ultimate stress and ultimate strain values.

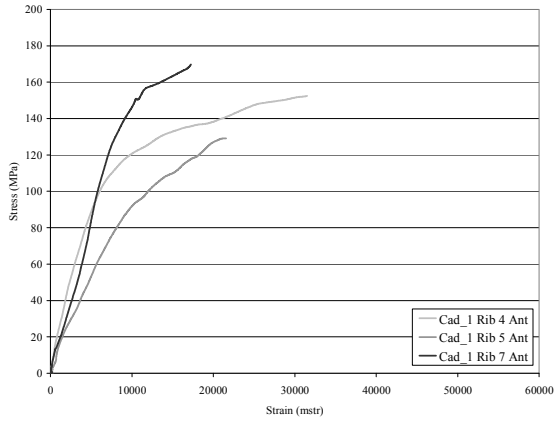

Figure 18: Sm1 anterior rib material response.

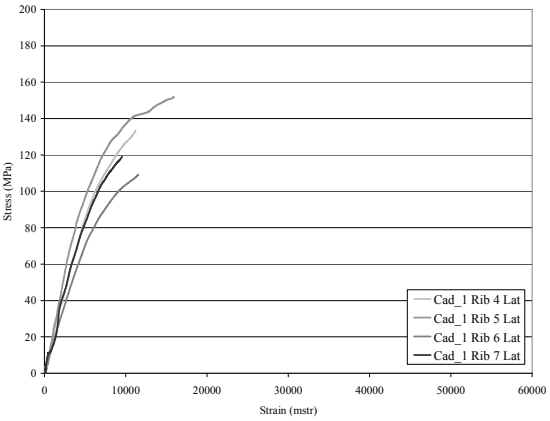

Figure 21: Sm1 lateral rib material response.

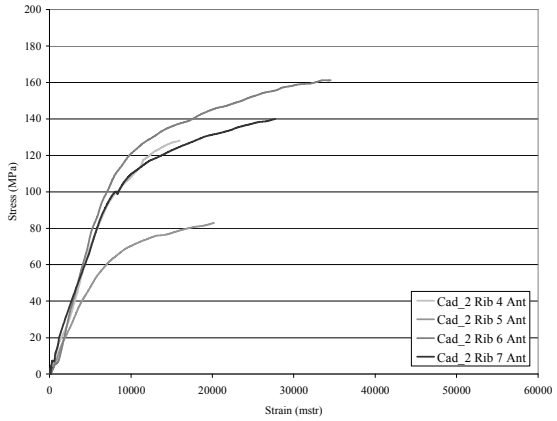

Figure 19: Sm2 anterior rib material response.

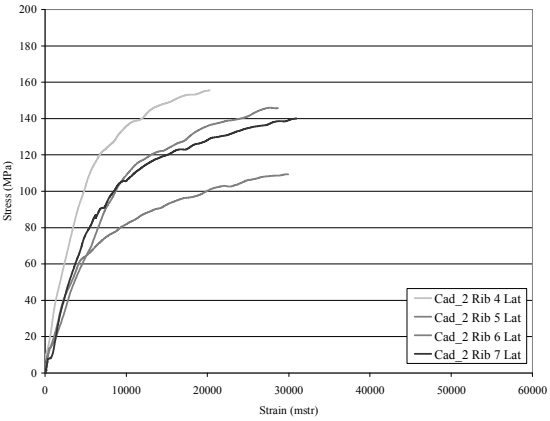

Figure 22: Sm2 lateral rib material response.

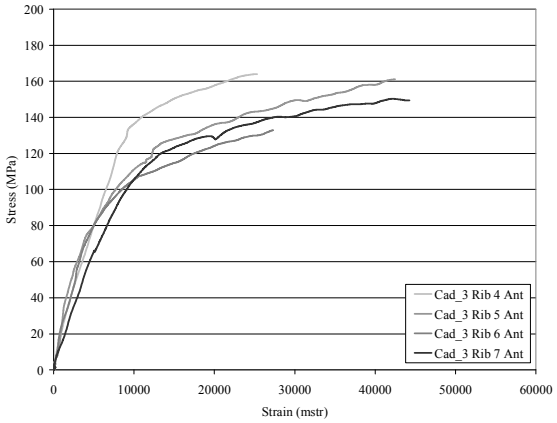

Figure 20: Sm3 anterior rib material response.

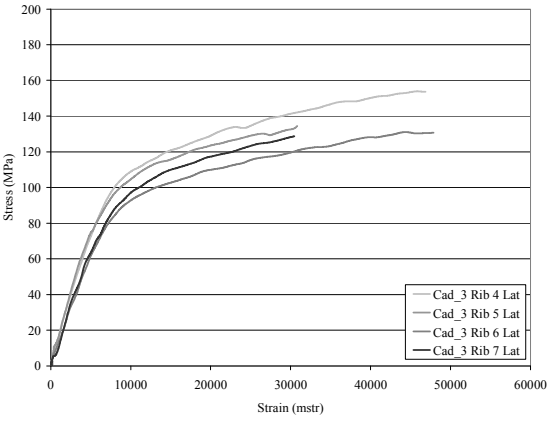

Figure 23: Sm3 lateral rib material response.

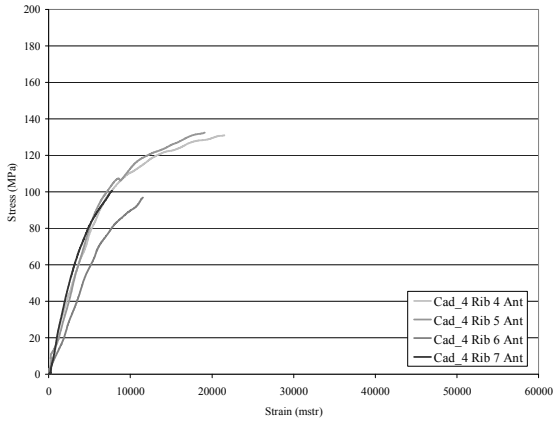

Figure 24: Sm4 anterior rib material response.

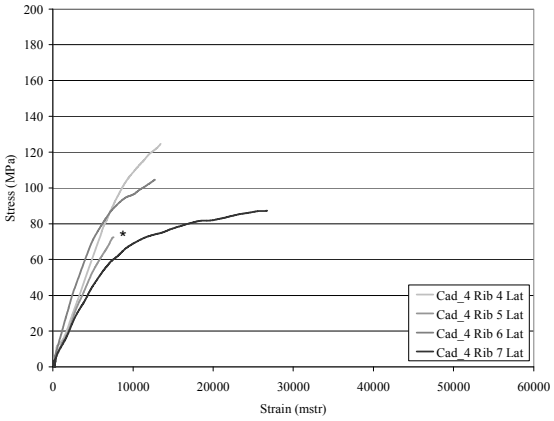

Figure 27: Sm4 lateral rib material response.

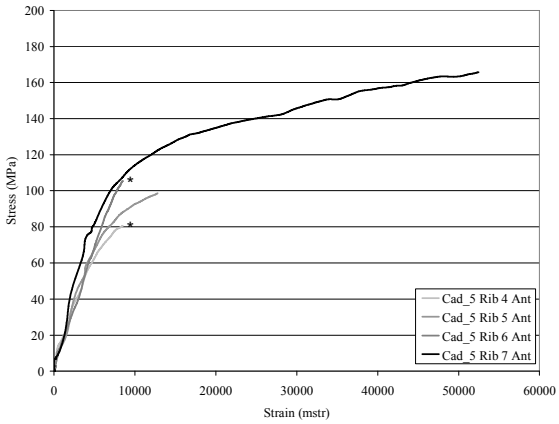

Figure 25: Sm5 anterior rib material response.

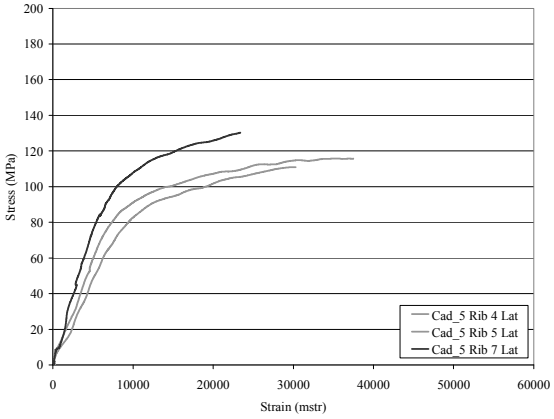

Figure 28: Sm5 lateral rib material response.

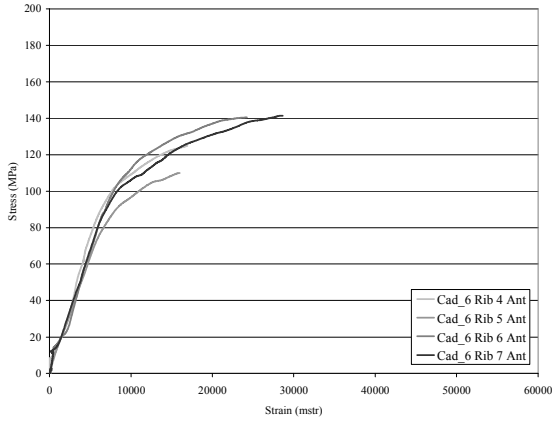

Figure 26: Sm6 anterior rib material response.

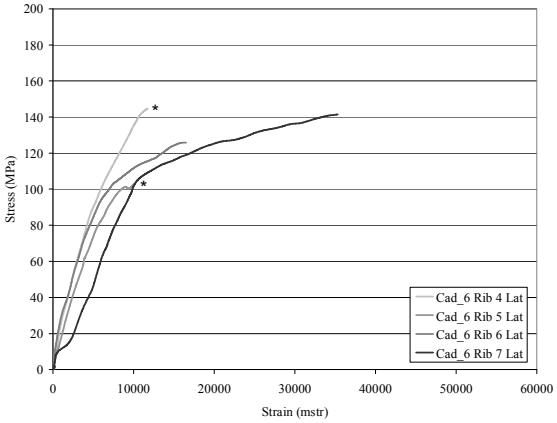

Figure 29: Sm6 lateral rib material response.

Table 10: Anterior tension coupon material property values.

Subject ID	Rib Number	Region	Ultimate Stress	Ultimate Strain	E
			MPa	μstrain	GPa
Sm1	4	Anterior	152.4	31491	16.9
Sm1	5	Anterior	129.0	21550	9.3
Sm1	7	Anterior	169.8	17255	15.6
Sm2	4	Anterior	128.1	15971	15.2
Sm2	5	Anterior	82.9	20178	9.3
Sm2	6	Anterior	161.2	34518	17.4
Sm2	7	Anterior	140.0	27750	12.5
Sm3	4	Anterior	164.0	25333	14.6
Sm3	5	Anterior	161.1	42459	18.7
Sm3	6	Anterior	132.9	27313	17.2
Sm3	7	Anterior	149.3	44285	12.6
Sm4	4	Anterior	131.0	21516	15.6
Sm4	5	Anterior	132.4	19103	16.2
Sm4	6	Anterior	96.8	11559	12.0
Sm4	7	Anterior	100.5	7790	20.5
Sm5	4	Anterior	*	*	12.3
Sm5	5	Anterior	98.7	12822	17.9
Sm5	6	Anterior	*	*	13.1
Sm5	7	Anterior	117.5	37848	11.5
Sm6	4	Anterior	124.9	16915	15.1
Sm6	5	Anterior	110.0	15984	12.3
Sm6	6	Anterior	140.6	24264	15.2
Sm6	7	Anterior	141.3	28635	13.4
Average			***131.6***	***24026***	***14.5***
Standard Deviation			***24.1***	***9942***	***2.9***

Note: * indicates that specimen broke outside the gage length

Table 11: Lateral tension coupon material property values.

Subject ID	Rib Number	Region	Ultimate Stress	Ultimate Strain	E
			MPa	μstrain	GPa
Sm1	4	Lateral	133.5	11229	16.2
Sm1	5	Lateral	151.9	15913	21.7
Sm1	6	Lateral	109.2	11540	13.5
Sm2	7	Lateral	119.6	9613	16.2
Sm2	4	Lateral	155.6	20255	21.0
Sm2	5	Lateral	145.8	28683	11.6
Sm2	6	Lateral	109.3	29921	13.4
Sm3	7	Lateral	140.0	30939	15.8
Sm3	4	Lateral	153.7	46889	13.6
Sm3	5	Lateral	134.5	30816	15.0
Sm3	6	Lateral	130.7	47865	10.5
Sm4	7	Lateral	128.7	30468	13.1
Sm4	4	Lateral	124.6	13442	12.6
Sm4	5	Lateral	*	*	10.4
Sm4	6	Lateral	104.7	12723	14.2
Sm5	7	Lateral	87.2	26768	8.3
Sm5	4	Lateral	111.0	30284	9.7
Sm5	5	Lateral	165.8	52480	15.3
Sm5	7	Lateral	130.3	23382	16.0
Sm6	4	Lateral	*	*	18.4
Sm6	5	Lateral	*	*	15.0
Sm6	6	Lateral	125.9	16532	15.9
Sm6	7	Lateral	141.4	35330	11.2
Average			***130.2***	***26253***	***14.3***
Standard Deviation			***19.6***	***12714***	***3.3***

Note: * indicates that specimen broke outside the gage length

Statistical Analysis

A mixed effect ANOVA showed that there were no statistically significant interaction effects between the between-subject variables and the within-subject variables (Table 12). A randomized block ANOVA showed that there was a significant interaction effect found for the ultimate stress between the within-subject variables. Therefore, any significance found with respect to region or rib level when evaluated independently should be regarded with caution.

Table 12: Table of interaction statistical significances for tension coupons.

Model	Interaction Effect	p-value		
		Ultimate Stress	Ultimate Strain	Modulus
1	Age * Region	0.53	0.91	0.70
1	Age * Rib Level	0.41	0.76	0.13
1	Mass * Region	0.14	0.96	0.26
1	Mass * Rib Level	0.45	0.82	0.78
1	BMD * Region	0.21	0.90	0.30
1	BMD * Rib Level	0.86	0.98	0.48
2	Region * Rib Level	0.05	0.71	0.75

Note: 1= mixed effects ANOVA; 2 = randomized block ANOVA.

Material Response by Region

The material properties were evaluated to determine if there were any significant differences with respect to anatomical region (Figure 30). A randomized block ANOVA, where each cadaver was treated as a block, was used to determine the significance of the material response with respect to anatomical region. Statistical significance was defined as a p-value less than or equal to 0.05. There were no significant differences in any material properties with respect to thoracic region.

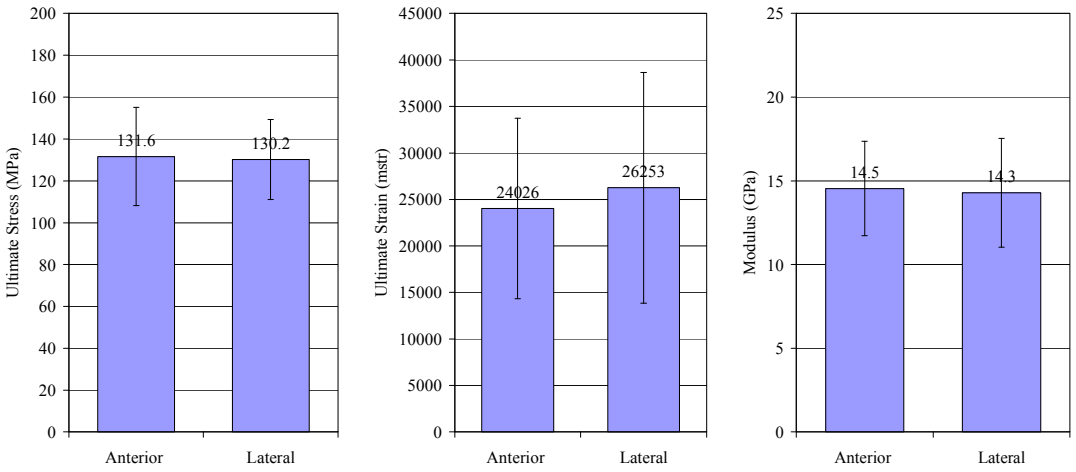

Figure 30: Average ultimate strain, ultimate stress, and modulus of anterior and lateral tension coupons.

Material Response by Rib Level

The material properties were evaluated to determine if there were any significant differences with respect to rib level (Figure 31). A randomized block ANOVA showed that there were no significance differences in the material response with respect to rib level.

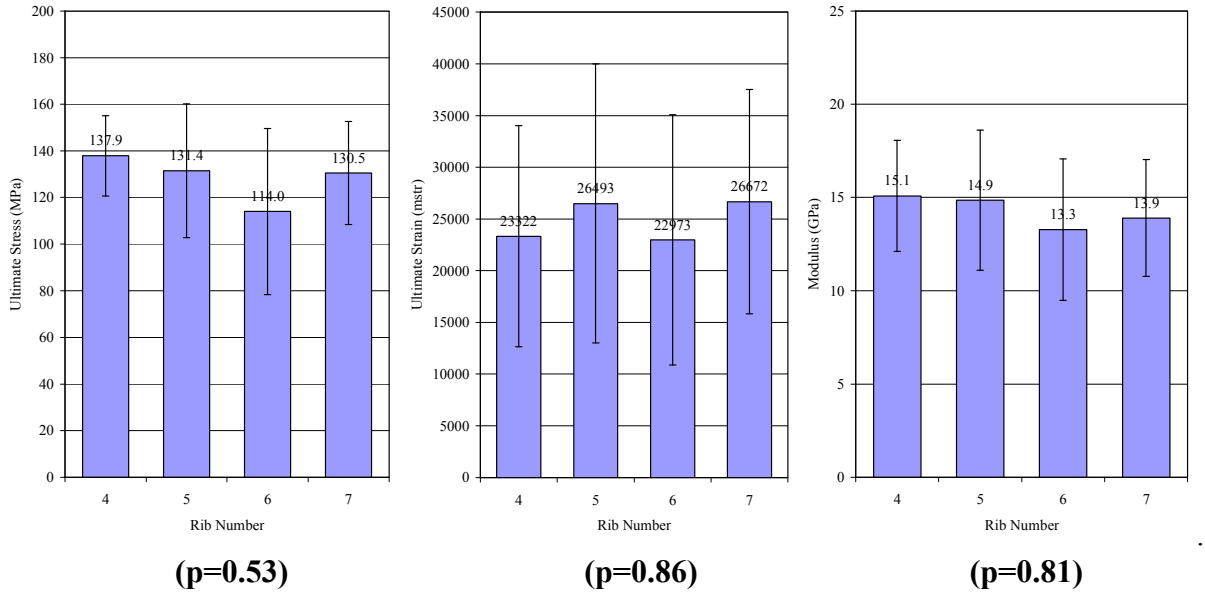

Figure 31: Average ultimate strain, ultimate stress, and modulus by rib level.

Variation between Cadavers

A Pearson Correlation analysis for the averaged data, by cadaver, was used to statistically analyze all continuous variables. However, there were no significant trends ($p \leq 0.05$, $abs(r) \geq 0.5$) found in the ultimate stress, ultimate strain, modulus or global BMD with respect to age. In addition, there were no significant trends found in the ultimate stress, ultimate strain, or modulus with respect to global BMD.

Whole Rib Three-Point Bending

The moment versus strain plots for each cadaver are presented in this section (Figure 32 to Figure 43). The average strain rate for all specimens was 0.7 s^{-1}. The structural response values for each anterior and lateral specimen are reported (Table 13 to Table 14). The peak values were defined as the point at which structural compromising occurred, i.e., the point at which further motion of the impactor produced no incremental increase of applied force (Stein and Granik 1979). The point at which the specimen became structurally compromised did not always coincide with a fracture on the tensile side.

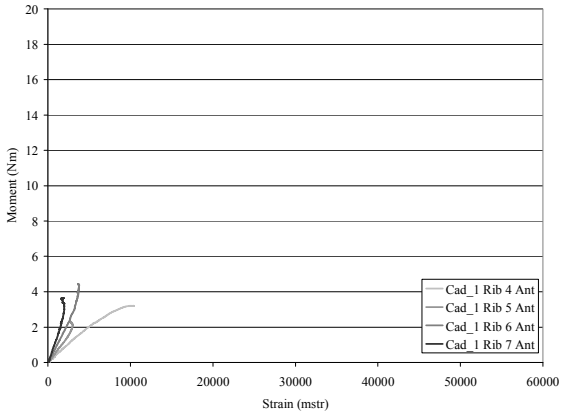

Figure 32: Sm1 anterior rib structural response.

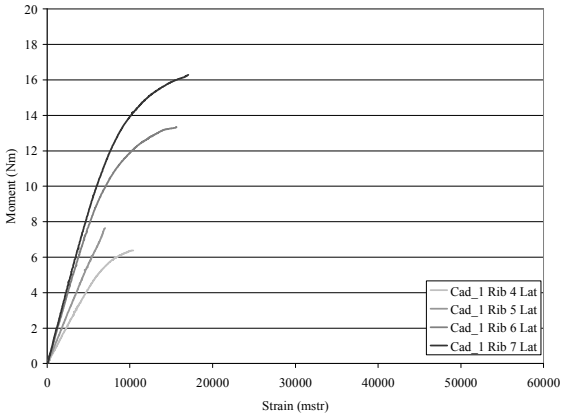

Figure 35: Sm1 lateral rib structural response.

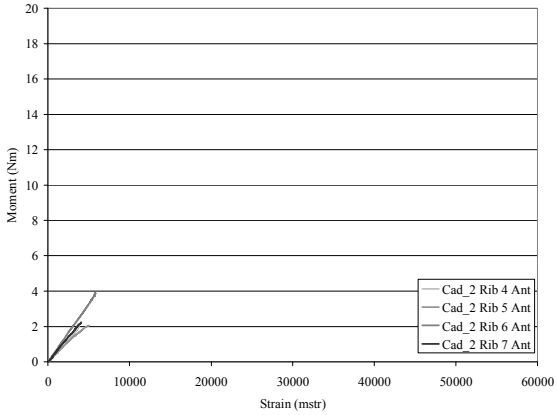

Figure 33: Sm2 anterior rib structural response.

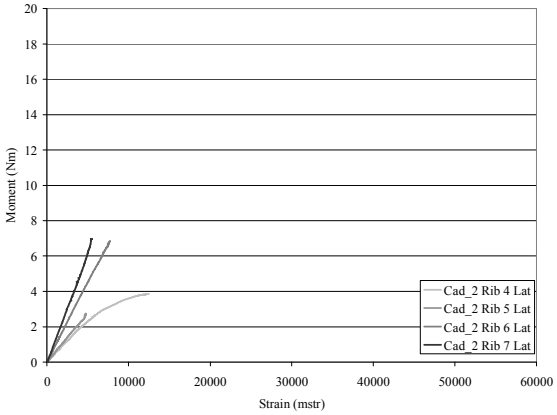

Figure 36: Sm2 lateral rib structural response.

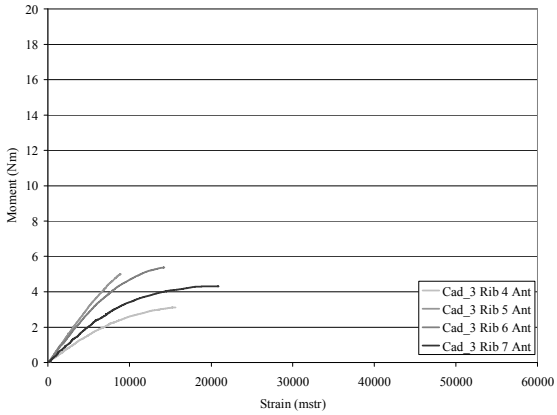

Figure 34: Sm3 anterior rib structural response.

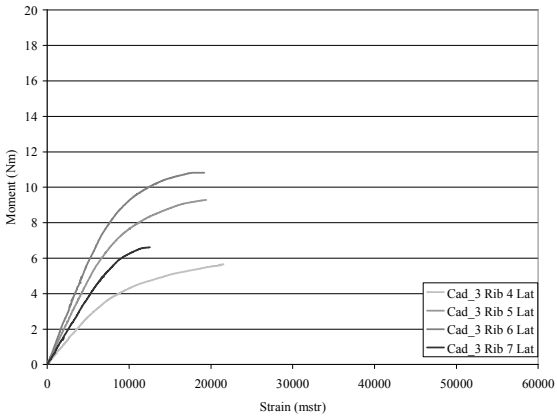

Figure 37: Sm3 lateral rib structural response.

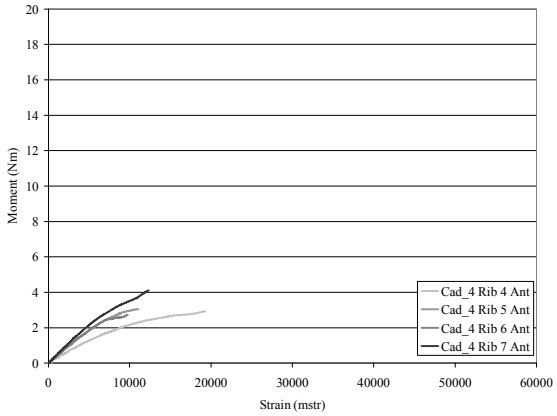

Figure 38: Sm4 anterior rib structural response.

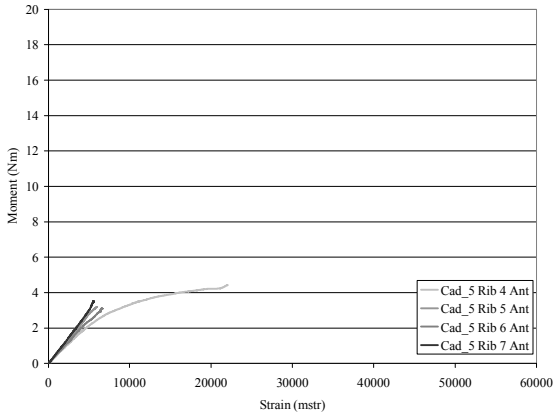

Figure 39: Sm5 anterior rib structural response.

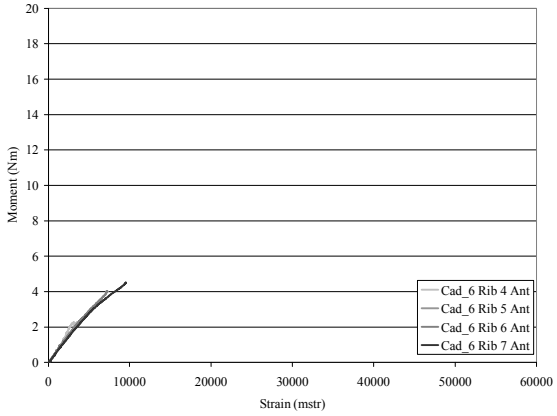

Figure 40: Sm6 anterior rib structural response.

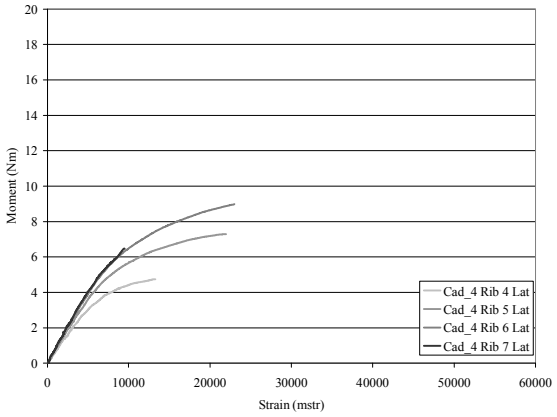

Figure 41: Sm4 lateral rib structural response.

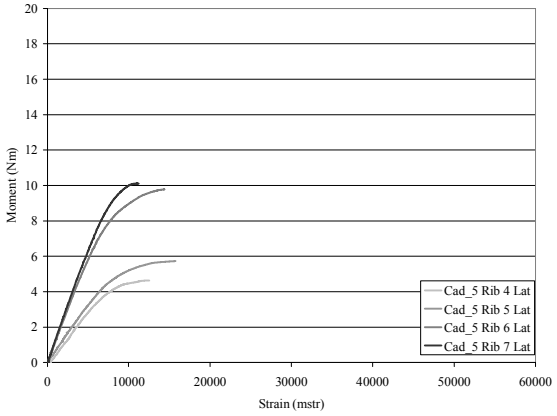

Figure 42: Sm5 lateral rib structural response.

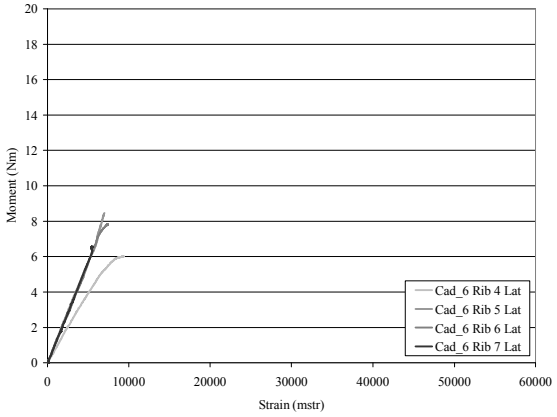

Figure 43: Sm6 lateral rib structural response.

Table 13: Anterior three-point bending specimen structural response values.

Subject ID	Rib Number	Region	Peak Force	Peak Moment	Peak Strain	Peak Stress	E	K
			N	Nm	µstrain	MPa	GPa	N/mm
Sm1	4	Anterior	155.0	3.2	10363	126.3	14.7	70.5
Sm1	5	Anterior	112.4	2.3	2649	75.1	20.2	89.5
Sm1	6	Anterior	214.8	4.4	3617	104.0	22.4	146.1
Sm1	7	Anterior	176.2	3.6	1885	74.0	29.9	130.5
Sm2	4	Anterior	102.7	2.1	3725	78.5	18.6	66.6
Sm2	5	Anterior	99.1	2.0	5048	85.2	18.6	69.8
Sm2	6	Anterior	187.8	3.9	5729	109.0	18.1	130.4
Sm2	7	Anterior	107.9	2.2	4030	67.8	16.6	99.1
Sm3	4	Anterior	151.3	3.1	15611	171.7	15.7	46.1
Sm3	5	Anterior	241.9	5.0	8904	143.6	17.5	113.6
Sm3	6	Anterior	260.3	5.4	14254	157.6	14.9	105.7
Sm3	7	Anterior	209.3	4.3	20756	199.0	16.5	72.5
Sm4	4	Anterior	141.6	2.9	19286	200.9	15.1	40.3
Sm4	5	Anterior	147.5	3.0	11067	169.4	19.7	55.5
Sm4	6	Anterior	131.8	2.7	9778	156.0	21.1	54.0
Sm4	7	Anterior	198.5	4.1	12358	171.0	17.2	79.8
Sm5	4	Anterior	214.3	4.4	22018	200.1	18.1	66.4
Sm5	5	Anterior	154.4	3.2	5998	122.5	21.3	67.6
Sm5	6	Anterior	150.4	3.1	6557	130.9	20.7	141.7
Sm5	7	Anterior	170.3	3.5	5527	109.9	18.7	85.9
Sm6	4	Anterior	114.5	2.4	3996	81.0	27.1	58.0
Sm6	5	Anterior	155.3	3.2	5722	95.1	17.2	101.0
Sm6	6	Anterior	194.8	4.0	7215	114.3	16.0	94.6
Sm6	7	Anterior	218.0	4.5	9497	147.8	18.1	144.1
Average			***167.1***	***3.4***	***8984***	***128.8***	***18.9***	***88.7***
Standard Deviation			***45.1***	***0.9***	***5777***	***42.6***	***3.6***	***32.1***

Table 14: Lateral three-point bending specimen structural response values.

Subject ID	Rib Number	Region	Peak Force	Peak Moment	Peak Strain	Peak Stress	E	K
			N	Nm	µstrain	MPa	GPa	N/mm
Sm1	4	Lateral	309.1	6.4	10407	161.9	23.1	137.6
Sm1	5	Lateral	370.3	7.6	7011	155.7	23.0	161.9
Sm1	6	Lateral	646.5	13.3	15642	198.3	22.5	328.3
Sm1	7	Lateral	787.6	16.5	17054	195.9	19.4	393.6
Sm2	4	Lateral	186.6	3.9	12476	162.6	18.4	53.5
Sm2	5	Lateral	133.7	2.8	4743	120.8	24.6	90.8
Sm2	6	Lateral	331.6	6.8	7752	149.3	19.6	191.9
Sm2	7	Lateral	337.6	7.0	5448	118.2	20.6	219.7
Sm3	4	Lateral	274.4	5.7	21544	195.5	16.9	97.7
Sm3	5	Lateral	450.3	9.3	19429	213.9	20.0	181.4
Sm3	6	Lateral	526.4	10.9	19181	200.4	19.6	236.5
Sm3	7	Lateral	320.3	6.6	12575	190.6	21.1	147.2
Sm4	4	Lateral	229.8	4.7	13283	184.6	23.3	91.4
Sm4	5	Lateral	353.0	7.3	21961	211.0	20.0	136.5
Sm4	6	Lateral	435.3	9.0	22848	223.5	18.0	175.6
Sm4	7	Lateral	313.7	6.5	9501	167.6	20.0	119.5
Sm5	4	Lateral	224.1	4.6	12532	181.2	23.4	107.5
Sm5	5	Lateral	277.4	5.7	15741	202.6	22.0	126.9
Sm5	6	Lateral	473.6	9.8	14357	219.5	25.0	215.4
Sm5	7	Lateral	490.2	10.1	11227	186.8	22.5	249.0
Sm6	4	Lateral	291.5	6.0	9435	166.3	21.0	149.0
Sm6	5	Lateral	410.6	8.5	7044	156.7	21.0	209.8
Sm6	6	Lateral	379.7	7.8	7491	149.0	21.9	206.6
Sm6	7	Lateral	318.6	6.6	5436	117.1	20.4	193.6
Average			***369.7***	***7.6***	***12671***	***176.2***	***21.1***	***175.9***
Standard Deviation			***144.8***	***3.0***	***5545***	***31.2***	***2.0***	***77.0***

Statistical Analysis

A mixed effect ANOVA showed that there were no statistically significant interaction effects found between the between-subject variables and the within-subject variables or between the within-subject variables (Table 15). A randomized block ANOVA showed that there were no interaction effects between the within-subject factors. Since there were no statistically significant interaction effects, each variable can be evaluated independently.

Table 15: Table of interaction statistical significances for three-point bending specimens.

Model	Interaction Effect	p-value			
		Peak Moment	**Peak Strain**	**Modulus**	**Stiffness**
1	Age * Region	0.44	0.85	0.95	0.39
1	Age * Rib Level	0.98	0.85	0.81	0.99
1	Mass * Region	0.21	0.70	0.92	0.28
1	Mass * Rib Level	0.36	0.76	0.86	0.17
1	BMD * Region	0.39	0.68	0.61	0.30
1	BMD * Rib Level	0.46	0.91	0.87	0.36
2	Region * Rib Level	0.09	0.07	0.92	0.21

Note: 1= mixed effects ANOVA; 2 = randomized block ANOVA.

Structural Response by Region

The structural response values were evaluated to determine if there were any significant differences with respect to anatomical region (Figure 44). A randomized block ANOVA showed that the lateral specimens had a significantly larger peak moment ($p<0.01$), peak strain ($p=0.03$), modulus ($p=0.05$), and stiffness ($p<0.01$) than the anterior specimens.

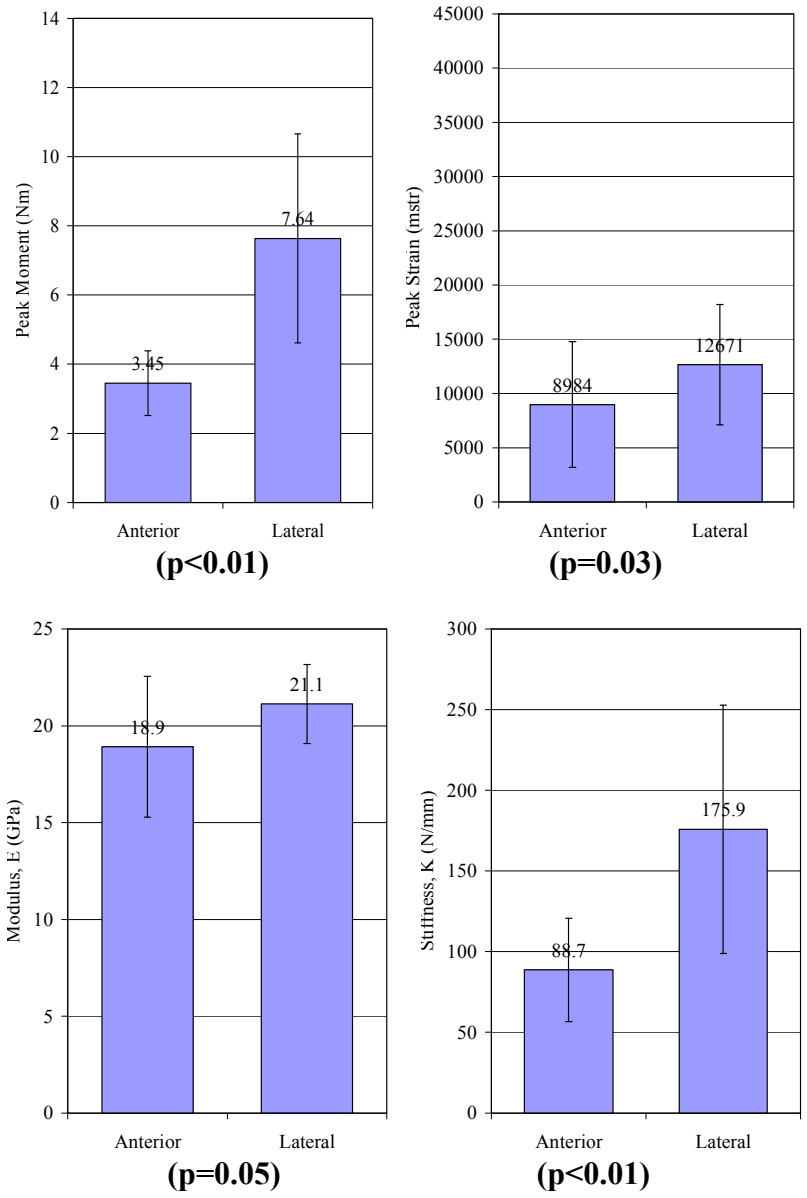

Figure 44: Average structural properties of three-point bending specimens by anatomical region.

Geometry by Region

The geometric values were evaluated to determine if there were any significant differences with respect to rib level (Figure 45 to Figure 47). A randomized block ANOVA showed that there were significant differences ($p<0.05$) in the cross-sectional geometry of the anterior specimens versus the lateral specimens. Specifically, anterior specimens were found to have significantly: smaller distance to the neutral axis ($p<0.01$), smaller area moment of inertia ($p<0.01$), larger ratio of distance to the neutral axis to area moment of inertia ($p<0.01$), smaller cortical bone cross-sectional area ($p<0.01$), and smaller radius of gyration ($p<0.01$) (Figure 46). The cortical bone thickness of anterior specimens was found to be significantly less than lateral specimens at the internal ($p<0.01$), superior ($p=0.03$), and inferior ($p<0.01$) (Figure 47). Although there were significant differences in the local mineral density ($p=0.01$) between the anterior and the lateral specimens, the difference was very small (Figure 48). The geometric property values for each anterior and lateral specimen are reported (Table 16 to Table 19).

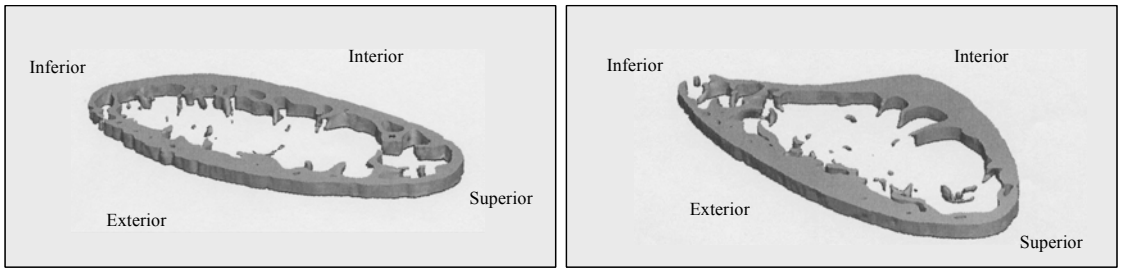

Figure 45: Isometric reconstruction for matched anterior (left) versus lateral (right) specimens.

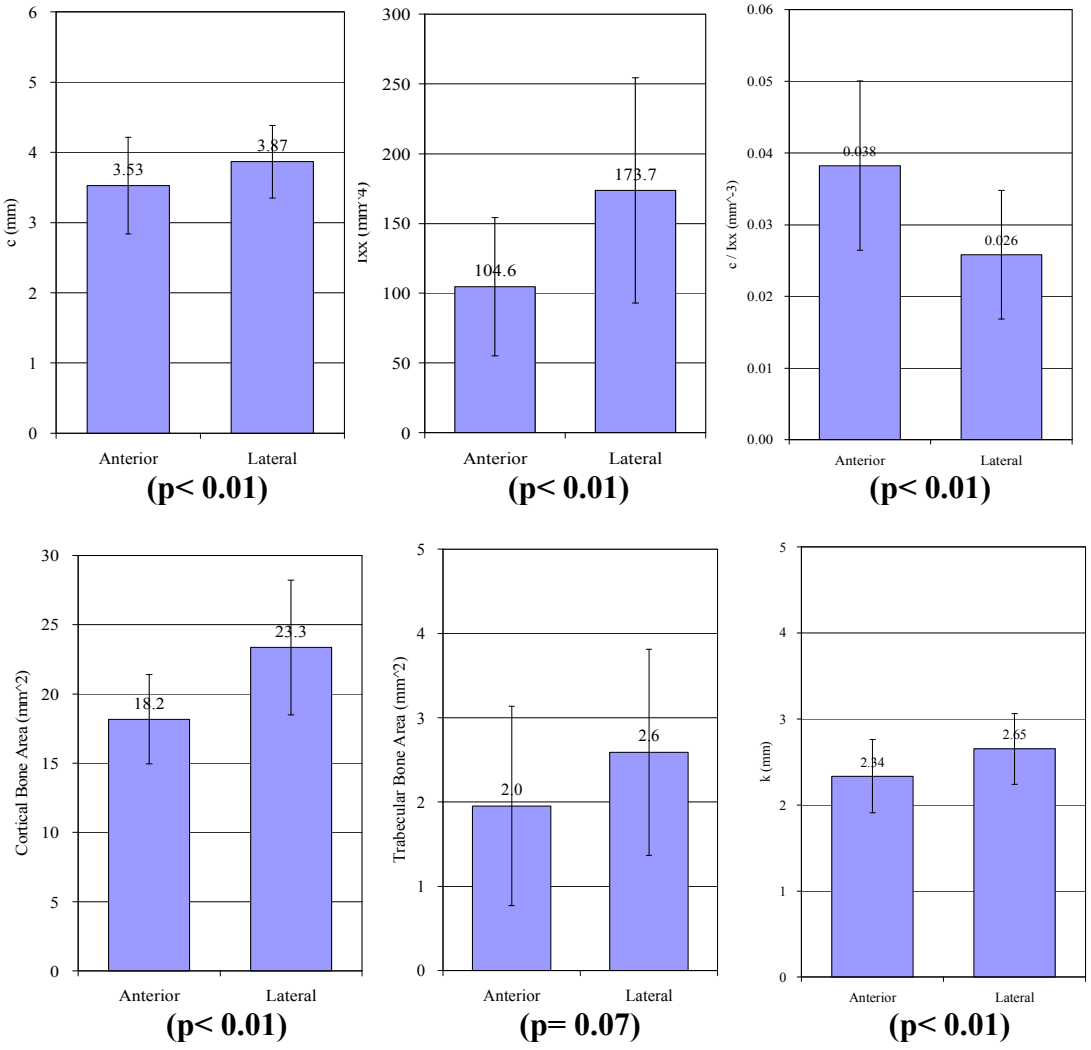

Figure 46: Geometric properties by anatomical region.

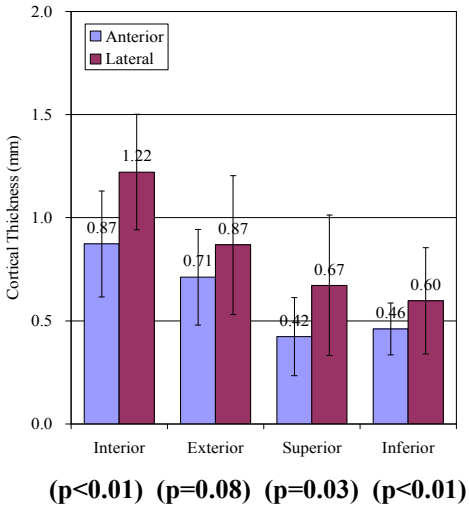

Figure 47: Cortical bone thickness by region.

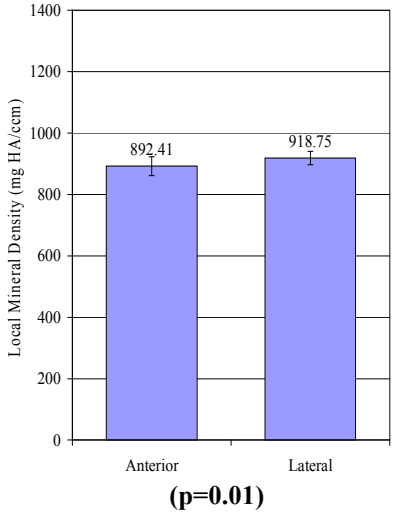

Figure 48: Local mineral density by region.

Table 16: Anterior three-point bending specimen geometric property values.

Subject ID	Rib Number	Region	Local Mineral Density	Ixx	c	Cortical Area	Trabecular Area	k
			(mg HA/ ccm)	(mm^4)	(mm)	(mm^2)	(mm^2)	(mm)
Sm1	4	Anterior	895.38	88.5	3.50	16.3	2.6	2.33
Sm1	5	Anterior	913.71	119.6	3.88	17.3	0.5	2.63
Sm1	6	Anterior	951.88	221.9	5.21	19.8	2.3	3.35
Sm1	7	Anterior	928.38	240.9	4.90	21.6	1.3	3.34
Sm2	4	Anterior	873.53	94.4	3.50	17.4	1.1	2.33
Sm2	5	Anterior	851.46	82.1	3.42	16.4	1.3	2.24
Sm2	6	Anterior	875.40	144.7	4.07	21.3	1.8	2.60
Sm2	7	Anterior	874.32	126.0	3.84	17.6	1.6	2.68
Sm3	4	Anterior	890.21	41.5	2.28	17.3	1.5	1.55
Sm3	5	Anterior	902.64	112.3	3.23	23.4	1.5	2.19
Sm3	6	Anterior	895.53	111.4	3.27	21.1	2.9	2.30
Sm3	7	Anterior	923.42	68.5	3.15	17.4	1.7	1.98
Sm4	4	Anterior	875.61	34.8	2.39	13.7	3.2	1.60
Sm4	5	Anterior	929.96	49.9	2.77	15.0	2.2	1.82
Sm4	6	Anterior	890.64	59.0	3.38	13.1	3.4	2.12
Sm4	7	Anterior	887.33	81.9	3.42	16.1	3.3	2.26
Sm5	4	Anterior	797.25	65.5	2.96	12.2	5.6	2.31
Sm5	5	Anterior	863.03	79.1	3.04	17.3	1.6	2.14
Sm5	6	Anterior	882.29	92.8	3.91	15.0	0.0	2.48
Sm5	7	Anterior	893.87	108.1	3.38	20.2	1.6	2.31
Sm6	4	Anterior	899.19	94.2	3.23	19.9	0.3	2.17
Sm6	5	Anterior	916.88	152.4	4.52	20.3	2.5	2.74
Sm6	6	Anterior	911.63	123.0	3.50	23.2	1.5	2.30
Sm6	7	Anterior	894.38	119.1	3.91	23.1	1.4	2.27
Average			***892.41***	***104.6***	***3.53***	***18.2***	***2.0***	***2.34***
Standard Deviation			***30.78***	***49.6***	***0.69***	***3.2***	***1.2***	***0.43***

Table 17: Lateral three-point bending specimen geometric property values.

Subject ID	Rib Number	Region	Local Mineral Density	Ixx	c	Cortical Area	Trabecular Area	k
			(mg HA/ ccm)	(mm^4)	(mm)	(mm^2)	(mm^2)	(mm)
Sm1	4	Lateral	955.77	143.7	3.65	20.0	2.2	2.68
Sm1	5	Lateral	952.89	207.1	4.22	21.5	2.4	3.10
Sm1	6	Lateral	937.87	298.7	4.48	28.9	1.5	3.22
Sm1	7	Lateral	944.34	406.6	4.90	35.9	2.0	3.36
Sm2	4	Lateral	868.64	81.9	3.46	21.7	0.8	1.94
Sm2	5	Lateral	902.86	86.8	3.80	16.4	1.9	2.30
Sm2	6	Lateral	909.40	191.5	4.18	23.0	1.9	2.88
Sm2	7	Lateral	909.83	257.5	4.37	22.3	1.6	3.40
Sm3	4	Lateral	917.60	84.9	2.93	19.7	2.8	2.08
Sm3	5	Lateral	912.85	171.6	3.95	25.8	2.5	2.58
Sm3	6	Lateral	915.00	224.4	4.14	26.7	3.3	2.90
Sm3	7	Lateral	889.06	123.9	3.57	24.4	2.1	2.25
Sm4	4	Lateral	914.43	78.1	3.04	16.8	4.2	2.16
Sm4	5	Lateral	908.47	111.5	3.23	20.8	5.3	2.32
Sm4	6	Lateral	918.82	128.2	3.19	27.1	4.8	2.18
Sm4	7	Lateral	875.47	143.9	3.72	20.0	5.7	2.68
Sm5	4	Lateral	928.96	89.3	3.50	15.5	2.3	2.40
Sm5	5	Lateral	939.02	99.9	3.53	16.5	1.8	2.46
Sm5	6	Lateral	921.69	196.3	4.41	27.1	1.8	2.69
Sm5	7	Lateral	912.35	238.7	4.41	26.9	2.2	2.98
Sm6	4	Lateral	936.93	138.8	3.84	23.2	2.2	2.45
Sm6	5	Lateral	928.81	221.9	4.10	24.5	2.4	3.01
Sm6	6	Lateral	934.06	237.8	4.52	26.4	2.5	3.00
Sm6	7	Lateral	914.79	204.9	3.65	29.2	2.0	2.65
Average			***918.75***	***173.7***	***3.87***	***23.3***	***2.6***	***2.65***
Standard Deviation			***21.53***	***80.8***	***0.52***	***4.9***	***1.2***	***0.41***

Table 18: Anterior three-point bending specimen cortical bone thickness values.

Subject ID	Rib Number	Region	Internal Thickness	External Thickness	Superior Thickness	Inferior Thickness
			(mm)	(mm)	(mm)	(mm)
Sm1	4	Anterior	0.66	0.45	0.44	0.53
Sm1	5	Anterior	0.94	0.44	0.43	0.37
Sm1	6	Anterior	1.04	0.79	0.43	0.53
Sm1	7	Anterior	1.09	0.77	0.37	0.54
Sm2	4	Anterior	0.65	0.63	0.36	0.50
Sm2	5	Anterior	0.70	0.47	0.40	0.33
Sm2	6	Anterior	1.35	0.63	0.16	0.19
Sm2	7	Anterior	0.87	0.75	0.17	0.27
Sm3	4	Anterior	0.72	1.00	0.53	0.49
Sm3	5	Anterior	1.23	0.86	0.59	0.58
Sm3	6	Anterior	1.15	1.13	0.18	0.48
Sm3	7	Anterior	0.92	1.05	0.59	0.44
Sm4	4	Anterior	0.49	0.45	0.90	0.55
Sm4	5	Anterior	0.76	0.58	0.61	0.54
Sm4	6	Anterior	0.74	0.47	0.53	0.48
Sm4	7	Anterior	0.78	0.86	0.43	0.71
Sm5	4	Anterior	0.34	0.40	0.07	0.20
Sm5	5	Anterior	0.97	0.62	0.38	0.42
Sm5	6	Anterior	0.96	0.60	0.22	0.55
Sm5	7	Anterior	1.09	1.13	0.25	0.30
Sm6	4	Anterior	0.43	0.64	0.43	0.47
Sm6	5	Anterior	0.84	0.74	0.68	0.58
Sm6	6	Anterior	1.15	0.54	0.57	0.50
Sm6	7	Anterior	1.09	1.07	0.43	0.48
Average			***0.87***	***0.71***	***0.42***	***0.46***
Standard Deviation			***0.26***	***0.23***	***0.19***	***0.13***

Table 19: Lateral three-point bending specimen cortical bone thickness values.

Subject ID	Rib Number	Region	Internal Thickness	External Thickness	Superior Thickness	Inferior Thickness
			(mm)	(mm)	(mm)	(mm)
Sm1	4	Lateral	1.12	0.56	0.58	0.80
Sm1	5	Lateral	1.26	0.74	0.38	0.77
Sm1	6	Lateral	1.44	1.43	0.62	0.73
Sm1	7	Lateral	1.83	1.20	0.63	0.68
Sm2	4	Lateral	0.82	1.22	1.92	0.88
Sm2	5	Lateral	0.90	0.42	0.57	0.51
Sm2	6	Lateral	1.28	0.59	0.49	0.33
Sm2	7	Lateral	1.26	1.04	0.39	0.22
Sm3	4	Lateral	1.13	0.72	0.48	0.73
Sm3	5	Lateral	1.50	0.80	0.87	0.68
Sm3	6	Lateral	1.44	0.97	0.54	0.70
Sm3	7	Lateral	1.00	0.91	1.04	0.42
Sm4	4	Lateral	0.99	0.52	0.93	0.48
Sm4	5	Lateral	0.89	0.68	0.93	0.46
Sm4	6	Lateral	1.21	0.66	0.94	1.46
Sm4	7	Lateral	1.18	0.71	0.35	0.32
Sm5	4	Lateral	0.79	0.53	0.58	0.47
Sm5	5	Lateral	0.82	0.91	0.43	0.56
Sm5	6	Lateral	1.11	1.75	0.30	0.80
Sm5	7	Lateral	1.70	1.38	0.53	0.63
Sm6	4	Lateral	1.44	0.73	0.96	0.44
Sm6	5	Lateral	1.53	0.67	0.61	0.43
Sm6	6	Lateral	1.34	0.57	0.57	0.30
Sm6	7	Lateral	1.37	1.13	0.51	0.51
Average			***1.22***	***0.87***	***0.67***	***0.60***
Standard Deviation			***0.28***	***0.34***	***0.34***	***0.26***

Structural Response by Rib Level

The structural responses of anterior and lateral specimens were evaluated independently to determine if there were any significant differences with respect to rib level (Figure 49). A randomized block ANOVA showed that both peak moment and peak strain were found to be significant with respect to rib level. The peak moment was found to be significant with respect to rib level for lateral specimens (p=0.02) but not anterior specimens (p=0.20). The peak strain was only found to be significant with respect to rib level for anterior specimens (p=0.05). The stiffness was found to be significant with respect to rib level for anterior specimens (p<0.01) and lateral specimens (p<0.01). The modulus (Ant p=0.93, Lat p=0.81) was not found to be significant with respect to rib level.

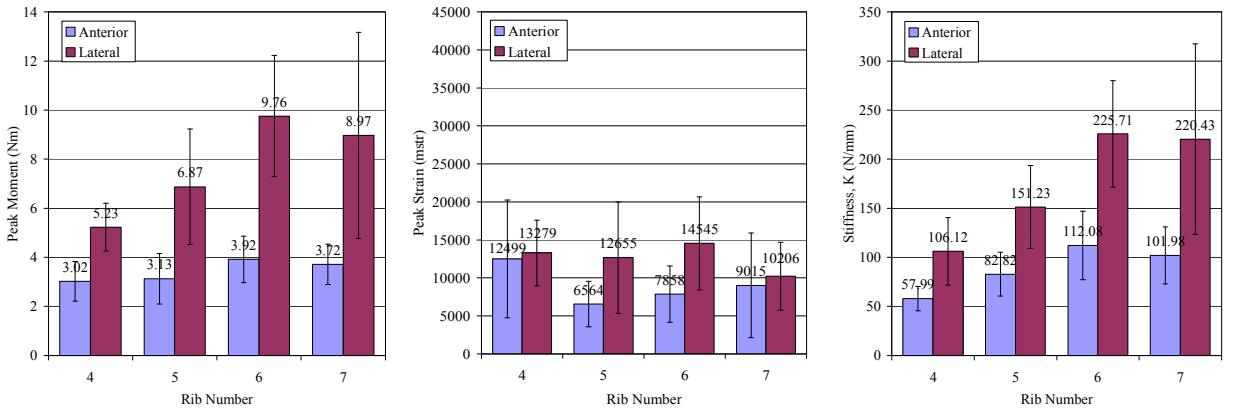

(Ant p=0.20, Lat p=0.02) **(Ant p= 0.05, Lat p=0.15)** **(Ant p< 0.01, Lat p<0.01)**

Figure 49: Average peak moment, peak strain, and stiffness of three-point bending specimens by rib level.

Geometry by Rib Level

The geometric values of anterior and lateral specimens were evaluated independently to determine if there were any significant differences with respect to rib level (Figure 50 to Figure 51). A randomized block ANOVA showed that there were significant differences in the cross-sectional geometry for both anterior and lateral specimens with respect to rib level. The internal and external cortical bone thickness were found to vary significantly with respect to rib level for anterior specimens ($p<0.01$), but not for lateral specimens (Figure 50). For anterior specimens, the distance to the neutral axis ($p<0.01$), the ratio of distance to the neutral axis to area moment of inertia ($p=0.02$), and the radius of gyration ($p=0.04$) were found to be significant with respect to rib level (Figure 51). For lateral specimens, the distance to the neutral axis ($p<0.01$), the area moment of inertia ($p<0.01$), the ratio of distance to the neutral axis to area moment of inertia ($p<0.01$), the cross sectional cortical bone area ($p<0.01$), and the radius of gyration ($p=0.03$) were found to be significant with respect to rib level (Figure 51).

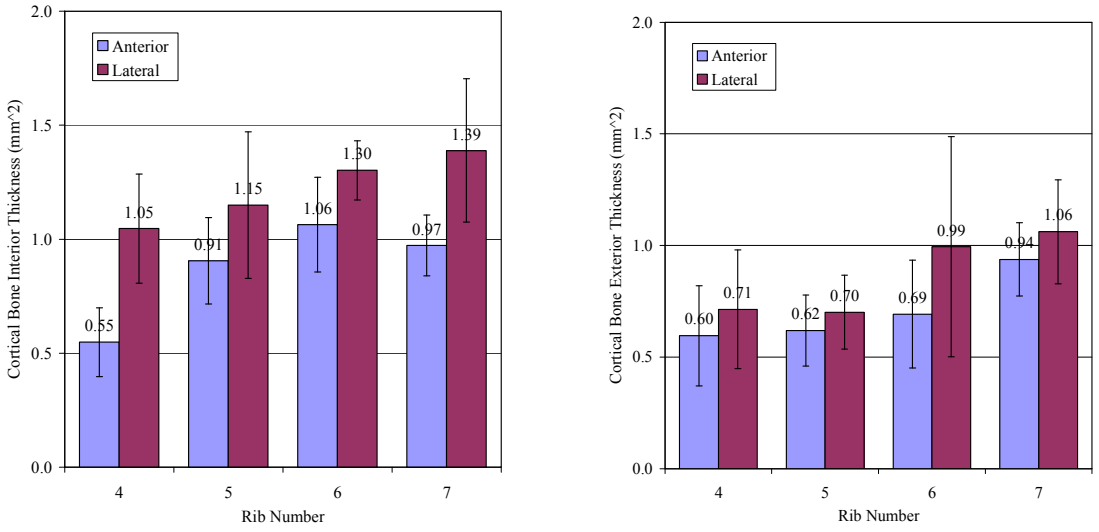

(Ant p< 0.01, Lat p= 0.16) **(Ant p< 0.01, Lat p=0.15)**

Figure 50: Cortical bone thickness by rib level.

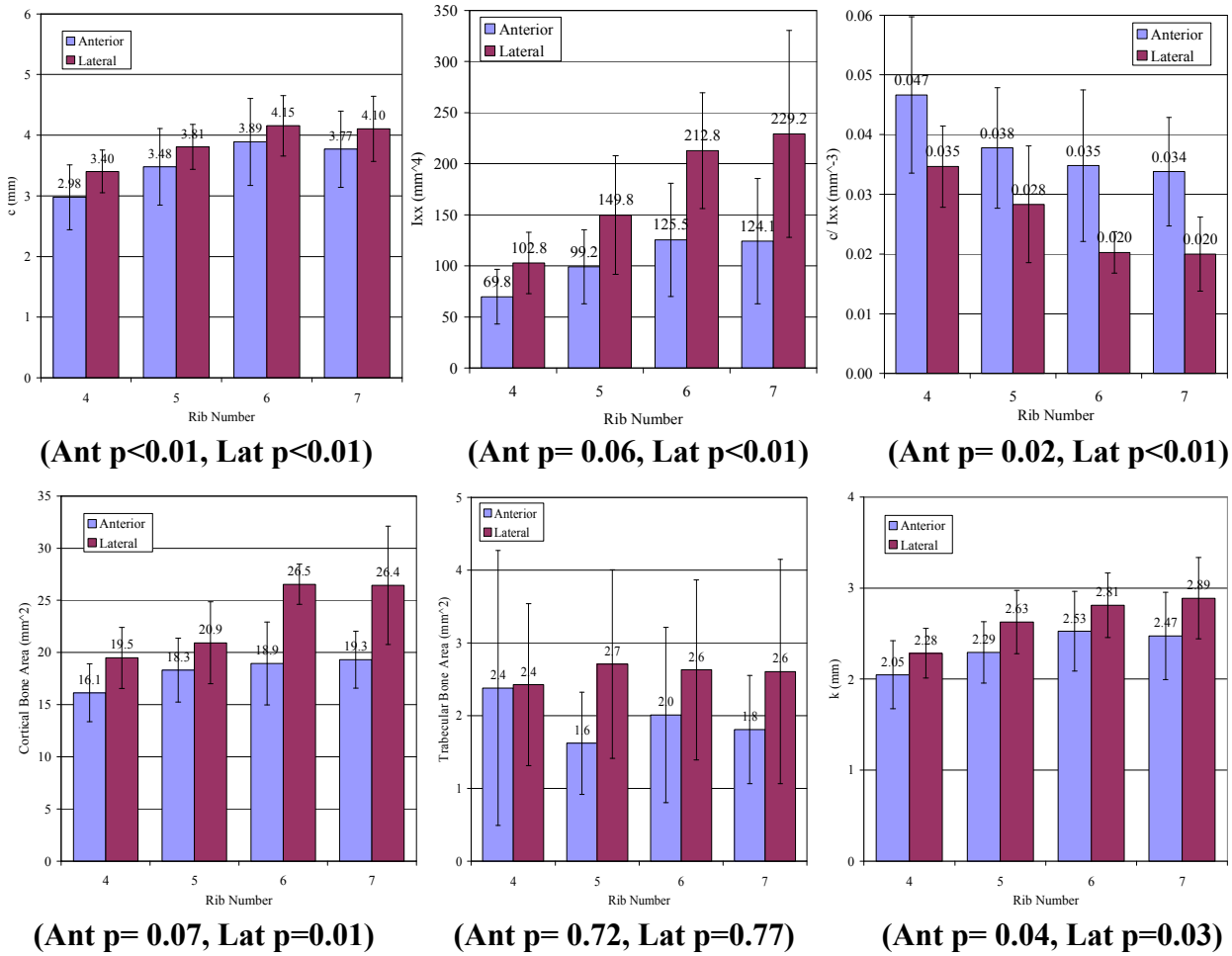

Figure 51: Geometric properties by rib level.

Variation between Cadavers

A Pearson Correlation analysis for the averaged data, by cadaver, was used to statistically analyze all continuous variables. However, there were no significant trends ($p \leq 0.05$, $abs(r) \geq 0.5$) found in the peak moment, peak strain, modulus, global BMD, or local mineral density with respect to age. There were no significant trends found in the peak moment, peak strain, or modulus with respect to global BMD. In addition, there was not a significant correlation between the local mineral density averaged by cadaver and the global BMD ($p = 0.30$, $r = 0.58$).

Discussion

This study describes the regional variation in material, structural, and geometrical properties of two regions in the thorax of six human subjects. This was done by performing 94 matched tests on human rib specimens; 46 tension coupon tests, 48 three-point bending tests. The highly controlled data set and specimen preparation techniques allowed for direct comparison between the two types of test results and the factors that contributed to each.

Variation by Region

The results of the tension coupon testing showed that the material response, i.e. ultimate stress, ultimate strain, and modulus, do not vary significantly with respect to anatomical region or rib level. This finding is consistent with the findings of Kemper et al. (2005). In addition, the overall averages of the current tension coupon testing are consistent with the results reported by Kemper et al. (2005) (Table 20). In contrast to these findings, Stitzel et al. (2003), who performed three-point bending tests on small rectangular cortical bone coupons, found an increase in the average stiffness and average ultimate stress for the cortical bone specimens located in the lateral portion of the ribs versus the anterior and posterior rib locations. Kemper et al. (2005) attributed the differences in regional variation findings to the fact that the specimens used by Stitzel et al. were very thin for three-point bending. In addition, trends in specimen thickness correlated with the trends seen with the regional variation of the material properties. For example, the average thickness of the anterior specimens, 0.49 ± 0.10 mm, was significantly lower than the average thickness of the lateral specimens, 0.57 ± 0.12 mm ($p<0.01$), and posterior specimens, 0.57 ± 0.12 mm ($p<0.01$). This was the same trend seen with the

significantly lower elastic modulus for the anterior specimens compared to the lateral and posterior specimens. It is suggested that the continuum assumption for three-point bending equations may no longer be valid for such small specimen thicknesses, and that this error is augmented with the smaller thickness specimens from the anterior regions. Given that an osteon is approximately 0.2 mm in diameter, the three-point bending tests on the anterior specimens put one-half of the coupon in tension, or the equivalent of approximately one osteon.

Table 20: Comparison of published material properties of human rib cortical bone tension coupons.

Author	N	Rate	Rib Level	Failure Stress	Failure Strain	Modulus
	subjects	(s^-1)		(MPa)	(μstrain)	(GPa)
Kemper et al. (2005)	6	0.5	1-12	124.2	27053	13.9
Current Study	6	0.6	4-7	130.9	25112	14.4

The results of the three-point bending test results are consistent with comparable rib sections of previous studies (Table 21). For both the anterior and lateral regions, the peak moment and corresponding strain were found to be consistent with the findings of Cormier et al. (2005). Yoganandan and Pintar (1998) reported a much lower peak moment and modulus, 3.8 Nm and 2.3 GPa respectively, for the lateral portion of the 7th rib. Granik and Stein (1973) reported a lower average modulus of 11.5 GPa for the lateral portion of ribs 6 and 7 combined. However, Granik and Stein (1973) performed tests under static loading conditions and Yoganandan and Pintar (1998) performed tests under quasi-static loading conditions. It is well known that bone is a viscoelastic material, and therefore is affected by the rate of loading (McElhaney and Byars, 1965; Wood, 1971; Crowninshield and Pope, 1974; Wright and Hayes, 1976; Carter et al., 1976; and Stein and Granik, 1979). In general, with increased loading rate the ultimate stress and

modulus increase, while the ultimate strain decreases. Another possible explanation for the differences in reported modulus values could be the method used to calculate the modulus. Granik and Stein (1973) and Yoganandan and Pintar (1998) calculated the modulus based on the impactor displacement, while the current study used a strain gage and calculated bending stress. Funk et al. (2004) reported that calculating material properties based on deflection data from whole bone three-point bending under predicted the elastic modulus by approximately 40%, when compared to strain gage data, due to the presence of shear and/ or a varying bending rigidity (EI) along the length of the bone.

Table 21: Comparison of published structural properties of whole human rib three-point bending specimens.

Author	N	Rate	Region	Rib Level	Peak Moment	Peak Strain	Modulus
	(subjects)	(mm/s)			(Nm)	(μstrain)	(GPa)
Cormier et al. (2005)	4	500-1000	Ant	3-7	4.0	5432	N/R
Current Study	6	172	Ant	4-7	3.5	8984	18.9
Granik & Stein (1973)	10	static	Lat	6 / 7	N/R	N/R	11.5
Yoganandan & Pintar (1998)	30	0.042	Lat	7 / 8	3.8 / 3.2	N/R	2.3/ 1.9
Cormier et al. (2005)	4	500-1000	Lat	2, 8-10	6.0	10741	N/R
Current Study	6	172	Lat	4-7	7.6	12671	21.1

With respect to anatomical region, it was found that the lateral specimens had a significantly larger peak moment, peak strain, modulus, and stiffness than the anterior specimens. The trends with respect to peak moment and strain are consistent with those reported by Cormier et al. (2005). However, Cormier et al. (2005) did not report the modulus. In addition, the moment of inertia and distance to the neutral axis increased when moving from the anterior region to the posterior region, which is consistent with the findings of Cormier et al. (2005). Logically, the

significantly lower geometric properties found in the anterior region versus lateral is a large contributing factor to the significantly lower structural response exhibited by specimens obtained from the anterior region of the thorax versus ones obtained from the lateral region.

An additional factor that may be contributing the regional differences found in the structural response is the mode of failure. As noted previously, the peak values were defined as the point at which structural compromising occurred, i.e. the point at which further motion of the impactor produces no increment of applied force (Stein and Granik 1979). In the current study, it was found that a number of specimens exhibited structural failure on the compression side of the rib at the point of impactor contact with no tensile fracture. Out of the 48 specimens, the majority of the specimens that demonstrated this failure mode were taken from the anterior region: 20 anterior and 12 lateral. This resulted in a decrease in the strength of the rib while maintaining structural integrity on the tension side, and therefore, a continued increase in measured strain. The authors are unaware of the clinical relevance with regard to this phenomenon.

The same phenomenon was reported by Cormier et al. (2005). Cormier et al. (2005) suggested that this could be a result of regional changes in the material properties. However, the results of the current study and those reported by Kemper et al. (2005) show that there are no significant differences in the tensile material properties of human rib cortical bone with respect to region. Therefore, the local structural failure at the point of loading and subsequent reduction in peak structural response values, seen by primarily anterior specimens, may be attributed to differences in geometry or bone modeling differences. A two-sample student t-test assuming unequal variance showed that none of the cortical shell thicknesses were found to be significant with

respect to failure mode: internal thickness ($p=0.19$), external thickness ($p=0.42$), superior thickness ($p=0.29$), and inferior thickness ($p=0.08$). A two-sample student t-test assuming unequal variance showed that there is significantly less ($p<0.01$) trabecular bone present in the specimens that exhibited local failure at the point of impactor contact versus specimens that exhibited tensile fractures. The specimens which failed at the point of impactor contact had an average trabecular area of 1.71 ± 0.7 mm^2, while specimens that failed on the tensile side had an average trabecular area of 3.40 ± 1.34 mm^2. This is an extremely interesting finding, because it implies that the cortical shell alone may not be thick enough to support a point load. Therefore, the significant differences found with respect to anatomical region could be an artifact of three-point bending methodology.

Variation by Rib Level

With respect to rib level, peak moment for lateral specimens ($p=0.02$), peak strain for anterior specimens ($p=0.05$), and stiffness for anterior and lateral specimens (Ant $p<0.01$; Lat $p<0.01$) were found to be significant. The peak moment for lateral specimens and stiffness for anterior and lateral specimens were found to increase from rib 4 to 6 and then decrease slightly from rib 6 to 7. The trend in peak strain for anterior specimens was less prominent, but seemed to decrease slightly from rib 4 to 7. The average modulus and average stiffness were not found to be significant ($p>0.05$) with respect to rib level for anterior or lateral specimens. Yoganandan and Pintar (1998) reported that the modulus of the 7th and 8th ribs was independent of location both vertically and horizontally on the thorax over this narrow range. Granik and Stein (1973) and Stein and Granik (1976) did not report on the differences between the structural response of the

6th and 7th ribs. Cormier et al. (2005) did not report whether or not the structural response of ribs 2 through 12 varied with respect to rib level.

In addition to the changes in structural response with respect to rib level, there were significant differences in the cross-sectional geometry with respect to rib level for both anterior and lateral specimens. Furthermore, the trends in geometry with respect to rib level coincide with the changes in peak moment with respect to rib level. For anterior specimens, the distance to the neutral axis ($p<0.01$), the ratio of the distance to the neutral axis to the area moment of inertia ($p=0.02$), and radius of gyration ($p=0.04$) were found to be significant with respect to rib level. For lateral specimens, the cortical bone cross-sectional area ($p=0.01$), area moment of inertia ($p<0.01$), the distance to the neutral axis ($p<0.01$), the ratio of the distance to the neutral axis to the area moment of inertia ($p<0.01$), and radius of gyration ($p=0.03$) were found to be significant with respect to rib level. These findings are similar to those of Cormier et al. (2005), who reported that the distance to the neutral axis increased from rib 2 to rib 6, and then decreased from rib 6 to rib 12. Cormier et al. (2005) also reported that the radius of gyration increased from rib 2 to 4 and decreased from rib 5 to rib 12. In the current study, the radius of gyration increased from rib 4 to rib 6 for anterior specimens and from rib 4 to rib 7 for lateral specimens. However, the differences between the trends in the current study and those reported by Cormier et al. (2005) are most likely due to subject variation as a result of differences in age, gender, or BMD. Yoganandan and Pintar (1998) reported that the cortical area and area moment of inertia of rib 7 were found to be statistically larger than rib 8, which is consistent with that of Cormier et al (2005).

Tension Coupons versus Three-Point Bending

Although three-point bending provides the overall structural response of human rib sections, there are inherent limitations that introduce uncertainty in the calculated material properties (Figure 52). First, three-point bending of whole rib sections is confounded by the irregular cross-sectional geometry and curvature of human ribs. Second, a paired student t-test for the means assuming unequal variance showed there was a significant ($p<0.01$) over estimation of the ultimate stress due to the fact that linear-elastic beam equations do not take plasticity into account (Figure 52-left). Although not significant ($p=0.22$) in the current data set, the use of a strain gage can underestimate the actual ultimate strain due to that fact that the strain gage was not always located exactly at the location of the fracture (Figure 52-center). It should be noted that only three-point bending specimens which exhibited tensile fractures were used for the ultimate stress and ultimate strain comparisons, while all specimens were used for the modulus comparison. The degree to which the reported peak strain varies from the actual is related to the distance from the point of fracture to the center of the strain gage, due to the strain distribution on the tensile side of the specimen. Finally, three-point bending of a whole rib section significantly overestimated the elastic modulus ($p<0.01$) (Figure 52-right).

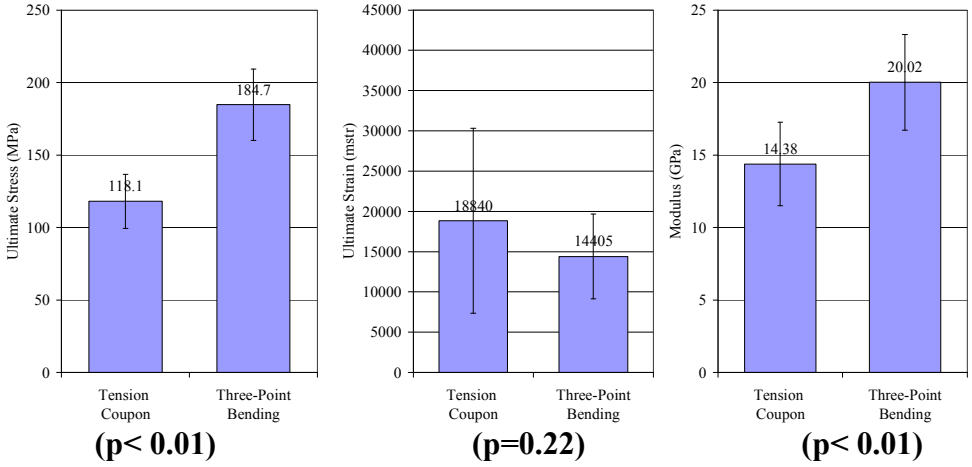

Figure 52: Matched material properties from tension coupons versus three-point bending specimens.

Variation between Cadavers

Unlike previous researchers, age was not found to have a significant influence on the mechanical properties of human bone in the current study. However, this is most likely the result of the fact that there were only six cadavers included in the current study. Kemper et al. (2005) reported that the elastic modulus of human rib cortical bone increased with age, while the ultimate strain decreased. However, these trends were also based upon only six cadavers rather than the general population. Sacreste et al. (1982) reported the peak bending stress and modulus of rib sections decrease with age. Lindahl and Lindren (1967) reported that the tensile material properties, ultimate stress and ultimate strain, of both femur and humerus cortical bone decreased with age, while the modulus of elasticity showed no significant changes with age. Burstein et al. (1976) reported that the tensile material properties, ultimate strain and energy, of tibia cortical bone decrease significantly with age. Although not significant, Burstein et al. (1976) reported that the modulus of elasticity of tibia cortical bone increased with age. However, Burstein et al. (1976) performed tension tests on the femoral cortical bone, and reported that ultimate stress, ultimate strain, elastic modulus, and energy significantly decrease with age. McCalden et al. (1993) reported that tensile material properties, ultimate strain and energy, of the femur significantly decrease with age, while the modulus of elasticity showed no significant changes with age. In addition, McCalden et al. (1993) reported that the energy in the elastic region did not change with age, while the energy in the plastic region significantly decreased with increasing age ($p<0.01$). When all of these studies are taken into consideration, the overall conclusion is that the ultimate strain and energy of cortical bone significantly decrease with age regardless of the skeletal location, while the relationship of ultimate stress and modulus with respect to age varies between individual skeletal locations due to tissue and/or structure differences.

The changes in material properties with respect to age have been attributed to a number of morphologic and compositional changes that occur as a result of aging (Kent et al. 2005). Burstein et al. (1976) attributed the differences between the matched tibia and femur specimens to differences at the tissue and structure or organ level, which vary based on the loading conditions the different bones are subjected to. McCalden et al. (1993) found that the amount of haversian bone and osteon size increase with age, and showed a clear inverse relationship between strength and haversian bone. It has been reported that remodeling causes a general increase in the porosity of cortical bone with advancing age, with an accompanying decrease in cortical bone density (Lindahl and Lindgren, 1967; Evans; 1974; McCalden et al.; 1993). In addition, wet and dry apparent densities of cortical bone, which are functions of both the rate of mineralization and porosity, have been shown to increase with increasing mechanical properties (Muellar et al., 1966; Carter and Hayes, 1976; Schaffler and Burr, 1986; Martin and Ishida, 1989; McCalden et al., 1993; Keller, 1994). Kemper et al. (2005) compared his data to data from studies involving bone biomechanics published by Hardy et al. (1997) and Kennedy et al. (2004) and reported that there was a large variation of cross-sectional area values versus the small variation of in the rate of mineralization and local mineral density. This is further supported by the finding of the current study, which showed that average local mineral density did not vary significantly with respect to age ($p=0.78$). This indicates that the amount of bone present changes with age or gender whereas the rate of mineralization remains fairly constant. This conclusion is consistent with the findings of Trotter and Peterson (1955), Muellar et al. (1966), McCalden et al. (1993), and Schaffler and Burr (1986).

Statistical Analysis

For the tension coupon testing, a randomized block ANOVA showed that there was a significant interaction effect found for the ultimate stress between the within-subject variables. However, it is extremely difficult to interpret this interaction effect, because the effect is different for every subject. Furthermore, this effect cannot truly be quantified because there is not enough information to look at the differences found for each subject. However, ultimate stress was not found to be significant with respect to region or rib level when evaluated independently. Therefore, the significant interaction effect for ultimate stress with respect to region and rib level can be ignored.

The conclusions drawn in the current study are based upon six cadavers rather than the general population. Due to the limited number of cadavers, two types of statistical models were used rather than a single more complicated one. Performing a more complicated analysis with only six cadavers would result in saturation of the model, which can lead to erroneous statistical significance. No statistically significant interaction effects were found between the between-subject variables and the within-subject variables, or between the within-subject variables. An analysis to determine interaction effects of between-subject variables, like gender and age, was not performed due to limited number of cadavers, which would result in a limited number of degrees of freedom and low power. Therefore, any results found in such an analysis would be weak.

Conclusions

The variables which contribute to the regional variation in the strength of human ribs were investigated through 94 matched tests on human rib specimens; 46 tension coupon tests, 48 three-point bending tests. The results of the tension coupon testing showed that there were no significant differences in material properties with respect to region or rib level: ultimate stress, ultimate strain, or elastic modulus. In contrast, lateral three-point bending specimens were found to have a significantly higher peak bending moment, peak strain, modulus, and stiffness than anterior specimens. The lateral three-point bending specimens also had a significantly larger area moment of inertia, larger distance to the neutral axis, smaller ratio of the distance to the neutral axis to area moment of inertia, larger cortical bone area, and larger radius of gyration than the anterior specimens. In addition, the peak moment, peak strain, and stiffness were found to vary significantly with respect to rib level. Similar to anatomical region, the changes in the structural response with respect to rib level were accompanied by significant changes in specimen geometry. For lateral specimens, the cortical bone area, area moment of inertia, distance to the neutral axis, ratio of the distance to the neutral axis to area moment of inertia, and radius of gyration were found to be significantly different with respect to rib level. For anterior specimens, distance to the neutral axis, ratio of the distance to the neutral axis to area moment of inertia, and radius of gyration were found to be significantly different with respect to rib level.

The results of the current study clearly illustrate that there is variation in the structural response of human ribs with respect to anatomical region and rib level, and this variation is due to changes in local geometry of each rib while the material properties remain constant within an individual

thorax. However, there can be significant variation in both the material and structural response between individuals due to the effects of age and gender (Figure 53).

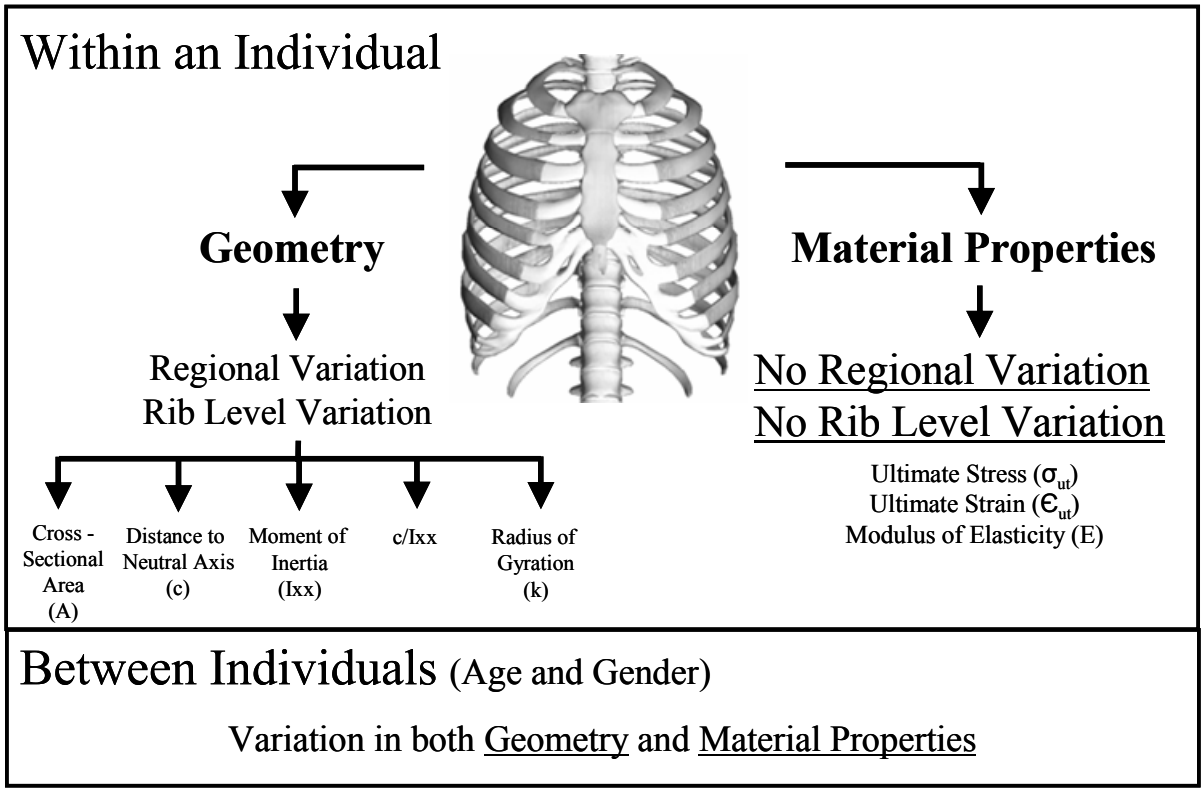

Figure 53: Variation within the human thorax that influences the overall structural response.

CHAPTER 4

Response of the Human Clavicle in Three-Point Bending: Effect of Loading Direction

Introduction

Clavicle fractures are classified as having an Abbreviated Injury Score (AIS) of 2, where AIS is a system used by researchers and trauma centers to rank and compare the severity of injuries on a scale of 1 (minor) to 6 (death) based on threat to life (Abbreviated Injury Scale, 2005). However, clavicle fractures can result in either temporary or long term loss of functional capacity. Housner and Kuhn (2003) reported that depending on the fracture type, clavicle fractures take 4 to 12 weeks to heal in adults. During this time, the range of motion and strength of the shoulder are limited. Mid-clavicle fractures are of special concern since they may lead to significant morbidity due to a high rate of nonunion, 22% to 33%, when treated non-operatively (Nordqvist, 2000).

Analysis of the National Automotive Sampling System-Crashworthiness Data System (NASS-CDS) showed that over 9,700 three-point belt restrained occupants incur a clavicle fracture every year. For occupants exposed to frontal automotive impacts, over 90% of the fractures occurred in the clavicle due to loading by the shoulder belt, as evidence by left clavicle fractures for drivers and right clavicle fractures for right front seat passengers. This injury pattern is consistent with the hypothesis that shoulder belt loading initiates clavicle fractures in frontal impacts. Therefore, understanding the biomechanics of clavicle fractures is an important factor in the optimization of seatbelt restraint systems.

There have only been two studies to the author's knowledge that have evaluated the biomechanical response of the human clavicle. Bolte et al. (2000) evaluated the strength of the clavicle by conducting three-point bending tests on six human clavicles at an impact rate of 0.5 mm/s. However, the direction of loading was not reported. Proubasta et al. (2002) conducted three-point bending tests on 5 intact clavicles dissected from fresh frozen human cadavers. Prior to testing, the distal ends were fixed in aluminum cylinders using polyester resin. Proubasta et al. (2002) applied the load in the anterior to posterior direction 3 cm from the midpoint, medial or lateral not reported, of a fixed 150 mm test span at a loading rate of 0.05 mm/s.

Although there have some studies that investigated the biomechanical response of the clavicle in three-point bending, these studies have been limited to a single loading direction and low impact speeds. The clavicle has a complex shape, and differences found in the structural response of the clavicle due to different loading angles could provide insight to possible methods to optimize seatbelt restraint design in order to minimize the risk of clavicle fractures. Therefore, the purpose of this study was to evaluate the biomechanical response of the human clavicle when subjected to dynamic three-point bending in two different loading directions: 0° and 45° from the transverse plane.

Methods

Dynamic three-point bending tests were performed at two loading angles on 20 human claviculae obtained from 10 unembalmed frozen and thawed post mortem human subjects ranging from 45 to 92 years of age (Table 22). Freezing was used as a means to preserve the specimens because

numerous previous studies have indicated that freezing does not significantly affect the material properties of cortical bone when frozen to a temperature of -20° C (Frankel, 1960; Sedlin, 1965; Weaver, 1966; Linde and Sorensen, 1993; Griffon et al., 1995; Hamer et al., 1996). Numerous authors have reported significant differences in the material properties of dry bone compared to wet bone (Yamada, 1970; Dempster, 1952; Evans, 1951). Therefore, gauze pads soaked in normal saline were wrapped around the specimens to maintain proper specimen hydration after the specimens were dissected from the bodies (Reilly et al., 1974).

Table 22: Subject information and anthropometric data for clavicle testing.

Test ID	Aspect	Subject Number	Gender	Age	Specimen Length
				(yrs)	(cm)
1	Right	Sf_C1	F	61	13.2
2	Left	Sm_C2	M	89	14.5
3	Right	Sm_C3	M	75	13.8
4	Left	Sm_C4	M	66	15.7
5	Left	Sm_C5	M	84	15.7
6	Left	Sm_C6	M	84	15.4
7	Right	Sf_C7	F	64	16.9
8	Right	Sm_C8	M	67	14.9
9	Right	Sf_C9	F	92	14.3
10	Left	Sm_C10	M	45	16.5
11	Left	Sf_C1	F	61	13.2
12	Right	Sm_C2	M	89	14.8
13	Left	Sm_C3	M	75	13.8
14	Right	Sm_C4	M	66	15.2
15	Right	Sm_C5	M	84	16.0
16	Right	Sm_C6	M	84	15.4
17	Left	Sf_C7	F	64	16.7
18	Left	Sm_C8	M	67	15.7
19	Left	Sf_C9	F	92	14.6
20	Right	Sm_C10	M	45	15.9

The right and left claviculae were randomly divided into two groups, where each group contained one specimen from each of the 10 matched pairs. Each group was subjected to an impact at either 0° or 45° from the transverse plane (Figure 54). Three-dimensional Computed Tomography (CT) scans of each clavicle were obtained prior to specimen preparation and testing to account for the irregular geometry of the clavicle cross section. An image processor was used to properly orient the three-dimensional CT reconstructions of the claviculae. Then the center of the clavicle corresponding to the point of load application in the experimental setup was located, based on the CT scans and experimental measurements, and a cross section was created. For the image analysis, the cross-sectional image was aligned such that the assumed loading direction was from the right (Figure 55). For specimens impacted 45º from the transverse plane, the image was rotated an additional 45º. The clavicle cross sections were then thresholded to obtain the cortical bone cross section, pixel value of 190/255, using the standard 8 bit black and white CT image imported into Photoshop © (Adobe Systems Inc., Adobe Photoshop). The 190 pixel value resulted in an acceptable cortical bone cross section for all specimens, and preserved the variation between certain claviculae with very thin cross sections and other healthier bones with thicker cortex. Finally, each cross-sectional CT image was converted to binary black (0) and white (1), where pixels designated as 1 represented bone (Figure 56). It should be noted that the material properties of the cortical bone were assumed to be homogeneous.

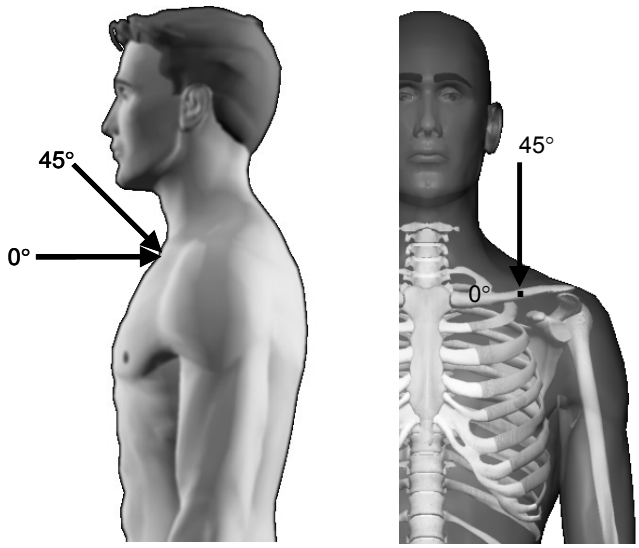

Figure 54: Clavicle impact locations (left and anatomical positions (right).

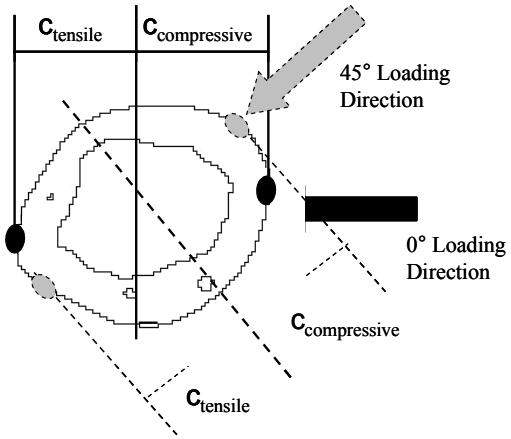

Figure 55: Sample image outline and assumptions for clavicle CT image processing.

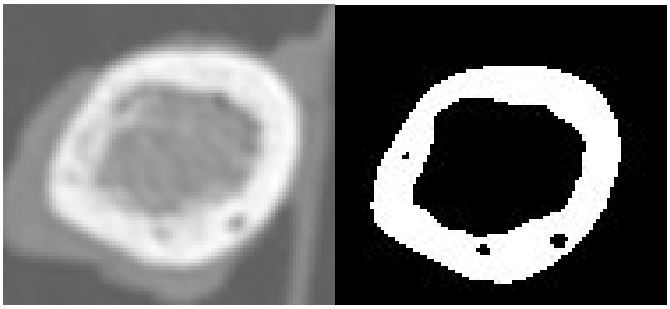

Figure 56: Sample clavicle cross section before (left) and after (right) thresholding.

Custom Matlab © (Matworks, Inc., Matlab-R12, Natick, MA) code was used to calculate the area moment of inertia (I), the distance from the neutral axis to the tensile surface (c), and the cortical bone cross-sectional area (A), using the thresholded binary CT image. The neutral axis of the image, which was assumed to be perpendicular to the loading direction, was found by first calculating the area of bone in each row of the image, which is the sum of ones in a given row multiplied by the pixel dimensions in millimeters. The area of bone in each row of pixels was multiplied by the distance that row was from an assumed neutral axis, and then summed above and below the assumed neutral axis. The neutral axis was determined to be the row in which the sum above the assumed neutral axis was equal to the sum below the assumed neutral axis. The distance to the neutral axis (c) was calculated by multiplying the number of rows between the neutral axis and the tensile side by the millimeters per pixel value. The area moment of inertia (I) about the neutral axis was found by calculating the area of bone in a row multiplied by the square of the distance that row was from the neutral axis, and then summing that value up for the entire image. The area of cortical bone (A) was calculated as the sum of ones over the entire image multiplied by the pixel dimensions in millimeters.

The primary component of the test setup was a servo-hydraulic Material Testing System (MTS Systems Corporation, MTS-810, Eden Prairie, MN) (Figure 57). The MTS utilized a hydraulic actuator and impactor head to load the claviculae in a dynamic three-point bending configuration at a displacement rate of 152 mm/s. This corresponded to a strain rate of 0.3 s^{-1} at the midpoint of the tensile side of the clavicle, which is consistent with the thoracic belt loading test results reported by Duma et al. (2005). Displacement was measured using the MTS internal linear variable displacement transducer (LVDT). A six-axis impactor load cell (Denton ATD, Inc.,

1968- 22 kN, Rochester Hills, MI) was used to measure loads exerted on the specimen by the impactor. An accelerometer (Endevco Corporation, 7264B-2000G, San Juan Capistrano, CA) was attached to the impactor head to allow for inertial compensation of the impactor load cell, using the mass between the clavicle and active axis of the load cell. The support structure was mounted to a three-axis reaction load cell (Denton ATD, Inc., 5768-11 kN, Rochester Hills, MI).

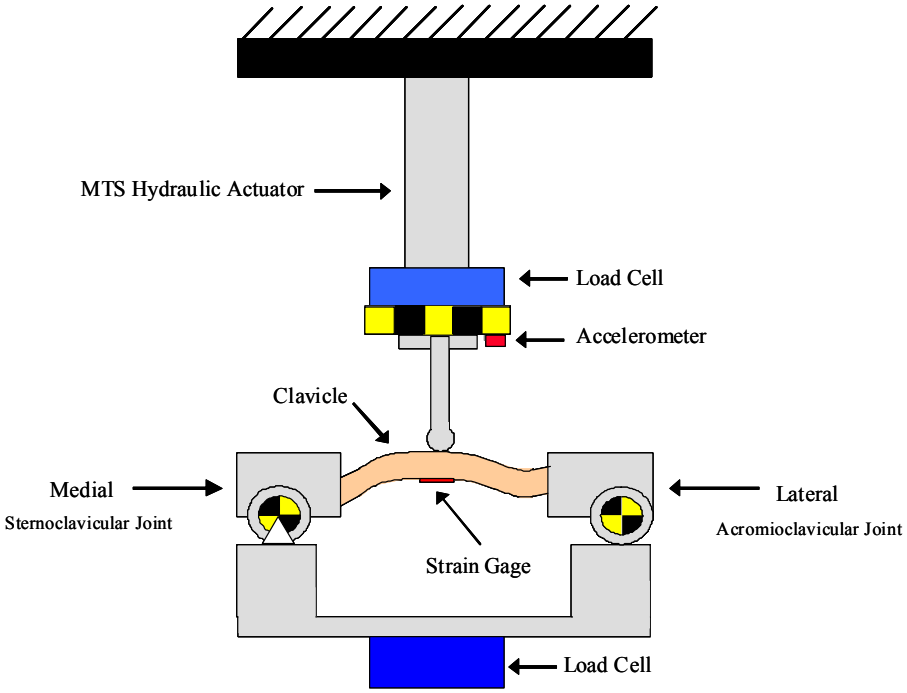

Figure 57: Clavicle three-point bending test setup.

To stabilize the clavicle in the three-point test configuration while maintaining loading in the desired plane, the ends were placed in rigid square aluminum potting cups, containing polymer filler (Bondo Corporation, Atlanta, GA). Special care was taken during the potting process to ensure that the claviculae were oriented in order to produce loading in the desired direction when placed on the three-point bending test setup. The sternoclavicular joint is a saddle-type of synovial joint but functions like a ball-and-socket joint, allowing rotation about all three axes but

not translation (Terry and Chopp, 2000; Moore and Dalley, 2006). Therefore, a cylindrical polymer roller was attached to the medial potting cup and pinned to allow for rotation but not translation. The acromioclavicular joint is a plane type of synovial joint, but movements at this joint are similar to those of the sternoclavicular joint (Williams et al., 1989). Specifically, the acromioclavicular joint allows axial rotation, anterior-posterior rotation, and superior-inferior rotation (Branch et al., 1996). In addition, since the sternoclavicular joint is the only articulation between the upper limb and the axial skeleton, the clavicle in its movement carries with it the scapula which glides on the external portion of the thorax. As a result, the lateral end of the clavicle is free to translate in all directions. Therefore, a cylindrical polymer roller was attached to the lateral end of the clavicle but not constrained laterally.

After potting, each clavicle was instrumented with a single-axial strain gage bonded to the tensile side, which was the side opposite of the impactor, at the mid-point of the specimen (Vishay Measurements Group, CEA-06-062UW-350, Malvern, PA). For specimens struck at 0° from the transverse plane, the tensile side corresponded to the posterior portion of the clavicle. For specimens struck at 45° from the transverse plane, the tensile side corresponded to the inferior-posterior portion of the clavicle. It should be noted that normal saline was sprayed directly on the samples to maintain proper specimen hydration during both specimen preparation and testing (Reilly et al., 1974).

All data channels were recorded at a sampling rate of 20 kHz (Iotech, Wavebook-16, Cleveland, OH). Data from the load cells and accelerometers were filtered to SAE channel filter class (CFC) 180 (SAE J211, 1995). The moment was calculated as one-half the inertially

compensated impactor force multiplied by one-half of the active span, which corresponds to the initial distance between the centers of the two rollers. The stiffness (K) was determined by performing a linear regression on the initial linear region of the force versus displacement curve (R^2>0.9), 10% to 40% of the peak force. After testing, the distance from the center of the strain gage to the point of fracture on the tension side was documented. In the case of a comminuted fracture, the measurement was taken from the closest fracture location.

Statistical analyses were performed on the structural response variables by performing a paired two sample t-test for means. In addition, statistical analyses were performed on the geometric variables: moment of inertia (I), distance to the neutral axis (c), and cortical bone area (A) by performing a paired two sample t-test for the means. Statistical significance was defined as a p-value ≤ 0.05. The goal of the statistical analysis was to determine if there were any statistical differences in structural properties or geometry with respect to impact direction.

Results

The clavicle strain time histories in the current study were found to be similar to that of observed shoulder belt loading performed on intact post mortem human subjects. This similarity was determined by comparing the strain time histories obtained in the clavicle three-point bending tests performed in the current study to those achieved in the male and female shoulder belt tests conducted by Duma et al. (2005) (Figure 58). All clavicle fractures occurred at approximately the mid-point between the supports. The claviculae fractured in the form of a transverse, oblique, or comminuted-wedge fracture, which are typical of three-point loading conditions (Figure 59).

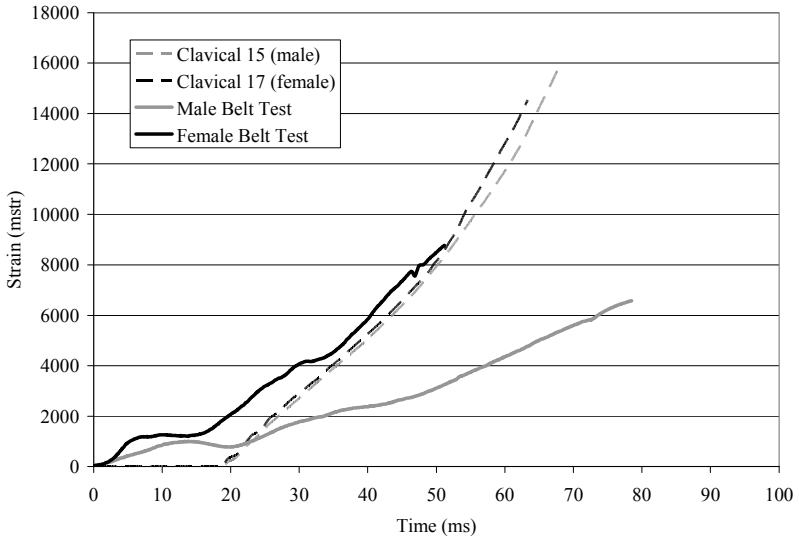

Figure 58: Comparison of strain rates between clavicle tests and belt loading tests (Duma et al. 2005).

Figure 59: Clavicle fracture types resulting from three-point bending.

The peak values were defined as the point at which structural compromising occurred, in other words, the point at which further motion of the impactor produced no incremental increase of applied force (Stein and Granik, 1976). The force versus deflection response was found to be similar for both test groups (Figure 60 and Figure 61). The average strain rate for all specimens was 0.3 s^{-1}. However, structural stiffness ($p=0.01$) and peak strain ($p<0.01$) were found to be statistically different between specimens struck at 0º versus 45º from the transverse plane. The

average peak structural values and corresponding standard deviations for both test groups were recorded (Table 23 and Table 24). The average geometric values and corresponding standard deviations for both test groups were recorded (Table 25 and Table 26).

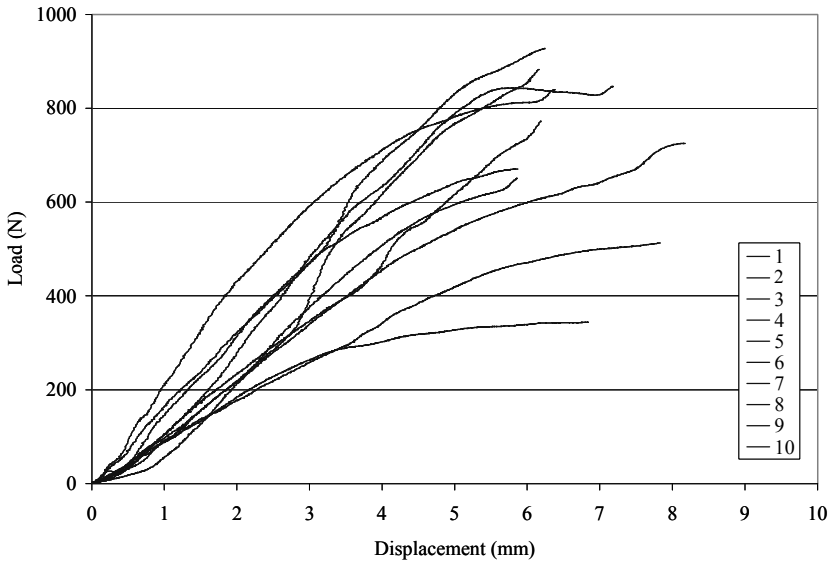

Figure 60: Impactor force vs. displacement for all 0º clavicle impact tests.

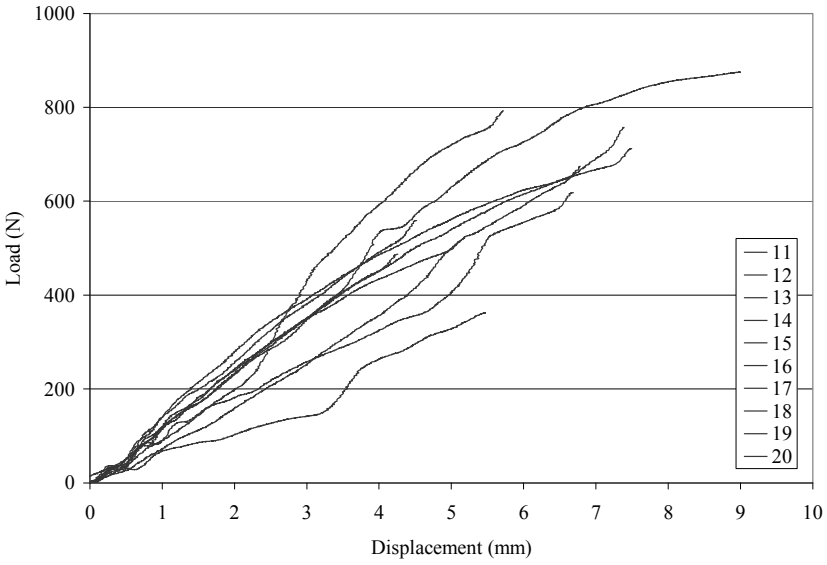

Figure 61: Impactor force vs. displacement for all 45º clavicle impact tests.

Table 23: Peak structural response values for 0˚ clavicle tests.

Test ID	Active Span	Peak Impactor		Peak Deflection	Stiffness	Peak Strain	Gage to Fracture
		Force	Moment				
	(m)	(N)	(Nm)	(mm)	(N/mm)	(µstrain)	(mm)
1	0.137	840	28.8	6.4	227.1	* 19870	6.0
2	0.148	651	24.1	5.9	163.9	19156	0.0
3	0.142	670	23.8	5.9	165.7	* 21096	4.0
4	0.159	883	35.1	6.2	128.3	* 18059	7.0
5	0.162	725	29.4	8.2	122.2	* 25443	6.0
6	0.159	513	20.4	7.8	83.3	* 18973	6.0
7	0.169	772	32.6	6.2	123.5	14282	16.0
8	0.154	847	32.6	7.2	196.8	17087	8.0
9	0.146	344	12.6	6.8	93.2	* 22919	16.0
10	0.163	928	37.8	6.2	159.0	* 20498	2.0
Average:		***717***	***27.7***	***6.7***	***146.3***	***19738***	***7.1***
Standard Deviation:		***181***	***7.6***	***0.8***	***44.9***	***3085***	***5.3***

Note: * indicates that strain gage failed prior to peak load.

Table 24: Peak structural response values for 45˚clavicle tests.

Test ID	Active Span	Peak Impactor		Peak Deflection	Stiffness	Peak Strain	Gage to Fracture
		Force	Moment				
	(m)	(N)	(Nm)	(mm)	(N/mm)	(µstrain)	(mm)
11	0.138	517	17.8	5.1	129.2	18065	6.0
12	0.150	793	29.7	5.7	105.5	17223	10.0
13	0.140	712	24.9	7.5	121.2	* 17556	6.0
14	0.156	487	19.0	4.3	121.5	10163	17.0
15	0.161	756	30.4	7.4	144.8	15898	7.0
16	0.161	674	27.1	6.8	95.7	16664	23.0
17	0.170	618	26.3	6.7	72.3	14536	17.0
18	0.164	559	22.9	4.5	131.5	9463	2.0
19	0.155	362	14.0	5.5	39.9	14184	26.0
20	0.175	875	38.3	9.0	116.0	* 19230	1.0
Average:		***635***	***25.1***	***6.2***	***107.8***	***15298***	***11.5***
Standard Deviation:		***157***	***7.0***	***1.5***	***31.4***	***3273***	***8.7***

Note: * indicates that strain gage failed prior to peak load.

Table 25: Cross-sectional geometry values for claviculae struck at 0˚.

Test ID	Impact Angle	I	c	c/I	A
		(mm^4)	(mm)	(mm^-3)	(mm^2)
1	0	542.8	5.6	0.010	65.4
2	0	737.8	6.3	0.009	48.1
3	0	439.9	5.5	0.013	49.8
4	0	881.8	6.6	0.007	57.6
5	0	546.6	5.6	0.010	49.3
6	0	292.1	5.3	0.018	26.5
7	0	940.5	6.6	0.007	72.9
8	0	832.8	5.9	0.007	46.0
9	0	373.1	6.2	0.017	28.5
10	0	896.3	6.0	0.007	68.5
Average		***648.4***	***6.0***	***0.010***	***51.3***
Standard deviation		***238.3***	***0.5***	***0.004***	***15.6***

Table 26: Cross-sectional geometry values for claviculae struck at 45˚.

Test ID	Impact Angle	I	c	c/I	A
		(mm^4)	(mm)	(mm^-3)	(mm^2)
11	45	326.9	4.1	0.010	64.4
12	45	544.3	5.3	0.013	40.4
13	45	347.4	4.3	0.010	54.2
14	45	548.3	5.8	0.012	48.4
15	45	741.4	5.4	0.011	65.6
16	45	352.0	4.5	0.007	40.1
17	45	503.6	4.4	0.013	66.6
18	45	674.1	5.4	0.009	46.9
19	45	284.9	5.5	0.008	27.2
20	45	832.1	6.5	0.019	67.3
Average		***515.5***	***5.1***	***0.011***	***52.1***
Standard deviation		***189.2***	***0.8***	***0.004***	***13.8***

The results indicate that there was no statistically significant difference in peak force (p=0.22), peak moment (p=0.30), or peak displacement (p=0.44) between specimens struck at 0º versus 45º from the transverse plane (Table 27). The results indicate that the area moment of inertia (I) (p=0.05) and distance to the neutral axis (c) (p=0.01) were significantly different between specimens struck at 0º versus 45º from the transverse plane (Table 28). However, neither the ratio of the distance to the neutral axis to the moment of inertia (p=0.60) nor the cortical bone area (A) (p=0.76) were found to be significantly different between the two test groups.

Table 27: Statistical analysis of structural response variables for 0º versus 45º tests.

Compression Group	Two Tail p-values				
	Peak Force	Peak Moment	Peak Displacement	Peak Strain	Stiffness
0º vs. 45º	0.22	0.30	0.44	<0.01*	0.01

Note: * Indicates that analysis of peak strain should be regarded with caution.

Table 28: Statistical analysis of cross-sectional geometry for 0º versus 45º specimens.

Compression Group	Two Tail p-values			
	I	c	c/I	A
0º vs. 45º	0.05	0.01	0.60	0.76

Discussion

This study investigated the effect of loading direction on the structural response of the human clavicle subjected to dynamic three-point bending. This was accomplished by performing 20 matched tests on whole human claviculae in two loading directions: 0º and 45º from the transverse plane. The controlled data set and specimen preparation techniques allowed for direct comparison between the two test conditions.

Although the results of the current study were found to be consistent with those reported by previous researchers, an accurate comparison between studies is confounded by differences in end conditions, loading rates, and specimen orientation (Table 29). For example, the average peak force in the current study was consistent with Bolte et al. (2000), but the loading rate in the current study was significantly larger. It is well known that bone is a viscoelastic material, and therefore is affected by the rate of loading (McElhaney and Byars, 1965; Wood, 1971; Crowninshield and Pope, 1974; Wright and Hayes, 1976; Carter et al., 1976; and Stein and Granik, 1979). Assuming that all other test conditions were similar, one would expect the peak force to increase with loading rate. However, the end conditions were different between the two studies. Therefore, the two studies can not be directly compared due to the possible variations in applied shear and/or axial torsion, both of which would effectively decrease the measured peak force. Regardless, the findings of previous authors are presented for completeness.

Table 29: Comparison of current study to previous clavicle three-point bending literature.

Author	End Conditions	Impact Direction	Loading Rate	Average Peak Force	Average Stiffness
		Degrees from Transverse Plane	(mm/s)	(N)	(N/mm)
Bolte et al. (2000)	Evenly Supported	N/R	0.50	667 (± 277)	N/R
Proubasta et al. (2002)	Fixed-Fixed	0 º	0.05	486 (± 179)	94.8 (± 4.9)
Current Study	Simply Supported	0 º	152.00	717 (± 181)	146.3 (± 44.9)
	Simply Supported	45 º	152.00	635 (± 157)	107.8 (± 31.4)

Note: N/R = Not Reported

With respect to loading direction, the results of the current study showed that there were no statistically significant differences in peak force ($p=0.22$), peak moment ($p=0.30$), or peak displacement ($p=0.44$) between specimens struck at 0º versus 45º from the transverse plane. In contrast, the structural stiffness ($p=0.01$) and peak strain ($p<0.01$) were found to be significantly different between specimens struck at 0º versus 45º from the transverse plane. However, the location of the fracture on the tension side of the specimens rarely corresponded to the location of the strain gage due to the complex fracture types. In addition, the strain gage occasionally failed prior to peak load. For these two reasons, the peak strain reported in this paper is less than the actual peak strain. The degree to which the reported peak strain varies from the actual is related to the distance from the point of fracture to the center of the strain gage, due to the strain distribution on the tensile side of the specimen, and the point at which the gage failed. Therefore, peak strain is not an appropriate comparison variable and should be regarded with caution.

Variations in the structural response of whole bone sections can be a result of changes in the bone geometry, bone material properties, or both. Due to the controlled matched data set, the differences in the structural response with respect to loading direction can be attributed to geometric differences and not material differences. The analysis of the clavicle cross-sectional geometry showed that the area moment of inertia ($p=0.05$) and distance to the neutral axis ($p=0.01$) were significantly different between specimens struck at 0º versus 45º from the transverse plane. However, the ratio of the distance to the neutral axis to the moment of inertia ($p=0.60$) and cross-sectional area ($p=0.76$) was not found to be significant with respect to loading direction. Therefore, differences in the structural stiffness were most likely a result of the overall geometry of the clavicle and not differences in the cross-sectional geometry. To explain, the clavicle has a complex geometry that can best be described as an "S" shape. If there is significant curvature, then the neutral axis will no longer coincide with the neutral axis and the stress distribution across the section will become more hyperbolic (Norton, 2000). In the case that the loading is applied perpendicular to the radius of curvature, the neutral axis will shift towards the center of curvature and more of the specimen will be placed in compression. Previous researchers have shown that elastic modulus of bone is lower in tension than compression (Evans and Bang, 1967; Reilly and Burstein, 1975; Burstein et al., 1976; Kemper et al., 2007b). Therefore, loading a curved bone in different directions could result in changes to the overall structural stiffness.

The results of the current study suggest that optimizing seatbelt designs to load the midpoint of the clavicle at 0º versus 45º from the transverse plane, or vise versa, during frontal belt loading would have no effect on whether or not a fracture will occur. However, there are other variables

which should be evaluated in order to determine if it is possible to optimize seatbelt designs to minimize the risk of clavicle fractures. Specifically, the location, medial or lateral of the midpoint, and distribution of the applied force could significantly affect the failure strength of the clavicle. Therefore, future studies should be conducted to investigate the effects of these variables in order to further the understanding of the biomechanical response of the clavicle in three-point bending. The results of such studies would provide researchers and safety engineers with valuable data which could lead to an optimized seatbelt restraint system to minimize the risk of clavicle fractures in frontal belt loading.

Conclusions

The results of the current study showed that the only significant difference between 0° and 45° clavicle impacts was the stiffness. Specifically, claviculae struck 45° from the transverse plane were less stiff than the claviculae struck 0° from the transverse plane. Due to the controlled matched data set, the difference in the structural response with respect to loading direction can be attributed to the complex geometry of the clavicle and not material differences. Finally, additional testing should be conducted to investigate the effects of the location and distribution of the applied load in order to more fully understand the biomechanical response of the clavicle in three-point bending.

CHAPTER 5

Response of the Human Thorax to Dynamic Shoulder Belt Loading

Introduction

The vast majority of thoracic impact research has focused on developing global criteria for predicting injury. These include force, acceleration, and displacement based criteria, as well as combinations of the above (Eppinger, 1976; Morgan et al., 1994; Kuppa and Eppinger, 1998). Recent work has focused on the prediction of injury due to different restraint systems. For example, the increase in thoracic injury severity with increased age for a given occupant size, restraint type, and crash type is well documented (Kallieris et al., 1974; Patrick et al., 1974; Eppinger, 1976; Viano, 1978; Alem et al., 1978; Kallieris and Mattern, 1979). The most common injury that occurs during sled tests with belted cadavers is rib fractures (Viano, 1978; Crandall et al., 1997; Kallieris et al, 1998). Also, it is known that rib fracture patterns vary by restraint type (Kallieris et al, 1998). Kent et al. (2001) evaluated the injury predictive value of hard tissue criteria by varying restraint conditions and found that compression is the best indicator of fracture risk. Moreover, there is a significant effect on the fracture patterns due to belt only, airbag only, and combined belt and airbag loading.

Kent (2002) noted that one of the problems with global methods used to develop thoracic injury criteria is that the criteria correlate with injury without necessarily being functionally related to injury, in contrast to stress and strain. Previous studies aimed at determining thoracic injury criteria generally rely on the same set of cadaver impact tests, which all provide censored injury data. In other words, it is not possible to determine the exact loads, accelerations, or

displacements at the time of fracture. Rather, one only knows that an injury occurred at some point during the impact test. In order to address this limitation, this study presents a method to generate non-censored rib fracture data. Although previous studies have shown the ability to detect selected rib fractures, no method has been successful at mapping the exact fracture timing of the entire thorax during dynamic belt loading. Therefore, the purpose of this study is to develop a method for determining non-censored rib fracture data and to present results from dynamic belt loading tests on the human cadaver thorax using this method.

Methods

This study presents a total of four dynamic non-destructive and four dynamic destructive thoracic shoulder belt loading tests that were performed using four cadavers. Two back support conditions and two compression levels were evaluated using a custom table top belt loading device. The details of the test subjects, instrumentation, experimental setup, and test methodologies are presented in this section.

Subject Information

Dynamic belt tests were performed on four frozen and thawed human cadavers (Table 30 and Table 31). It should be noted that chest depth measurements were taken from the middle of the sternum, i.e. midpoint between the superior portion of the manubrium and the inferior portion of the gladiolus, to the back of the thorax. For comparison with the standard population, the bone mineral density (BMD) of each cadaver was determined by the Osteogram technique (Hardy et al. 2001a; Stitzel et al., 2003; Kemper et al., 2005). For this technique, the left hand of each cadaver was x-rayed next to an aluminum calibration wedge. The x-ray was then processed by

CompuMed Incorporated (CompuMed, Inc., Los Angeles, CA) to obtain the BMD, T-Score, and Z-score for each subject. This type of BMD measurement, however, only provides an indication of overall bone quality and does not account for local changes in bone density or composition. Therefore, the BMD obtained through this method is referred to as the "global BMD." The T-score is the number of standard deviations from the average value of healthy living individuals between 25 and 50 years of age. The Z-score is the number of standard deviations from the average value of healthy living individuals of similar age. The World Health Organization classifies normal bone as T-scores of -1.0 or greater, osteopenia as T-scores between -1.0 and -2.5, and osteoporosis as T-scores below -2.5 (Wolf and Pfleger, 2003).

Table 30: Subject and Osteogram data for cadavers used in belt loading.

Subject ID	Gender	Age	Mass	Height	BMD	T-score	Z-score
		(years)	(kg)	(cm)			
Sm_B1	Male	73	84.4	173	75.7	-3.2	-1.4
Sf_B2	Female	73	45.4	154	73.7	-3.4	-0.7
Sm_B3	Male	65	76.8	183	110.1	-0.1	1.1
Sf_B4	Female	69	50.9	155	72.4	-3.5	-1.0

Table 31: Subject anthropometry for cadavers used in belt loading.

Subject ID	Chest Circumference		Chest Breadth	Chest Depth
	Maximum	Center of Sternum		
	(mm)	(mm)	(mm)	(mm)
Sm_B1	1140	1070	370	230
Sf_B2	700	740	280	165
Sm_B3	813	787	305	235
Sf_B4	813	813	305	254

Thoracic Strain Gages

Cadavers Sm_B1 and Sf_B2 were instrumented with a total of 47 strain gages; 26 single-axial strain gages (Vishay Measurements Group, CEA-06-062UW-350, Malvern, PA) and 7

rectangular rosette strain gages (Vishay Measurements Group, CEA-06-062UR-350, Malvern, PA) (Figure 62). The first "R" in the rib strain gage labels stands for "Rib". Similarly, the first letters on the clavicle and sternum strain gage labels "CR", "SU", and "SL" stand for clavicle, upper sternum, and lower sternum respectively. The first number represents the number of the rib. The second letter "R" or "L" stands for the right side or left side of the thorax, respectively. The first letter after the dash, "S" or "R", stands for single-axis or rosette strain gage. The gages were numbered one to three bilaterally for ribs containing multiple gages. The number "1" gage corresponded to the gage closest to the sternum on each side, and the number "3" gage was the most distal gage from the sternum. The last letter "A", "B", or "C" only concerned the rosette strain gages and identified the gage position within the rosette. For example, the strain gage label R3R-R3A stands for gage A of a rosette on the lateral right side of rib 3.

Cadavers Sm_B3 and Sf_B4 were instrumented with a total of 26 single-axial strain gages (Vishay Measurements Group, CEA-06-062UW-350, Malvern, PA) (Figure 63). The strain gages were located on the lateral external surface of ribs 2-10 as well as the anterior external surface of ribs 3, 4, and 5. In addition, single-axial strain gages were placed on the right clavicle and the center of the sternum. For the strain gage labeling, the first "R" in the rib strain gage labels stands for "Rib". Similarly, the first letters on the clavicle "CR" and sternum "ST" strain gage labels stand for clavicle and sternum, respectively. The number represents the number of the rib. The second letter "R" or "L" stands for the right side or left side of the thorax, respectively. It should be noted that for the female gages R-6-A and L-6-A were not applied to the thorax because preexisting fractures were documented prior to testing.

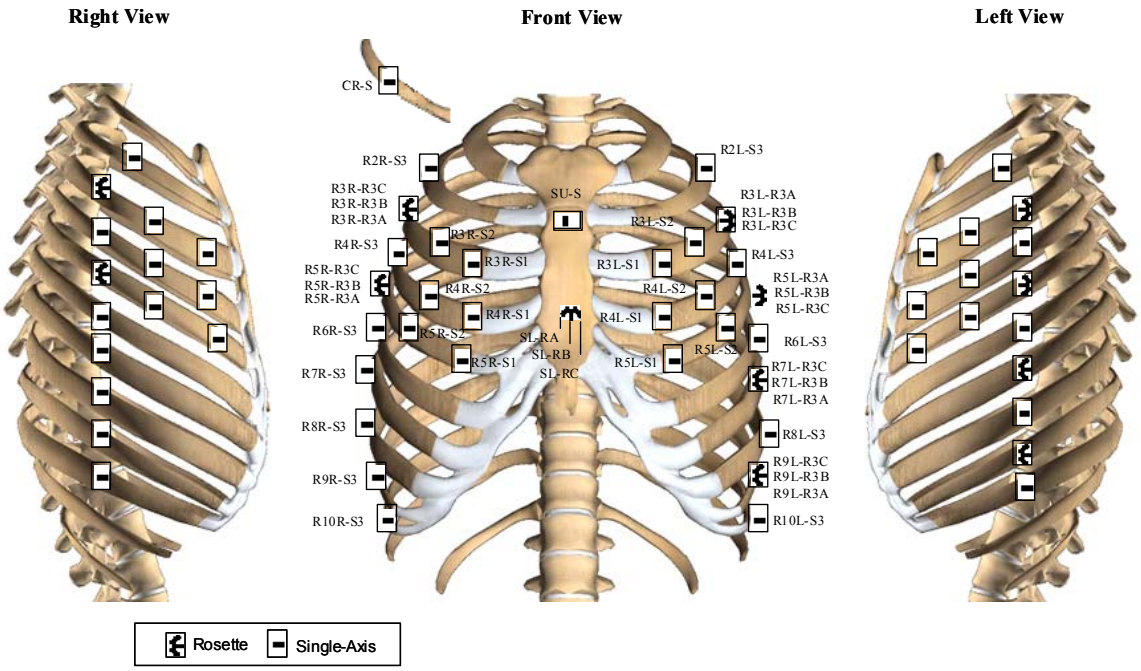

Figure 62: Strain gage locations for cadavers Sm_B1 and Sm_B2.

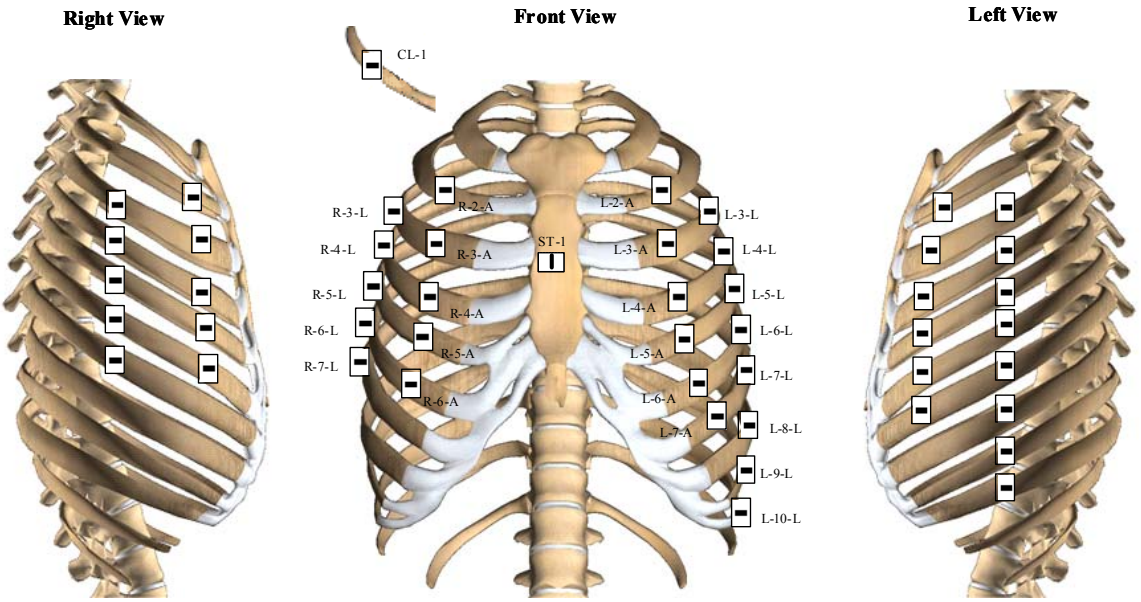

Figure 63: Strain gage locations for cadavers Sm_B3 and Sm_B4.

A number of detailed steps were taken in order to apply the strain gages to the ribs. First, the skin was carefully removed from the rib cage. Once the location of each strain gage was determined, the soft tissue and periosteum were removed from the external surface of the rib, and the bone was swabbed with ether to locally dry the bone. Upon drying, an acidic solution (Vishay Micro-Measurement, Conditioner A, Shelton, CT) was applied to the surface with a clean piece of gauze in order to etch the surface of the bone. Then a basic solution (Vishay Micro-Measurement, Neutralizer 5A, Shelton, CT) was applied to the surface in order to neutralize the acidic solution. The gage was removed from its case and prepared for mounting by applying a catalyst (Vishay Micro-Measurement, M-Bond 200 Catalyst, Shelton, CT) to the underside of the gage. Next, an adhesive (Vishay Micro-Measurement, M-Bond 200 Adhesive, Shelton, CT) was applied to the bone and the gage was quickly pushed over the adhesive in a rolling manner. The strain gage was covered with a small piece of latex and was held with firm pressure for 3 minutes (Figure 64 and Figure 65). Special care was taken to align each gage with the axis of the rib. The strain gage wire was strain relieved with a zip tie placed around the rib. Finally, the skin covering the rib cage was sutured back together.

Figure 64: Example thoracic strain gage attachment for belt loading tests.

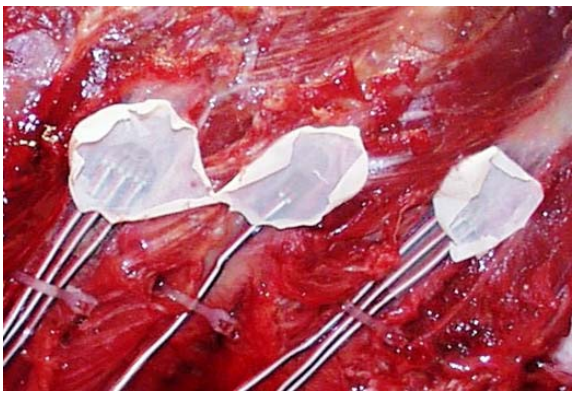

Latex Cover in Place

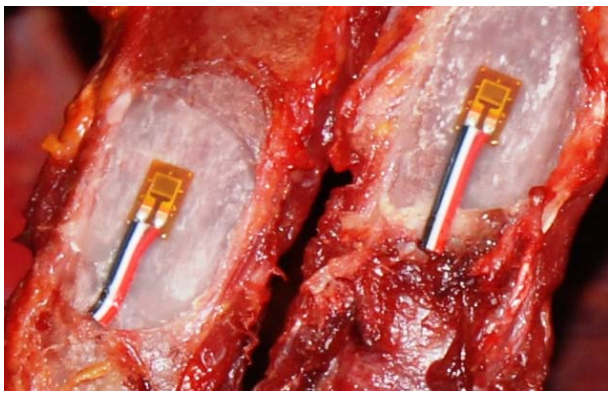

Latex Cover Removed after Testing

Figure 65: Strain gages shown mounted to the human cadaver ribs.

The strain output from the three gages that composed each rosette was used to calculate the first and second principal strains and the angle Phi (Φ). Phi was defined as the angle from the gage reference axis (labeled X-Y) to the first principal axis (Figure 66). In order to compare the direction of the first principal strain in relation to the axis of the rib, the angle from the axis of the rib (measured by the B gage of the rosette) to the first principal axis, defined as Theta (θ), was calculated. The first and second principal strains and the angles were calculated with the following equations (Equations 4-6).

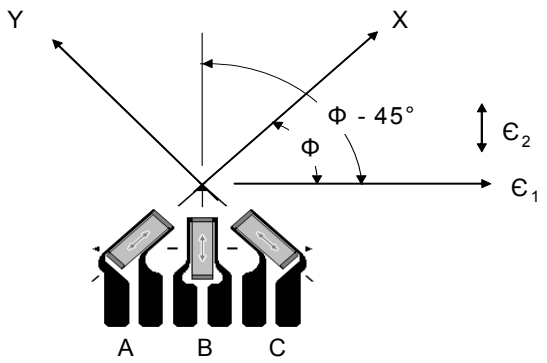

Figure 66: The angle Φ in reference to the gage reference axis, principal axis, and axis of gage B.

$$\varepsilon_{1,2} = \frac{\varepsilon_A + \varepsilon_C}{2} \pm \frac{1}{\sqrt{2}}\sqrt{(\varepsilon_A - \varepsilon_B)^2 + (\varepsilon_B - \varepsilon_C)^2} \qquad \text{(Eqn. 4)}$$

$$\phi_{1,2} = \frac{1}{2}\tan^{-1}\left(\frac{2\varepsilon_B - \varepsilon_A - \varepsilon_C}{\varepsilon_A - \varepsilon_C}\right) \qquad \text{(Eqn. 5)}$$

$$\theta_{1,2} = \left(\frac{1}{2}\tan^{-1}\left(\frac{2\varepsilon_B - \varepsilon_A - \varepsilon_C}{\varepsilon_A - \varepsilon_C}\right)\right) - 45^\circ \qquad \text{(Eqn. 6)}$$

Where:

ϵ_A = Strain output from gage A of the rosette

ϵ_B = Strain output from gage B of the rosette

ϵ_C = Strain output from gage C of the rosette

θ_1 = the angle from the axis of the rib to the first principal axis

θ_2 = the angle from the axis of the rib to the second principal axis

These equations were derived from the Mohr diagram for strain. It should be noted that the Mohr diagram for strain plots 2Φ, and due to the fact that $\tan 2\Phi = \tan 2(\Phi + 90)$, the equation for Φ can give either the angle from the axis of the rib to the first or second principal axis. The ambiguity was easily resolved by applying the following rules. In the case that $\theta_{1,2} = \theta_2$, θ_1 was obtained by simply adding 90 degrees to θ_2. This was done on a case by case basis.

1) If $\epsilon_A > \epsilon_C$, then $\theta_{1,2} = \theta_1$

2) If $\epsilon_A < \epsilon_C$, then $\theta_{1,2} = \theta_2$

Experimental Setup

The primary components of the belt loading system were a material testing machine (MTS Systems Corporation, MTS-810, Eden Prairie, MN) and a rigid loading table (Figure 67 and Figure 68). The thorax of each cadaver was placed over a rigid plate that distributed the applied load over four load cells to measure the reaction loads of the thorax. The 5 cm wide nylon loading belt was situated 40° from the sagittal plane of the body. The orientation of the belt simulated a passenger side seat belt, going over the right clavicle and left side of the abdomen. A series of wire cables and pulleys connected the hydraulic piston of the MTS, which loaded the cable/belt system at the desired rate. The locations of the pulleys were adjustable to accommodate cadavers of various sizes as well as to alter the angle of the belt relative to the table top. A slack reducer, connecting the primary wire cables to two secondary wire cables, served to displace the ends of the loading belt equally as well as remove slack from the system. The deflection of the thorax was measured using three string potentiometers (Space Age Control, 160, Palmdale, CA) that were attached to the belt at the center of the sternum. Percent chest compression was defined as the ratio of chest depth during the test to the chest depth measured prior to the test. Additionally, an accelerometer (Endevco Corporation, 7264B-2000G, San Juan Capistrano, CA) was mounted on the belt at the sternum and load cell plate to acquire chest acceleration and table vibration. Belt tension was measured with two load cells (Interface, Inc., SSM-AJ, 13kN, Scottsdale, AZ) placed in line with the belt. Four additional load cells (Denton ATD, Inc., 5768-11 kN, Rochester Hills, MI), (Denton ATD, Inc., 1968-22 kN, Rochester Hills, MI), (Denton ATD, Inc., 1716A-13 kN, Rochester Hills, MI) where located between the cadaver and loading table. The forces from all four load cells were summed to obtain the total reaction force.

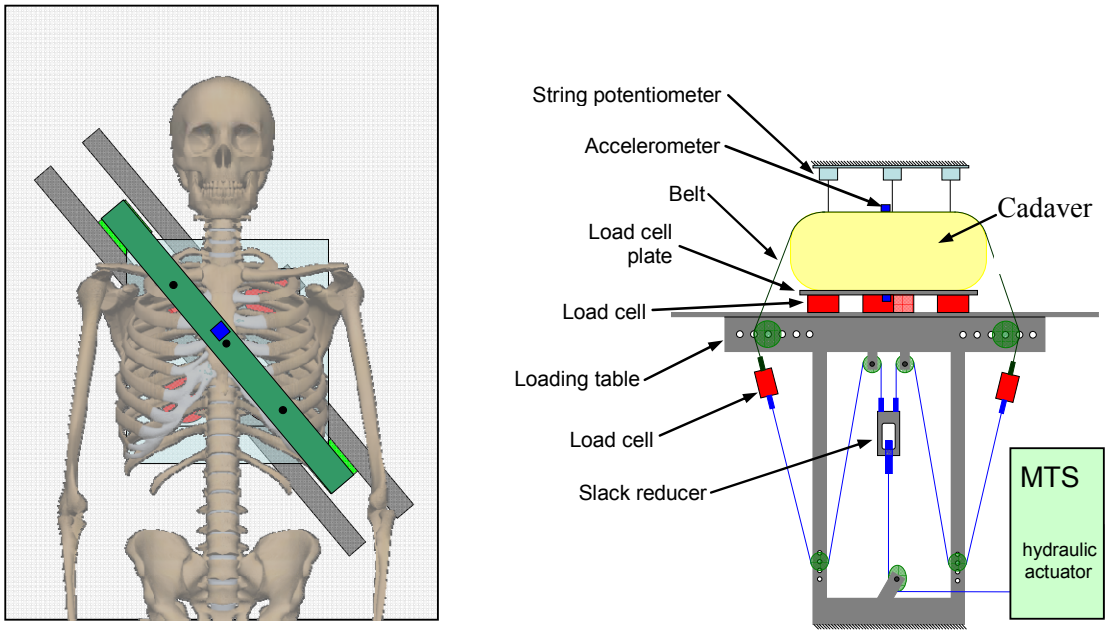

Figure 67: Top and oblique view of belt loading system.

Figure 68: Oblique views of actual belt loading system.

Testing Configurations

Four types of tests were performed: an 8% chest compression test with a flat back support; an 8% chest compression test with a custom spine support box; a maximum chest compression test with the flat back support, and a maximum chest compression test with a custom spine support box. The spine support box was designed support to the thorax on either side of the spinous process, which allowed free motion at the costovertebral joints. The design of the spine support bracket was similar to that used by Ali and Kent (2005). The spine support bracket used for this series of tests; however, was constructed of modular sections of varying height. This provided the ability to customize the bracket to the spinal curvature of a specific cadaver (Figure 69). The spine support bracket was assembled to support the spine from approximately T1 to L1 of each cadaver. The order of the testing was varied between cadavers in order to determine if there were any artifacts due to a specific back support condition (Table 32).

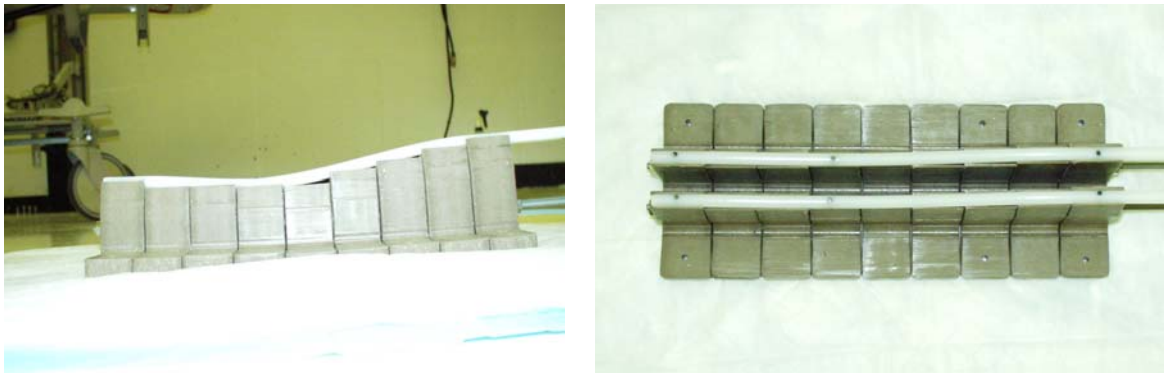

Side View Top View

Figure 69: Custom spine support bracket used for belt loading tests.
Note: Bracket for cadaver Sm_B3 shown.

Table 32: Belt loading test matrix.

Subject ID	Test Order	Back Support	Goal Compression
Sm_B1	1	Flat	Maximum Compression
Sf_B2	2	Flat	Maximum Compression
Sm_B3	3	Flat	8 % of Original Chest Depth
Sm_B3	4	Spine Box/Bracket	8 % of Original Chest Depth
Sm_B3	5	Spine Box/Bracket	Maximum Compression
Sf_B4	6	Spine Box/Bracket	8 % of Original Chest Depth
Sf_B4	7	Flat	8 % of Original Chest Depth
Sf_B4	8	Spine Box/Bracket	Maximum Compression

In order to minimize differences in the thoracic response due to multiple loading, each cadaver was preconditioned prior to each test by placing a large flat 9.07 kg mass on the thorax five times for 10 seconds at one minute intervals. Before each test the MTS was used to slightly pretension the belt (75-80 N for the male, 58-75 N for the female). In order to simulate *in vivo* conditions, the test subjects' pulmonary systems were inflated to 14 kPa immediately prior to each test, which corresponds to the mean inspiration pressure, with a tracheostomy tube connected to a pressure regulator. The depth of the inflated chest was then measured and recorded.

Results

Non-Destructive Belt Loading Tests

The total reaction force versus percent compression response for the two back support conditions was similar for both cadavers Sm_B3 and Sf_B4 (Figure 70 and Figure 71). The total force; however, was slightly higher for the tests with the flat back support for both cadavers; 13% higher for the male, and 17% for the female. The individual strains at 8% chest compression for the two back support conditions were compared for Sm_B3 and Sf_B4 (Table 33 and Table 34). The percent difference was calculated by taking the absolute value of the difference in peak strain between the two back support conditions divided by the average peak strain between the two back support conditions multiplied by 100.

For cadaver Sm_B3, the majority of the strain gages had similar strain values for both tests. However, there were a few strain gages that had significantly higher outputs for the test in which the spine box was used. For cadaver Sf_B4, rib fractures were detected on strain gages: R-4-R, L-5-A, and L-7A after performing the 8% compression test with the spine box. Given that the test with the spine box was performed first on cadaver Sf_B4, it is difficult to make a direct comparison between tests for these rib locations. In addition, strain gages for the anterior side on rib six were not applied due to pre-existing fractures documented prior to testing. Although the majority of the strain gages had similar strain values for both tests, there were a few strain gages that had significantly higher outputs for the test in which the spine box was used.

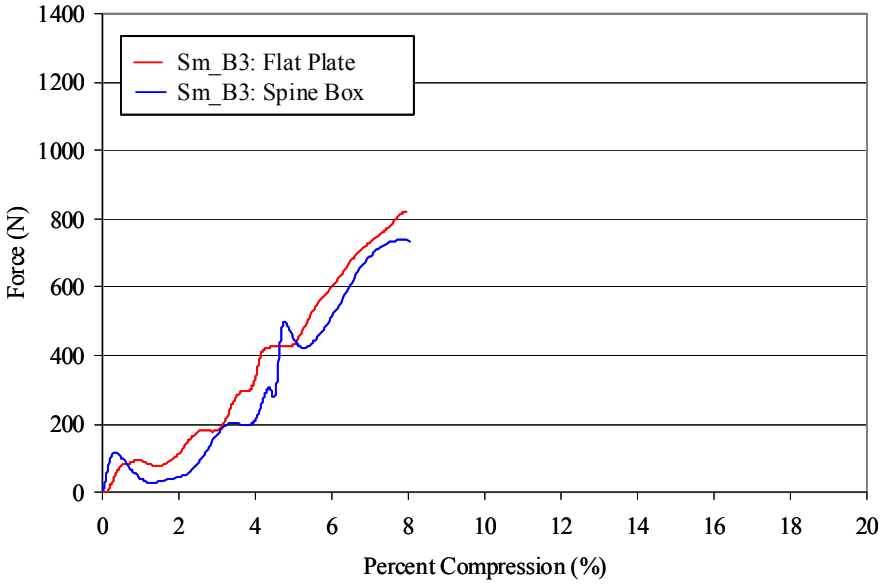

Figure 70: Comparison between back support conditions- Force vs. Compression – Sm_B3.

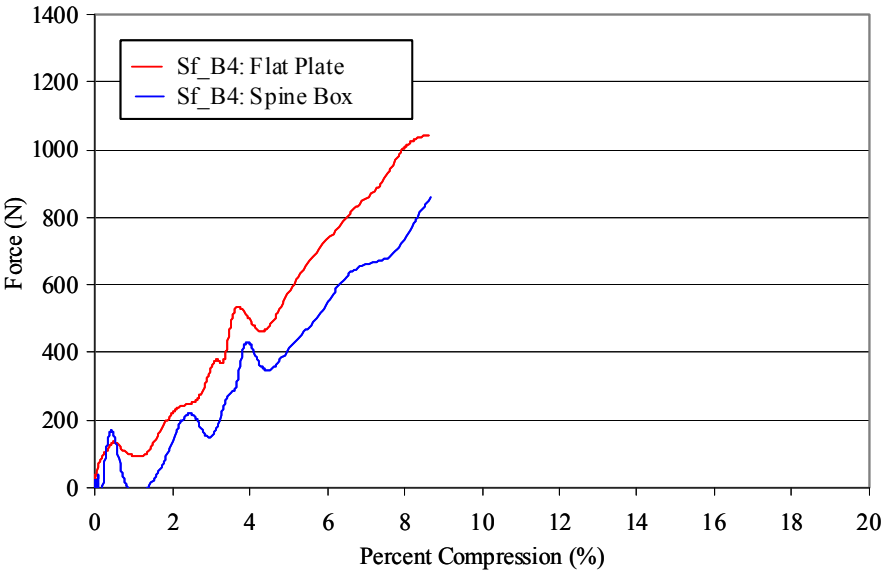

Figure 71: Comparison between back support conditions- Force vs. Compression – Sf_B4.

Table 33: Comparison between back support conditions- peak strain - Cadaver Sm_B3.

Region	Strain Gage ID	Flat Plate Peak Strain (μstrain)	Spine Box Peak Strain (μstrain)	Percent Difference (μstrain)
Clavicle & Sternum Gages	SG-CL	-228.3	-141.2	47.1
	SG-ST	-845.0	-439.5	63.1
Right Anterior Strain Gages	SG-R2A	431.8	-115.3	345.7
	SG-R3A	2582.6	2255.5	13.5
	SG-R4A	1806.8	1849.4	2.3
	SG-R5A	1122.8	1280.0	13.1
	SG-R6A	363.9	434.4	17.6
Right Lateral Strain Gages	SG-R3L	2667.1	2355.3	12.4
	SG-R4L	1889.6	2174.4	14.0
	SG-R5L	514.0	1055.7	69.0
	SG-R6L	194.3	700.3	113.1
	SG-R7L	-20.1	320.1	226.9
Left Anterior Strain Gages	SG-L2A	897.4	1674.0	60.4
	SG-L3A	2158.9	2268.4	4.9
	SG-L4A	2685.5	3014.4	11.5
	SG-L5A	1703.9	2329.9	31.0
	SG-L6A	1181.2	1464.8	21.4
	SG-L7A	1412.7	1282.4	9.7
Left Lateral Strain Gages	SG-L3L	1041.3	777.6	29.0
	SG-L4L	954.8	838.1	13.0
	SG-L5L	1986.7	2163.1	8.5
	SG-L6L	2810.7	3188.1	12.6
	SG-L7L	2807.3	2941.5	4.7
	SG-L8L	2751.9	2866.3	4.1
	SG-L9L	1428.1	1353.6	5.4
	SG-L10L	609.0	596.4	2.1

Table 34: Comparison between back support conditions- peak strain - Cadaver Sf_B4.

Region	Strain Gage ID	Flat Plate Peak Strain (µstrain)	Spine Box Peak Strain (µstrain)	Percent Difference (µstrain)
Clavicle & Sternum Gages	SG-CL	-38.4	393.4	243.3
	SG-ST	1032.8	1132.1	9.2
Right Anterior Strain Gages	SG-R2A	653.7	189.6	110.1
	SG-R3A	*	*	*
	SG-R4A	199.3	3925.8	180.7
	SG-R5A	1146.7	1692.2	38.4
	SG-R6A	*	*	*
Right Lateral Strain Gages	SG-R3L	*	*	*
	SG-R4L	173.4	146.2	17.0
	SG-R5L	-333.4	99.8	370.8
	SG-R6L	444.7	764.9	52.9
	SG-R7L	395.5	433.0	9.1
Left Anterior Strain Gages	SG-L2A	2688.2	2229.6	18.6
	SG-L3A	*	*	*
	SG-L4A	1266.0	1438.7	12.8
	SG-L5A	-11.1	-2101.9	197.9
	SG-L6A	*	*	*
	SG-L7A	-778.9	-3581.1	128.5
Left Lateral Strain Gages	SG-L3L	*	*	*
	SG-L4L	-623.0	-39.9	175.9
	SG-L5L	632.5	351.7	57.1
	SG-L6L	728.1	1224.5	50.8
	SG-L7L	-276.3	-60.0	128.6
	SG-L8L	4744.1	5148.0	8.2
	SG-L9L	3884.6	4311.3	10.4
	SG-L10L	2640.8	3569.0	29.9

Note: * Indicates that a fracture was detected after the first test.

Destructive Belt Loading Tests

In order to validate that thoracic loading rates during the destructive belt loading tests were representative of that observed in an actual severe crash, the data from the current study was compared to data obtained from actual 48 kph sled tests performed on human cadavers (Figure 72). It can be seen that the thoracic deflection rates produced from the tests in the current study closely match those seen in actual sled tests.

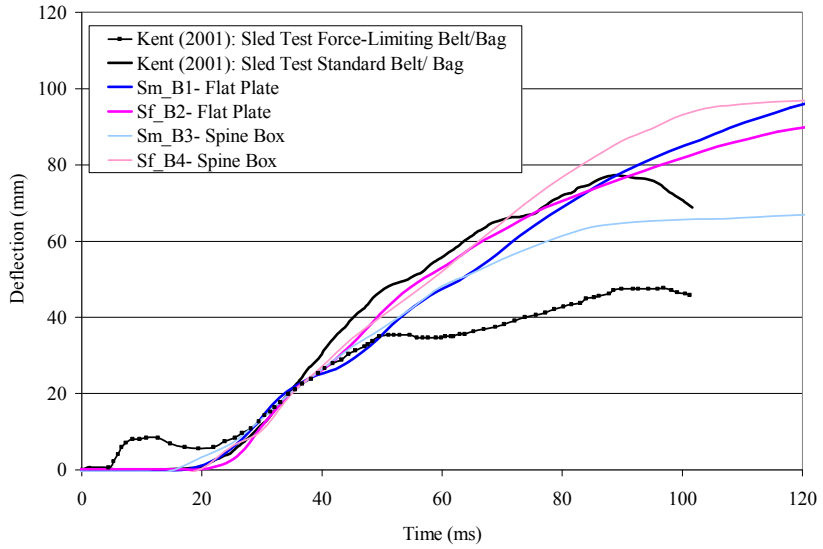

Figure 72: Chest deflection rate of cadavers in a 48 kph Sled Test (Kent, 2001) versus current study data.

The total reaction force versus percent compression was plotted for all destructive belt loading tests (Figure 73). Although the full travel of the MTS (15 cm) was used to fully compress the chest of each cadaver, the chest deflection and chest compression values at the point of peak force varied for each cadaver (Table 35). The MTS was actuated at 150 cm/s, which compressed the cadaver thoraces at a rate of 0.94 m/s to 1.0 m/s. The difference in the rate of the MTS and the rates seen by the cadavers was due to inertial effects and friction in the cable system. The

effective stiffness of the thorax under these conditions was determined by performing a linear regression of the force vs. percent deflection plots from 0% to 20% compression (Table 35). The differences in thoracic stiffness are most likely due to cadaver variation.

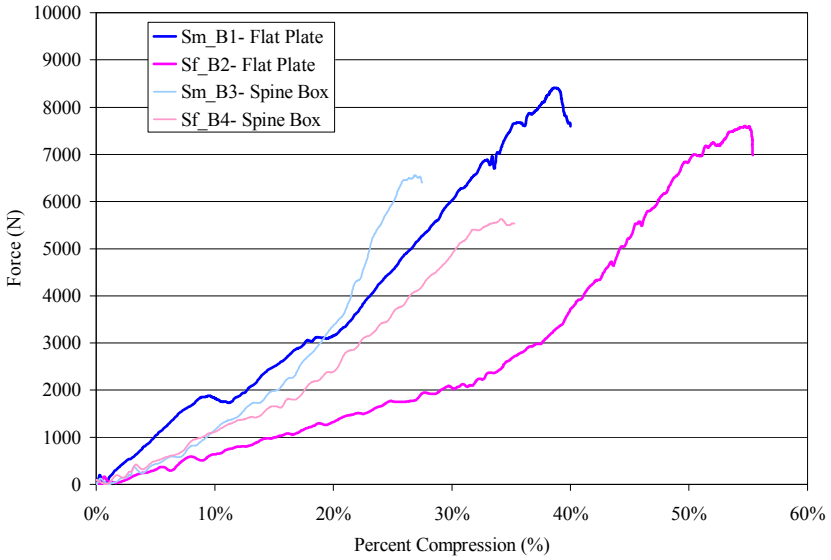

Figure 73: Force versus percent compression for destructive belt loading tests.

Table 35: Peak chest deflection and compression for destructive belt loading test.

Subject ID	Back Support	Chest Loading Rate	Thoracic Stiffness	Chest Deflection at Peak Force	Chest Compression at Peak Force
		(m/s)	(N/ % deflection)	(mm)	(%)
Sm_B1	Flat	0.97	16897.8	97.0	38.8
Sf_B2	Flat	0.94	6580.1	90.2	54.7
Sm_B3	Spine Box	1.00	13619.3	64.2	27.3
Sf_B4	Spine Box	1.30	11188.9	86.7	34.1

Principal Strain Results

The first principal strain, second principal strain, and the axial strain were plotted along with the angle from the axis of the rib to the first principal axis (Figure 74). In general, it was found that the first principal strain and the axial strain closely matched up to the time of the first fracture. In

some cases the first principal strain and the axial strain continued to follow each other after the fracture and in other cases they did not. This could be due to either broken or damaged gages and or the complex loading seen after the fracture.

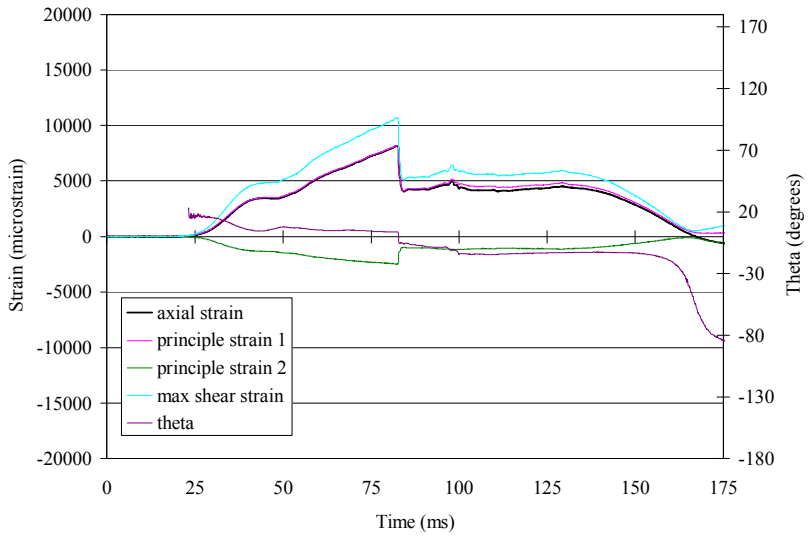

Figure 74: Axial strain, first and second principal strain, and theta vs. time example plot.

Note: Rosette R3R for Sm_B1- rigid back shown.

The maximum of the first and second principal strain before or at the first fracture were compared to the peak axial strain for each cadaver (Table 36 and Table 37). The peak strains before or at the time of the first fracture were used because the strain could no longer be reported with confidence after the rib fracture due to the complexity of loading and possibility of damage to the gage. If no fracture occurred, then the strains reported were those that corresponded to the time at which the absolute maximum strain out of the three occurred. In some the cases where the rib was too small to adequately support all three gages of the rosette the data was suspect and

thereby not reported in this section. Additionally, if one or more of the gages that composed each rosette broke during the test the data was omitted from this section.

Table 36: Axial strain vs. first principal strain for the cadaver Sm_B1- flat plate.

Rosette	Thorax Location		Peak Gage B Strain (µstrain)	Peak Principal Strain 1 (µstrain)	Percent Difference (%)	Peak Principal Strain 2 (µstrain)	θ (degrees)
R3R	Rib 3	Right Side	22111	23105	4.4	-8996	10.2
R5R	Rib 5	Right Side	8165	8223	0.7	-2465	3.8
R3L	Rib 3	Left Side	5890	6406	8.4	-636	-15.1
R5L	Rib 5	Left Side	6499	6661	2.5	-1605	-8.1
R7L	Rib 7	Left Side	6618	6773	2.3	-1792	-7.8
R9L	Rib 9	Left Side	3033*	3482*	13.8*	1844*	-17.0*

Note: * indicates not measured at a time of fracture.

Table 37: Axial strain vs. first principal strain for the cadaver Sf_B2- flat plate.

Rosette	Thorax Location		Peak Gage B Strain (µstrain)	Peak Principal Strain 1 (µstrain)	Percent Difference (%)	Peak Principal Strain 2 (µstrain)	θ (degrees)
R3R	Rib 3	Right Side	5246	6142	15.7	-1581	19.9
R5R	Rib 5	Right Side	4641	4986	7.2	-3386	10.8
SL	Sternum	Lower	-4860*	12819*	444.3*	-5864*	76.6*
R3L	Rib 3	Left Side	2046	2325	12.8	-896	-18.1
R5L	Rib 5	Left Side	10109	10109	0.0	2735	0.1
R7L	Rib 7	Left Side	11357	11881	4.5	-674	12.6

Note: * indicates not measured at a time of fracture.

Injury Analysis

The rib fracture locations were determined by performing a post-test injury analysis on each cadaver using a detailed necropsy of the thorax. The number of rib fractures for each cadaver is summarized in Table 38. The distribution of rib fractures was documented for each cadaver (Figure 75 to Figure 78). Sf_B4 had three pre-existing fractures which were not included in the

fracture analysis: two bilaterally on rib three, and one on rib six on the left side of the thorax. There were no injuries to the internal organs.

The AIS (Abbreviated Injury Scale, 2005) has multiple definitions for AIS=3 injury level based on rib fractures: ≥ 3 rib fractures without flail- any location unilateral or bilateral; fractures with flail- not further specified; unilateral fractures with flail- not further specified; and unilateral fractures with flail- 3 to 5 ribs with multiple fractures. The AIS defines flail chest as three or more ribs fractured in more than one location, i.e. posterior lateral and anterior lateral, and/or results in paradoxical chest motion. Paradoxical chest motion is defined as breathing which results in all or part of a lung inflating during inspiration and ballooning out during expiration; the opposite of normal chest motion. Paradoxical chest motion occurs when multiple ribs are no longer rigidly attached to the rest of the rib cage due to fractures in two or more places. The AIS definition for AIS=4 injury level based on rib fractures is unilateral fractures with flail- > 5 ribs with multiple fractures. Using rib fractures as the parameter, AIS injury level was determined to be AIS=3 for all cadavers except cadaver Sf_B2, which was determined to be AIS=4.

Table 38: Summary of rib fractures resulting from the destructive belt loading tests.

Subject ID	Back Support Condition	Clavicle Fractures	Sternum Fractures	Rib Fractures			AIS
				Left Side	Right Side	Total	
Sm_B1	Flat Rigid Plate	Right	None	8	4	12	3
Sf_B2	Flat Rigid Plate	None	Yes	14	6	20	4
Sm_B3	Spine Box/ Bracket	None	Yes	9	4	12	3
Sf_B4	Spine Box/ Bracket	None	None	5	3	8	3

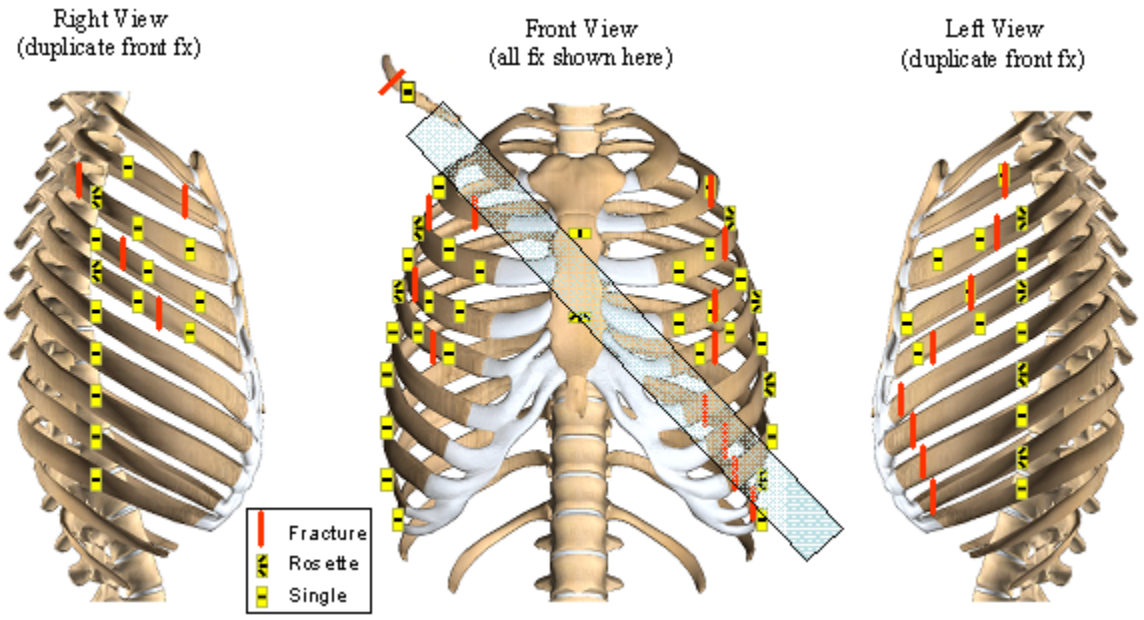

AIS=3

Figure 75: Location of strain gages and fractures for cadaver Sm_B1- flat plate.

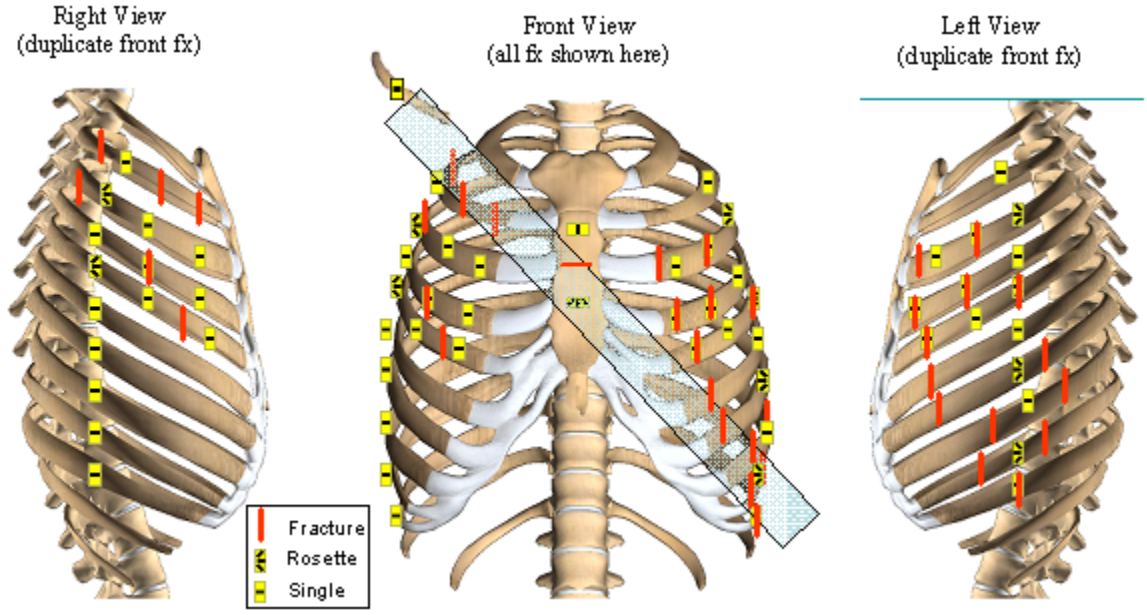

AIS=4

Figure 76: Location of strain gages and fractures for cadaver Sf_B2- flat plate.

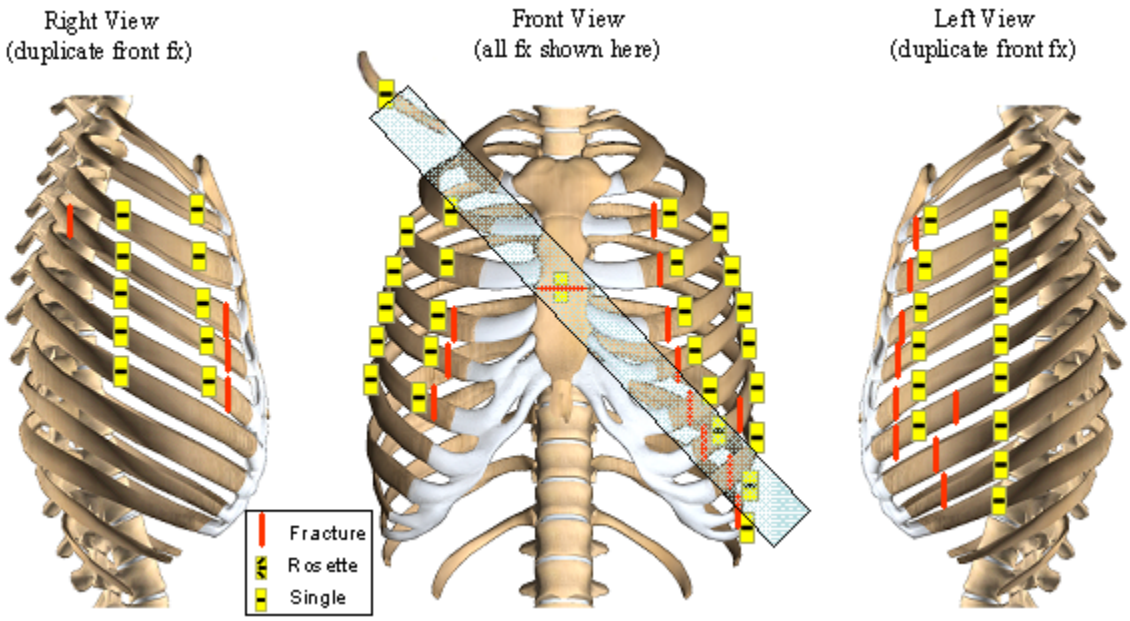

AIS=3

Figure 77: Location of strain gages and fractures for cadaver Sm_B3- spine box.

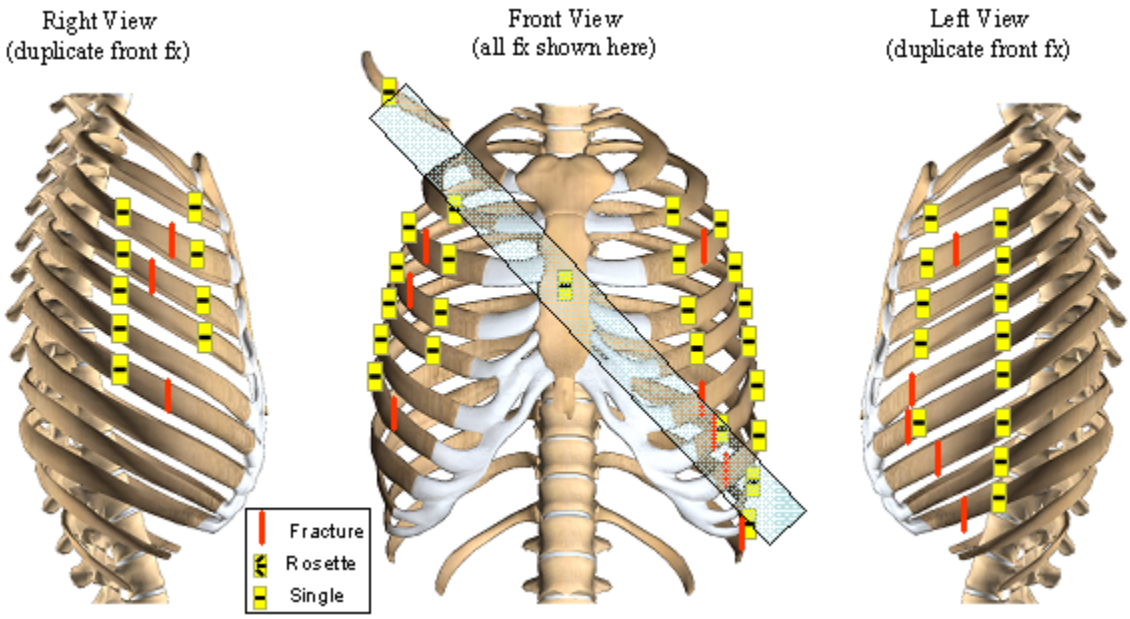

AIS=3

Figure 78: Location of strain gages and fractures for cadaver Sf_B4- spine box.

Rib Fracture Timing

The time histories of each strain gage were analyzed to determine the time at which each rib fracture occurred (Figure 79). The time of fracture could then be directly correlated to rib deflection (Table 39 to Table 42). The fractures that occurred directly under gages are of particular interest because the failure strain at the time of fracture could be obtained from these gages. The rib fracture timing with respect to the back support condition, spine box versus flat rigid plate, was evaluated for both male and female cadavers (Figure 80 and Figure 81). The tests performed in this study show a similar progression of rib fractures regardless of the back support condition. For all cadavers, all rib fractures occurred within the first 35% compression of the thorax. As a general trend, the first series of fractures were on the left side of the thorax where the belt passed over the abdominal region. The ribs in the upper thoracic region on the right side fractured next.

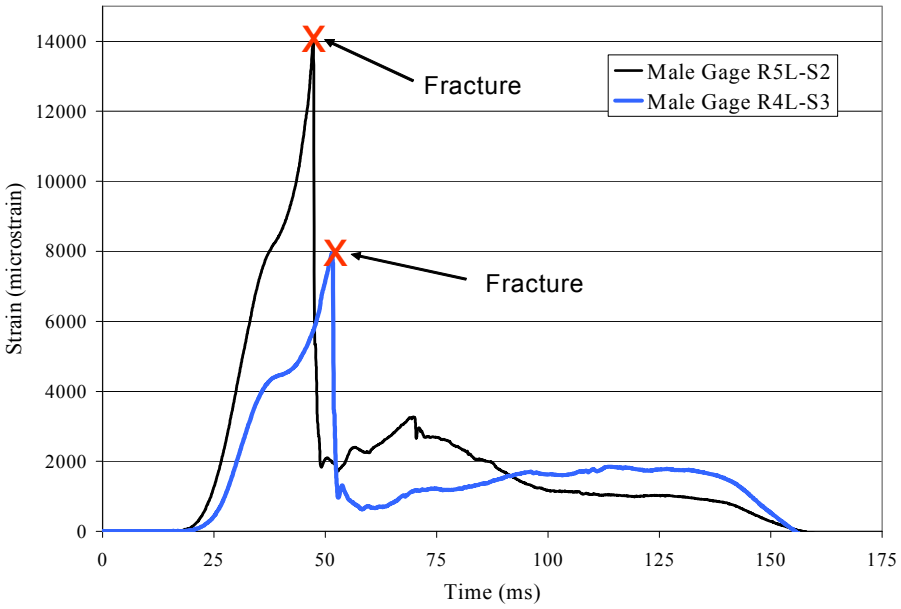

Figure 79: Determination of rib fracture timing during belt loading.

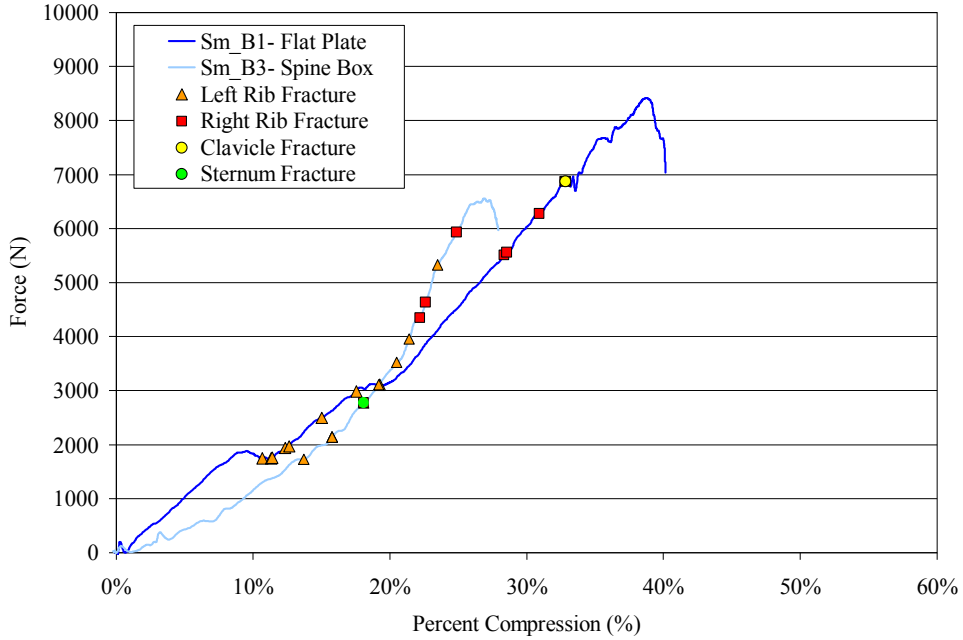

Figure 80: Male rib fracture timing with respect to back support condition.

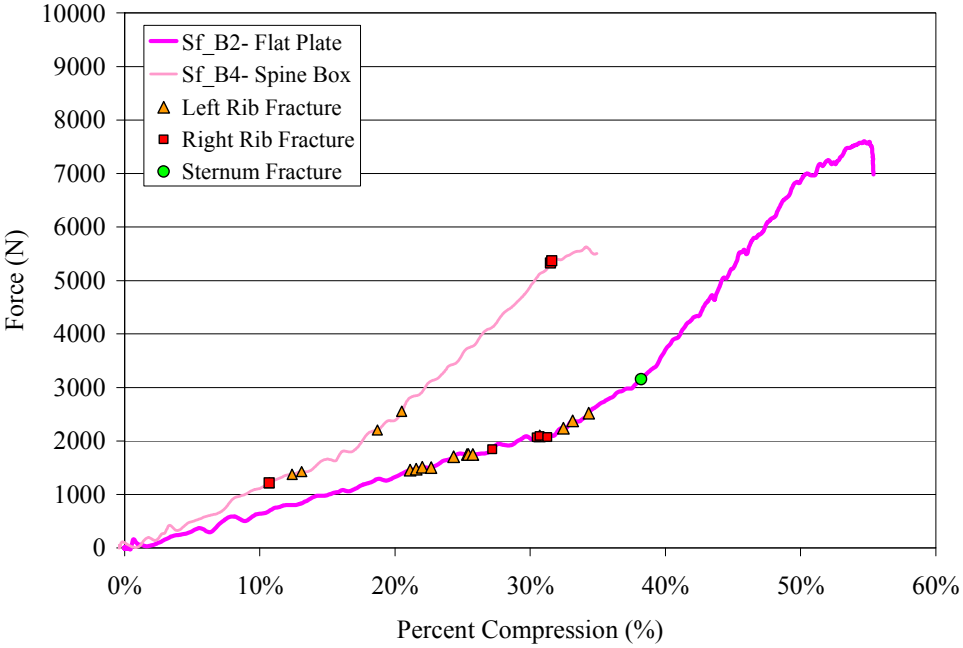

Figure 81: Female rib fracture timing with respect to back support condition.

Table 39: Fracture locations and timing for the cadaver Sm_B1.

Gage Location		Fracture Location from Closest Gage	Closest Gage	Time	Chest Compression	Strain at Time of Fracture
				(ms)	(%)	(µstrain)
Right Side	Clavicle	oblique, 25 mm lateral of	CR-S	95.5	32.86	-6577
	Rib 2	60 mm medial of gage	R2R-S3	81.9	28.29	13685
	Rib 3	10 mm lateral of rosette	R3R-R3B	88.9	30.87	22111
	Rib 4	30 mm lateral of gage	R4R-S2	95.2	32.77	13758
	Rib 5	15 mm medial of gage	R5R-S2	82.6	28.57	7252
	Rib 6	none	-----	-----	-----	-----
	Rib 7	none	-----	-----	-----	-----
	Rib 8	none	-----	-----	-----	-----
	Rib 9	none	-----	-----	-----	-----
	Rib 10	none	-----	-----	-----	-----
Left Side	Clavicle	none	-----	-----	-----	-----
	Rib 2	**immediately under gage**	**R2L-S3**	**53.9**	**16.42**	**11590**
	Rib 3	20 mm lateral of gage	R3L-S2	55.8	17.55	13328
	Rib 4	**immediately under gage**	**R4L-S2**	**51.4**	**15.09**	**15576**
	Rib 5	15 mm lateral of gage	R5L-S1	47.3	12.63	11741
	Rib 6	90 mm medial of gage	R6L-S3	44.7	11.42	6961
	Rib 7	80 mm medial of rosette	R7L-R3B	42.7	10.67	6618
	Rib 8	60 mm medial of gage	R8L-S3	46.7	12.36	3873
	Rib 9	60 mm medial of rosette	R9L-R3B	44.5	11.33	2284
	Rib 10	none	-----	-----	-----	-----
	sternum	none	-----	-----	-----	-----

Table 40: Fracture locations and timing for the cadaver Sf_B2.

Gage Location		Fracture Location from Closest Gage	Closest Gage	Time	Chest Compression	Strain at Time of Fracture
				(ms)	(%)	(µstrain)
Right Side	clavicle	none	-----	-----	-----	-----
	Rib 2	20 mm medial of gage	R2R-S3	52.3	27.2	2238
		60 mm medial of gage				
		30 mm lateral of gage				
	Rib 3	30 mm lateral of rosette	R3R-R3B	57.2	30.5	5246
	Rib 4	**immediately under gage**	**R4R-S2**	**57.6**	**30.7**	**6114**
	Rib 5	25 mm medial of gage	R5R-S2	58.6	31.3	4846
	Rib 6	none	-----	-----	-----	-----
	Rib 7	none	-----	-----	-----	-----
	Rib 8	none	-----	-----	-----	-----
	Rib 9	none	-----	-----	-----	-----
	Rib 10	none	-----	-----	-----	-----
Left Side	clavicle	none	-----	-----	-----	-----
	Rib 2	none	-----	-----	-----	-----
	Rib 3	10 mm medial of gage	R3L-S1	61.6	33.1	-8181
		immediately under gage	**R3L-S2**	**46.5**	**21.6**	**10907**
	Rib 4	**immediately under gage**	**R4L-S1**	**50.2**	**25.3**	**-7257**
		immediately under gage	**R4L-S2**	**49.1**	**24.4**	**9028**
	Rib 5	**immediately under gage**	**R5L-S1**	**50.3**	**25.4**	**-17193**
		immediately under rosette	**R5L-R3B**	**47.5**	**22.7**	**10109**
	Rib 6	85 mm medial of gage	R6L-S3	46.9	22.0	12211
	Rib 7	15 mm lateral of gage	R7L-R3B	46.1	21.1	11357
		80 mm medial of gage	R7L-R3B	60.6	32.5	-2772
	Rib 8	30 mm medial of gage	R8L-S3	50.7	25.8	2119
		30 mm lateral of gage				
	Rib 9	30 mm medial of gage	R9L-R3B	57.6	30.7	1540
		25 mm lateral of gage		63.3	34.2	-2976
	Rib 10	**immediately under gage**	**R10L-S3**	**63.1**	**34.2**	**6610**
	sternum	between the two sternum gages	SL-RB	70.3	38.1	-2110

Table 41: Fracture locations and timing for the cadaver Sm_B3.

Gage Location		Fracture Location from Closest Gage	Closest Gage	Time	Chest Compression	Strain at Time of Fracture
				(ms)	(%)	(µstrain)
Right Side	Clavicle	None	-----	-----	-----	-----
	Rib 2	None	-----	-----	-----	-----
	Rib 3	None	-----	-----	-----	-----
	Rib 4	17 mm medial of gage	R-4-A	58	22.2	4300
		50 mm posterior of gage	R-4-L	67	24.9	6500
	Rib 5	15 mm medial of gage	R-5-A	59	22.6	3600
	Rib 6	11 mm medial of gage	R-6-A	47	18.1	1150
	Rib 7	None	-----	-----	-----	-----
	Rib 8	None	-----	-----	-----	-----
	Rib 9	None	-----	-----	-----	-----
	Rib 10	None	-----	-----	-----	-----
Left Side	Clavicle	None	-----	-----	-----	-----
	Rib 2	10 mm medial of gage	L-2-A	47	18.1	4000
	Rib 3	17 mm medial of gage	L-3-A	42	15.8	4600
	Rib 4	23 mm medial of gage	L-4-A	42	15.8	9200
	Rib 5	19 mm medial of gage	L-5-A	62	23.5	5500
	Rib 6	20 mm medial of gage	L-6-A	37	13.7	2000
	Rib 7	15 mm medial of gage	L-7-A	42	15.8	1600
		36 mm medial of gage	L-7-A	52	20.5	1000
	Rib 8	87 mm medial of gage	L-8-L	49	19.2	10300
	Rib 9	77 mm medial of gage	L-9-L	55	21.4	9900
	Sternum	**immediately under gage**	**ST-1**	**47**	**18.1**	**2000**

Table 42: Fracture locations and timing for the cadaver Sf_B4.

Gage Location		Fracture Location from Closest Gage	Closest Gage	Time	Chest Compression	Strain at Time of Fracture
				(ms)	(%)	(μstrain)
Right Side	Clavicle	None	-----	-----	-----	-----
	Rib 2	None	-----	-----	-----	-----
	Rib 3	55 mm lateral of gage	R-3-A	25	10.7	-4300
	Rib 4	32 mm medial of gage	R-4-L	70	31.6	10800
	Rib 5	None	-----	-----	-----	-----
	Rib 6	None	-----	-----	-----	-----
	Rib 7	190 mm medial of gage	R-7-L	68	31.5	6800
	Rib 8	None	-----	-----	-----	-----
	Rib 9	None	-----	-----	-----	-----
	Rib 10	None	-----	-----	-----	-----
Left Side	Clavicle	None	-----	-----	-----	-----
	Rib 2	None	-----	-----	-----	-----
	Rib 3	30 mm lateral of gage	L-3-A	43	18.7	10000
	Rib 4	None	-----	-----	-----	-----
	Rib 5	None	-----	-----	-----	-----
	Rib 6	120 mm medial of gage	L-6-L	31	13.1	2000
	Rib 7	5 mm medial of gage	L-7-A	28	12.4	-5000
	Rib 8	135 mm medial of gage	L-8-L	25	10.7	9000
	Rib 9	None	-----	-----	-----	-----
	Rib 10	60 mm medial of gage	L-10-L	45	20.5	8200
	Sternum	None	-----	-----	-----	-----

Discussion

The thoracic testing conditions presented in this study are similar to those presented by Kent et al. (2003) in that they present thoracic data due to diagonal belt loading at a rate that corresponds to the thoracic loading rate seen in a 48 kph crash. Kent et al. (2003) determined the effective stiffness of the thorax under these conditions by performing a linear regression of the force versus percent deflection plots. These effective stiffness values for the male tests varied from 6,459 to 9,919 (N/% deflection) and from 7,102 to 15,420 (N/% deflection) for the female tests. The same method was performed on the force versus percent compression data presented in this study. The effective stiffness values for the male and female tests presented in the current study at were 13,619.3 to 16,897.8 (N/% deflection) for the male cadavers and 6,580.1 to 11,188.9 (N/% deflection) for the female cadavers. It is important to note that there were oscillations in the Kent et al. (2003) data during the initial loading phase which resulted in negative force. This indicates a tension force while the thorax was being compressed. Therefore, the Kent et al. (2003) stiffness data are likely lower than the actual response during the initial loading phase.

The comparison of back support conditions showed that there is no considerable difference between using a flat rigid plate and a spine box. For both cadavers, the stiffness was almost identical between tests performed with a flat rigid plate and those with a spine box. For male and female cadavers, the majority of the strain gages have similar strain values for both test conditions. However, there were a few strain gages that have significantly higher outputs for the test in which the spine box was used. Given the relatively low magnitudes of strain measured during these non-destructive tests, the difference in strain observed between the two back support conditions could be attributed to differences in the location of the belt relative to these gages.

The reaction force data was plotted versus the percent chest deflection data for these tests along with the fracture timing and corresponding AIS injury timing (Figure 82 to Figure 85). The timing of AIS=3 corresponded to the point at which the third rib fracture occurred. The timing of AIS=4 corresponded to the point at which six ribs had more than one fracture. For male cadavers, AIS=3 occurred at 13% -16% chest compression. For female cadavers, AIS=3 occurred at 13%-22% chest compression. The data from the current study was then compared to the thoracic injury criteria for the 50^{th} percentile male and 5^{th} percentile female Hybrid III frontal impact dummies as defined by NHTSA, which represents a 50% risk of an AIS=3 injury level. NHTSA has defined the injury criterion for the 50^{th} percentile Hybrid III dummy as a chest deflection of 63 mm, which corresponds to a 28%-30% chest deflection. The injury criterion for the 5th percentile female Hybrid III dummy has been defined as a chest deflection of 52 mm which corresponds to a 22%-24% chest deflection. The range of percent chest deflections is due to the variations in dummy chest thickness as a result of tolerances set by the manufacturer (Denton ATD, Inc.). The injury timing data presented in this study clearly shows that AIS $\geq$ 3 thoracic injuries in frontal belt loading occur at considerably lower chest deflections than the current respective male and female frontal thoracic injury criteria.

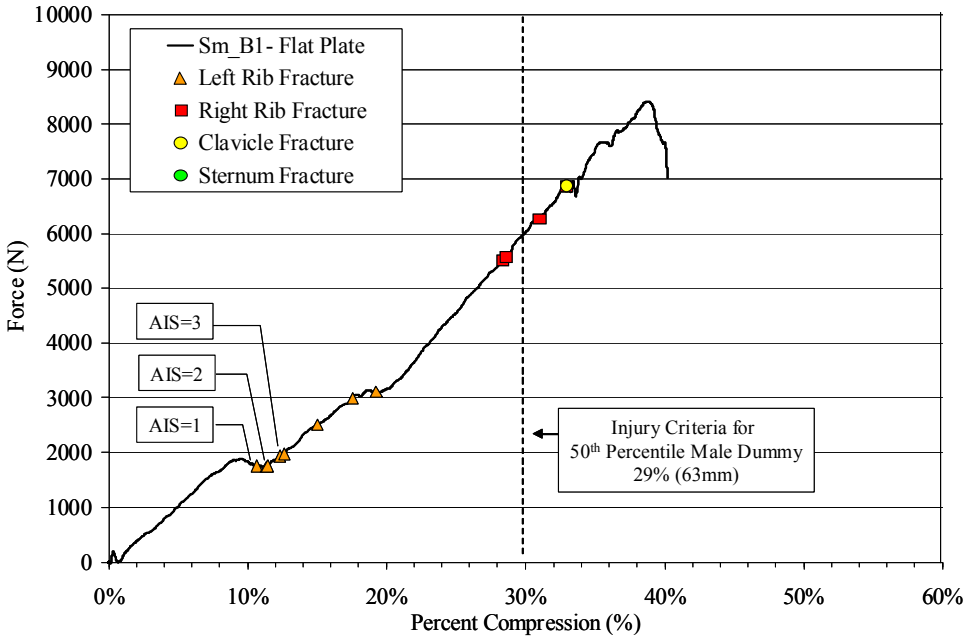

Figure 82: AIS injury timing due to belt loading for cadaver Sm_B1.

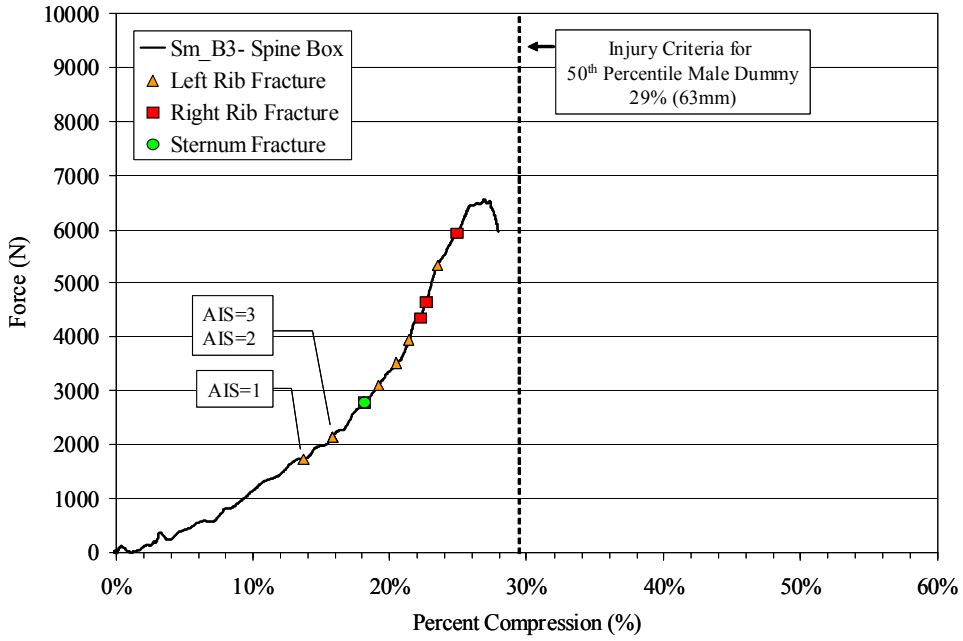

Figure 83: AIS injury timing due to belt loading for cadaver Sm_B3.

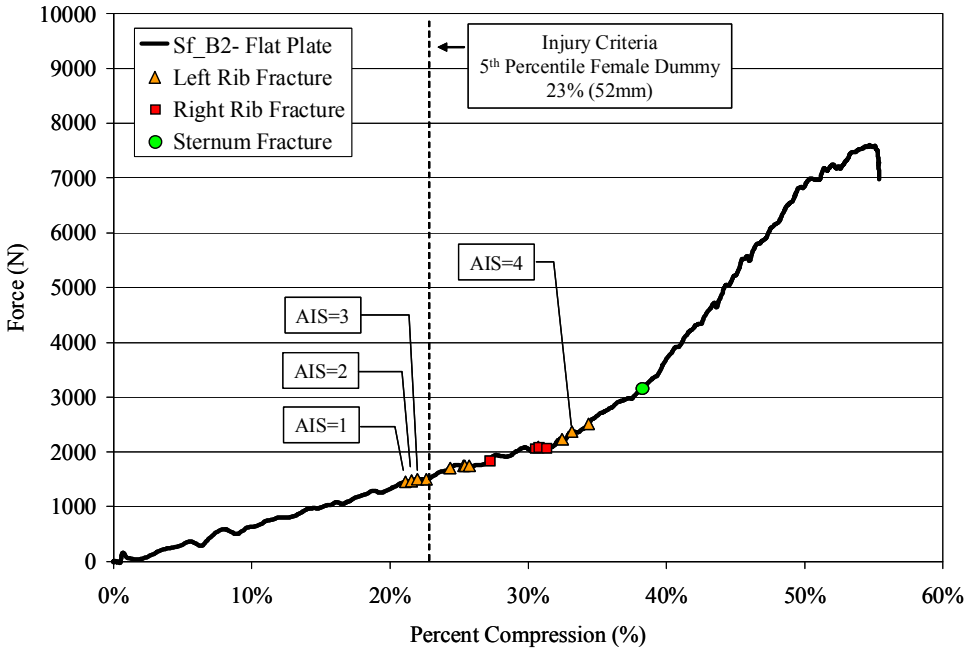

Figure 84: AIS injury timing due to belt loading for cadaver Sf_B2.

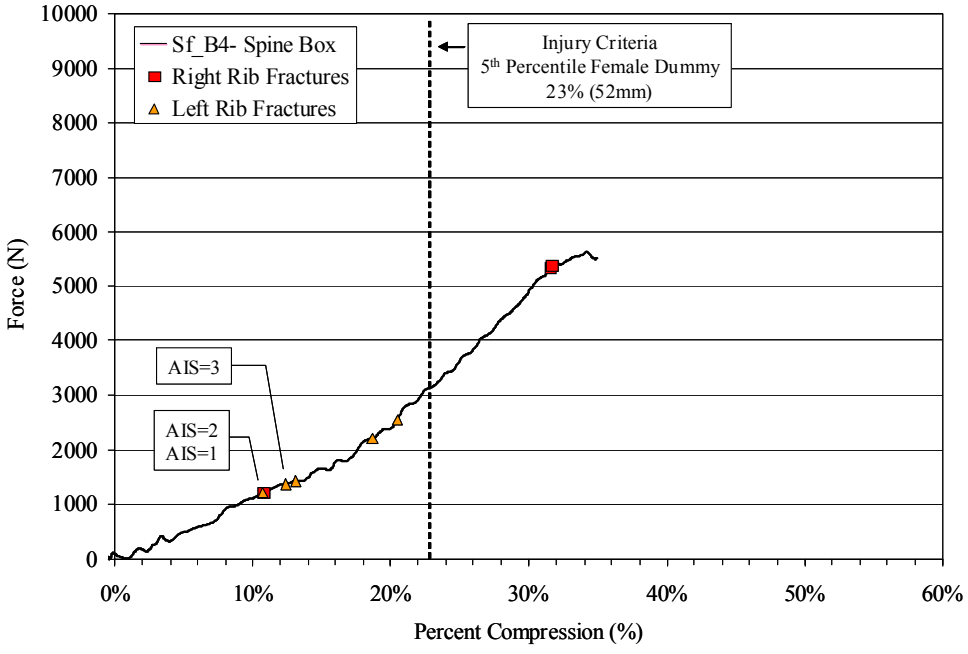

Figure 85: AIS injury timing due to belt loading for cadaver Sf_B4.

Conclusions

The novel thoracic strain gage technique presented in this study allowed for the precise determination of the time of fracture for each rib for the first time in the history of thoracic research. In addition, for the first time the exact point at which the different thoracic AIS scores occurred could be identified with the time of rib fracture data. All rib fractures occurred within the first 35% compression of the thorax for each cadaver. The first series of fractures were on the left side of the thorax where the belt passed over the abdominal region. The ribs on the upper right hand side of the thorax fractured second. In addition, the strain gage data showed that the majority of the ribs sustained tensile loading until the time of fracture. The gages that showed predominately compressive loading, with the exception of a few gages, were primarily the rosette element gages not aligned with the axis of the rib, the clavicle gage, or the gages on the sternum. The comparison of the principal strain to the axial strain resulted in several important findings. Specifically, all of the ribs with strain gage rosettes failed in tension, and the first principal strain was greater than or equal to the axial strain. However, the value of theta (θ) and the difference between the principal strain and the axial strain were small up to the time of the fracture. This finding indicates that the direction of the first principal strain was very close to the axis of the rib, which implies that axial strain measurements are essentially the peak values. The comparison of back support conditions showed that there is no considerable difference between using a flat rigid plate and a spine box. Therefore, articulation of the costovertebral joint has little to no effect on thoracic response during frontal belt loading. Overall, this study not only demonstrates a new methodology for determining rib fracture timing but also provides crucial data needed for interpreting thoracic injury criteria and developing new computational models of the thorax.

CHAPTER 6

Influence of Arm Position on Human Thoracic Response during Dynamic Lateral Impacts

Introduction

Side impact automotive collisions have been reported to account for 27% of all automotive crash fatalities annually, which equates to approximately 10,000 annual automotive fatalities (Lund, 2000; Kuppa et al., 2003). It has been reported that thoracic injuries are the most common type of serious injury (AIS≥3) to vehicle occupants in both near side and far side crashes which do not involve a rollover (Samaha et al., 2003; Gabler et al., 2005). In addition, laboratory studies have shown that rib fractures are the most frequent thoracic MAIS in side impacts (Morgan et al., 1986; Viano, 1989; Pintar et al., 1997; Kuppa et al., 2003).

There have been numerous human cadaver studies that have investigated the tolerance of the thorax in side impact loading through a variety of test methodologies. The current acceleration based thoracic side impact injury criteria, Thoracic Trauma Index (TTI), was developed by the National Highway Traffic Safety Administration (NHTSA) based on the results of two types of side impact tests involving instrumented human cadavers: whole body acceleration toward a rigid or padded wall using a sled and Opel Kadett car body struck with a moveable barrier (Klaus and Kallieris, 1982; Klaus and Kallieris, 1983; Klaus et al., 1984; Eppinger et al., 1984; Morgan et al., 1986). Since the NHTSA test series, a number of researchers have investigated the tolerance of the thorax through cadaver sled tests, which involve a short deceleration or

acceleration of an instrumented human cadaver toward a rigid or padded wall to simulate real-world side impacts (Cavanaugh et al, 1990; Irwin et al., 1993; Cavanaugh et al, 1993; Zhu et al, 1993; Cavanaugh et al, 1996; Pintar et al., 1997; Koh et al., 2001; Yoganandan et al., 2007). The majority of these studies were aimed at determining the effect of shoulder engagement, pelvis engagement, and different types of energy absorbing foam on the injury tolerance of the thorax. Pendulums and pneumatic impactors have been used to evaluate the stiffness and tolerance of the rib cage as a result of a lateral or oblique impact to the thorax (Chung et al., 1999; Cesari et al., 1981; Viano et al., 1989; Robbins et al., 1994; Shaw et al, 2006;). All of the previous studies aimed at determining the most appropriate thoracic injury criteria in side impact loading have provided significant contributions to the literature. However, the injury criteria based on the results of these studies rely primarily on censored rib fracture data (Morgan et al., 1986; Viano, 1989; Pintar et al., 1997; Kuppa et al., 2003). In other words, only the total number of rib fractures resulting from a given impact is known. Therefore, the force and thoracic deflection corresponding to the injury timing could not be determined.

Although there have been numerous studies that have investigated the tolerance of the thorax in side impact loading, research regarding the effect of the arm on the response and tolerance of the thorax is quite limited. In fact, there are only two studies to the author's knowledge that have investigated the influence of the arm on thoracic response in a controlled study. Stalnaker et al. (1979) conducted free-fall drop tests from 1 m onto a rigid surface, which engaged the cadavers from the shoulder to the pelvis, with the arm either rotated upward and forward (approximately 90 degrees to the thorax) or rotated forward such that an angle of 20 degrees was formed between the arm and the thoracic spine. The results of this study showed that peak thoracic

deflection was reduced when the arm was placed at 20 degrees. Cesari et al. (1981) performed a series of pendulum impacts to the lateral portion of the thorax to simulate real-world side impact collisions with the arm placed either parallel to the thorax or with no arm involvement, i.e. the rib cage only. The impactor speed was incrementally increased until a thoracic fracture was produced. The results of the study showed that an increased impact speed was necessary to produce thoracic fractures when the arm was placed parallel with the thorax versus when there was no arm involvement. Cesari et al. (1981) concluded that when the arm is placed parallel to the thorax it distributes impactor force on the thorax and decreases impactor penetration.

The studies performed by Stalnaker et al. (1979) and Cesari et al. (1981) clearly show that the arm provides some protection against thoracic injury compared to impacts directly to the rib cage. However, it is difficult to determine how the position of the arm relative to the thorax affects the thoracic response due to the differences in loading rate, instrumentation, and boundary conditions between the two studies. Therefore, the primary purpose of the current study is to evaluate the influence of arm position on thoracic response and injury severity resulting from side impacts in one controlled study. In addition, rib fracture timing is investigated using thoracic strain gages and correlated to rib deflection.

Methods

This study presents a total of sixteen non-destructive side impact tests and four destructive side impact tests performed using four male cadavers. Six impact conditions and two impactor surfaces were evaluated using a custom test seat and pneumatic impactor. The details of the test subjects, instrumentation, experimental setup, and test methodologies are presented in this section.

Subject Information

This study was performed using a total of four male unembalmed frozen and thawed human cadavers (Table 43 and Table 44). For comparison with the standard population, the bone mineral density (BMD) of each cadaver was determined by the Osteogram technique (Hardy et al. 2001a; Stitzel et al., 2003; Kemper et al., 2005). For this technique, the left hand of each cadaver was x-rayed next to an aluminum calibration wedge. The x-ray was then processed by CompuMed Incorporated (CompuMed, Inc., Los Angeles, CA) to obtain the BMD, T-Score, and Z-score for each subject. This type of BMD measurement, however, only provides an indication of overall bone quality and does not account for local changes in bone density or composition. Therefore, the BMD obtained through this method is referred to as the "global BMD." The T-score is the number of standard deviations from the average value of healthy living individuals between 25 and 50 years of age. The Z-score is the number of standard deviations from the average value of healthy living individuals of similar age. The World Health Organization classifies normal bone as T-scores of -1.0 or greater, osteopenia as T-scores between -1.0 and -2.5, and osteoporosis as T-scores below -2.5 (Wolf and Pfleger, 2003).

Table 43: Subject information for cadavers used in side impact testing.

Subject ID	Gender	Age (yr)	Weight (kg)	Height (cm)	Global BMD	T- Score	Z- Score
Sm_S1	M	61	69.1	167	72.1	-3.6	-2.2
Sm_S2	M	47	64.3	170	142.0	2.9	2.4
Sm_S3	M	56	63.2	165	90.1	-1.9	-1.0
Sm_S4	M	49	71.8	170	109.4	-0.1	0.3
50th Percentile Male							
Schneider et al. (1983)		38 (average)	76.7	175	N/A	N/A	N/A

Note: N/A is Not Applicable

Table 44: Subject thoracic anthropometry for cadavers used in side impact testing.

Measurement		Subject ID					50th Percentile Male
		Sm_S1	Sm_S2	Sm_S3	Sm_S4		Schneider et al.
Thorax depth (mid-sternum)	(cm)	20.3	19.7	22.4	24.4		23.6
Thorax circumference (mid-sternum)	(cm)	91.4	83.8	86.4	88.9		103.9
Chest width at rib 5	(cm)	29.1	28.7	26.2	26.2		30.4
Chest width at rib 7	(cm)	30.3	30.2	26.9	27.7		34.9
Chest width at rib 9	(cm)	32.4	31.0	27.9	28.7		N/R

Note: N/R is Not Reported

Instrumentation

The cadavers were instrumented with 12 single-axis accelerometers, up to 18 thoracic strain gages, 3 thoracic rods, and up to 22 photo targets prior to testing (Figure 86 and Figure 87). All accelerometers and photo targets were rigidly attached to boney structures using bone screws. Cadaver accelerations were recorded with single-axis accelerometers (Endevco Corporation 7264B, 2000 G, San Juan Capistrano, CA) mounted to three axis cubes on the sternum, T1, T12, and sacrum. Photo targets were rigidly attached to the head, sternum, spine, sacrum, and ilium using bone screws.

Lateral rib deflection was measured by placing rods through the thorax (Stalnaker et al., 1979; Patrick et al., 1967; Hardy et al., 2001b). It should be noted that the thoracic organs were not moved prior to inserting the rods through the thorax. Therefore, the rods penetrated through the lungs and possibly the heart. The metal rods were hollow to minimize inertial effects. The weight, length, outer diameter, and inner diameter of the thoracic rods were 0.05 kg, 457.2 mm, 9.5 mm, and 8.5 mm, respectively. The rods were attached to the internal portion of the rib on the struck side with zip ties placed around the rib and through holes in the rod. On the opposite side, the rods were attached to string potentiometers (Space Age Control Inc. 160-1705,

539.75mm, Palmdale, CA), which were rigidly attached to the thorax with a custom mounting plate. As the thorax is compressed laterally, the rods are pushed out of the thorax which causes the potentiometer cable to spool out, measuring rib deflection. The nominal displacement cable tension range for the potentiometers was 2 N to 5 N (full retraction to full extraction). For all tests, the potentiometer string was extracted approximately 1 inch (4.7% of full extraction) prior to the test. Therefore, the resistance of the potentiometers can be considered negligible when compared to the stiffness of the rib cage. It should be noted that because the thoracic rods used to measure deflection were attached to the internal portion of the struck ribs, the deflection measurement does not include the deflection of the skin, soft tissue, or clothing surrounding the external portion of the thorax.

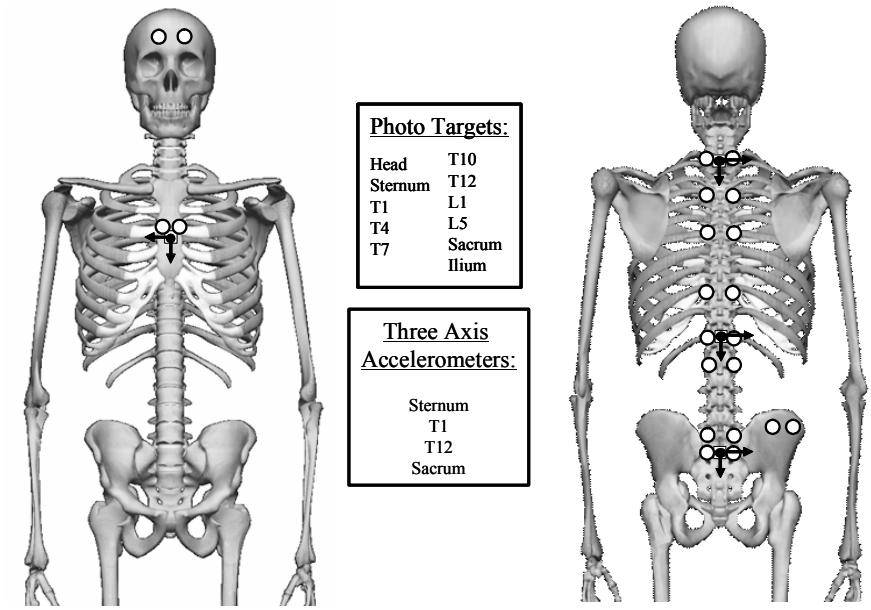

Figure 86: Location of photo targets and accelerometers for side impact testing.

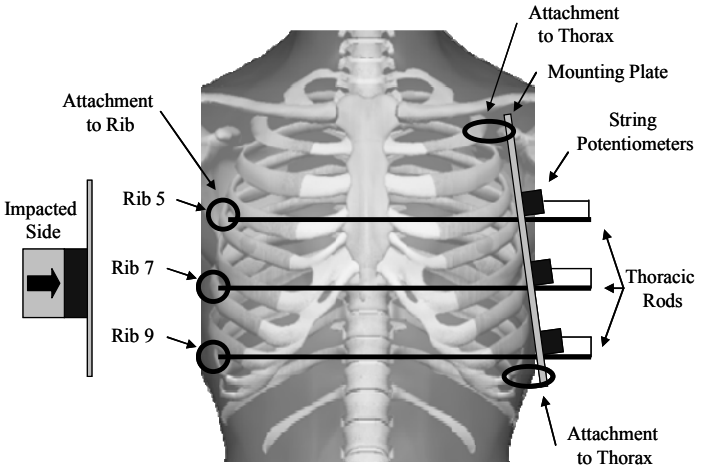

Figure 87: Thoracic deflection measurement methodology for side impact testing**.**

For cadavers Sm_S1 and Sm_S2, a total of 12 single-axis strain gages (Vishay Micro-Measurement, CEA-06-062UW-350, Shelton, CT) were applied to the external surface of the right and left lateral region of ribs 3 through 8. For cadavers 3 and 4, a total of 18 single-axis strain gages were applied to the external surface of the right and left lateral region of ribs 3 through 8, and the right posterior region of ribs 3 through 8 of cadavers 3 and 4 (Figure 88 and Table 45).

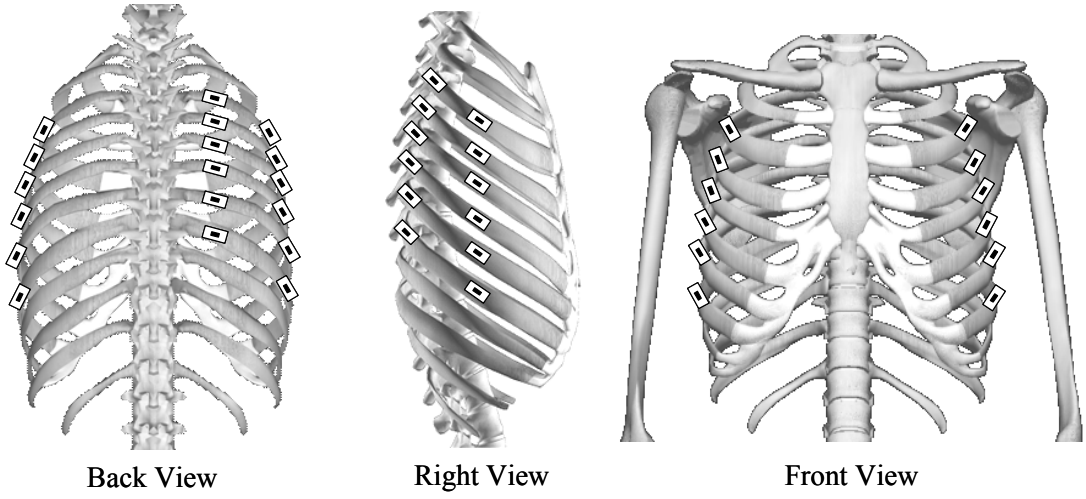

Figure 88: Thoracic strain gage locations for side impact testing.
Note: Cadavers Sm_S1 and Sm_S2 did not have posterior strain gages.

Table 45: Locations of strain gages for side impact testing.

Thoracic Strain Gages		Circumferential Measurement from	Subject ID			
			Sm_S1	Sm_S2	Sm_S3	Sm_S4
			(cm)	(cm)	(cm)	(cm)
Left Side	Lateral Rib 3	sternum	17.8	16.5	15.0	15.2
	Lateral Rib 4	sternum	18.4	17.1	18.0	15.2
	Lateral Rib 5	sternum	19.7	19.1	19.0	16.5
	Lateral Rib 6	sternum	18.4	19.7	20.0	16.5
	Lateral Rib 7	sternum	20.3	21.6	20.5	18.4
	Lateral Rib 8	sternum	21.0	21.6	21.0	18.4
Right Side	Lateral Rib 3	sternum	17.8	19.7	15.0	15.2
	Lateral Rib 4	sternum	18.4	20.3	17.0	15.2
	Lateral Rib 5	sternum	19.7	21.0	17.0	15.9
	Lateral Rib 6	sternum	20.3	21.6	17.0	16.5
	Lateral Rib 7	sternum	21.6	21.0	15.0	16.5
	Lateral Rib 8	sternum	21.6	22.2	18.0	17.8
	Posterior Rib 3	Spine	N/A	N/A	9.0	10.0
	Posterior Rib 4	Spine	N/A	N/A	9.5	10.0
	Posterior Rib 5	Spine	N/A	N/A	10.0	11.0
	Posterior Rib 6	Spine	N/A	N/A	10.0	11.0
	Posterior Rib 7	Spine	N/A	N/A	11.0	12.0
	Posterior Rib 8	Spine	N/A	N/A	10.0	12.0

Note: N/A is Not Applicable

Once the location of each strain gage was determined the soft tissue and periosteum were removed, and the bone was swabbed with ether to locally dry the bone. Upon drying, an acidic solution (Vishay Micro-Measurement, Conditioner A, Shelton, CT) was applied to the surface with a clean piece of gauze in order to etch the surface of the bone. Then a basic solution (Vishay Micro-Measurement, Neutralizer 5A, Shelton, CT) was applied to the surface in order to neutralize the acidic solution. The gage was removed from its case and prepared for mounting by applying a catalyst (Vishay Micro-Measurement, M-Bond 200 Catalyst, Shelton, CT) to the underside of the gage. Next, an adhesive (Vishay Micro-Measurement, M-Bond 200 Adhesive, Shelton, CT) was applied to the bone and the gage was quickly pushed over the adhesive in a

rolling manner. The strain gage was covered with a small piece of latex and held with firm pressure for 3 minutes. Special care was taken to align each gage with the axis of the rib. Finally, the strain gage wire was strain relieved with a zip tie placed around the rib.

Experimental Setup

The primary component of the side impact experimental setup was a custom pneumatic impactor, which accelerated an impacting cart constrained by rails to a desired speed via a piston (Figure 89). Prior to impact, the piston loses contact with the cart due to a limited piston stroke, resulting in an impact with finite energy. The displacement of the impacting cart, i.e. impactor stroke, was limited via a steel cable having a set length. The impactor was instrumented with a five-axis load cell (Denton ATD, Inc., 1968, 22,240 N, Rochester Hills, MI) and a single-axis accelerometer (Endevco Corporation 7264B, 2000 G, San Juan Capistrano, CA). A custom test seat was designed and fabricated to allow a cadaver to be placed in a seated position (Figure 90). The use of an adjustable back support bar allowed a clear line of sight to the posterior photo targets while maintaining the normal posture and upper body load on the pelvis and spine. The adjustable back support bar maintained the cadaver in an automotive-like seated posture by simply adjusting the position of the bar anterior-posterior and/or inferior-superior. After adjustment, the seatback angle was checked to ensure it was approximately 20 degrees from vertical. Neither the shoulders nor thorax were attached to the bar. However, the head was held upright with the use of paper tape placed around the forehead and attached to the bar on the right and left side of the cadaver. This tape was cut approximately half way through on both sides in order to ensure that the tape would break when the cadaver was struck. A Teflon ® sheet was placed between the cadaver and the seat pan to minimize friction (Cavanaugh et al. 1993).

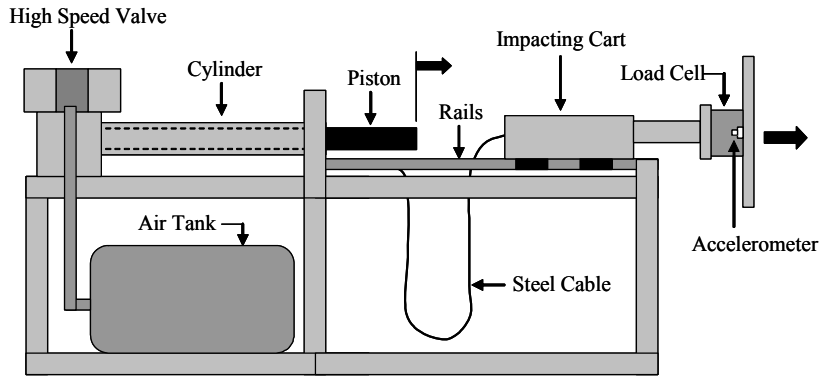

Figure 89: Custom pneumatic impactor for side impact testing.

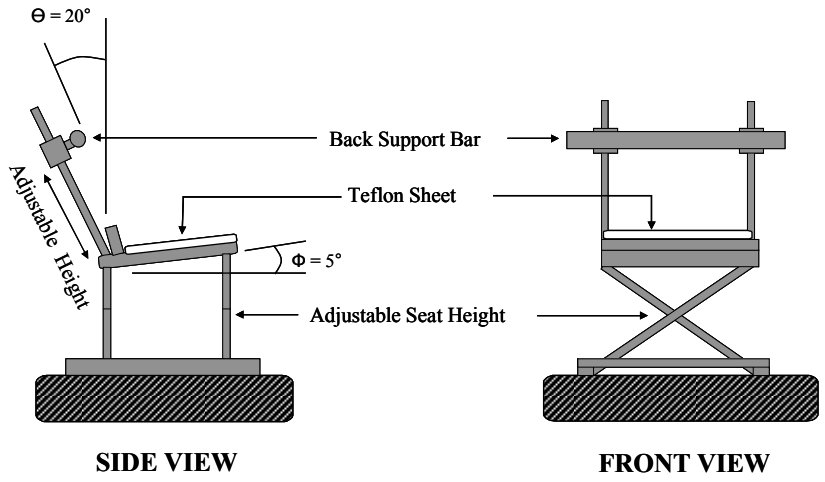

Figure 90: Custom side impact test seat for side impact testing.

Testing Configurations

Non-Destructive Testing

A total of sixteen non-destructive thoracic side impact tests were performed using four cadavers with a custom pneumatic impactor. Four non-destructive test conditions were evaluated for each cadaver (Figure 91 and Table 46). The order of the impact conditions was varied between cadavers to separate the effect of test order from the cadaver response. It should be noted that the vasculature was not pressurized prior to testing.

The objective of the non-destructive testing was to obtain sufficient thoracic displacement without inducing injury in order to evaluate the effect of the arm while controlling for subject variation. The non-destructive thoracic testing in the current study was conducted at a speed of 3 m/s with an impactor mass of 16 kg, which resulted in an impact energy of 72 Joules. This impact energy was based on the non-destructive impact energy used by Shaw et al. (2006). Shaw et al. (2006) conducted non-destructive lateral and oblique thoracic impacts at a speed of 2.5 m/s with an impactor mass (m) of 23 kg, which resulted in an impact energy of 73 Joules. Shaw et al. (2006) determined a non-destructive impact velocity by performing a work-energy balance, assuming a completely plastic impact (Equations 7 and 8). The energy was determined based on the observations of previous researchers (Kuppa 2004, Viano 1989). Viano (1989) found an average normalized force response (F) of 2.25 kN from low energy impacts. Kuppa (2004) performed a statistical analysis on data from several lateral sled tests and reported that a rib deflection (Δx) of 30 mm has a zero percent probability of injury. Although the tests performed by Shaw et al. (2006) were intended to be non-destructive, rib fractures were observed in 3 of the 7 cadavers tested. Since rib fractures could compromise the structural integrity of the thorax and contaminate data obtained from subsequent non-destructive tests, a lower impactor mass was used in the current study to lower the risk of inducing rib fractures

$$F * \Delta x = \frac{1}{2}\left(m * v^2\right) \qquad \text{(Eqn. 7)}$$

$$v = \sqrt{\frac{2 * F * \Delta x}{m}} \qquad \text{(Eqn. 8)}$$

The impacting surface for the non-destructive testing was a flat rigid aluminum plate with a height of 25 cm and a width of 25 cm. Special care was taken while positioning the cadaver to ensure that the impacting plate did not strike the pelvis. It should be noted that for the shoulder and rib impact the impactor height was raised relative to all other impact conditions. After each impact, the strain gage data were evaluated and the thorax was palpated to ensure that no gross rib fractures occurred.

In order to compare the effect of arm position on thoracic response directly, a set amount of intrusion was simulated for all tests. Kuppa (2004) analyzed data from several lateral sled tests and reported that rib deflection of 30 mm has a zero percent probability of injury. In order to account for the compression of soft tissue and clothing as well as cadaver motion away from the impactor, an additional 40 mm of impact stroke was added. The custom pneumatic impactor is an open loop system, and does provide a controlled displacement. Therefore, the cadavers were positioned relative to the impactor so that the maximum impactor stroke would be 70 mm medial of the lateral most portion of the thorax (Figure 92). This was done by first determining the point of maximum impactor stroke, which was controlled by a steel cable tethering the impacting cart to the impactor frame. A mark was placed on the back support bar at a measured distance of 70 mm inboard of the point of maximum impactor stroke. The cadaver was then placed in a seated position so that the lateral portion of the struck side of the thorax was inline with the 70-mm mark. Finally, the arm was placed in the desired position using an overhead rope. Once the cadaver was placed in the final seated position, measurements were taken to obtain the position of anatomical structures relative to the center of the impactor plate (Figure 93 and Table 47).

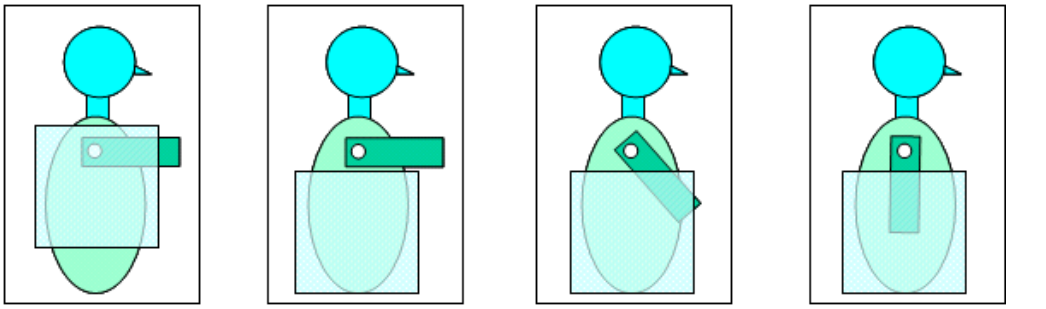

Figure 91: Non-destructive side impact locations and arm positions.

Table 46: Non-destructive thoracic side impact test matrix.

Test ID	Subject ID	Impact Side	Arm Position	Impactor Mass	Impactor Speed	Impact Surface	Impact Location
Tside1_1	Sm_S1	Left	90º	16 kg	3 m/s	25 x 25 cm	shoulder & ribs
Tside1_2	Sm_S1	Left	90º	16 kg	3 m/s	25 x 25 cm	ribs
Tside1_3	Sm_S1	Left	45º	16 kg	3 m/s	25 x 25 cm	arm & ribs
Tside1_4	Sm_S1	Left	parallel to thorax	16 kg	3 m/s	25 x 25 cm	arm & ribs
Tside2_1	Sm_S2	Right	90º	16 kg	3 m/s	25 x 25 cm	shoulder & ribs
Tside2_2	Sm_S2	Right	90º	16 kg	3 m/s	25 x 25 cm	ribs
Tside2_3	Sm_S2	Right	45º	16 kg	3 m/s	25 x 25 cm	arm & ribs
Tside2_4	Sm_S2	Right	parallel to thorax	16 kg	3 m/s	25 x 25 cm	arm & ribs
Tside3_1	Sm_S3	Right	90º	16 kg	3 m/s	25 x 25 cm	shoulder & ribs
Tside3_2	Sm_S3	Right	parallel to thorax	16 kg	3 m/s	25 x 25 cm	arm & ribs
Tside3_3	Sm_S3	Right	45º	16 kg	3 m/s	25 x 25 cm	arm & ribs
Tside3_4	Sm_S3	Right	90º	16 kg	3 m/s	25 x 25 cm	ribs
Tside4_1	Sm_S4	Right	90º	16 kg	3 m/s	25 x 25 cm	shoulder & ribs
Tside4_2	Sm_S4	Right	parallel to thorax	16 kg	3 m/s	25 x 25 cm	arm & ribs
Tside4_3	Sm_S4	Right	45º	16 kg	3 m/s	25 x 25 cm	arm & ribs
Tside4_4	Sm_S4	Right	90º	16 kg	3 m/s	25 x 25 cm	ribs

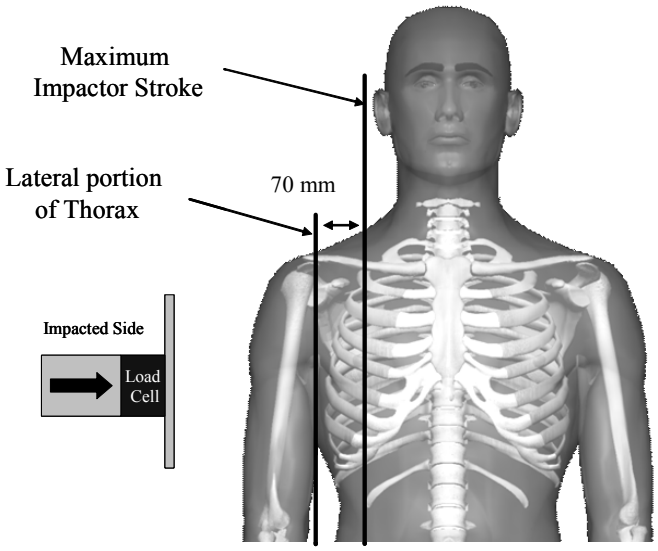

Figure 92: Cadaver positioning for controlled impactor displacement.

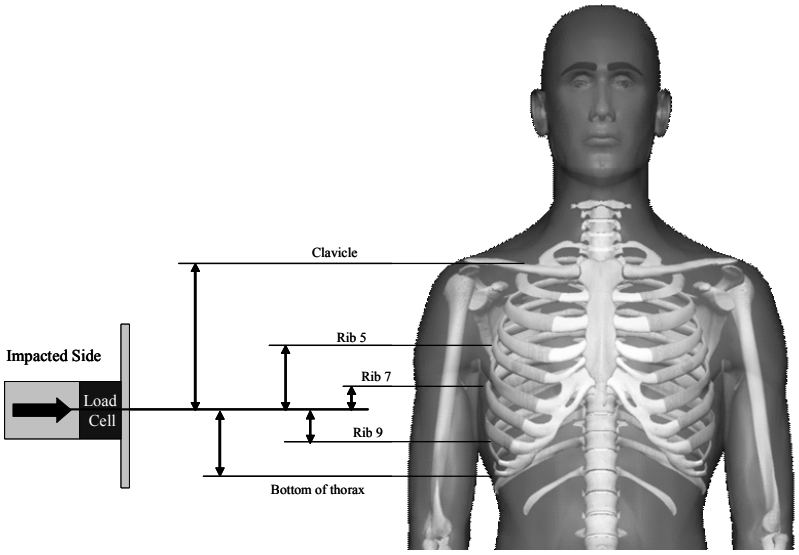

Figure 93: Center of impactor plate relative to anatomical landmarks.

Table 47: Center of impactor plate relative to anatomical locations for non-destructive side impact tests.

	Measurement of Anatomical Locations Relative to Impactor Center					
	Top of Shoulder	Clavicle Center	Rib 5	Rib 7	Rib 9	Bottom of Rib Cage
Test ID	(cm)	(cm)	(cm)	(cm)	(cm)	(cm)
Tside1_1	16	6	-3	-11	-17	-21
Tside1_2	24	14	7	-0	-6	-10
Tside1_3	24	15	7	-0	-6	-10
Tside1_4	18	14	8	1	-5	-9
Tside2_1	20	8	-4	-13	-19	-24
Tside2_2	26	18	6	-3	-8	-12
Tside2_3	25	17	5	-4	-9	-13
Tside2_4	21	19	8	-1	-6	-10
Tside3_1	14	10	0	-6	-15	-18
Tside3_2	23	19	9	3	-6	-9
Tside3_3	23	19	9	3	-6	-9
Tside3_4	25	21	11	5	-4	-7
Tside4_1	13	8	-3	-10	-16	-22
Tside4_2	25	20	9	3	-4	-10
Tside4_3	25	20	9	3	-4	-10
Tside4_4	25	20	9	3	-4	-10

It should be noted that multiple impact tests were performed on the same subject to eliminate the effects of variability between subjects. If only a single impact condition was performed on each subject the variability between subjects could effectively mask any changes in response with respect to different loading conditions (Kent et al. 2004). It should be noted, however, that repeated loading could potentially result in changes in the stiffness of the soft tissue and micro-fractures of the ribs. However, the potential effects of repeated loading were considered negligible in the current study for two primary reasons. First, based on the results of Hardy et al. (2001) the low impact energy used in the non-destructive testing is unlikely to have a considerable effect on the soft tissue response. Hardy et al. (2001) conducted repeated abdominal impacts on a single cadaver with a 48 kg rigid bar at 3 m/s, 6 m/s, and 9 m/s. Hardy

et al. (2001) repeated each loading rate more than once, while varying the order, and found no considerable changes in the force versus penetration response at any of the loading rates due to repeated loading. Second, the order of the test conditions was varied between cadavers in order to separate the effect of test order from the cadaver response.

Destructive Testing

A total of four destructive thoracic side impact tests were performed using four male cadavers with a custom pneumatic impactor after the non-destructive testing was completed. One impact area and two arm positions were evaluated using a speed of 12 m/s and an impactor mass of 23.4 kg (Figure 94 and Table 48). It should be noted that the vasculature was not pressurized prior to testing.

The objective of the destructive testing was to induce injuries in order to evaluate the effect of the arm on the rib fracture patterns and corresponding injury level. The impactor mass of 23.4 kg was based on the destructive pendulum testing performed by Viano et al. (1989). The impacting surface was a flat rigid aluminum plate with a height of 41.5 cm and a width of 25.5 cm. The cadavers were positioned using the same procedure as the non-destructive testing. The impactor stroke was set to the maximum impactor stroke of 250 mm for the destructive tests in order to ensure that the impact would result in thoracic injuries. Once the cadaver was placed in the final seated position, measurements were taken to obtain the position of important anatomical structures relative to the center of the impactor plate (Figure 93 and Table 49). Special care was taken while positioning the cadaver to ensure that the impacting plate did not strike the pelvis.

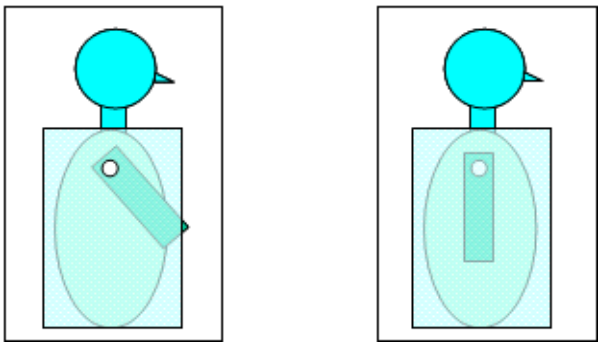

Shoulder, Arm, & Ribs
Arm at 45º

Shoulder, Arm, & Ribs
Arm parallel with thorax

Figure 94: Destructive thoracic side impact locations and arm positions.

Table 48: Destructive thoracic side impact test matrix.

Test ID	Subject ID	Impact Side	Arm Position	Impactor Mass	Impactor Speed	Impact Surface	Impact Location
Tside1_5	Sm_S1	Right	45º	23.4 kg	12 m/s	41.5 x 25.5 cm	shoulder, arm, & ribs
Tside2_5	Sm_S2	Right	45º	23.4 kg	12 m/s	41.5 x 25.5 cm	shoulder, arm, & ribs
Tside3_5	Sm_S3	Right	parallel with thorax	23.4 kg	12 m/s	41.5 x 25.5 cm	shoulder, arm, & ribs
Tside4_5	Sm_S4	Right	parallel with thorax	23.4 kg	12 m/s	41.5 x 25.5 cm	shoulder, arm, & ribs

Table 49: Center of impactor plate relative to anatomical locations for destructive side impact tests.

Test ID	Measurement of Anatomical Locations Relative to Impactor Center					
	Top of Shoulder	Clavicle Center	Rib 5	Rib 7	Rib 9	Bottom of Rib Cage
	(cm)	(cm)	(cm)	(cm)	(cm)	(cm)
Tside1_5	8	9	-1	-8	-14	-18
Tside2_5	9	15	-2	-10	-15	-19
Tside3_5	11	15	1	-5	-14	-17
Tside4_5	10	15	-1	-8	-14	-20

Data Acquisition and Analysis

During the impact, the impactor plate contacted a trigger strip, consisting of two strips of copper tape, secured to the outermost portion of the cadaver, arm or thorax, to activate the data acquisition for each test. Data from the load cell, accelerometers, and strain gages were recorded at a sampling rate of 15 kHz with an Analog-to-Digital conversion resolution of 16 bits using an Iotech Wavebook with WBK16 strain gage modules (Iotech WBK16, Cleveland, OH). The cadaver kinematics were recorded using two high-speed video cameras (front view and back view) operating at a rate of 1,000 frames per second (Vision Research, Phantom IV, Wayne, NJ). All channels except for the strain gages were filtered to SAE channel filter class (CFC) 180 (SAE J211, 1995). The inertially compensated impactor force (F_{IC}) was calculated by summing the measured impactor force (F_I) and inertial force (Equation 9). The inertial force was calculated by taking the product of the impactor acceleration (a_I) and the inertial compensation mass (m), which is the impacting plate mass and ½ the load cell mass.

$$F_{IC} = F_I + a_I m \qquad \text{(Eqn. 9)}$$

In order to minimize the variations in subject response due to individual geometry and inertial properties, the force, rib deflection, and time were scaled according to the procedures detailed in the International Standards Organization (ISO) technical report ISO/TR-9790:1999 for a two mass system, which is an extension of the technique developed by Mertz (1984). The scaling factors for a two mass system are defined below (Equations 10-13). The time, impactor force, and displacement were multiplied by the respective scaling factor for a given cadaver to normalize the response to that of a 50th percentile male. In the scaling factor equations, M_I is the

impactor mass, M_c is the effective thoracic mass of the cadaver, M_s is the effective thoracic mass of a standard subject, V_s is the standard impactor velocity, V_c is the cadaver impact velocity, R_m is the thoracic mass ratio, and R_k is the thoracic stiffness ratio.

- Time Factor $$R_t = (R_m/R_k)^{1/2}(M_I + M_c)^{1/2}(M_I + M_s)^{-1/2} \quad \text{(Eqn. 10)}$$

- Impactor Force Factor $$R_f = (V_s/V_c)(R_m \times R_k)^{1/2}(M_I + M_c)^{1/2}(M_I + M_s)^{-1/2} \quad \text{(Eqn. 11)}$$

- Thoracic Displacement Factor $$R_x = (R_m/R_k)^{1/2}(M_I + M_c)^{1/2}(M_I + M_s)^{-1/2} \quad \text{(Eqn. 12)}$$

- Thoracic Acceleration Factor $$R_a = (R_k/R_m)^{1/2}(M_I + M_c)^{1/2}(M_I + M_s)^{-1/2} \quad \text{(Eqn. 13)}$$

The effective thoracic mass was calculated for each test by dividing the thoracic impulse by its change in velocity (Equation 14). In Equation 12, a_p is the acceleration versus time history of the impactor, a_T is the lateral acceleration versus time history of T1, and τ is the impact duration $\Delta V = Vo$. The thoracic mass for the standard subject was calculated for each impact condition by multiplying the mass of the 50th percentile adult male, 76 kg, by the average ratio of the effective thoracic mass to the cadaver's total body mass for each test condition (Equation 15).

$$M_c = \left[\int_\tau M_p a_p dt\right] \Big/ \left[\int_\tau a_T dt\right] \quad \text{(Eqn. 14)}$$

$$M_s = \left(M_c / M\right)_{AVG} (76kg) \quad \text{(Eqn. 15)}$$

The thoracic mass ratio, R_m, and thoracic stiffness, R_k, are defined below (Equations 16 and 17). According to Mertz (1984), thoracic stiffness is proportional to the characteristic length, L, assuming geometrically similar structures with the same elastic modulus. This assumption is rooting in the equal strain- equal velocity scaling proposed by Eppinger et al. (1984). Schneider et al. (1983) reported the chest breadth of a 50th percentile male measured at the nipple to be 349 mm. This was used as the characteristic length value in the calculation of all scaling factors. In the equations below, K_c is the thoracic stiffness of the cadaver, K_s is the thoracic stiffness of a standard 50th percentile subject, L_c is the cadaver chest breadth, and L_s is the chest breadth of an adult 50th percentile male.

$$R_m = M_s / M_c \qquad \text{(Eqn. 16)}$$

$$R_k = K_s / K_c = L_s / L_c \qquad \text{(Eqn. 17)}$$

Rib compression was calculated by taking the ratio of non-scaled rib deflection to the initial chest breadth multiplied by 100 (Equation 18). In this equation, $X_{Rib(N)i}$ is the non-scaled rib deflection measured at rib(N) of cadaver(i) and $L_{Rib(N)i}$ is the initial chest breadth measured at rib(N) of cadaver(i).

$$Compression = (X_{Rib(N)i} / L_{Rib(N)i}) * 100 \qquad \text{(Eqn. 18)}$$

Results

Non-Destructive Testing

The scaled impactor force, peak scaled rib deflections, and peak rib strains resulting from the non-destructive tests are presented in this section. The scaling factors, effective thoracic masses, impactor velocities, thoracic mass ratios, and thoracic stiffness ratios for each test were tabulated (Table 50).

High-speed video stills of the non-destructive testing performed on cadaver 3 are provided as exemplar qualitative kinematics (Figure 95). For the test in which the shoulder was directly loaded, both the arm and shoulder translated and rotated medially with continued impactor displacement. For the test conducted with the arm placed at 45 degrees, the arm translated and rotated medially with continued impactor displacement. For the test conducted with the arm parallel with the thorax, the arm remained between the impactor and thorax throughout the test. It is important to note that the impacting cart did not reach the maximum allowed penetration in any of the non-destructive tests due to energy lost through soft tissue deflection, thoracic deflection, and the inertia/ motion of the thorax. Therefore, the impactor penetration was always limited by the interaction with the cadaver and not by the cable. It should also be noted that no considerable changes to the arm or shoulder were observed after each impact.

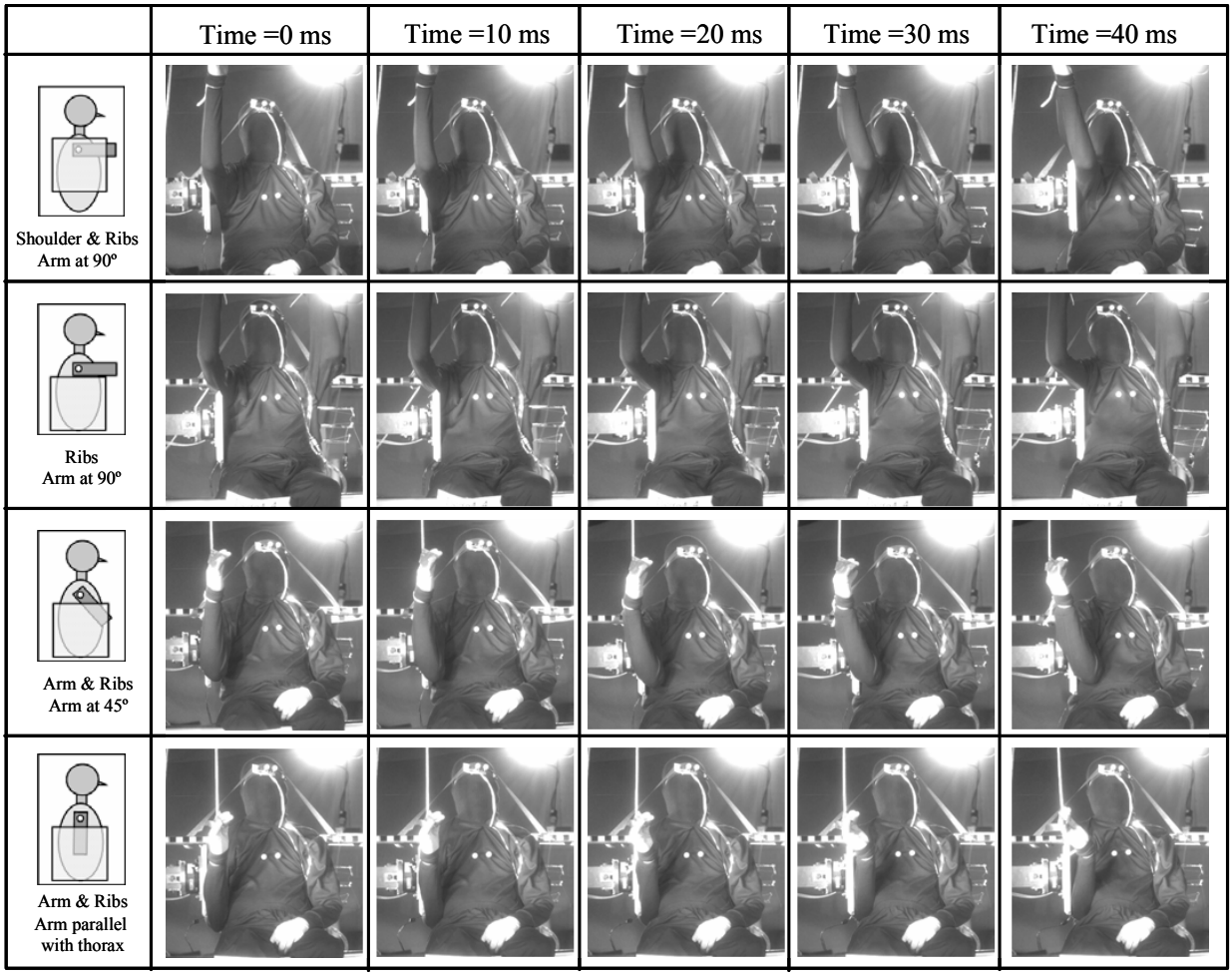

Figure 95: High-speed video stills of cadaver Sm_S3 non-destructive tests.

Table 50: Velocities, effective masses, characteristic ratios, and scaling factors.

Test ID	Test Condition	Body Mass	Velocity		Effective Thoracic Mass			Characteristic Ratios				Scaling Factors					
		M	V_s	V_s/V_i	M_c	M_c/M	M_s	Mass	Stiffness			Time	Impactor Force	Thoracic Acceleration	Thoracic Displacement		
		(kg)	(m/s)	-	(kg)	(%)	(kg)	R_m	R_k_5	R_k_7	R_k_9	R_t	R_f	R_a	R_x_5	R_x_7	R_x_9
Tside1_1	Arm 90: Shoulder and Ribs	69.1	2.54	1.18	37	53.5%	37.0	1.00	1.20	1.15	1.08	0.93	1.27	1.07	0.91	0.93	0.96
Tside2_1	Arm 90: Shoulder and Ribs	64.3	2.61	1.15	28.5	44.3%	37.0	1.30	1.22	1.16	1.14	0.97	1.29	0.87	0.95	0.97	0.98
Tside3_1	Arm 90: Shoulder and Ribs	63.2	2.69	1.12	31.6	50.0%	37.0	1.17	1.33	1.30	1.26	0.90	1.30	1.00	0.89	0.90	0.91
Tside4_1	Arm 90: Shoulder and Ribs	71.8	2.59	1.16	33.5	46.7%	37.0	1.10	1.33	1.26	1.22	0.90	1.32	1.03	0.88	0.90	0.92
Tside1_2	Arm 90: Ribs	69.1	3.06	0.98	32.3	46.7%	31.9	0.99	1.20	1.15	1.08	0.93	1.05	1.09	0.91	0.93	0.96
Tside2_2	Arm 90: Ribs	64.3	2.56	1.17	17.5	27.2%	31.9	1.82	1.22	1.16	1.14	1.05	1.42	0.67	1.02	1.05	1.06
Tside3_4	Arm 90: Ribs	63.2	2.69	1.12	29.2	46.2%	31.9	1.09	1.33	1.30	1.26	0.89	1.29	1.06	0.88	0.89	0.90
Tside4_4	Arm 90: Ribs	71.8	2.60	1.15	34.1	47.5%	31.9	0.93	1.33	1.26	1.22	0.88	1.28	1.19	0.86	0.88	0.90
Tside1_3	Arm 45:Arm and Ribs	69.1	3.08	0.97	36.3	52.5%	38.7	1.07	1.20	1.15	1.08	0.94	1.06	1.02	0.92	0.94	0.97
Tside2_3	Arm 45:Arm and Ribs	64.3	2.69	1.12	27.2	42.3%	38.7	1.42	1.22	1.16	1.14	0.99	1.27	0.80	0.96	0.99	0.99
Tside3_3	Arm 45:Arm and Ribs	63.2	2.64	1.14	32.3	51.1%	38.7	1.20	1.33	1.30	1.26	0.90	1.33	0.98	0.89	0.90	0.92
Tside4_3	Arm 45: Arm and Ribs	71.8	2.64	1.14	41.5	57.8%	38.7	0.93	1.33	1.26	1.22	0.88	1.26	1.19	0.86	0.88	0.90
Tside1_4	Arm Parallel with Thorax :Arm and Ribs	69.1	3.09	0.97	35.1	50.8%	40.7	1.16	1.20	1.15	1.08	0.95	1.06	0.95	0.93	0.95	0.98
Tside2_4	Arm Parallel with Thorax :Arm and Ribs	64.3	2.65	1.13	28.1	43.7%	40.7	1.45	1.22	1.16	1.14	0.99	1.29	0.79	0.96	0.99	1.00
Tside3_2	Arm Parallel with Thorax: Arm and Ribs	63.2	2.71	1.11	38.1	60.3%	40.7	1.07	1.33	1.30	1.26	0.89	1.27	1.08	0.87	0.89	0.90
Tside4_2	Arm Parallel with Thorax: Arm and Ribs	71.8	2.82	1.06	42.5	59.2%	40.7	0.96	1.33	1.26	1.22	0.89	1.19	1.17	0.86	0.89	0.90
Tside1_5	Arm 45: Shoulder, Arm, and Ribs	69.1	11.87	1.01	23.6	34.2%	29.2	1.24	1.20	1.15	1.08	0.97	1.14	0.91	0.96	0.98	1.01
Tside2_5	Arm 45: Shoulder, Arm, and Ribs	64.3	11.99	1.00	27.4	42.6%	29.2	1.06	1.22	1.16	1.14	0.94	1.09	1.02	0.92	0.94	0.95
Tside3_5	Arm Parallel with Thorax : Shoulder, Arm, and Ribs	63.2	12.23	0.98	28.5	45.1%	34.6	1.21	1.33	1.30	1.26	0.91	1.15	0.98	0.90	0.92	0.93
Tside4_5	Arm Parallel with Thorax : Shoulder, Arm, and Ribs	71.8	12.18	0.99	33	46.0%	34.6	1.05	1.33	1.26	1.22	0.90	1.11	1.08	0.87	0.90	0.92

Impactor Force

The scaled impactor force time histories were found to be consistent in both magnitude and shape between subjects for each impact condition (Figure 96 to Figure 99). The peak scaled impactor force was plotted, both by cadaver and averaged by impact condition, to evaluate differences between the four non-destructive test conditions (Figure 100 and Table 51).

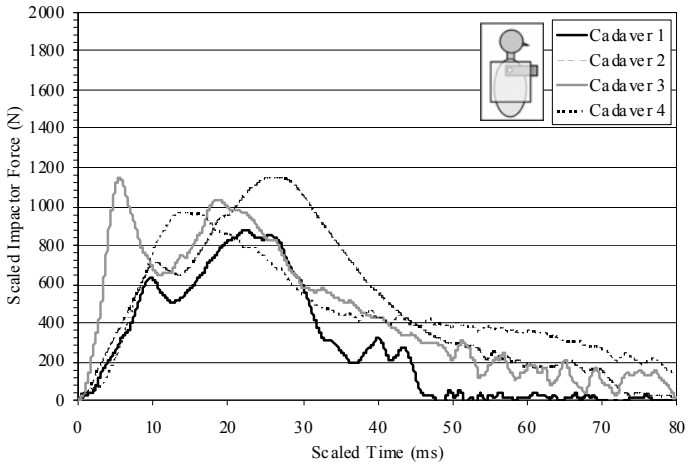

Figure 96: Scaled impactor force time history for non-destructive tests- Shoulder/Ribs: Arm 90.

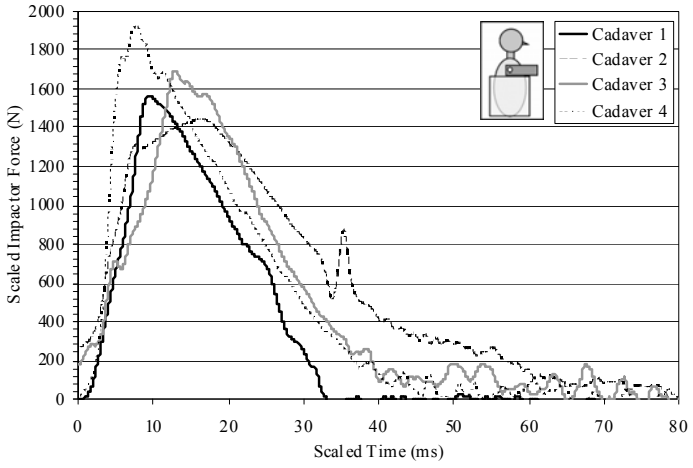

Figure 97: Scaled impactor force time history for non-destructive tests- Ribs: Arm 90.

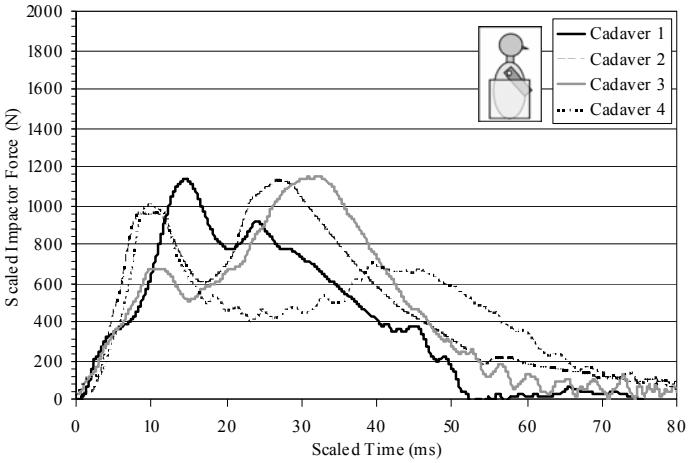

Figure 98: Scaled impactor force time history for non-destructive tests- Arm/Ribs: Arm 45.

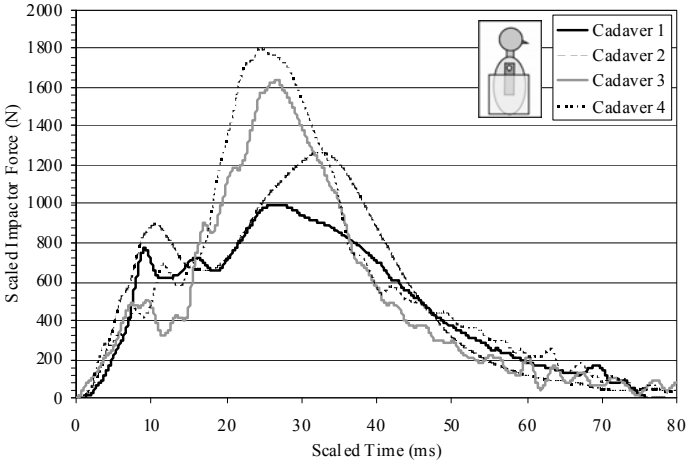

Figure 99: Scaled impactor force time history for non-destructive tests- Arm/Ribs: Arm Parallel to Thorax.

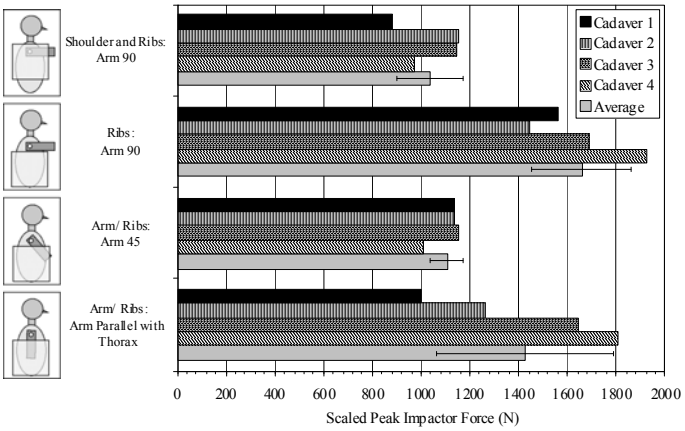

Figure 100: Peak impactor force by cadaver for all non-destructive side impact tests.

Table 51: Peak impactor force for all non-destructive side impact tests.

Test ID	Test Condition	Peak Inertially Compensated Impactor Force	Peak Scaled Impactor Force
		(N)	(N)
Tside1_1	Arm 90: Shoulder and Ribs	777.1	878.2
Tside2_1	Arm 90: Shoulder and Ribs	891.6	1150.2
Tside3_1	Arm 90: Shoulder and Ribs	884.2	1149.4
Tside4_1	Arm 90: Shoulder and Ribs	736.5	972.2
	Average	822.4	822.4
	Standard Deviation	77.5	77.5
Tside1_2	Arm 90: Ribs Only	1680.3	1562.7
Tside2_2	Arm 90: Ribs Only	1018.9	1446.9
Tside3_4	Arm 90: Ribs Only	1310.8	1690.9
Tside4_4	Arm 90: Ribs Only	1506.6	1928.4
	Average	1379.1	1379.1
	Standard Deviation	283.6	283.6
Tside1_3	Arm 45: Arm and Ribs	1208.7	1136.1
Tside2_3	Arm 45: Arm and Ribs	893.1	1134.2
Tside3_3	Arm 45: Arm and Ribs	866.5	1152.5
Tside4_3	Arm 45: Arm and Ribs	799.7	1007.6
	Average	945.2	942.0
	Standard Deviation	180.4	182.1
Tside1_4	Arm Parallel with Thorax : Arm and Ribs	1050.3	997.8
Tside2_4	Arm Parallel with Thorax : Arm and Ribs	981.7	1266.4
Tside3_2	Arm Parallel with Thorax : Arm and Ribs	1292.7	1641.7
Tside4_2	Arm Parallel with Thorax : Arm and Ribs	1515.5	1803.4
	Average	1210.0	1210.0
	Standard Deviation	243.4	243.4

Rib Deflection

The peak scaled rib 5, rib 7, and rib 9 deflections were plotted by cadaver to evaluate differences between the four non-destructive test conditions (Figure 101 to Figure 103). In addition, the peak scaled rib 5, rib 7, and rib 9 deflections were plotted averaged by impact condition (Figure 104). The peak rib deflections, peak scaled rib deflections, and peak rib compressions were tabulated (Table 52).

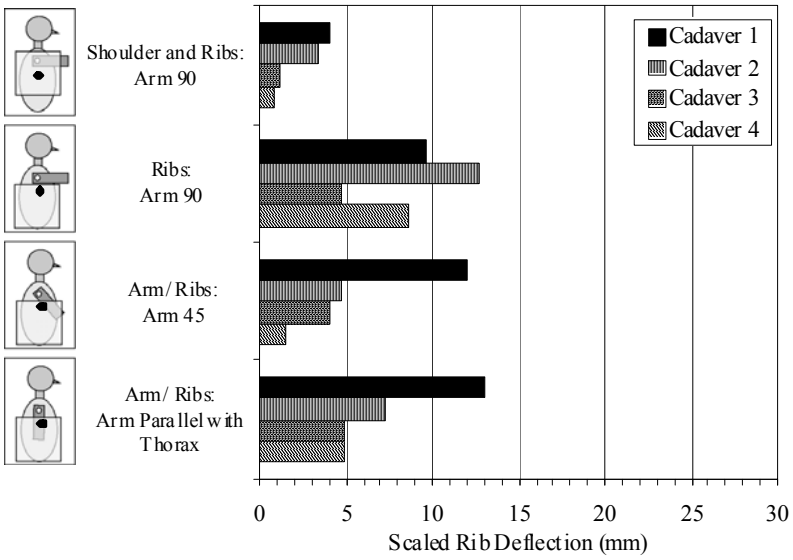

Figure 101: Peak rib 5 deflection for all non-destructive side impact tests.

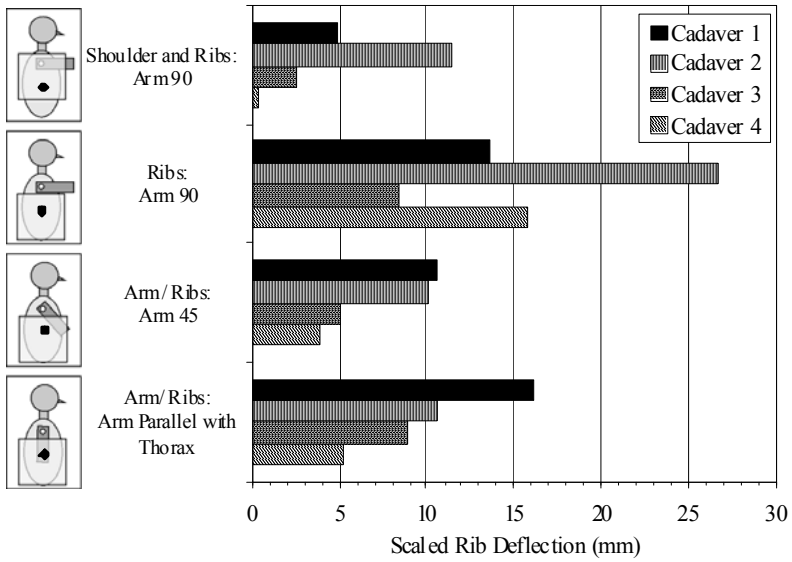

Figure 102: Peak rib 7 deflection for all non-destructive side impact tests.

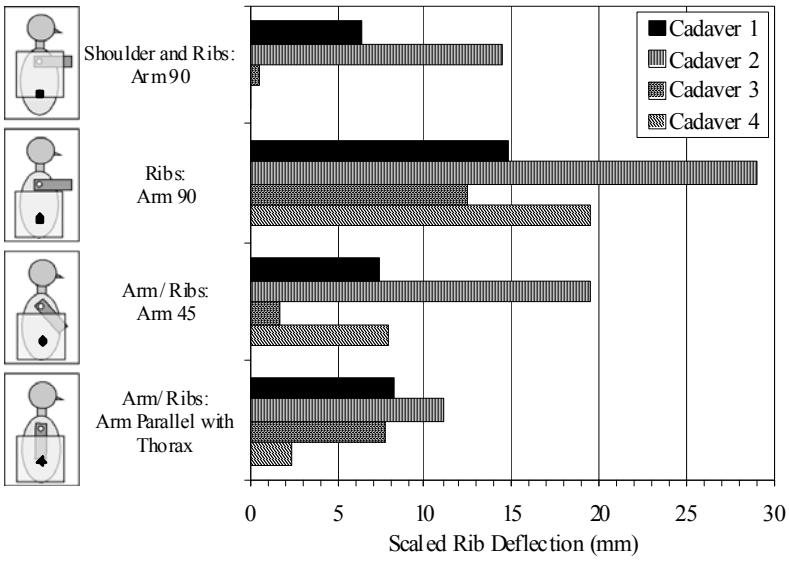

Figure 103: Peak rib 9 deflection for all non-destructive side impact tests.

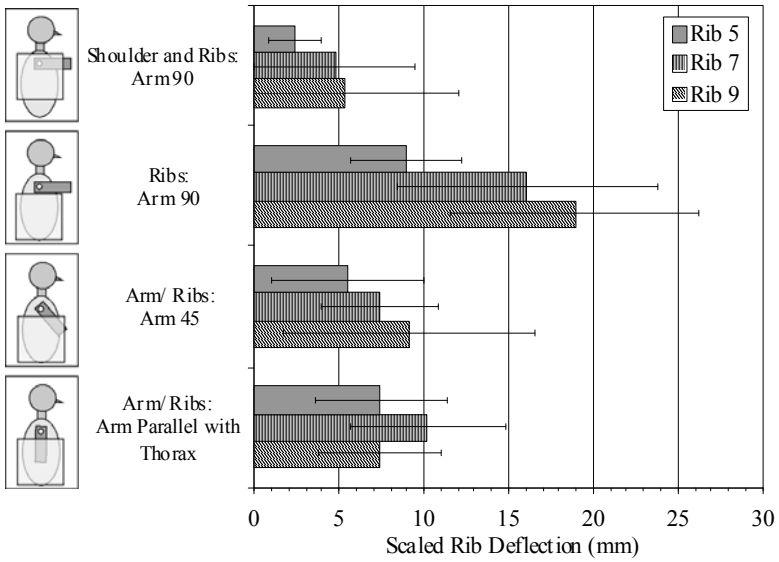

Figure 104: Average peak rib deflection averaged by side impact test condition.

Table 52: Peak lateral thoracic deflections for all non-destructive tests.

Test ID	Test Condition	Non-Scaled Deflection			Scaled Deflection			Compression		
		Rib 5 (mm)	Rib 7 (mm)	Rib 9 (mm)	Rib 5 (mm)	Rib 7 (mm)	Rib 9 (mm)	Rib 5 (%)	Rib 7 (%)	Rib 9 (%)
Tside1_1	Arm 90: Shoulder and Ribs	4.43	5.27	6.74	4.03	4.90	6.47	1.52	1.74	2.08
Tside2_1	Arm 90: Shoulder and Ribs	3.50	11.72	14.74	3.33	11.36	14.44	1.22	3.88	4.75
Tside3_1	Arm 90: Shoulder and Ribs	1.38	2.78	0.54	1.22	2.50	0.50	0.52	1.03	0.20
Tside4_1	Arm 90: Shoulder and Ribs	0.90	0.35	0.06	0.79	0.32	0.05	0.34	0.13	0.02
Tside1_2	Arm 90: Ribs	10.61	14.66	15.44	9.66	13.63	14.82	3.65	4.84	4.76
Tside2_2	Arm 90: Ribs	12.36	25.35	27.33	12.61	26.61	28.97	4.31	8.39	8.82
Tside3_4	Arm 90: Ribs	5.40	9.43	13.80	4.75	8.39	12.42	2.06	3.51	4.95
Tside4_4	Arm 90: Ribs	10.05	17.90	21.52	8.64	15.75	19.37	3.84	6.46	7.50
Tside1_3	Arm 45: Arm and Ribs	13.01	11.27	7.61	11.97	10.59	7.38	4.47	3.72	2.35
Tside2_3	Arm 45: Arm and Ribs	4.89	10.22	19.55	4.69	10.12	19.36	1.70	3.38	6.31
Tside3_3	Arm 45: Arm and Ribs	4.50	5.61	1.96	4.01	5.05	1.80	1.72	2.08	0.70
Tside4_3	Arm 45: Arm and Ribs	1.65	4.36	8.78	1.42	3.84	7.91	0.63	1.57	3.06
Tside1_4	Arm Parallel with Thorax : Arm and	13.97	17.00	8.47	12.99	16.15	8.30	4.80	5.61	2.61
Tside2_4	Arm Parallel with Thorax : Arm and	7.50	10.74	11.11	7.20	10.63	11.11	2.61	3.56	3.59
Tside3_2	Arm Parallel with Thorax : Arm and	5.52	9.99	8.52	4.80	8.89	7.67	2.11	3.71	3.05
Tside4_2	Arm Parallel with Thorax : Arm and	5.64	5.83	2.65	4.85	5.19	2.39	2.15	2.11	0.93

Rib Strain

The primary loading mode, tension or compression, on the external portion of the ribs was determined for all tests. For example, the primary loading mode for lateral strain gages on the struck and non-struck side was compression, while the primary loading mode for the posterior gages on the struck side was tension for the test condition when only the ribs were struck (Figure 105). In the event that the primary loading mode of one rib of one cadaver did not follow the trend seen by the other cadavers and/ or the adjacent ribs, the peak value in the mode that did correspond with the general trend was reported along with an asterisk (*) (Table 53 to Table 55). In the event that a rib experienced both tensile and compressive loading, the peak value in the mode that corresponded with the general trend of the other cadavers and adjacent ribs was reported. The peak rib strain in the primary mode of loading was averaged by rib level and region, for each non-destructive test type, over all cadavers (Figure 106 to Figure 109).

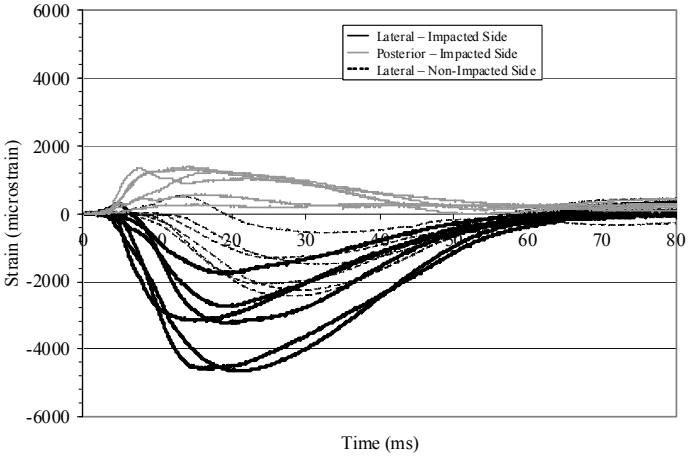

Figure 105: Example strain vs. time plot showing primary loading modes during a Rib: Arm 90 impact.

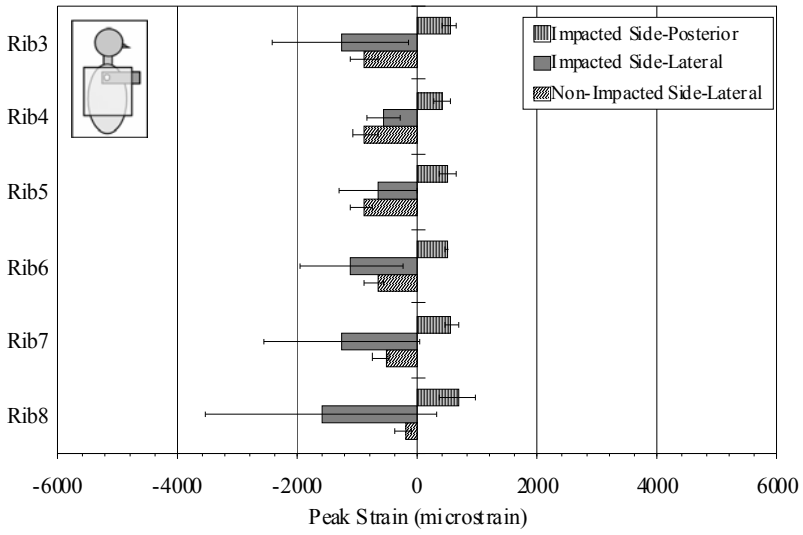

Figure 106: Primary loading mode average peak rib strain- Shoulder/ Ribs: Arm 90.
Note: Posterior strain was only obtained for cadavers 3 and 4.

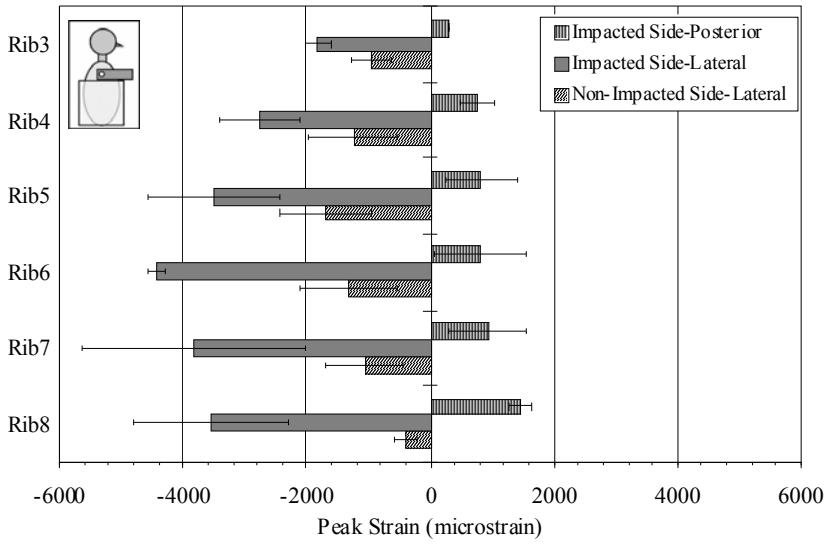

Figure 107: Primary loading mode average peak rib strain- Ribs: Arm 90.
Note: Posterior strain was only obtained for cadavers 3 and 4.

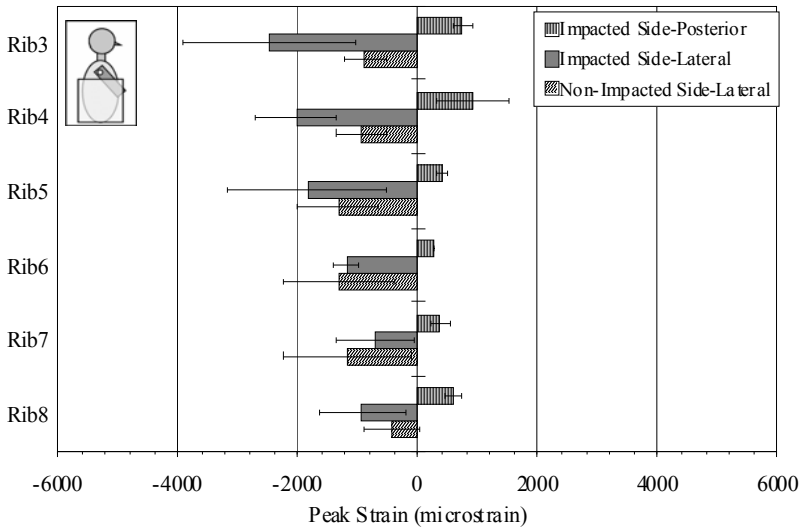

Figure 108: Primary loading mode average peak rib strain- Arm/ Ribs: Arm 45.
Note: Posterior strain was only obtained for cadavers 3 and 4.

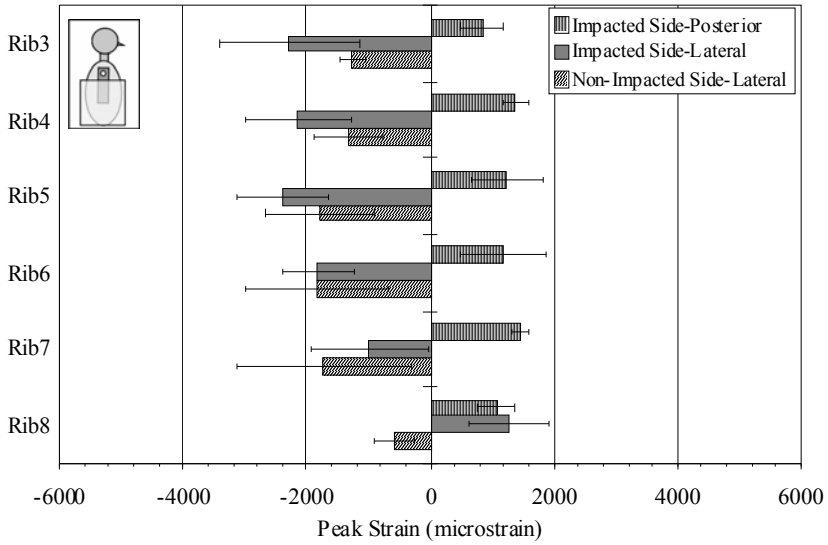

Figure 109: Primary loading mode average peak rib strain- Arm/ Ribs: Arm Parallel with Thorax.
Note: Posterior strain was only obtained for cadavers 3 and 4.

Table 53: Primary loading mode peak rib strain on struck side- lateral region.

Test ID	Test Condition	Region	Struck Side					
			Rib8	Rib7	Rib6	Rib5	Rib4	Rib3
			(µstrain)	(µstrain)	(µstrain)	(µstrain)	(µstrain)	(µstrain)
Tside1_1	Arm 90: Shoulder and Ribs	Lateral	-1965	-1903	-1315	-1655	B/G	-2961
Tside2_1	Arm 90: Shoulder and Ribs	Lateral	-4202	-2809	-1871	-408	-874	-775
Tside3_1	Arm 90: Shoulder and Ribs	Lateral	-160	-140	B/G	-317	-549	-943
Tside4_1	Arm 90: Shoulder and Ribs	Lateral	-106*	-242	-179	-319	-320	-424
Tside1_2	Arm 90: Ribs Only	Lateral	-6196	-5274	-4205	-4554	B/G	-2617
Tside2_2	Arm 90: Ribs Only	Lateral	-3766	-4663	-4416	-4430	-3596	-1492
Tside3_4	Arm 90: Ribs Only	Lateral	-1075	-826	B/G	-1846	-1990	-1357
Tside4_4	Arm 90: Ribs Only	Lateral	-3154	-4580	-4652	-3243	-2739	-1777
Tside1_3	Arm 45: Arm and Ribs	Lateral	-917	-249*	-1274	-3611	B/G	-4651
Tside2_3	Arm 45: Arm and Ribs	Lateral	-1828	-1368	-1347	-1396	-2751	-1663
Tside3_3	Arm 45: Arm and Ribs	Lateral	-81*	-69*	B/G	-1890	-1870	-1801
Tside4_3	Arm 45: Arm and Ribs	Lateral	-883	-1153	-939	-472	-1443	-1781
Tside1_4	Arm Parallel with Thorax : Arm and Ribs	Lateral	2211	-23*	-1246	-3277	B/G	-3942
Tside2_4	Arm Parallel with Thorax : Arm and Ribs	Lateral	1128	-529	-1852	-1704	-1864	-1749
Tside3_2	Arm Parallel with Thorax : Arm and Ribs	Lateral	815	-1201	B/G	-1811	-1474	-1418
Tside4_2	Arm Parallel with Thorax : Arm and Ribs	Lateral	941	-2204	-2402	-2775	-3122	-2034

Note: B/G = Broken Gage; N/A = Not Applicable;* indicates that the value is not in the primary mode of loading

Table 54: Primary loading mode peak rib strain on struck side- posterior region.

Test ID	Test Condition	Region	Struck Side					
			Rib8 (μstrain)	Rib7 (μstrain)	Rib6 (μstrain)	Rib5 (μstrain)	Rib4 (μstrain)	Rib3 (μstrain)
Tside1_1	Arm 90: Shoulder and Ribs	Posterior	N/A	N/A	N/A	N/A	N/A	N/A
Tside2_1	Arm 90: Shoulder and Ribs	Posterior	N/A	N/A	N/A	N/A	N/A	N/A
Tside3_1	Arm 90: Shoulder and Ribs	Posterior	885	631	501	593	503	621
Tside4_1	Arm 90: Shoulder and Ribs	Posterior	439	471	445	398	321	435
Tside1_2	Arm 90: Ribs Only	Posterior	N/A	N/A	N/A	N/A	N/A	N/A
Tside2_2	Arm 90: Ribs Only	Posterior	N/A	N/A	N/A	N/A	N/A	N/A
Tside3_4	Arm 90: Ribs Only	Posterior	1571	501*	273*	410	952	289
Tside4_4	Arm 90: Ribs Only	Posterior	1307	1380	1333	1243	579	300
Tside1_3	Arm 45: Arm and Ribs	Posterior	N/A	N/A	N/A	N/A	N/A	N/A
Tside2_3	Arm 45: Arm and Ribs	Posterior	N/A	N/A	N/A	N/A	N/A	N/A
Tside3_3	Arm 45: Arm and Ribs	Posterior	503*	258*	249*	463	1339	858
Tside4_3	Arm 45: Arm and Ribs	Posterior	696	488	248	326	480	631
Tside1_4	Arm Parallel with Thorax : Arm and Ribs	Posterior	N/A	N/A	N/A	N/A	N/A	N/A
Tside2_4	Arm Parallel with Thorax : Arm and Ribs	Posterior	N/A	N/A	N/A	N/A	N/A	N/A
Tside3_2	Arm Parallel with Thorax : Arm and Ribs	Posterior	1280	1361	674	827	1246	601
Tside4_2	Arm Parallel with Thorax : Arm and Ribs	Posterior	871	1569	1655	1640	1520	1097

Note: N/A = Not Applicable;* indicates that the value is not in the primary mode of loading

Table 55: Primary loading mode peak rib strain on non-struck side- lateral region.

Test ID	Test Condition	Region	Non-Struck Side					
			Rib8	Rib7	Rib6	Rib5	Rib4	Rib3
			(µstrain)	(µstrain)	(µstrain)	(µstrain)	(µstrain)	(µstrain)
Tside1_1	Arm 90: Shoulder and Ribs	Lateral	-347	-706	-839	-1110	-938	-920
Tside2_1	Arm 90: Shoulder and Ribs	Lateral	-359	B/G	-652	-856	-979	-524
Tside3_1	Arm 90: Shoulder and Ribs	Lateral	-98	-595	-837	-1020	-1061	-1137
Tside4_1	Arm 90: Shoulder and Ribs	Lateral	-39	-306	-371	-547	-604	-945
Tside1_2	Arm 90: Ribs Only	Lateral	-678	-1425	-1772	-2406	-1793	-947
Tside2_2	Arm 90: Ribs Only	Lateral	-252	B/G	-649	-1096	-528	-511
Tside3_4	Arm 90: Ribs Only	Lateral	-157	-278	-622	-754	-588	-1024
Tside4_4	Arm 90: Ribs Only	Lateral	-581	-1499	-2273	-2448	-2087	-1319
Tside1_3	Arm 45: Arm and Ribs	Lateral	-1085	-2432	-2697	-2277	-1426	-1213
Tside2_3	Arm 45: Arm and Ribs	Lateral	-387	B/G	-867	-1186	-868	-521
Tside3_3	Arm 45: Arm and Ribs	Lateral	-184	-615	-1140	-1226	-1072	-1151
Tside4_3	Arm 45: Arm and Ribs	Lateral	-37*	-500	-625	-629	-429	-635
Tside1_4	Arm Parallel with Thorax : Arm and Ribs	Lateral	-1083	-3307	-3572	-3067	-2126	-1489
Tside2_4	Arm Parallel with Thorax : Arm and Ribs	Lateral	-363	B/G	-1081	-1612	-1039	B/G
Tside3_2	Arm Parallel with Thorax : Arm and Ribs	Lateral	-431	-587	-1461	-1203	-905	-1201
Tside4_2	Arm Parallel with Thorax : Arm and Ribs	Lateral	-471	-1283	-1233	-1279	-1180	-1097

Note: B/G = Broken Gage; N/A = Not Applicable;* indicates that the value is not in the primary mode of loading

Destructive Testing

The scaled impactor force, peak scaled rib deflections, and injury documentation resulting from the destructive tests are presented in this section. High-speed video stills of the destructive testing performed on each cadaver are provided for qualitative kinematics (Figure 110). For both tests conducted with the arm placed at 45 degrees, the arm translated and rotated medially with continued impactor displacement, exposing the thorax to direct impactor loading by the impactor plate. For both tests conducted with the arm parallel with the thorax, the arm remained between the impactor and thorax throughout the test. It is important to note that the impacting cart did not reach the maximum allowed penetration in any of the destructive tests due to energy lost through soft tissue deflection, thoracic deflection, and the inertia/ motion of the thorax. Therefore, the impactor penetration was always limited by the interaction with the cadaver and not by the cable.

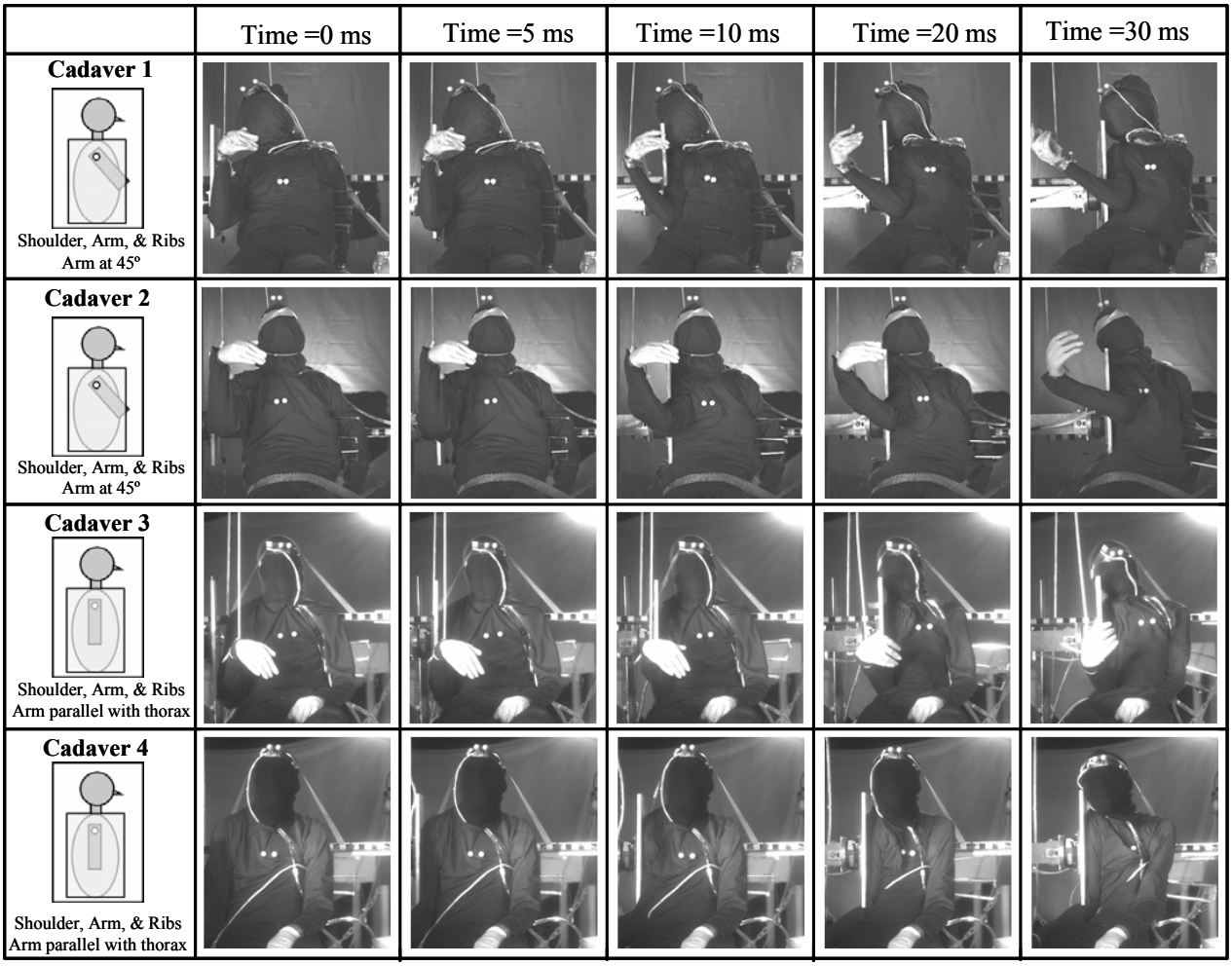

Figure 110: High-speed video stills of all destructive side impact tests.

Impactor Force and Rib Deflection

The scaled impactor force time histories for the destructive impact tests were plotted by impact condition (Figure 111 and Figure 112). In addition, the peak scaled and non-scaled impactor forces were tabulated (Table 56). The peak scaled rib 5, rib 7, and rib 9 deflections were plotted by cadaver and test type for the destructive testing (Figure 113).

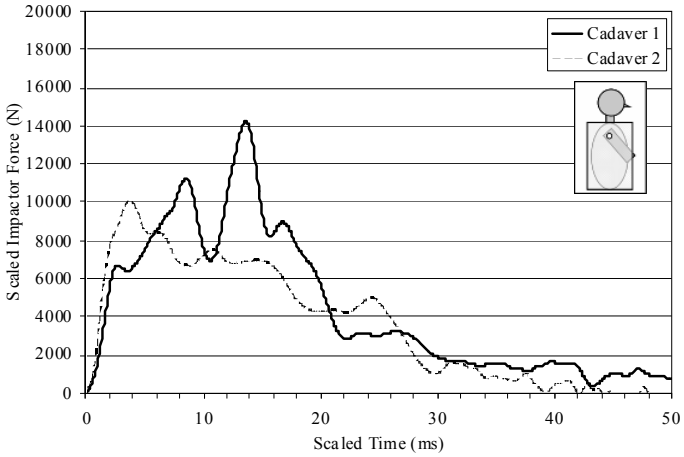

Figure 111: Scaled impactor force time history for destructive side impact tests- Arm 45.

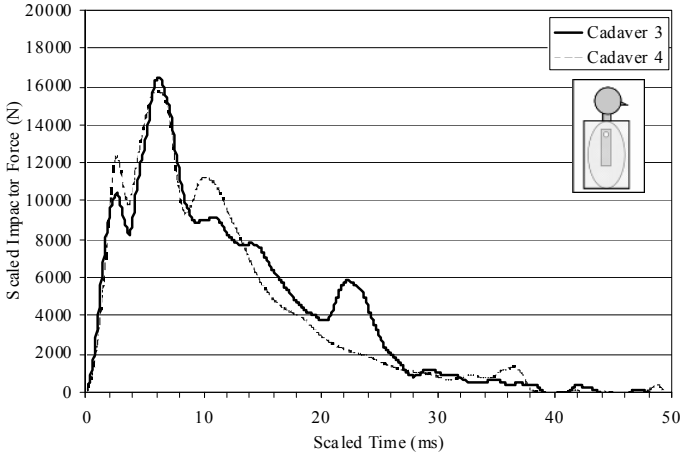

Figure 112: Scaled impactor force time history for destructive side impact tests- Arm Parallel with Thorax.

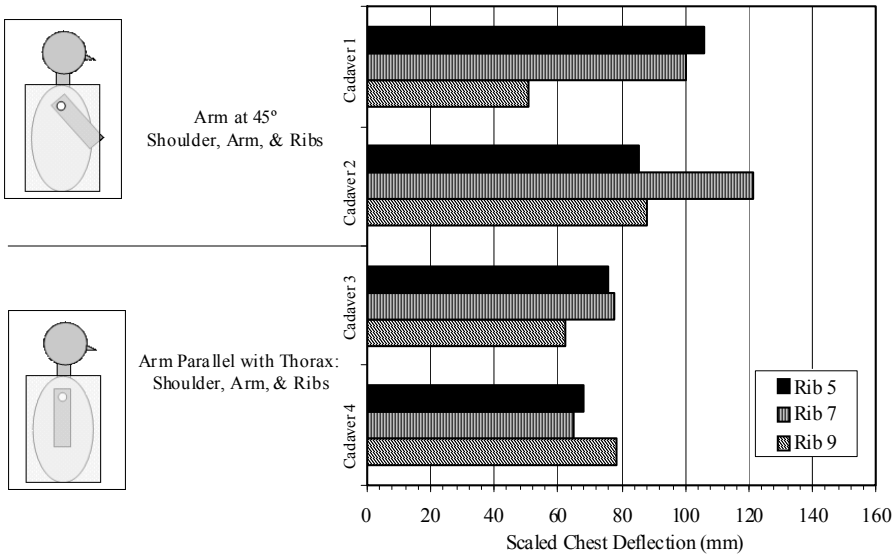

Figure 113: Peak rib deflections for all destructive side impact tests.

Table 56: Peak impactor force for all destructive side impact tests.

Test ID	Test Condition	Peak Inertially Compensated Impactor Force	Peak Scaled Impactor Force
		(N)	(N)
Tside1_5	Arm 45: Shoulder, Arm and Ribs	13926.2	14204.7
Tside2_5	Arm 45: Shoulder, Arm and Ribs	9259.7	10093.1
	Average	11593.0	11593.0
	Standard Deviation	3299.7	3299.7
Tside3_5	Arm Parallel with Thorax	14348.2	16500.4
Tside4_5	Arm Parallel with Thorax	14181.7	15741.6
	Average	14264.9	14264.9
	Standard Deviation	117.8	117.8

Injury Documentation

The skeletal and soft tissue injuries documented during the post-test dissection are presented in this section (Table 57, Figure 114 to Figure 117). Note that the number and distribution of observed injuries were almost identical with respect to impact condition. In addition, both cadavers struck with the arm placed at 45 degrees had approximately twice as many rib fractures

as the cadavers struck with the arm placed parallel with the thorax. Using rib fractures as the parameter for AIS injury level, tests conducted with the arm at 45 degrees resulted in a higher AIS injury level (AIS=4 for both cadavers) versus tests conducted with the arm parallel with the thorax (AIS=3 for both cadavers) due to the increased number of ribs with multiple fractures which resulted in a flail chest. The AIS (Abbreviated Injury Scale, 2005) defines flail chest as three or more ribs fractured in more than one location, i.e. posterior lateral and anterior lateral, and/or results in paradoxical chest movement. In addition, both cadavers struck with the arm placed at 45 degrees had lacerations to internal organs where cadavers struck with the arm placed parallel with the thorax did not. It should be noted that there were no observed injuries to the arm in any of the cadavers.

Table 57: Summary of observed skeletal and soft tissue injuries due to side impact loading.

Impact Condition		Struck Side		Non-Struck Side		Soft Tissue Injuries
		Shoulder	Thorax	Shoulder	Thorax	
Shoulder/ Ribs/ Arm: Arm 45	Sm_S1	None	9 Posterior Rib Fractures 12 Anterior/ Lateral Rib Fractures	None	1 Lateral Rib Fracture	Spleen Laceration
	Sm_S2	1 Clavicle Fracture	10 Posterior Rib Fractures 11 Anterior/ Lateral Rib Fractures	None	2 Lateral Rib Fracture	Spleen Laceration Liver Laceration
Shoulder/ Ribs/ Arm: Arm Parallel with Thorax	Sm_S3	1 Clavicle Fracture	2 Posterior Rib Fractures 5 Anterior/ Lateral Rib Fractures	Sternoclavicular Dislocation	3 Lateral Rib Fracture	None
	Sm_S4	Sternoclavicular Dislocation	2 Posterior Rib Fractures 5 Anterior/ Lateral Rib Fractures	None	3 Lateral Rib Fracture	None

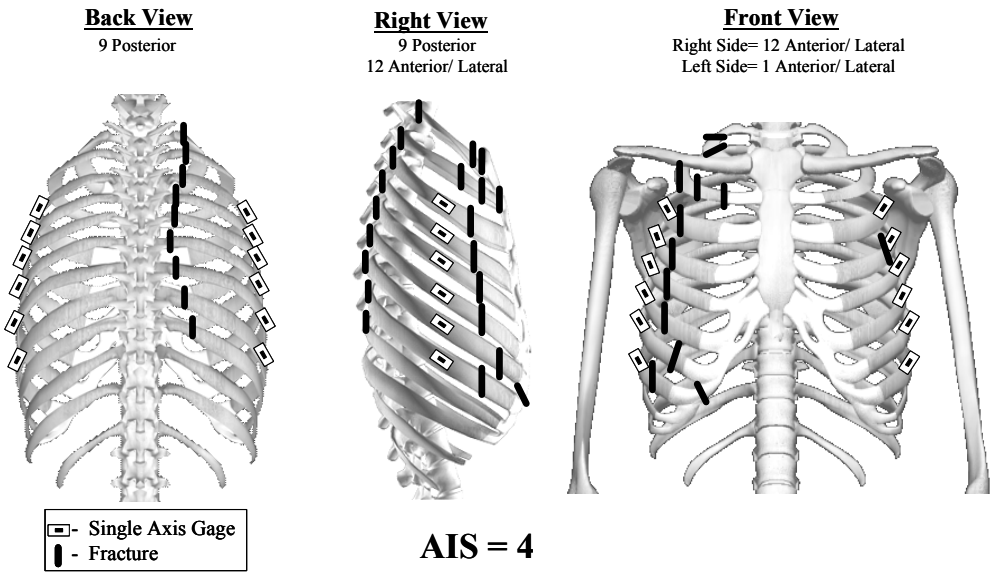

Figure 114: Rib fracture and strain gage locations for cadaver Sm_S1 destructive test - Arm 45.

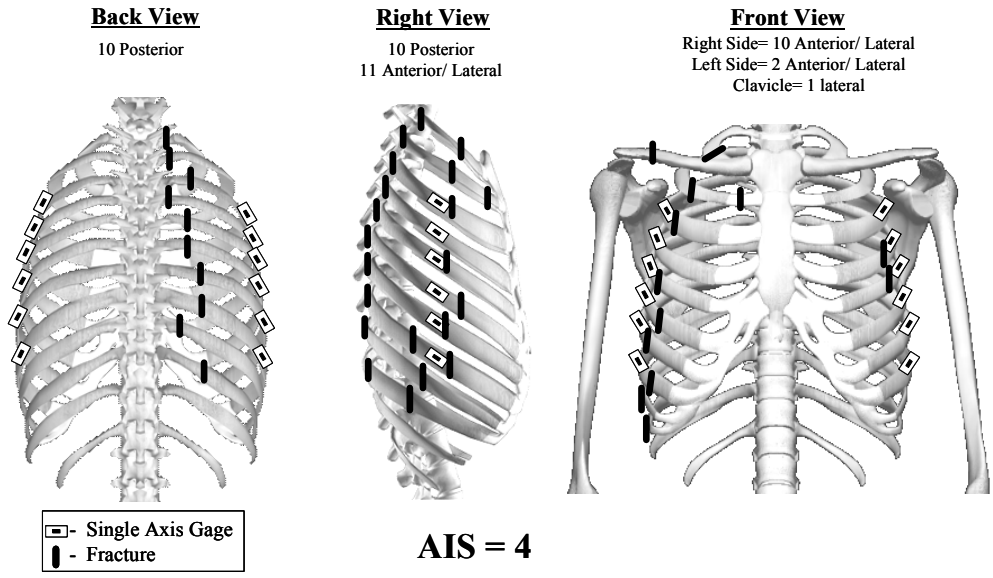

Figure 115: Rib fracture and strain gage locations for cadaver Sm_S2 destructive test - Arm 45.

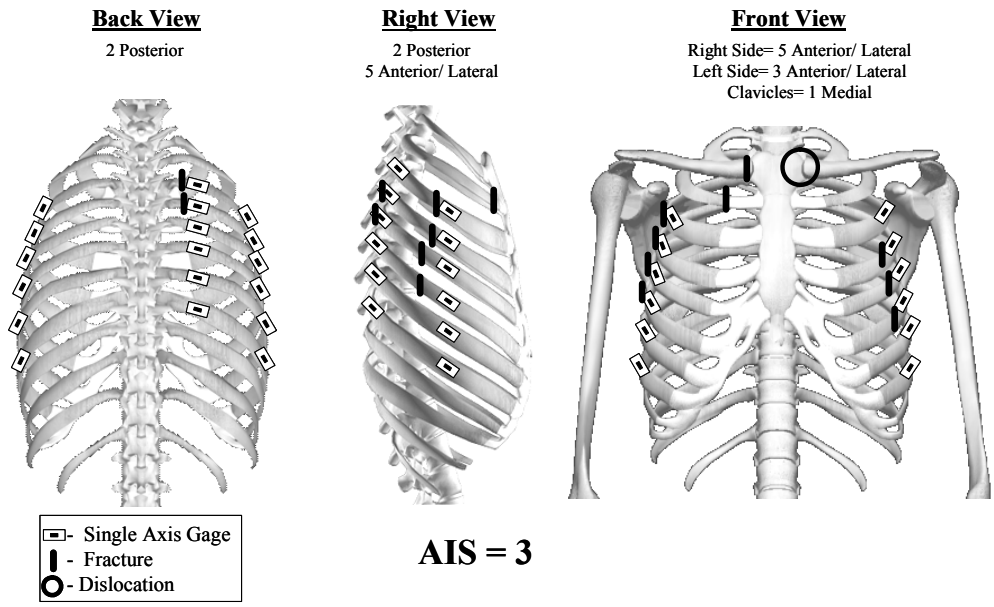

Figure 116: Rib fracture and strain gage locations for cadaver Sm_S3 destructive test - Arm Parallel with Thorax.

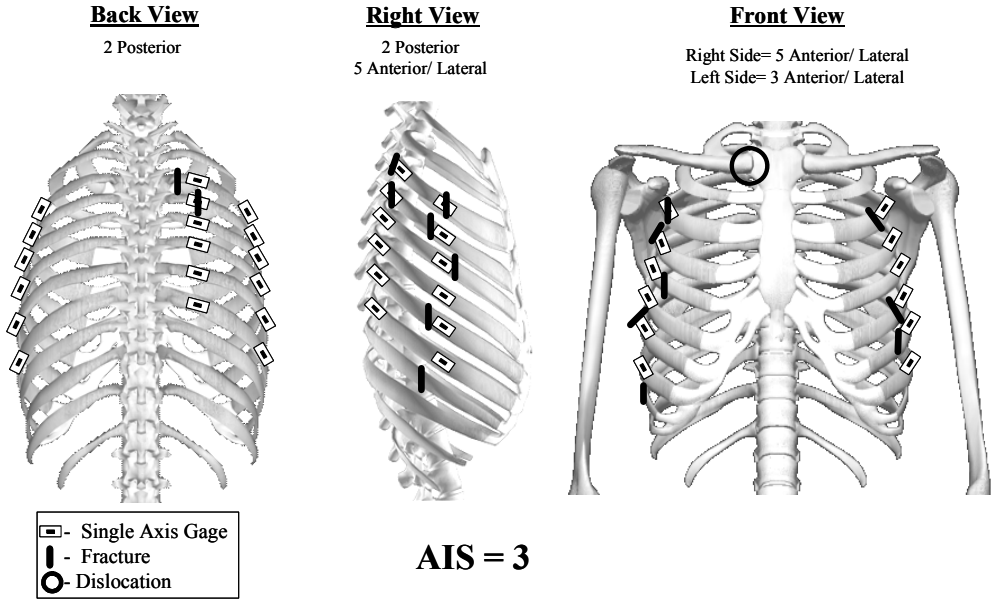

Figure 117: Rib fracture and strain gage locations for cadaver Sm_S4 destructive test - Arm Parallel with Thorax.

Rib Fracture Timing

The time histories of each strain gage were analyzed to determine the time at which each rib fracture occurred (Figure 118). The time of fracture could then be directly correlated to rib deflection (Table 58 to Table 61). The fractures that occurred directly under gages are of particular interest because the failure strain at the time of fracture could be obtained from these gages. The scaled rib 5, rib 7, and rib 9 deflections were plotted versus time with the fracture timing and corresponding AIS injury level, using rib fractures as the parameter for AIS (Figure 119 to Figure 122). Each rib fracture was plotted along the scaled rib 5, rib 7, and rib 9 deflection time histories in order to provide injury timing with respect to different rib deflection measurement locations. Due to the lack of posterior strain gages on the struck side of the thorax, the timing of the AIS 4 injury level could not be determined for cadavers 1 and 2. It should also be noted that the Abbreviated Injury Scale (2005) has multiple definitions for AIS=3 injury level based on rib fractures: ≥ 3 rib fractures without flail- any location unilateral or bilateral; fractures with flail- not further specified; unilateral fractures with flail- not further specified; and unilateral fractures with flail- 3 to 5 ribs with multiple fractures. In the current study, the timing of AIS=3 corresponded to the point at which the third rib fracture occurred.

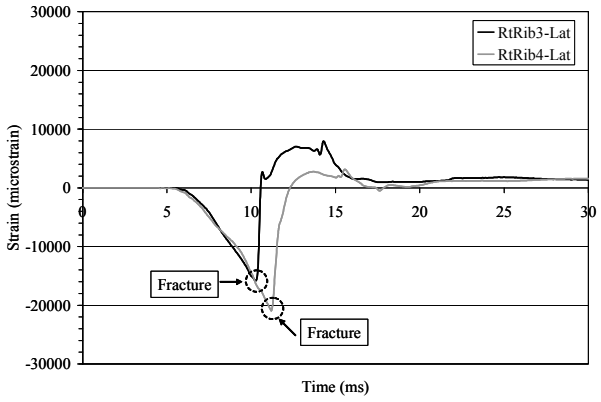

Figure 118: Determination of rib fracture timing.

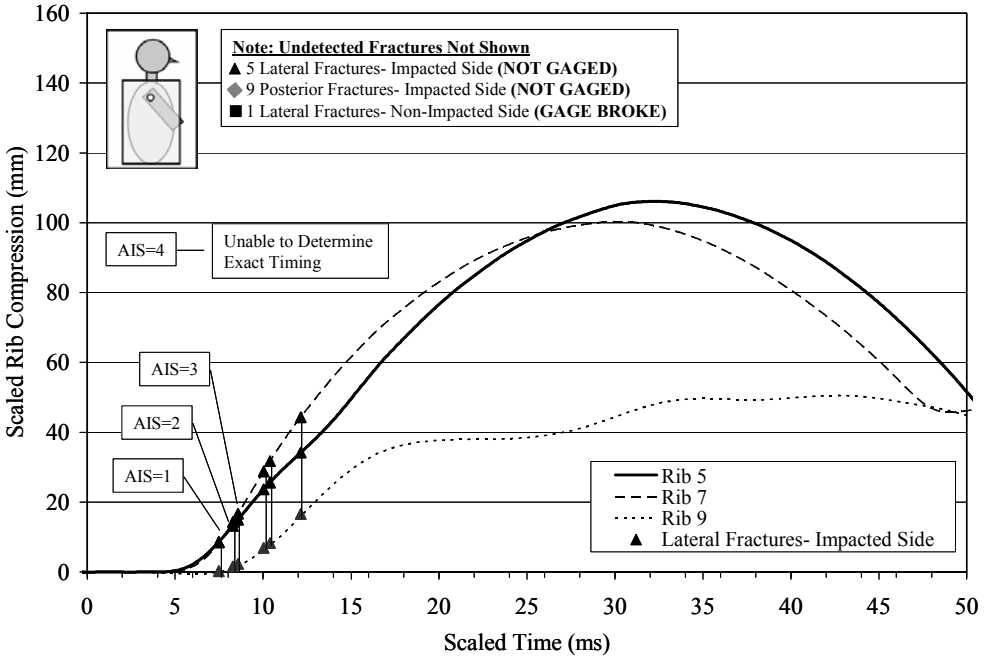

Figure 119: Rib fracture timing for cadaver Sm_S1 destructive side impact test. Shoulder/Arm/ Ribs: Arm 45

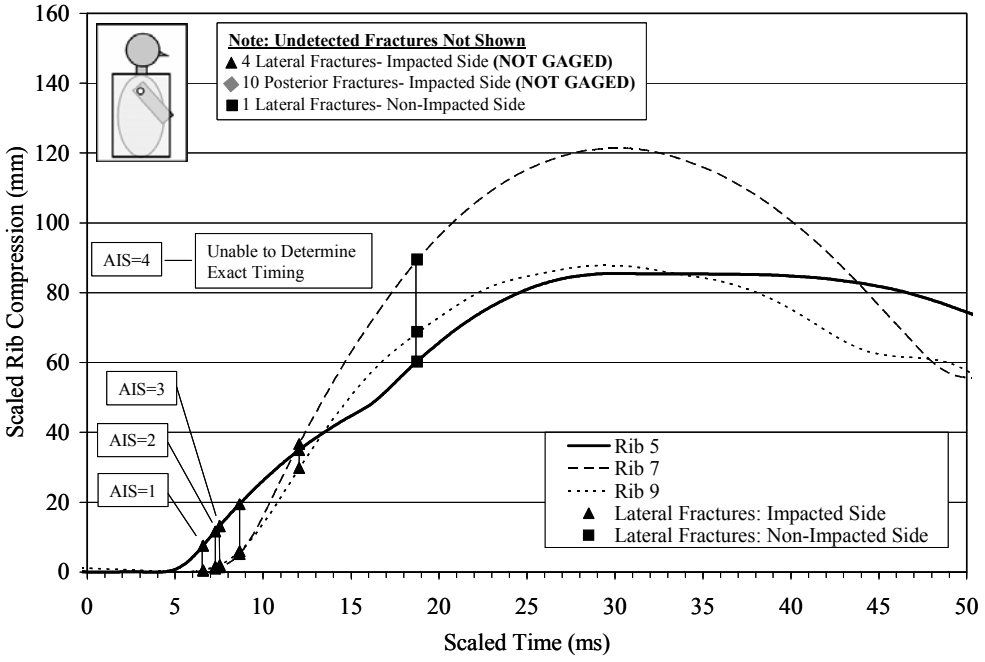

Figure 120: Rib fracture timing for cadaver Sm_S2 destructive side impact test. Shoulder/Arm/ Ribs: Arm 45.

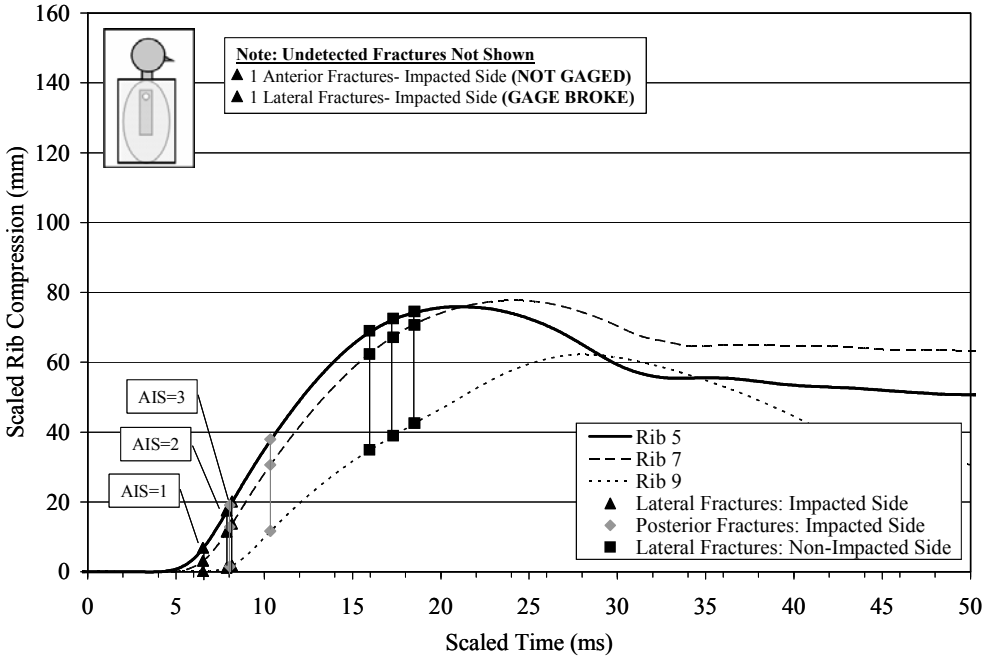

Figure 121: Rib fracture timing for cadaver Sm_S4 destructive side impact test. Shoulder/Arm/ Ribs: Arm Parallel with Thorax.

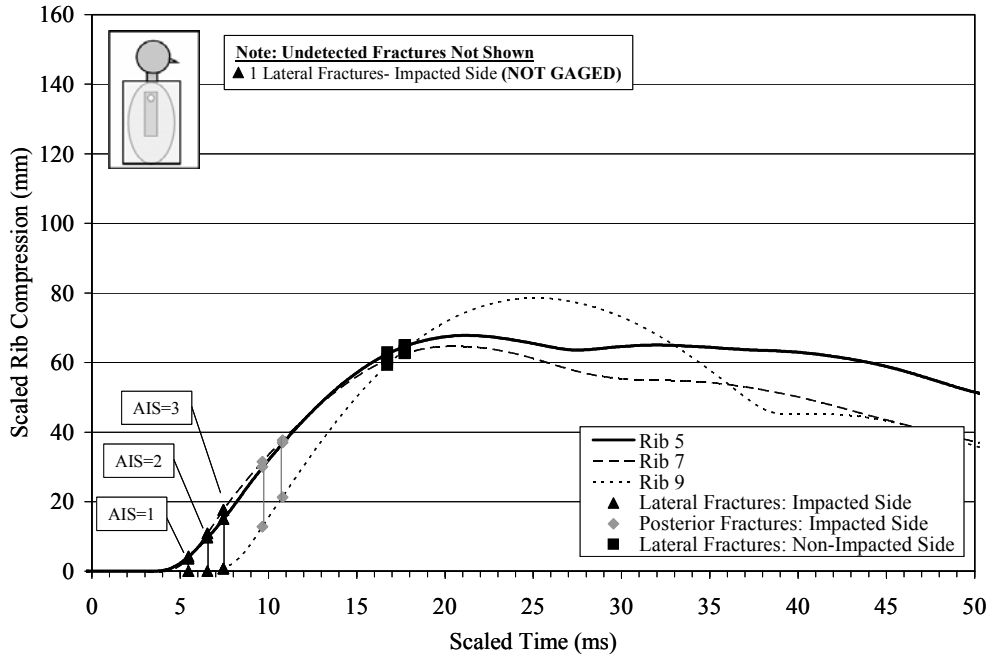

Figure 122: Rib fracture timing for cadaver Sm_S5 destructive side impact test. Shoulder/Arm/ Ribs: Arm Parallel with Thorax

Table 58: Rib fracture locations, fracture time, strain, and chest deflection for cadaver Sm_S1. Shoulder/Arm/Ribs: Arm 45

Region and Rib Number		Strain Gage (Yes/No)	Fracture Location	Strain at Time of Fracture	Non-Scaled Deflection			Scaled Deflection			Compression		
					Rib 5	Rib 7	Rib 9	Rib 5	Rib 7	Rib 9	Rib 5	Rib 7	Rib 9
				(µstrain)	(mm)	(mm)	(mm)	(mm)	(mm)	(mm)	(%)	(%)	(%)
Lateral -Struck Side	1	No	13 mm from sternum center 19 mm from sternum center	----	----	----	----	----	----	----	----	----	----
	2	No	32 mm from sternum center 57 mm from sternum center 108 mm from sternum center	----	----	----	----	----	----	----	----	----	----
	3	Yes	20 mm anterior of gage	-8878.9	15.6	17.0	2.3	15.0	16.7	2.3	5.4	5.6	0.7
	4	Yes	32 mm anterior of gage	-13600.3	35.7	45.2	16.4	34.2	44.3	16.6	12.3	14.9	5.1
	5	Yes	43 mm anterior of gage	-13808.3	24.7	29.4	6.8	23.7	28.8	6.8	8.5	9.7	2.1
	6	Yes	57 mm anterior of gage	-12621.1	13.8	14.6	1.6	13.3	14.3	1.6	4.7	4.8	0.5
	7	Yes	73 mm anterior of gage	-15771.8	26.7	32.4	8.2	25.7	31.7	8.3	9.2	10.7	2.5
	8	Yes	45 mm anterior of gage	-10893.5	9.0	8.6	0.3	8.6	8.4	0.3	3.1	2.8	0.1
	9	No	No Fracture	----	----	----	----	----	----	----	----	----	----
	10	No	No Fracture	----	----	----	----	----	----	----	----	----	----
Posterior- Struck Side	1	No	13 mm lateral of rib-spine joint	----	----	----	----	----	----	----	----	----	----
	2	No	19 mm lateral of rib-spine joint	----	----	----	----	----	----	----	----	----	----
	3	No	13 mm lateral of rib-spine joint	----	----	----	----	----	----	----	----	----	----
	4	No	6 mm lateral of rib-spine joint	----	----	----	----	----	----	----	----	----	----
	5	No	6 mm lateral of rib-spine joint	----	----	----	----	----	----	----	----	----	----
	6	No	0 mm lateral of rib-spine joint	----	----	----	----	----	----	----	----	----	----
	7	No	6 mm lateral of rib-spine joint	----	----	----	----	----	----	----	----	----	----
	8	No	19 mm lateral of rib-spine joint	----	----	----	----	----	----	----	----	----	----
	9	No	32 mm lateral of rib-spine joint	----	----	----	----	----	----	----	----	----	----
	10	No	No Fracture	----	----	----	----	----	----	----	----	----	----
Lateral -Non-Struck Side	1	No	No Fracture	----	----	----	----	----	----	----	----	----	----
	2	No	No Fracture	----	----	----	----	----	----	----	----	----	----
	3	Yes	No Fracture	----	----	----	----	----	----	----	----	----	----
	4	Yes	5 mm posterior of gage	B/G	B/G	B/G	B/G	B/G	B/G	B/G	B/G	B/G	B/G
	5	Yes	No Fracture	----	----	----	----	----	----	----	----	----	----
	6	Yes	No Fracture	----	----	----	----	----	----	----	----	----	----
	7	Yes	No Fracture	----	----	----	----	----	----	----	----	----	----
	8	Yes	No Fracture	----	----	----	----	----	----	----	----	----	----
	9	No	No Fracture	----	----	----	----	----	----	----	----	----	----
	10	No	No Fracture	----	----	----	----	----	----	----	----	----	----

Note: B/G= Broken Gage

Table 59: Rib fracture locations, fracture time, strain, and chest deflection for cadaver Sm_S2. Shoulder/Arm/Ribs: Arm 45

Region and Rib Number		Strain Gage (Yes/No)	Fracture Location	Strain at Time of Fracture	Non-Scaled Deflection			Scaled Deflection			Compression		
					Rib 5	Rib 7	Rib 9	Rib 5	Rib 7	Rib 9	Rib 5	Rib 7	Rib 9
				(μstrain)	(mm)	(mm)	(mm)	(mm)	(mm)	(mm)	(mm)	(mm)	(mm)
Lateral -Struck Side	1	No	86 mm from sternum center	----	----	----	----	----	----	----	----	----	----
	2	No	25 mm from sternum center 127 mm from sternum center	----	----	----	----	----	----	----	----	----	----
	3	Yes	**Immediately under gage**	-14156.0	8.2	0.4	0.6	7.5	0.4	0.5	2.8	0.1	0.2
	4	Yes	No Fracture	----	----	----	----	----	----	----	----	----	----
	5	Yes	**Immediately under gage**	-10136.0	37.9	38.8	31.3	34.9	36.5	29.8	13.2	12.8	10.1
	6	Yes	51 mm anterior of gage	-5560.0	12.6	1.1	1.6	11.6	1.0	1.5	4.4	0.4	0.5
	7	Yes	**Immediately under gage**	-7343.8	14.3	1.4	2.1	13.1	1.4	2.0	5.0	0.5	0.7
	8	Yes	45 mm posterior of gage 20 mm anterior of gage	-9090.3	21.1	5.4	6.3	19.4	5.1	6.0	7.4	1.8	2.0
	9	No	172 from sternum center	----	----	----	----	----	----	----	----	----	----
	10	No	229 from sternum center	----	----	----	----	----	----	----	----	----	----
Posterior- Struck Side	1	No	13 mm lateral of rib-spine joint	----	----	----	----	----	----	----	----	----	----
	2	No	19 mm lateral of rib-spine joint	----	----	----	----	----	----	----	----	----	----
	3	No	32 mm lateral of rib-spine joint	----	----	----	----	----	----	----	----	----	----
	4	No	0 mm lateral of rib-spine joint	----	----	----	----	----	----	----	----	----	----
	5	No	19 mm lateral of rib-spine joint	----	----	----	----	----	----	----	----	----	----
	6	No	19 mm lateral of rib-spine joint	----	----	----	----	----	----	----	----	----	----
	7	No	44 mm lateral of rib-spine joint	----	----	----	----	----	----	----	----	----	----
	8	No	44 mm lateral of rib-spine joint	----	----	----	----	----	----	----	----	----	----
	9	No	16 mm lateral of rib-spine joint	----	----	----	----	----	----	----	----	----	----
	10	No	64 mm lateral of rib-spine joint	----	----	----	----	----	----	----	----	----	----
Lateral -Non-Struck Side	1	No	No Fracture	----	----	----	----	----	----	----	----	----	----
	2	No	No Fracture	----	----	----	----	----	----	----	----	----	----
	3	Yes	No Fracture	----	----	----	----	----	----	----	----	----	----
	4	Yes	15 mm anterior of gage	N/D	N/D	N/D	N/D	N/D	N/D	N/D	N/D	N/D	N/D
	5	Yes	18 mm anterior of gage	-5295.7	65.5	94.9	72.4	60.2	89.2	68.8	22.8	31.4	23.3
	6	Yes	No Fracture	----	----	----	----	----	----	----	----	----	----
	7	Yes	No Fracture	----	----	----	----	----	----	----	----	----	----
	8	Yes	No Fracture	----	----	----	----	----	----	----	----	----	----
	9	No	No Fracture	----	----	----	----	----	----	----	----	----	----
	10	No	No Fracture	----	----	----	----	----	----	----	----	----	----

Note: N/D= Not Determined

Table 60: Rib fracture locations, fracture time, strain, and chest deflection for cadaver Sm_S3. Shoulder/Arm/Ribs: Arm Parallel with Thorax

Region and Rib Number		Strain Gage (Yes/No)	Fracture Location	Strain at Time of Fracture	Non-Scaled Deflection			Scaled Deflection			Compression		
					Rib 5	Rib 7	Rib 9	Rib 5	Rib 7	Rib 9	Rib 5	Rib 7	Rib 9
				(µstrain)	(mm)	(mm)	(mm)	(mm)	(mm)	(mm)	(mm)	(mm)	(mm)
Lateral -Struck Side	1	No	No Fracture	----	----	----	----	----	----	----	----	----	----
	2	No	51 mm from sternum center	----	----	----	----	----	----	----	----	----	----
	3	Yes	13 mm posterior of gage	-16220.1	19.4	12.5	1.2	17.4	11.5	1.1	7.4	4.6	0.4
	4	Yes	20 mm posterior of gage	-11183.7	22.3	15.0	1.9	20.1	13.8	1.8	8.5	5.6	0.7
	5	Yes	55 mm posterior of gage	-6501.1	7.6	3.5	0.1	6.8	3.2	0.1	2.9	1.3	0.0
	6	Yes	45 mm posterior of gage	B/G	B/G	B/G	B/G	B/G	B/G	B/G	B/G	B/G	B/G
	7	Yes	No Fracture	----	----	----	----	----	----	----	----	----	----
	8	Yes	No Fracture	----	----	----	----	----	----	----	----	----	----
	9	No	No Fracture	----	----	----	----	----	----	----	----	----	----
	10	No	No Fracture	----	----	----	----	----	----	----	----	----	----
Posterior- Struck Side	1	No	No Fracture	----	----	----	----	----	----	----	----	----	----
	2	No	No Fracture	----	----	----	----	----	----	----	----	----	----
	3	Yes	10 mm posterior of gage	7491.0	21.1	14.0	1.6	19.0	12.9	1.5	8.1	5.2	0.6
	4	Yes	10 mm posterior of gage	11350.0	42.0	33.5	12.6	37.8	30.8	11.7	16.1	12.4	4.5
	5	Yes	No Fracture	----	----	----	----	----	----	----	----	----	----
	6	Yes	No Fracture	----	----	----	----	----	----	----	----	----	----
	7	Yes	No Fracture	----	----	----	----	----	----	----	----	----	----
	8	Yes	No Fracture	----	----	----	----	----	----	----	----	----	----
	9	No	No Fracture	----	----	----	----	----	----	----	----	----	----
	10	No	No Fracture	----	----	----	----	----	----	----	----	----	----
Lateral -Non-Struck Side	1	No	No Fracture	----	----	----	----	----	----	----	----	----	----
	2	No	No Fracture	----	----	----	----	----	----	----	----	----	----
	3	Yes	No Fracture	----	----	----	----	----	----	----	----	----	----
	4	Yes	22 mm anterior of gage	-4786.6	80.3	73.4	42.0	72.3	67.5	39.0	30.7	27.3	15.0
	5	Yes	10 mm anterior of gage	-8540.5	76.4	68.1	37.6	68.8	62.7	35.0	29.2	25.3	13.5
	6	Yes	11 mm anterior of gage	-7668.1	82.6	77.2	45.8	74.3	71.0	42.6	31.6	28.7	16.4
	7	Yes	No Fracture	----	----	----	----	----	----	----	----	----	----
	8	Yes	No Fracture	----	----	----	----	----	----	----	----	----	----
	9	No	No Fracture	----	----	----	----	----	----	----	----	----	----
	10	No	No Fracture	----	----	----	----	----	----	----	----	----	----

Note: B/G= Broken Gage

Table 61: Rib fracture locations, fracture time, strain, and chest deflection for cadaver Sm_S4. Shoulder/Arm/Ribs: Arm Parallel with Thorax

Region and Rib Number		Strain Gage (Yes/No)	Fracture Location	Strain at Time of Fracture	Non-Scaled Deflection			Scaled Deflection			Compression		
					Rib 5	Rib 7	Rib 9	Rib 5	Rib 7	Rib 9	Rib 5	Rib 7	Rib 9
				(μstrain)	(mm)	(mm)	(mm)	(mm)	(mm)	(mm)	(mm)	(mm)	(mm)
Lateral -Struck Side	1	No	No Fracture	----	----	----	----	----	----	----	----	----	----
	2	No	No Fracture	----	----	----	----	----	----	----	----	----	----
	3	Yes	**Immediately under gage**	-15680.1	11.1	12.1	0.0	9.6	10.9	0.0	4.2	4.4	0.0
	4	Yes	13 mm posterior of gage	-20914.3	17.1	19.5	0.9	14.9	17.6	0.8	6.6	7.1	0.3
	5	Yes	19 mm anterior of gage	-4191.7	4.8	4.1	0.0	4.2	3.7	0.0	1.8	1.5	0.0
	6	Yes	No Fracture	----	----	----	----	----	----	----	----	----	----
	7	Yes	19 mm anterior of gage	-8663.6	17.1	19.5	0.9	14.9	17.6	0.8	6.6	7.1	0.3
	8	Yes	No Fracture	----	----	----	----	----	----	----	----	----	----
	9	No	171 from sternum center	----	----	----	----	----	----	----	----	----	----
	10	No	No Fracture	----	----	----	----	----	----	----	----	----	----
Posterior- Struck Side	1	No	No Fracture	----	----	----	----	----	----	----	----	----	----
	2	No	No Fracture	----	----	----	----	----	----	----	----	----	----
	3	Yes	25 mm medial of gage	9800.7	34.3	35.0	14.0	29.8	31.5	12.9	13.1	12.6	4.9
	4	Yes	**Immediately under gage**	14142.0	42.2	41.9	23.3	36.8	37.7	21.4	16.1	15.1	8.1
	5	Yes	No Fracture	----	----	----	----	----	----	----	----	----	----
	6	Yes	No Fracture	----	----	----	----	----	----	----	----	----	----
	7	Yes	No Fracture	----	----	----	----	----	----	----	----	----	----
	8	Yes	No Fracture	----	----	----	----	----	----	----	----	----	----
	9	No	No Fracture	----	----	----	----	----	----	----	----	----	----
	10	No	No Fracture	----	----	----	----	----	----	----	----	----	----
Lateral -Non-Struck Side	1	No	No Fracture	----	----	----	----	----	----	----	----	----	----
	2	No	No Fracture	----	----	----	----	----	----	----	----	----	----
	3	Yes	5 mm anterior of gage	-17608.0	72.0	67.7	64.8	62.6	60.9	59.6	27.5	24.5	22.6
	4	Yes	No Fracture	----	----	----	----	----	----	----	----	----	----
	5	Yes	No Fracture	----	----	----	----	----	----	----	----	----	----
	6	Yes	20 mm anterior of gage	-6261.2	74.4	69.6	69.4	64.7	62.7	63.9	28.4	25.2	24.2
	7	Yes	18 mm anterior of gage	-4827.8	74.2	69.5	69.2	64.6	62.6	63.6	28.4	25.1	24.1
	8	Yes	none	----	----	----	----	----	----	----	----	----	----
	9	No	none	----	----	----	----	----	----	----	----	----	----
	10	No	none	----	----	----	----	----	----	----	----	----	----

Discussion

This study investigated the effect of arm position on thoracic response and injury severity in side impacts. A total of sixteen non-destructive side impact tests and four destructive side impact tests were performed using four male cadavers. The controlled data set, test methodology, and thoracic instrumentation allowed for direct comparison of the thoracic response between the different impact conditions. The factors which contributed to differences in thoracic response between impact conditions are discussed in the following sections.

Impactor Force

The non-destructive tests performed in this study showed that both the shape and magnitude of the impactor force time history varied with respect to impact condition. When the four non-destructive tests are compared to one another, it is clear that impacts involving either the arm or shoulder reduced the maximum impactor force in the low-energy impacts. The impactor force was highest when only the thorax was struck because there was only a thin layer of soft tissue between the rib cage and impactor, which provided virtually no dampening prior to the loading of the thorax. The impactor force was lowest during the shoulder impact due to considerable displacement of the shoulder prior to loading the thorax. Therefore, the force response observed in the shoulder impacts was due primarily to the inertial response of the shoulder and arm, which has a relatively low mass compared to the thorax, and the compression of soft tissue.

All impact conditions, except the impact which only involved the ribs, resulted in two peaks in the impactor force time history. The first peak was due to the inertial and compressive response of the arm and/or shoulder while the second peak was due to the inertial and compressive

response of the thorax. When the two low-energy arm impacts were compared to one another, the first peak in impactor force was found to be larger when the arm was placed at 45 degrees compared to when the arm was placed parallel to the thorax due to the larger inertial response of the arm prior to loading of the ribs. To explain, when the arm was placed parallel to the thorax the arm had a limited amount of space to accelerate and translate before loading the lateral portion of the thorax, resulting in a relatively small inertial response (Figure 123). Conversely, when the arm was placed at 45 degrees the arm had considerably more space to translate and rotate medially about the shoulder joint before loading the anterior-lateral portion of the thorax (Figure 123). In addition, more mass of the arm was accelerated by the impactor prior to loading the thorax when the arm was placed at 45 degrees. This was due to the fact that when the arm was placed at 45 degrees only the upper portion of the arm loaded the ribs initially, while the mass of the lower portion of the arm and the mass of the forearm were accelerated until loading the anterior-lateral portion of the thorax. Consequently, the dissipation of more impactor energy prior to the loading of the rib cage resulted in a lower second peak in impactor force when the arm was placed at 45 degrees compared to when the arm was parallel with the thorax.

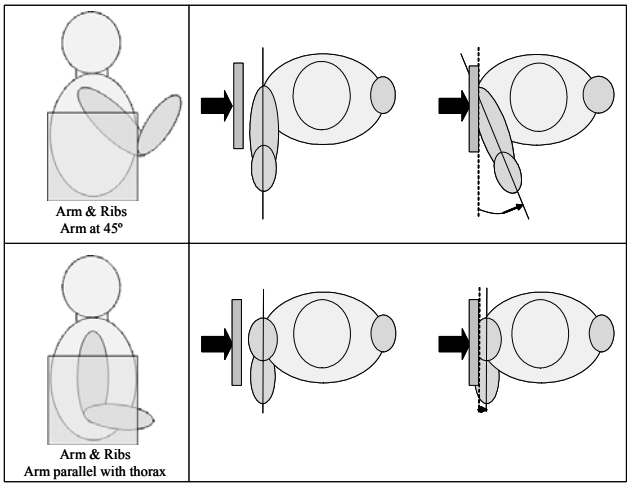

Figure 123: Illustration of arm motion for arm at 45 degrees versus parallel with thorax.

Rib Deflection

In the current study, rib deflection was measured using hollow thoracic rods attached to the internal portion of ribs 5, 7, and 9. Therefore, the deflection measurement reported in the current study does not include the deflection of the skin, soft tissue, or clothing surrounding the external portion of the thorax. Previous side impact studies have determined chest deflection with either a strain gage based chestband placed around the entire thorax or by taking the difference in the locations of photo targets, tracked by film analysis, placed on the ribs or spine and impacting surface (Irwin et al., 1993; Cavanaugh et al., 1993; Pintar et al., 1997; Viano, 1998; Shaw et al., 2006;). Consequently, these methods result in deflection measurements which include both skeletal and soft tissue compression. Therefore, the rib deflection measurements reported in the current study may be lower than the chest deflection measurements reported in previous studies.

The non-destructive testing showed that the peak rib deflections exhibited similar trends with respect to impact condition as the peak impactor force. In general, rib deflections were found to be largest when only the ribs were struck and lowest when the shoulder was struck. For all cadavers, the rib 5 and rib 7 peak deflections were found to be larger when the arm was placed parallel with the thorax versus when the arm was placed at 45 degrees. There was no consistent trend found for rib 9 peak deflections between the parallel and 45 degrees arm positions. Although the trends in peak rib deflection with respect to impact condition were not consistent for all cadavers, a certain amount of variability between subjects is expected due to factors which were not accounted for in the scaling procedure: modulus of elasticity of the ribs and thoracic anthropometry. However, the average peak rib deflection, which provides an overall means of comparison, clearly shows that all rib deflections were decreased when the arm was struck and

further decreased when the shoulder was struck. This finding is consistent with those reported by Stalnaker et al. (1979). In addition, the average peak rib 5 and rib 7 deflections were found to be larger when the arm was placed parallel with the thorax versus when the arm was placed at 45 degrees for all cadavers. This trend was due to the larger inertial response of the arm when placed at 45 degrees versus parallel with the thorax, which absorbed more impactor energy prior to the loading of the ribs.

The destructive testing showed that the peak rib 5 and rib 7 deflections for both cadavers struck with the arm placed parallel to the thorax were lower than the two cadavers struck with the arm at 45 degrees. Although this seemingly contradicts the trends observed in the non-destructive testing, the number of rib fractures should be taken into account. To explain, the cadavers struck with the arm at 45 degrees had approximately three times as many rib fractures on the struck side as the cadavers struck with the arm parallel with the thorax. In addition, a fracture timing analysis, discussed in a later section- *Rib Fracture Timing,* showed that the fractures on the struck side occurred well before the peak rib deflection. Logically, the thorax becomes structurally compromised as more ribs are fractured which, in turn, results in an increase in rib deflection with continued loading. Therefore, the increased peak rib deflection observed in the cadavers struck with the arm at 45 degrees versus cadavers struck with the arm parallel to the thorax was a result of the increased number of rib fractures on the struck side, which is discussed in a later section- *Fracture Patterns*.

Rib Strain

The rib strain in the current study was measured using single-axis strain gages attached directly to the external portions of the ribs at specific locations. In order to apply strain gages to the external portion of the ribs, the soft tissue and periosteum had to be removed from the rib at the location of the gage application. However, based on the results presented in Chapter 2 this technique does not have a significant effect on the structural response of the ribs. It should be noted that the strain gages only provide a local measurement of rib strain. Consequently, the peak strain values reported in the current study correspond to the peak strain at the location of the strain gage and not the peak strain along the length of the rib. However, the peak strain values reported in the current study can be directly compared between the different impact conditions.

In both the non-destructive and destructive testing, the rib strain gage data showed that the primary loading mode of the ribs varied with respect to thoracic region, i.e. circumferential distance from the spine or sternum. In general, the external portions of the ribs on the lateral region of both the struck and non-struck sides were placed in compression. This finding suggests that during side impact loading the sternum is displaced anteriorly away from the spine. This is consistent with previous side impact studies which quantified the contour of the thorax during side impact loading using chestbands (Pintar et al., 1997; Shaw et al, 2006). Unlike the lateral portions of the thorax, the posterior region of the struck side was placed in tension. This can be explained when the posterior boundary condition and natural curvature of the ribs are taken into account. The ribs are attached to the spine through the costovertebral joint, which allows only minimal rotation. In addition, the radius of curvature of the ribs decreases considerably just

lateral of the spine. As the lateral portion of the thorax was compressed, the curvature of the posterior region of the ribs was forced to increase, resulting in tension on the external portion of the posterior region.

The average peak rib strain on the lateral portion of the struck side exhibited similar trends with respect to impact condition as the average peak impactor force and average peak rib deflections in the non-destructive tests. The highest average peak rib strains on the lateral portion of the struck side were observed when only the ribs were struck. This was due to the fact that all the impactor energy was dissipated by the inertia and deflection of only the ribs. The average peak rib strain of the upper ribs on the lateral region of the struck side was lowest when only the shoulder was struck. This was due to the inertia and deflection of the shoulder and arm, which dissipated the majority of the impactor energy before loading the upper ribs. However, the average peak rib strain of the lower ribs was found to be larger for this impact condition versus the two arm impact conditions. This was due to the rotation of the torso about the x-axis of the pelvis, away from the impactor, as the shoulder was loaded and compressed exposing the lower ribs to loading of primarily cadaver Sm_S2. The comparison of the two arm impact conditions showed that the average peak strain on the lateral portions of the lower ribs on the struck side were slightly higher when the arm was placed parallel with the thorax versus 45 degrees. Logically, this was due to the direct load transmission to the lateral portion of the lower ribs through the arm when the arm was parallel to the thorax.

The average peak rib strain on the posterior portion of the struck side was found to vary with respect to impact condition in the non-destructive tests. However, the differences in average

peak rib strain on the posterior portion of the struck side with respect to impact condition were not as prominent as those seen in the average peak rib strain on the lateral portion of the struck side. In addition, the rib strain on the posterior portion of the ribs was only obtained for cadavers 3 and 4. Unlike the average peak rib strain on the lateral portion of the struck side, the average peak rib strain on the posterior region was highest when the arm was placed parallel to the thorax for all ribs except rib 8. This was most likely due to the wider contact area on the ribs from the arm, which resulted in rib deflection closer to the posterior region than when only the ribs were struck. The impact involving only the ribs resulted in higher posterior strain on the lower ribs than the impact when the arm was placed at 45 degrees. This was due to the more direct transmission of load to the lower ribs during the rib only impact. The average peak rib strain of the posterior region of the upper ribs was found to be higher when the arm was at 45 degrees versus the shoulder impact. This was because the inertia and compression of the arm and shoulder dissipated more impactor energy during the shoulder impact prior to loading the upper ribs.

The average peak rib strain on the lateral portion of the non-struck side was also found to vary with respect to impact condition in the non-destructive tests. Similar to the average peak rib strain on the posterior portion of the struck side, the average peak rib strain on the lateral region of the non-struck side was highest when the arm was placed parallel to the thorax. This was mostly likely due to the increased time to peak force during the impacts with the arm placed parallel with the thorax compared to the rib only impact, which allowed the non-struck side of the rib cage more time to respond. The average peak strain on the lateral portion of the non-struck upper ribs was found to be higher for the ribs only impact than the arm at 45 degrees

impacts. This was due to the increased impactor force and rib deflection observed in the rib only impact.

Rib Fracture Patterns

The post-test dissection showed that both the number and distribution of rib fractures was consistent with respect to impact condition, i.e. the arm position. In addition, approximately twice as many rib fractures were observed when the arm was placed at 45 degrees versus parallel to the thorax. Specifically, cadavers struck with the arm placed at 45 degrees had posterior rib fractures on almost every rib of the struck side, while cadavers struck with the arm placed parallel with the thorax only had two. In addition, cadavers struck with the arm placed at 45 degrees had considerably more lateral rib fractures on the lower ribs of the struck side. Given that the mass, velocity, stroke, and area of the impactor were held constant for both impact conditions, the differences in the observed rib fractures between the two impact conditions could be attributed to either subject variation, the influence of the arm position, or a combination of both.

It has been well established in the literature that the fracture tolerance of the bone is related to subject age, BMD, and cross-sectional geometry. Previous side impact studies involving human cadavers have shown that thoracic injury tolerance decreases with age regardless of impact direction (Eppinger et al., 1984; Kallieris et al., 1992; Cavanaugh et al., 1993; Zhou et al., 1996). In addition, studies involving tension coupon tests of isolated cortical bone have shown that ultimate strain decreases significantly with increasing age (Lindahl and Lindren, 1967; Yamada, 1970; Burstein et al., 1976; McCalden et al., 1993; Kemper et al., 2005;). However, the cadavers

used in the current study were all males with ages within approximately one decade of each other. Therefore, it is unlikely that differences in age contributed considerably to the number and distribution of rib fractures. With respect to BMD, previous studies have shown that the strength of cortical bone significantly decreases with decreasing apparent wet and dry density (Muellar et al., 1966; Carter and Haynes, 1976; Martin and Ishida, 1989; Schaffler and Burr, 1988; McCalden et al., 1993; Keller, 1994). In the current study, one subject with a low global BMD and one subject with a high global BMD were used for each impact condition and the fracture pattern was virtually identical with respect to impact condition. For example, one cadaver struck with the arm at 45 degrees had a normal global BMD (cadaver Sm_S2) while the other (cadaver Sm_S1) had a global BMD indicating osteoporosis. Again, global BMD only provides an indication of overall bone quality and does not account for local changes in BMD or composition. However, the fracture pattern was virtually identical between the two cadavers, and cadaver Sm_S2 had one more fracture than cadaver Sm_S1. Therefore, it is unlikely that differences in global BMD contributed considerably to the number and distribution of rib fractures.

When comparing the differences in the observed rib fractures between the two arm positions, the load path to the thorax resulting from arm position should be considered. When the arm was placed at 45 degrees, the impact force was initially transmitted to the anterior/lateral region of the upper ribs after the initial deflection of the shoulder and soft tissue of the arm. This resulted in multiple fractures to the upper ribs on the struck side. Unlike the non-destructive testing, the inertial and compressive responses of the arm and shoulder were not large enough to dissipate a considerable amount of impactor force before the ribs were loaded during the destructive tests

due to the significantly larger impact energy. Therefore, with continued impactor displacement the arm and shoulder rotated medially exposing the lateral region of the lower ribs to direct impactor loading. This resulted in a large number of posterior fractures on the struck side and anterior/ lateral fractures of the lower ribs on the struck side. When the arm was placed parallel to the thorax the impactor force was transmitted to lateral portions of both the upper and lower ribs on the struck side after the initial deflection of the shoulder and soft tissue of the arm. As opposed to when the arm was placed at 45 degrees, the arm remained between the ribs and impactor throughout the duration of the test. This resulted in fewer fractures on the struck side due to the distribution of force over a larger area and increased energy absorption by the arm due to the compression of more soft tissue than when the arm was placed at 45 degrees.

Rib Fracture Timing

The analysis of the strain gage time histories showed that, in general, the rib fracture timing varied with respect to thoracic region, i.e. the circumferential distance from the spine or sternum. For both cadavers struck with the arm parallel to the thorax, lateral fractures on the struck side occurred first, followed by posterior fractures on the struck side, and lastly lateral fractures on the non-struck side. For the second cadaver struck with the arm at 45 degree (cadaver Sm_S2), lateral fractures on the struck side occurred first, followed by lateral fractures on the non-struck side. Due to a lack of strain gages on the posterior region, the timing of the posterior fractures relative to the lateral portions of the struck and non-impact sides could not be determined for the two cadavers struck with the arm at 45 degrees. Using scaled rib 5 deflection, lateral fractures on the struck side occurred between 4.2 mm and 34.9 mm, posterior fractures on the struck side occurred between 19.0 mm and 37.8 mm, and lateral fractures on the non-struck side occurred

between 60.2 mm and 74.3 mm. It should be noted that no fractures were observed at similar rib 5 deflections during the non-destructive tests due to the considerably lower impact velocity compared to that of the destructive tests. To explain, it has been well established in the literature that bone is a viscoelastic material and that the ultimate strain decreases with increased loading rate (McElhaney and Byars, 1965; Wood, 1971; Crowninshield and Pope, 1974; Wright and Hayes, 1976; Carter et al., 1976; and Stein and Granik 1979).

The fracture timing results of the current study could lead to a greatly improved side impact criterion. This is due to the fact that the fracture timing analysis showed that all rib fractures occurred before peak compression. The observation that rib fractures occur before peak chest compression has been made by previous researchers investigating the tolerance of the thorax in frontal loading (Kroell et al., 1974; Duma et al., 2005). Using rib fractures as the parameter for AIS level, it was found that an AIS=1 injury level occurred at a scaled chest deflections of 4.2 mm to 8.6 mm (2% to 3% compression), AIS=2 at 9.6 to 17.4 mm (4% to 7% compression), and AIS=3 at 13.1 mm to 20.1 mm (5% to 9% compression) measured at rib five. It is important to note that despite all of the strain gages used in this study, the fracture timing could not be determined for every rib fracture. Consequently, the rib deflections corresponding to a given AIS injury level cannot be considered exact. To explain, it is possible that some of the rib fractures with unknown timing occurred before the rib fractures reported to correspond to a given injury level. This would result in AIS injury levels corresponding to lower rib deflections than those reported in the current study. However, if the fractures with unknown timing occurred after the rib fractures reported to correspond to a given injury level, the timing of the AIS injury

levels reported in the current study would not change. Therefore, the AIS injury level timing and corresponding rib deflections reported in the current study can be considered conservative.

Limitations and Future Studies

There are several factors to consider when interpreting the results of this study. First, only four cadavers were used in the current study, all of which were males of approximately the same age and weight. Although the similarities between cadavers helped minimize the variation in thoracic response between subjects, additional testing should be conducted to determine the effects of age, mass, and gender. Another limitation of the study was that only one impactor mass and velocity was used for the non-destructive testing. Additional testing should be conducted to determine the impactor energy threshold which no longer results in decreased rib deflection and strain, due to the inertial and compressive response of the arm, when the arm is placed at 45 degrees compared to when it is parallel with the thorax. For the destructive testing, the shoulder was directly loaded during both impact conditions. Additional destructive tests should be conducted to provide rib fracture data when the shoulder is not involved in the impact as well as when neither the arm nor shoulder is involved in the impact. Lastly, the fracture timing of the posterior portion of the ribs and corresponding point of AIS=4 could not be obtained for the destructive tests when the arm was placed at 45 degrees due to a lack of posterior gages. Therefore, additional tests could be conducted with posterior strain gages on the struck side to obtain this data.

Conclusions

In the current study, the effect of arm position on thoracic response and injury severity in side impacts was investigated by performing a total of sixteen non-destructive side impact tests and four destructive side impact tests on four human male cadavers. The primary loading mode of the ribs varies with respect to thoracic region during side impact loading. In general, the external portions of the ribs on the lateral region of both the struck and non-struck side are placed in compression while the external portion of the ribs on the posterior region of the struck side are placed in tension. In the low-energy side impacts, impacting the arm and/or shoulder reduces the impact forces, rib deflections, and rib strains compared to the values obtained when impacting only the ribs. In high-energy, rigid surface side impacts, the position of the arm has a considerable affect on both the total number and distribution of rib fractures. In the high-energy, rigid surface side impacts, rib fracture timing generally varies with respect to the thoracic region. For both cadavers struck with the arm parallel with the thorax, lateral fractures on the struck side occurred first, followed by posterior fractures on the struck side, and lastly lateral fractures on the non-struck side. For the second cadaver struck with the arm at 45 degree (cadaver 2), lateral fractures on the struck side occurred first, followed by lateral fractures on the non-struck side. In the high-energy, rigid surface side impacts, all rib fractures occurred before peak chest compression. Using the number and location of rib fractures as the measure of thoracic AIS injury level, for the high energy, rigid surface side impacts, AIS=1 level injury occurred at Rib 5 scaled deflections of 4.2 mm to 8.6 mm (2% to 3% compression), AIS=2 at 9.6 to 17.4 mm (4% to 7% compression), and AIS=3 at 13.1 mm to 20.1 mm (5% to 9% compression).

CHAPTER 7

Research Summary and Expected Publications

Research Summary

This dissertation provides new and significant research to the field of injury biomechanics. The specific research objectives focus on providing material, structural, and global thoracic skeletal response data not currently addressed in the literature. The general methods and subsequent conclusions of the five controlled studies performed answer multiple scientific questions which are summarized below.

The effect of the periosteum, application of a strain gage, and hydration level on the structural response of human ribs was determined by performing 48 dynamic three-point bending tests. In order to eliminate the confounding effects of material and geometric variation between individuals, each condition was evaluated by performing tests on matched specimens obtained from the right and left side of the thorax. Based on the results of this study, the following conclusions were made:

- The removal of the periosteum does not have a significant effect on the structural response of human ribs.
- The removal of the periosteum and application of a strain gage does not have a the significant effect on the structural response of human ribs.
- There is no significant difference in the structural response of the human ribs stored in saline-soaked gauze versus those immersed in saline.

The effect of loading direction on the biomechanical response of the human clavicle was determined by performing 20 dynamic three-point bending tests. For this study, two impact directions were evaluated: 0° from the transverse plane, and 45° from the transverse plane. Tests were performed on matched claviculae obtained from the right and left side in order to eliminate the confounding effects of material and geometric variation between individuals. Based on the results of this study, the following conclusions were made:

- The structural response of the human clavicle is significantly stiffer when struck 0° from the transverse plane versus 45° from the transverse plane.
- Due to the controlled matched data set, the difference in the structural response with respect to loading direction can be attributed to the complex geometry of the clavicle and not material differences.

The variables which contribute to the regional variation in the strength of human ribs were investigated through 94 matched tests on human rib specimens: 46 tension coupon tests and 48 three-point bending tests. The cross-sectional geometry of the three-point bending specimens was quantified using microCT imaging. Based on results of this study, the following conclusions were made:

- The results of the tension coupon testing showed that there are no significant differences in material properties with respect to rib region and level.
- The results of the three-point bending testing showed that the structural response of human ribs varies significantly with respect to anatomical region and rib level.

- The local cross-sectional geometry of human ribs was found to significantly vary with respect to anatomical region and rib level, and these variations correspond to variations in structural response.

The thoracic response due to frontal belt loading was examined with respect to two back support conditions, flat rigid plate versus spine box, by performing 4 non-destructive and 4 destructive tests on 4 human cadavers using a table-top belt loader. The spine box was designed to support the thorax while allowing costovertebral joint articulation. Rib strain and fracture timing was quantified with the use of both single-axis and rosette strain gages attached to the ribs. Based on the results of this study, the following conclusions were made:

- There is no considerable effect on thoracic response with respect to the two back support conditions during frontal belt loading.
- The strain gage rosettes showed that the direction of the first principal strain is essentially in line with the main axis of the rib.
- Rib fracture timing generally varies with respect to the thoracic region: fractures on the left side occur first followed by fractures on the upper right side of the thorax.
- All rib fractures occur within 35% thorax compression.
- Using rib fractures as the parameter for AIS level, AIS=3 occurs at of 13% - 16% chest compression for male cadavers and 13% - 22% chest compression for female cadavers.

The influence of arm position on thoracic response and injury severity during dynamic side impact loading was determined by performing 20 tests, 16 non-destructive and 4 destructive, on 4 human cadavers with the use of a custom pneumatic impactor. Rib strain and fracture timing were quantified with the use of single-axis strain gages attached to the ribs. Based on the results of this study, the following conclusions were made:

- The primary loading mode of the ribs varies with respect to thoracic region: the lateral region of both the struck and non-struck side is placed in compression while the posterior region of the struck side is placed in tension.
- The involvement of the shoulder or arm in side impact loading both attenuates and distributes impactor energy, resulting in decreased impactor force, lateral rib deflection, and strain relative to direct impacts to the rib cage.
- In high-energy side impact tests, larger peak rib deflection and injury severities are observed when the arm is positioned at 45 degrees versus parallel with the thorax.
- Rib fracture timing generally varies with respect to the thoracic region: lateral fractures on the struck side occur first, then posterior fractures on the struck side, and lastly lateral fractures on the non-struck side.
- In high-energy side impacts, all rib fractures occur before peak chest compression.
- Using rib fractures as the parameter for AIS level, AIS=1 injury level occurs at a scaled chest deflections of 4.2 mm to 8.6 mm (2% to 3% compression), AIS=2 at 9.6 to 17.4 mm (4% to 7% compression), and AIS=3 at 13.1 mm to 20.1 mm (5% to 9% compression) measured at rib five.

The research presented in this dissertation has yielded a comprehensive set of experimental thoracic skeletal response data not previously addressed in the literature. The results of the rib and clavicle studies outlined in this dissertation provide crucial material, structural, and geometric validation data needed to improve current thoracic FEMs used to assess thoracic injury risk in automotive collisions. In addition, the results of the thoracic belt loading and side impact studies provide novel global response data that can be used to validate and improve both FEMs and ATDs. The devolvement of FEMs and ATDs with improved thoracic injury risk assessment capabilities would provide researchers and safety engineers with a more accurate tool to evaluate the effectiveness of both new and existing safety restraint technologies, which are integral in the mitigation of thoracic injuries and fatalities.

In addition to validation data, this dissertation demonstrates a methodology for determining rib fracture timing in both frontal belt loading and side impact loading, which could augment and clarify the foundation of thoracic injury criteria. The current thoracic injury criteria for both frontal and side impact dummies are inherently limited by the fact that they were developed based on the results of cadaveric studies which rely primarily on censored rib fracture data. In other words, it is not possible to determine the exact loads, accelerations, or displacements at the time of fracture. Rather, it is only known that an injury occurred at some point during the impact test. Consequently, these studies rely on statistical regression models to develop injury risk functions with respect to global criteria, such as peak chest deflection. The methodology for quantifying rib fracture timing in both frontal belt loading and side impact loading outlined in this dissertation allows for the determination of the exact thoracic deflections which correspond to each injury severity level, defined by the abbreviated injury scale (AIS).

The injury timing data presented in this dissertation clearly shows that AIS ≥ 3 thoracic injuries in both frontal belt loading and side impacts occur at considerably lower chest deflections than the current respective frontal and side impact thoracic injury criteria. The FMVSS for frontal impacts (FMVSS 208- Moving Deformable Barrier) specifies that the chest compression cannot exceed 63 mm (29% chest compression) for the belted male dummy and 52 mm (23% chest compression) for the belted female dummy during a 40 kph impact, which corresponds to a 50% risk of an AIS ≥ 3. The frontal belt loading outlined in this dissertation shows that AIS=3 occurs at 13% - 16% chest compression for male cadavers and 13% - 23% chest compression for female cadavers. The new FMVSS side impact pole test (FMVSS 214- Pole) specifies that the lateral rib deflection of the belted male dummy cannot exceed 44 mm, which corresponds to a 50% risk of an AIS ≥ 3. The destructive side impact loading outlined in this dissertation shows that AIS=3 occurs at 13.1 mm to 20.1 mm (5% to 9% compression) measured at rib five.

Although the research presented in this dissertation indicates that the thoracic injury criteria for both frontal and side impact dummies could be greatly improved, these studies were performed on a limited number of cadavers. In order to develop a robust thoracic injury threshold, additional testing using the methods outlined for determining rib fracture timing with respect to thoracic deflection in both frontal belt loading and side impact loading needs to be performed. Logically, the development of improved, more stringent thoracic injury criteria for both frontal and side impact dummies could potentially lead to safer automobiles and the reduction of both thoracic injuries and fatalities observed in real-world automotive collisions.

Expected Publications

The research in this dissertation answers multiple scientific questions previously not addressed in the literature. It is expected that each of the studies outlined in this dissertation will be published in a scientific journal. In addition, the research may also be presented at relevant scientific conferences. Currently, it is expected that the research outlined in chapters two through six will be published as shown (Table 62).

Table 62: Publication plan for research presented in this dissertation.

Dissertation Chapter	**Topic/ Focus**	**Journal Submissions** *(Conference Publications)*
Chapter 2	The Effect of the Periosteum, Strain Gages, and Hydration on the Structural Response of Human Ribs	Journal of Applied Biomechanics *(Biomedical Sciences Instrumentation)*
Chapter 3	The Biomechanics of Human Ribs: Material and Structural Properties from Dynamic Tension and Bending Tests	Stapp Car Crash Journal
Chapter 4	Biomechanical Response of the Human Clavicle: The Effects of Loading Direction on Bending Properties	Journal of Applied Biomechanics *(Biomedical Sciences Instrumentation)*
Chapter 5	Determining Non-Censored Rib Fracture Data during Dynamic Belt Loading Tests on the Human Thorax Dynamic Belt Loading Tests on the Human Thorax: Influence of Back Support	Journal of Anatomy Journal of Applied Biomechanics *(Enhanced Safety of Vehicles)* *(Biomedical Sciences Instrumentation)*
Chapter 6	The Influence of Arm Position on Thoracic Response in Dynamic Side Impacts	Stapp Car Crash Journal

REFERENCES

Alem, N., Bowman, B., Melvin, J., and Benson, J. (1978) Whole-body human surrogate response to three-point harness restraint. Proc. 22nd Stapp Car Crash Conference, 22: 361-399. Society of Automotive Engineers, Warrendale, PA.

Bolte, J., Hines, M., McFadden, J., & Saul, R. (2000). Shoulder response characteristics and injury due to lateral glenohumeral joint impacts. *Stapp Car Crash Journal, 44,* 261-280.

Branch, T., Burdette, H., Shahriari, A., Carter, F., & Hutton, W. (1996). The role of the acromioclavicluar ligaments and the effect of distal clavicle resection. *The American Journal of Sports Medicine, 24(3)*, 293-297.

Burstein, A., Currey, J., Victor, H., and Reilly D. (1972) The ultimate properties of bone tissue: the effect of yielding. Journal of Biomechanics, 5: 35-44.

Burstein, A., Reilly D., and Martens M. (1976) Aging of bone tissue: mechanical properties. *Journal of Bone and Joint Surgery*, 58-A(1): 82-86.

Carter, D., and Haynes, W. (1976) The compressive behavior of bone as a two-phase porous structure. *Journal of Bone and Joint Surgery*, 59-A: 954- 962.

Cavanaugh, J., Walilko, T., Malhotra, A., Zhu, Y., and King, A. (1990) Biomechanical response and injury tolerance of the pelvis in twelve sled side impacts. Proc. 34th Stapp Car Crash Conference, 34, pp: 1–12. Society of Automotive Engineers, Warrendale, PA.

Cavanaugh, J. M. (1993) The biomechanics of thoracic trauma. In Accidental Injury Biomechanics and Prevention, ed A. M. Nahum and J. W. Melvin, 362-390. Springer- Verlag, New York.

Cavanaugh, J., Walilko, T., Chung, J., and King, A. (1996) Abdominal injury and response in side impact. Proc. 40th Stapp Car Crash Conference, 40: 1–16. Society of Automotive Engineers, Warrendale, PA.

Cesari, D., Ramet, M., and Bloch, J. (1981) Influence of arm position on thoracic injuries in side impact. Proc. 25th Stapp Car Crash Conference, 25: 270-297. Society of Automotive Engineers, Warrendale, PA.

Cesari, D. and Bouquet, R. (1990) Behavior of Human Surrogates under Belt Loading. Proc. 34th Stapp Car Crash Conference, 34: 73-82, Society of Automotive Engineers, Warrendale, PA.

Cesari, D. and Bouquet, R., (1994) Comparison of Hybrid III and Human Cadaver Thoracic Deformations. Proceedings of the 38th Stapp Car Crash Conference, 38, Society of Automotive Engineers, Warrendale, PA.

Charpail E., Trosseille X., Philippe P., Laporte S., Lavaste F., and Vallancien G. (2005) Characterization of PHMS Ribs: A New Methology, *Stapp Car Crash Journal*, 49: 183-198.

Chung, J. Cavanaugh, J., King, A., Koh, S., and Deng, Y. (1999) Thoracic Injury mechanisms and biomechanical responses in lateral velocity pulse impacts. Proceedings of the 43rd Stapp Car Crash Conference. 43, Society of Automotive Engineers, Warrendale, PA.

Cormier, J., Stitzel, J., Duma, S., and Matsuoka, F. (2005) Regional variation in the structural response and geometrical properties of human ribs. Proc. 49th Association for the Advancement Automotive Conference, Boston, MA.

Crandall, J., Bass, C., Pilkey, W., Miller, H., Sikorski, J., and Wilkins, M. (1997) Thoracic response and injury with belt, driver side airbag and force limited belt restraint systems. *International Journal of Crashworthiness,* 2(1): 119-132.

Cromack, J., and Ziper, H. (1975) Three-point belt induced injuries: a comparison between laboratory surrogates and real world accident victoms. Proc. 19th Stapp Car Crash Conference. 19: 1-22. Society of Automotive Engineers, Warrendale, PA.

Crowninshield, R., and Pope M. (1974) The response of compact bone in tension at various strain rates. *Annals of Biomedical Engineering,* 2: 217-225.

DaPonte, J. , Clark, M., Nelson, P., Sadowski, T., Wood, E. (2006) Quantitative confirmation of visual improvements to micro-CT bone density images. Proceedings of the SPIE. 6246: 62460D.

Dempster, W., and Lippicoat R. (1952) Compact bone as a non-isotropic material. *Amer. J. Anat*. 91: 331-362.

Duma, S., Stitzel, J., Kemper, A., McNally, C., Kennedy, E., and Matsuoka, F. (2005) Non-censored rib fracture data from dynamic belt loading tests on the human cadaver thorax. Proc. 19th International Technical Conference on the Enhanced Safety of Vehicles. NHTSA, Washington, D.C.

Eppinger, R. (1976) Prediction of thoracic injury using measurable experimental parameters. Proc. 6th International Technical Conference on the Enhanced Safety of Vehicles, 6: 770-779.

Eppinger, R., Marcus, J., and Morgan, R. (1984) Development of dummy and injury index for NHTSA's thoracic side impact protection research program. Society of Automotive Engineers, Warrendale, PA.

Evans, F., and Lebow, M. (1951) Regional differences in some of the physical properties of the human femur. *Journal Appl. Physiol*., 3: 563-572.

Evans, F., and Vincentelli, R. (1974) Relationships of the compressive properties of human cortical bone to histological structure and calcification. *Journal of Biomechanics,* 7 :1-10.

Evans, F., & Lebow, M. (1951). Regional differences in some of the physical properties of the human femur. *Journal of Applied. Physiology*, 3: 563-572.

Evans, F., & Bang, S. (1967). Differences and relationships between the physical properties and microscopic structure of human femoral, tibia, and fibular cortical bone. *American Journal of Anatomy*, 120: 79-88.

Elhagediab, A., and Rouhana, S. (1998) Patterns of abdominal injury in frontal automotive crashes. Proc. 16th International Technical Conference on the Enhanced Safety of Vehicles, 16: 327-337, NHTSA, Washington, D.C.

Fondrk, M., Bahniuk, E., Davy, D., et al. (1988). Some viscoelastic characteristics of bovine and human cortical bone. *Journal of Biomechanics*, 21(8): 623-630.

Fondrk, M., Bahniuk, E., & Davy D. (1999). Inelastic strain accumulation in cortical bone during rapid transient tensile loading. *Journal of Biomechanical Engineering*, 121(6): 616-621.

Frankel, V.H. (1960) The femoral neck. Function. Fracture mechanism. Internal fixation. An experimental study. Almqvist and Wiskell, Goteborg, Sweden..

Funk, J, Kerrigan, J, and Crandall, J. (2004) Dynamic bending tolerance and elastic-plastic material properties of the human femur. Proc. 48th Association for the Advancement Automotive Conference. 48: 216-233. Key Biscayne, FL.

Gabler, H, Digges, K., Fildes, B., and Sparks, L. (2005) Side impact risk for belted far side passenger vehicle occupants. Society of Automotive Engineers, Warrendale, PA.

Granik, G., and Stein, I. (1973) Human ribs: static testing as a promising medical application. *Journal of Biomechanics*, 8: 237-240.

Griffon, D.J., Wallace, L.J., and Bechtold, J. (1995) Biomechal properties of canine corticocancellous bone frozen in normal saline solution. *Am. J. Vet. Res.,* 56 : 822.

Hamer, A., Strachen, J., Black, M., Ibbotson, C., Stockley, I., and Elson, R. (1996) Biomechanical properties of cortical allograft bone using a new method of bone strength measurement. A comparison of fresh, fresh-frozen and irradiated bone. *Journal of Bone and Joint Surgery*, 78B: 363.

Hardy, W., Lawrence, W., Reed, M., and Ricci, L. (1997) Biomechanical investigation of airbag-induced upper-extremity injuries. Proc. 39th Stapp Car Crash Conference, 39: 1-22. Society of Automotive Engineers, Warrendale, PA.

Hardy, W., Schneider, L., and Rouhana, S. (2001a) Prediction of airbag-induced forearm fractures and airbag aggressivity. *Stapp Car Crash Journal*, 45: 511-534.

Hardy, W., Schneider, L., and Rouhana, S. (2001b) Abdominal impact response to rigid-bar seatbelt, and airbag loading. *Stapp Car Crash Journal*, 45:131-149.

Housner, J., & Kuhn, J. (2003) Clavicle fractures. *The Physician and Sports Medicine*, 31(12): 30-36.

International Standards Organization (ISO) Road vehicles– Anthropometric side impact dummy-Lateral impact response requirements to assess the biofidelity of the dummy, ISO/TR 9790:1999(E).

Irwin, A.L., Walilko, T.J., Cavanaugh, J.M., Zhu, Y., and King, A.I. (1993) Displacement of the shoulder and thorax in lateral sled impacts. Proceedings of the 37th Stapp Car Crash Conference, 37: 165-173.

Ito, M. (2005) Assessment of bone quality using micro-computed tomography (micro-CT) and synchrotron micro-CT. Jou*rnal Bone Miner Metab.*, 23 Suppl: 115-21.

Kallieris, D., and Mattern, R. (1979) Shoulder belt forces and thorax injuries. Proc. 7th International Research Council on the Biomechanics of Impact, 7: 171-183.

Kallieris, D., Schmidt, G., Barz, J., Mattern, R., and Schulz, F. (1974) Response and vulnerability of the human body at different impact velocities in simulated three-point belted cadaver tests. Proc. 2nd International Research Council on the Biomechanics of Impact, 2: 196-209

Kallieris, D., Mattern, R., McIntosh, A., and Boggasch, F. (1992) The biofidelity of EuroSID 1 and BioSID. Paper 922518. Proc. 36th Stapp Car Crash Conference, 36: 103-117. Society of Automotive Engineers, Warrendale, PA.

Kallieris, D., Zerial, P.D., Rizzetti, A., and Mattern, R. (1998) Prediction of thoracic injuries in frontal collisions. Proc. 18th International Technical Conference on the Enhanced Safety of Vehicles, 18: 1550-1563.

Keller, T.S. (1994) Predicting to compressive mechanical behavior of bone. *Journal of Biomechanics*, 27(9): 1159-1168.

Klaus, G., Sinnhuber, R., Hoffman, G., Kalleris, D., and Mattern, R. (1984) Side impact—a comparison between dummies and cadavers, correlations between cadaver loads and injury severity. Proc. 28th Stapp Car Crash Conference, 28: 237–259. Society of Automotive Engineers, Warrendale, PA.

Kemper, A., McNally, C., Kennedy, E., Rath, A., Manoogian, S., Stitzel, J., and Duma, S., (2005) Material Properties of Human Rib Cortical Bone from Dynamic Tension Coupon Testing. *Stapp Car Crash Journal,* 49: 199-230.

Kemper, A., McNally C., Pullins, C., Freeman, L. & Duma, S, (2007a). The biomechanics of human ribs: Material and structural properties from dynamic tension and bending tests. *Stapp Car Crash Journal, 51,* 235-273.

Kemper, A., McNally, C., Kennedy, E., et al. (2007b). The Material properties of human tibia cortical bone in tension and compression: Implications for the tibia index. Proceedings of the 20th Enhanced Safety of Vehicles Conference, Lyon, France.

Kemper A., McNally C., Kennedy E., Manoogian S., and Duma S. (2008) The Influence of Arm position on Thoracic Response in Side Impacts. *Stapp Car Crash Journal*, 52: 379-420.

Kennedy, E., Hurst, W., Stitzel, J., Cormier, J., Hansen, G., Smith, E., and Duma, S. (2004) Lateral and posterior dynamic bending of the mid-shaft femur: fracture risk curves for the adult population. *Stapp Car Crash Journal,* 48: 27-51.

Kent, R. (2002) Dynamic response of the thorax: Restraint specific hard tissue injury. Ph.D. Dissertation, University of Virginia.

Kent, R., Crandall, J., Bolton, J., Prasad, P., Nusholtz, G., and Mertz, H. (2001) The influence of superficial soft tissues and restraint condition on thoracic skeletal injury prediction. *Stapp Car Crash Journal,* 45: 183-204.

Kent, R., Sherwood, C., Lessley, D., Overby, B. (2003). Age-Related Changes in the Effective Stiffness of the Human Thorax Using Four Loading Conditions. International Research Council on the Biomechanics of Impact, Lisbon Portugal.

Kent, R., Henary, B., Matsuoka, F. (2005a) On the fatal crash experience of older drivers. Proc. AAAM. 49: 371-391.

Kent, R., Lee S., Darvish, K., Wang, S., Poster, C., Lange, A., Brede, C., Lange, D., and Matsuoka, F. (2005b) Structural and Material Changes in the Aging Thorax and Their Role in Crash Protection for Older Occupants. *Stapp Car Crash Journal,* 49: 231-249.

Klaus, G., and Kalleris, D. (1982) Side impact—a comparison between HSRI, APROD and HYBRID II dummies and cadavers. Ninth International Tech Conference on Experimental Safety Vehicles, Kyoto, Japan.

Klaus, G., and Kalleris, D. (1983) Side impact—a comparison between HSRI, APROD and HYBRID II dummies and cadavers. Proc. 27th Stapp Car Crash Conference, 27: 365–381. Society of Automotive Engineers, Warrendale, PA.

Koh, S., Cavanaugh, J., Zhu, J. (2001) Injury response of the shoulder in lateral sled tests. *Stapp Car Crash Journal,* 45: 101–141.

Kroell, C., Schneider, D., and Nahum, A. (1974) Impact Tolerance of the Human Thorax II. Procedings of the 18th Stapp Car Crash Conference. SAE International, Warrendale, PA.

Kuppa, S., and Eppinger, R. (1998) Development of an improved thoracic injury criterion. Proc. 42nd Stapp Car Crash Conference, 42: 139-154.

Kuppa, S., Eppinger, R.H., McKoy, F., Nguyen, T, Pintar, F.A., and Yoganandan, N. (2003) Development of side impact thoracic injury criteria and their application to the modified ES-2 dummy with rib extensions. *Stapp Car Crash Journal,* 47: 189-210.

Kuppa, S. (2004) Injury criteria for side impact dummies. Docket Number NHTSA-2004-17694. U.S. Department of Transportation, Washington, D.C.

L'Abbe, R., Dainty, D., Newman, J., (1982) An Experimental Analysis of Thoracic Deflection Response to Belt Loading." Proceedings of the 7th International Research Council on the Biomechanics of Impact Conference, Bron, France, 7: 184-194.

Lindahl, O., and Lindren, G.H. (1967) Cortical bone in man. *Acta. Orthop. Scandinava,* 38: 141-147.

Linde, F., and Sorenson, H. (1993) The effect of different storage methods on the mechanical properties of trabecular bone. *Journal of Biomechanics,* 26: 1249.

Littell, R., Milliken, G., Storp, W., and Wolfinger, R. (1996) SAS system for mixed models. SAS Institute; Inc, Cary, NC.

Lund, A.K. (2000) Recommended procedures for evaluating occupant injury risk from deploying side airbags. International Standard Organization.

Martin, R., and Ishida, J. (1989) The relative effects of collagen fiber orientation, porosity, density, and mineralization, on bone strength. *Journal of Biomechanics,* 22(5): 419-426.

Mertz, H. (1984) A Procedure for normalizing impact response data. Society for AutomotiveEngineers, Warrendale, PA.

McCalden, R., McGeogh, J., Barker, M., et al. (1993) Age-related changes in the tensile properties of cortical bone. *Journal of Bone and Joint Surgery,* 75(8): 1193-1205.

McElhaney, J., & Byars, E. (1965). Dynamic response of biological materials. ASME. Publ. 65-WA/Huf-9.

Milliken, G., and Johnson, D. (1984) Analysis of messy data. Volume 1: designed experiments. Wadsworth Inc., Belmont, CA.

Mohr, M., Abrams, E., Engel, C., Long, W., and Bottlang, M. (2007) Geometry of human ribs pertinent to orthopedic chest-wall reconstruction. Journal of Biomechanics, 40: 1310-1317.

Moore, K., & Dalley, A. (2006). Clinically Oriented Anatomy, 5th Edition. Lippincot Williams & Wilkins, New York.

Morgan, R. , Marcus, J. , and Eppinger, R. (1986) Side Impact – the Biofidelity of NHTSA's Proposed ATD and Efficacy of TTI. Proc. 13th Stapp Car Crash Conference, 13: 27-40. Society of Automotive Engineers, Warrendale, PA.

Morgan, R., Eppinger, R., Haffner, M., Kallieris, D., Miltner, E., Mattern, R., Yoganandan, N., Pintar, F.., Sances, A., Kuppa, S., Sharpless, C., Crandall, J., Pilkey, W., and Klopp, G.(1994) Thoracic trauma assessment formulations for restrained drivers in simulated frontal impacts. *Stapp Car Crash Journal,* 38: 15-34.

Muellar, K., Trias, A., and Ray, R. (1966) Bone density and composition. Age-related and phathological changes in water and mineralization content. *Journal Bone and Joint Surgery,* 48-A: 140-148.

Nordqvist, A., Petersson, C., & Redlund-Johnell, I. (1993). The Natural course of lateral clavicle fractures: 15 (11-21) Year follow-up of 110 Cases. *Acta Orthopaedic-Scand*inavian, 64(1): 87-91.

Norton, R. (2000). Machine Design: An Integrated Approach 2nd Ed. Prentice Hall, New Jersey.

Patrick L. (1976) Frontal force impact tolerance of the human thorax. The Human Thorax-Anatomoy, Injury, and Biomechanics. SAE P-67, Dearborn, MI.: 37-48.

Patrick, L., Mertz, H., and Kroell, C. (1967) Cadaver Knee, Chest and Head Impact Loads. Proc. 10th Stapp Car Crash Conference, 10: 168-182. Society of Automotive Engineers, Warrendale, PA.

Patrick, L.M., Anderson, A., and Bohlin, N. (1974) Three-point harness accident and laboratory data comparison. *Stapp Car Crash Journal,* 18: 201-282.

Pintar, F., Yoganandan, N., Hines, M., Maltese, M., McFadden, J., Saul, R., Eppinger, R., Khaewpong, N., and Kleinberger, M. (1997) Chestband Analysis of Human Tolerance to Side Impact. Proc. 41st Stapp Car Crash Conference, 41: 63-74. Society of Automotive Engineers, Warrendale, PA.

Proubasta, I., Itarte, J., Caceres, E., et al. (2002). Biomechanical evaluation of fixation of clavicle fractures. *Journal of the Southern Orthopedic Association*, 11(3): 148-152.

Ramet, M., and Cesari, D. (1979) Behavior of restrained dummies and cadavers in frontal impacts. Proc. 7th International Research.

Reilly, D.T., Burstein, A.H., and Victor, H.F. (1974) The elastic modulus for bone. *Journal of Biomechanics,* 7: 271-275.

Reilly, D., & Burstein, A. (1975). The elastic and ultimate properties of compact bone tissue. *Journal of Biomechanics,* 8(6): 393-405.

Rouhana S., Bedewi P., Kankanala S., Prasad P., Zwolinski J., Meduvsky A., Rupp J., Jeffreys T. and Schneider L., (2003) Biomechanics of 4-p seat belt systems in frontal impacts, *Stapp Car Crash Journal,* 47: 367-399.

Robbins, D., Lehman, R., and Augustyn, K., (1994). Prediction of thoracic injuries as a function of occupant kinematics. In: Bachaitis, S. (Ed.), Biomechanics of Impact Injury and Injury Tolerances of the Thorax–Shoulder Complex: 1109–1118.

Sacreste, J., Brun-Cassen, F., Fayon, A., Tarriere, C., Got, C., Patel, A. (1982) Proposal for a thorax tolerance level in side impacts based on 62 tests performed with cadavrs having known bone condition. SAE 821157.

Samaha, R., and Elliott, D. (2003) NHTSA Side Impact Research: Motivation for Upgraded Test Procedures, Eighteenth International Technical Conference on the Enhanced Safety of Vehicles, Paper No. 492, National Highway Traffic Safety Administration, Washington, D.C.

SAE, 1995, "Instrumentation for Impact Test," SAE J211/1 MAR 1995, 1995 SAE Handbook Volume 4 - On-Highway Vehicles & Off-Highway Machinery, Society of Automotive Engineers, Warrendale, PA.

Schaffler, M.B., and Burr, D.B. (1988) Stiffness of compact bone: effects of porosity and density. *Journal of Biomechanics*, 21(1): 13-16.

Schneider, L., Robbins, D., Pflueg, M., and Snyder, R. (1983) Development of anthropometrically based design specifications for an advanced adult anthropomorphic dummy family. Contract No. DTNH22-80-C-07502, University of Michigan Trnasportation Research Institute, Ann Arbor.

Sedlin, E. (1965) A rheological model for cortical bone. *Acta Orthop. Scand.,* 83: 1.

Shaw, J., Herriott, R., McFadden, J., Donnelly, B., and Bolte, J. (2006) Oblique and lateral impact response of the PMHS thorax. *Stapp Car Crash Journal,* 50: 146-167.

Stalnaker, R., Tarriere, C., Fayon, A., Walfisch, G., Balthazard, M., Masset, J., Got, C., and Patel, A. (1979) Modification of part 572 dummy for lateral impact according to biomechanical data. Proc. 23rd Stapp Car Crash Conference, 23: 843-872. Society of Automotive Engineers, Warrendale, PA.

Stein, I., and Granik, G. (1979). Rib structure and bending strength: *An autopsy study. Calcif. Tiss Res.,* 20: 66-73.

Stitzel, J., Cormier, J., Barretta, J., Kennedy, E., Smith, E., Rath, A, and Duma, S. (2003) Defining regional variation in the material properties of human rib cortical bone and its effect on fracture prediction. *Stapp Car Crash Journal,* 47: 243- 265.

Terry, G., & Chopp T. (2000). Functional anatomy of the shoulder. *Journal of Athletic Training,* 35(3): 248-255.

Trosseille, X., Baubrit, P., Leport, T., and Vallancien, G. (2008) Rib Cage Strain Patterns as a Function of Chest Loading Configuration, *Stapp Car Crash Journal*, 52: 205-231.

Trotter, M., and Perterson, R. (1955) Ash weight of human skeletons in percent of their dry fat-free weight. Anatomical Record, 123: 341-358.

Turner, C., & Burr, D. (2001). Experimental techniques for bone mechanics. In Bone Biomechanics Handbook, Second Edition, CRC Press, Washington D.C.

Viano, D.C. (1978) Thoracic injury potential. Proc. 6th International Research Council on the Biomechanics of Impact: 142-156.

Viano, D. (1989) Biomechanical Responses and Injuries in Blunt Lateral Impact. Proc. 33rd Stapp Car Crash Conference, 33: 113-142. Society of Automotive Engineers, Warrendale, PA.

Weaver, J.K. (1966) The microscopic hardness of bone. *Journal Bone and Joint Surgery*, 48-A: 273.

Williams, P., Warwick, R. Dyson, M., & Bannister, L. (1989). Gray's Anatomy, 37th Edition. Churchill Livingston Inc., New York.

Wood, J.L. (1971) Dynamic response of human cranial bone. *Journal of Biomechanics*, 4: 1-12.

Wolf, A. and Pfeger, B. (2003) Polict and Practice- Burden of major musuloskeletal conditions. Bulletin of the World Helath Organization, 81(9): 646-656.

Wright, T., and Hayes, W. (1976) Tensile testing of bone over a wide range of strain rates: effects of strain rate, microstructure and density. Medical and Biological Engineering Nov: 671-679.

Yamada, H. (1970). Strength of Biological Materials. Williams and Wilkins Co., Baltimore, MD.

Yeuheui, H.A. and Draughn, R.A. (2000) Mechanical testing of bone and the bone-implant interface. CRC Press LLC, New York.

Yoganandan, N., and Pintar, F.A. (1998) Biomechanics of human thoracic ribs. *Journal of Biomechanical Engineering*, 120: 100-104

Yoganandan, N., Pintar, F.A., Stemper, B.D., Gennarelli, T.A., and Weigelt, J.A. (2007) Biomechanics of side impact: Injury criteria, aging, occupants, and airbag technology. *Journal of biomechanics*, 40: 227-243.

Zhou, Q., Rouhana, S., and Melvin, J. (1996) Age effects on thoracic injury tolerance. Society of Automotive Engineers, Warrendale, PA.

Zhu, Y., Cavanaugh, J., and King, A., (1993). Pelvic biomechanical response and padding benefits in side impact based on a cadaveric test series. Proc. 37th Stapp Car Crash Conference, 37: 223–233. Society of Automotive Engineers, Warrendale, PA.